



**Investigation of Nrf2 activity measures for assessing  
the toxicological and pharmacological effects of drugs**

Thesis submitted in accordance with the requirements of the University  
of Liverpool for the degree of Doctor of Philosophy

By

Fiona Mutter

March 2018

## **Declaration**

This thesis is the result of my own work. The material contained within this thesis has not be presented, nor is currently being presented, either wholly or in part for any other degree qualification.

Fiona Mutter

This research was conducted in the Department of Molecular and Clinical Pharmacology and the MRC Centre for Drug Safety Science of the University of Liverpool.

## Contents

<b>Abstract</b> .....	6
<b>Acknowledgements</b> .....	8
<b>Publications</b> .....	9
<b>Abbreviations</b> .....	10
<b>Chapter 1</b> General introduction.....	13
<b>Chapter 2</b> Bioluminescent imaging of Nrf2 reveals localised chemical stress associated with drug-induced organ toxicity .....	52
<b>Chapter 3</b> Blood-based analysis of the Nrf2 pathway .....	105
<b>Chapter 4</b> Investigation of putative Nrf2-regulated genes in human hepatocytes.....	137
<b>Chapter 5</b> Use of Nrf2 reporter genes to assess the potencies of novel sulforaphane analogues .....	181
<b>Chapter 6</b> General discussion .....	201
<b>References</b> .....	212
<b>Appendix</b> .....	232

## List of figures and tables

Figure 1.1 Bioactivation of paracetamol.....	19
Figure 1.2 Overview of the Nrf2-Keap1 pathway .....	24
Figure 1.3 Functional domains of Nrf2 and Keap1 .....	25
Table 1.1 Human genes positively regulated by Nrf2.....	31
Figure 1.5 The Glutathione system.....	38
Figure 1.6 Overview of the OKD48 reporter .....	45
Figure 1.7 Nrf2 inducing compounds.....	49
Figure 2.1 Calculation of region of interest .....	58
Table 2.2 Drug-induced liver injury scoring criteria.....	62
Table 2.3 Drug-induced kidney injury score criteria.....	62
Table 2.4 Antibody concentration and conditions for Western blot.....	65
Table 2.5 Mouse qPCR primer sequences .....	68
Table 2.6 qPCR Program .....	68
Figure 2.2 Basal expression of glutathione and Nrf2 pathway activity in Nrf2-Luc mice.....	70
Figure 2.3 In and ex vivo bioluminescence of Nrf2-Luc mice exposed to Sodium Arsenite (13 mg/kg).....	71
Figure 2.4 Elevated serum alanine transaminase in wild-type mice exposed to a single dose of APAP (300 mg/kg).....	73
Figure 2.5 Glutathione depletion in wild-type mice exposed to a single dose of paracetamol (300 mg/kg).....	73
Figure 2.6 Upregulation of the Nrf2-pathway in wild-type mice exposed to a single dose of paracetamol (300 mg/kg). .....	74
Figure 2.7 Serum alanine transaminase significantly elevated in male and female Nrf2-Luc mice exposed to paracetamol (300 mg/kg).....	76
Figure 2.8 In vivo bioluminescence induced in male Nrf2-Luc mice exposed to paracetamol (300 mg/kg).....	77
Figure 2.9 Ex vivo bioluminescence induced in male Nrf2-Luc mice exposed to paracetamol (300 mg/kg).....	78
Figure 2.10 In vivo bioluminescence induced in female Nrf2-Luc mice exposed to paracetamol (300 mg/kg).....	80
Figure 2.11 Ex vivo bioluminescence induced in female Nrf2-Luc mice exposed to paracetamol (300 mg/kg) .....	81
Figure 2.12 Serum alanine transaminase and ex vivo bioluminescence in male and female Nrf2-Luc mice exposed to paracetamol (300 mg/kg) .....	82
Figure 2.13 Immunohistochemistry of livers from male Nrf2-Luc mice exposed to paracetamol (300 mg/kg) .....	85
Figure 2.12 Immunohistochemistry of livers from female Nrf2-Luc mice exposed to paracetamol (300 mg/kg) .....	87

Figure 2.15 Nrf2-Luc signal corresponds with upregulation of the Nrf2 pathway in livers of female Nrf2-Luc mice exposed to paracetamol (300 mg/kg) .....	88
Figure 2.16 Endogenous Nrf2 pathway activity in the livers and kidneys of wild-type mice exposed to paracetamol (300 mg/kg).....	89
Figure 2.17 Serum blood urea nitrogen significantly elevated in female Nrf2-Luc mice exposed to cisplatin (20 mg/kg).....	91
Figure 2.18 In vivo bioluminescence induced in female Nrf2-Luc mice exposed to Cisplatin (20 mg/kg).....	92
Figure 2.19 Ex vivo bioluminescence induced in female Nrf2-Luc mice exposed to Cisplatin (20 mg/kg).....	93
Figure 2.20 Serum BUN and ex vivo bioluminescence in female Nrf2-Luc mice exposed to cisplatin (20 mg/kg) .....	94
Figure 2.21 Immunohistochemistry of female Nrf2-Luc mice exposed to Cisplatin (20 mg/kg) .....	97
Figure 2.22 Gene and protein expression in kidneys of female Nrf2-Luc mice exposed to Cisplatin (20 mg/kg) .....	98
Figure 2.23 Gene expression in livers of female Nrf2-Luc mice exposed to Cisplatin (20 mg/kg) .....	99
Table 3.1 Additional Mouse qPCR primers .....	110
Figure 3.1 – Validation of organ specific primers .....	114
Figure 3.2 Induction of Nrf2 pathway in whole blood following a toxic dose of paracetamol .....	117
Figure 3.3 – Increased liver-specific gene expression in whole blood of paracetamol-treated mice.....	118
Figure 3.4 – Muted elevation of serum alanine transaminase in response to N-acetylcysteine exposure following paracetamol toxicity.....	121
Figure 3.5 – Muted necrosis and Hmox1 staining in mice administered N-acetylcysteine in response to paracetamol toxicity .....	122
Figure 3.6 – Gene expression in tissues and whole blood from mice treated with paracetamol and N-acetylcysteine.....	124
Figure 3.7 Induction of Nrf2 pathway in tissues and whole blood by CDDO-Me .....	128
Figure 3.8 Upregulation of the Nrf2 pathway in response to chronic exposure to CDDO-Me .....	130
Table 4.1 Wild-type and mutated ARE sequences within synthesised constructs .....	142
Table 4.2 Q5 polymerase PCR reaction conditions.....	143
Table 4.3 Insert digestion reaction .....	144
Table 4.4 Colony screening reactions .....	145
Table 4.5 Human qPCR primers .....	148

Figure 4.1 Work flow of microarray hit comparison with existing datasets.....	150
Figure 4.2 Alignment of ChIP-Seq peaks with predicted antioxidant response elements...	154
Table 4.6 Genes with antioxidant response elements responsive to sulforaphane.....	155
Figure 4.3 Gene expression in primary human hepatocytes exposed to CDDO-Me .....	162
Figure 4.4 Gene expression in HepG2 cells exposed to CDDO-Me.....	163
Figure 4.5 Confirmation of pGL4 clones by Sanger sequencing .....	165
Figure 4.6 Potential ARE sites within the SRXN1 promotor.....	166
Figure 4.7 pGL4-construct response to CDDO-Me in HEK293T cells .....	168
Figure 4.8 pGL4-construct response to CDDO-Me in HepG2 cells.....	169
Figure 4.9 Optimisation of NRF2 overexpression by pSB-tet-NRF2.....	171
Figure 4.10 pGL4-construct response to NRF2 overexpression in HepG2 cells.....	172
Figure 4.11 Induction of wild-type but not mutant pGL4-SRXN1 constructs following NRF2 activation .....	174
Table 5.1 Annealed oligo cloning primers.....	186
Figure 5.1 Decreased luciferase NRF2-reporter activity following toxicity .....	188
Figure 5.2 5xARE reporter construction .....	191
Figure 5.3 Response of pGL4-5xARE reporter to CDDO-Me in HepG2 cells .....	192
Figure 5.4 Response of pGL4-5xARE reporter to NRF2 overexpression .....	193
Figure 5.5 Response of pGL4-NQO1 and 5xARE reporter constructs to sulforaphane analogues in HepG2 cells .....	195
Table A1 Putative NRF2-regulated gene bioinformatic analysis.....	232
Figure A1 NQO1 WT GeneMill plasmid map.....	235
Figure A2 pGL4.20 plasmid map .....	235
Figure A3 Sub-cloning promoter regions into the pGL4.20 vector .....	236
Figure A4 NQO1 WT GeneMill plasmid map.....	237
Figure A5 pSB-tet-Nrf2 plasmid map .....	237
Table A2 Summary of EVGEN analogue potencies .....	238
Figure A6 Sulforaphane analogues with non-defined CD values.....	243
Figure A7 Sulforaphane analogues with CD values greater than 20 $\mu$ M .....	244
Figure A8 Sulforaphane analogues with CD values between 15 and 20 $\mu$ M .....	247
Figure A9 Sulforaphane analogues with CD values between 10 and 15 $\mu$ M .....	248
Figure A10 Compounds in the SFX-01 program with CD values less than 10 $\mu$ M .....	251

## Abstract

The transcription factor Nuclear factor erythroid 2-related factor 2 (NRF2) orchestrates the expression of a battery of cytoprotective genes containing antioxidant response elements (AREs) within their promoter sequences. Activation of the NRF2 pathway has been implicated in the early stages of drug-induced toxicity, a major cause of drug attrition and public risk, and therefore holds potential as a pre-clinical marker of chemical entities liable to toxicity. Conversely, the upregulation of NRF2 activity holds great therapeutic potential. Many NRF2 modulating agents are currently undergoing clinical trials for the treatment of pathologies with an underlying oxidative stress component. The establishment of sensitive, accurate methods to monitor induction of the transcription factor are therefore vital. This thesis focuses on the characterisation of novel methods to measure NRF2 pathway activation following both toxic and therapeutic stimulation.

In chapter 2, I use the transgenic Nrf2-Luciferase (Nrf2-Luc) mouse model (Oikawa et al., 2012), to test the hypothesis that localised activation of NRF2 represents an early marker of chemical stress associated with organ-specific drug toxicity. Following a hepatotoxic dose of paracetamol (APAP) a bioluminescent signal was observed in the liver but not kidneys or lungs of the Nrf2-Luc mice. On a cellular level, luciferase and Haem oxygenase 1 (Hmox1) staining colocalised around the centrilobular region, consistent with the known pathology of APAP. In response to a nephrotoxic dose of cisplatin, kidney specific bioluminescence was detected and colocalised with activation of the endogenous NRF2 pathway in tubular epithelial cells. A key finding was that activation of organ-specific bioluminescence correlated well with established biomarkers for liver and kidney injury respectively, highlighting the ability of NRF2 to reflect localised cellular insults associated with overt organ toxicity.

Despite the emerging role of NRF2 as a marker of the response to drug toxicity and a therapeutic target, there are currently no non-invasive methods for monitoring NRF2 pathway activation in patients. In chapter 3 of this thesis, I hypothesised that organ-specific chemical perturbation instigates changes in NRF2 pathway activity in murine whole blood, providing potential markers of organ-specific injury. Here I provide evidence for the induction of NRF2-regulated genes in whole blood following exposure of C57BL/6 mice to APAP or the therapeutic NRF2-activating compound, CDDO-Me. The induction of NRF2-regulated transcripts, including *Hmox1*, was muted in mice administered APAP and the clinically used antidote, *N*-acetylcysteine (NAC). Insight into blood-based activity of the NRF2 pathway may provide evidence for the role of NRF2 in response to drug toxicity in humans and will be an important pharmacodynamic marker with the emergence of NRF2 modulators as therapeutic drugs.

Primary human hepatocytes (PHH) are one of the most physiologically relevant *in vitro* systems for modelling drug-induced hepatotoxicity. However, the NRF2 pathway is not well characterised in these cells. In chapter 4, based on previous, unpublished microarray data of NRF2 pathway modulation in PHH, a group of potentially novel NRF2-regulated genes were identified: Coagulation factor II receptor-like 2 (*F2RL2*), NmrA-like family domain containing 1 pseudogene (*LOC344887*) and Tripartite Motif Containing 16 Like (*TRIM16L*). Following identification of potentially active cis-ARE sites in the promoters of these genes, I assessed direct activation by NRF2 using luciferase-based promoter-reporter assays. Despite evidence in multiple microarray datasets from our bioinformatic analysis that these genes are indeed modulated by NRF2, wild-type and mutant reporter constructs failed to produce differential luminescent responses in transfected HepG2 cells exposed to CDDO-Me or following over-expression of NRF2. During consideration of the well-established Nrf2-regulated gene *SRXN1* as a positive control, I noticed two consecutive ARE sites within the region identified by Singh

*et al.* to which NRF2 directly binds (Singh et al., 2009). Promotor-reporter analysis implicated both sequences in the activation of *SRXN1* transcription as only cells transfected with the wild-type *SRXN1* construct produced luminescence in response to Nrf2-activation. These data indicate the necessity of extended AREs for the activation of NRF2-regulated genes.

The emergence of NRF2-activating compounds in the clinic highlights the application of therapeutic induction of the NRF2-dependent oxidative stress responses. The isothiocyanate, sulforaphane is among the most well studied clinical activators of NRF2. However due to its limited shelf life, stabilised analogues are needed. In the final experimental chapter of this thesis, I summarise data generated in collaboration with Evgen Pharma to assess the potencies of novel analogues of sulforaphane. Utilizing the H4Ile-8AREL reporter cell line, I show analogues with variable methane bridge length and sulfoxide group exhibited reduced potency towards NRF2 compared to the parent compound sulforaphane. The potencies of a subgroup of analogues as inducers of other luminescent reporters: pGL4-NQO1 and pGL4-5xARE, in a human liver cell line were also recorded. A key finding was the similar rank order of potencies of this subset of compounds in both cell lines. Development of sensitive assays for the *in vitro* assessment of NRF2 activators will be of increasing value as the number of therapeutic NRF2-modulating compounds entering the clinic grow.

The establishment of robust methods to monitor NRF2 activation will inform key events underlying toxicity and provide insight into the subtle changes resulting in upregulation of the oxidative stress response to provide either an adaptive phenotype or one that is overwhelmed in resulting toxicity. Documentation of these mechanisms at a tissue or cellular level will inform adverse outcome pathways (AOPs), improving risk assessment frameworks. The specific stimuli NRF2 responds to must be thoroughly characterised to define the role of NRF2 and other stress response pathways following exposure to chemical and/or oxidative stressors. Conversely, development of effective, novel NRF2 inducers for use in the clinic requires sensitive screening platforms to determine the pharmacodynamic effects of these compounds.



## **Acknowledgements**

This work would not have been possible without the support of several people. I would like to express my sincere thanks to them all. First and foremost, I would like to thank my supervisor, Dr. Ian Copple. Thank you for your guidance, constructive questions and insightful advice, without which this thesis would never have been finished.

Special thanks to Dr. Shiva Foorotan for her endless patience and encouragement. You have taught me so much and I will miss eating your Iranian rice. Dr. Nick Harper who made a significant and much appreciated contribution to the plasmid construction in this thesis. Thank you for sharing your time and expertise. Thanks also to Dr. Olympia Gianfrancesco and the other members of White Block for giving me a crash course in cloning techniques.

I am grateful to Prof. Anja Kipar for conducting the histopathological work. Thank you to Pam, Rhys, Edita and the rest of the technical team at the BSU and CPI. Thanks also to Dr. Ben Francis for statistical assistance. I would also like to thank Dr. Takao Iwawaki for providing us with the Nrf2-Luc mice and Jonathan Pho for permission to use his constructs.

Particular thanks to lab members, past and present, for making working at the MRC CDSS that much more enjoyable during the highs and lows of research. Thank you, Charles, for the many interesting conversations, despite the jazz music. Thanks also to Nathalie, Jo, Lawrence, Jess, Constance, Emma, Beth, Sarah, Rob, James, Amy, Carol and Sean. Special thanks to Fang for dragging me to yoga and the therapeutic baking sessions. I would also like to thank Niraj, for the pep talks and for nodding your head in the sea of people at the end of year talks. Thank you Tushar for volunteering to proof-read multiple chapters. Thanks also to Shiquan and Zohra for always knowing the right thing to say, on those rare occasions outside the lab. Thank you, Paul and Yanru for the excellent cups of tea.

I am deeply grateful for the love and support from my family, and their occasional parcels of food. Chris, thank you for your patience, humour and endless support throughout writing this thesis.

And finally, Mum, thank you for all that you do.

## **Publications**

**Mutter FE**, Park BK, Copple IM. (2015) Value of monitoring Nrf2 activity for the detection of chemical and oxidative stress. *Biochemical Society Transactions*. 2015;43(4):657-662.

Forootan SS\*, **Mutter FE\***, Kipar A, Iwawaki T, Goldring CE, Kitteringham NR, Park BK, Copple IM (2017) Real-time *in vivo* imaging reveals localised Nrf2 stress responses associated with direct and metabolism-dependent drug toxicity. *Scientific Reports*. 2017:16084 (\*joint first authors).

Copple IM, den Hollander W, **Mutter FE**, Maggs JL, Shelton LM, Olayanju A, Rainbow L, Fang Y, Sutherland JJ, Ellis EC, Moro SM, Ingelman-Sundberg M, Malik H, Goldring CE, Kitteringham NR, van de Water B, Stevens JL, Park BK (2018) Complex responses of NRF2-associated gene sets to chemical insult in primary human hepatocytes – Implications for prediction of chemical stress. *Submission pending*.

## Abbreviations

·OH	Hydroxyl radical
8-OH-dG	8-hydroxydeoxyguanosine
ADRs	Adverse drug reactions
AGEs	Advanced glycation end products
AKR1C2	Aldo-Keto reductase family 1, member C2
ALT	Alanine transaminase
Ambp	$\alpha$ -1-microglobulin/bikunin precursor
AOP	Adverse outcome pathway
AOPPs	Advanced oxidation protein products
APAP	Acetaminophen
Apoa2	Apolipoprotein A2
Aqp2	Aquaporin 2
ARE	Antioxidant response element
ASK1	Apoptosis signalling-regulating kinase 1
ASK-1	Apoptosis signal-regulated kinase
ASN	Sodium arsenite
ATM	Ataxia-telangiectasia mutated
BAC	Bacterial artificial chromosome
BACH1	BTB and CNC homolog 1
BCL-2	B-cell lymphoma 2
BSA	Bovine serum albumin
BTB	Bric-a-brac/tram-track/broad complex
BUN	Blood urea nitrogen
bZIP	Basic leucine zipper
CD	Critical dose
CdCl <sub>2</sub>	Cadmium chloride
cGMP	Cyclic guanosine monophosphate
CHD	Coronary heart disease
CML	N(6)-carboxymethyllysine
CO <sub>3</sub> <sup>-</sup>	Carbon trioxide
CONFIRM	Comparator and an oral fumarate in relapsing-remitting multiple sclerosis
COPD	Chronic obstructive pulmonary disease
cpYFP	Circulatory permuted yellow fluorescent protein)
CREB	cAMP response element binding protein
CRET	Chemiluminescence resonance energy transfer
CSA	Cyclosporine A
CTR	C-terminal region
DCF	2',7'-dichlorofluorescein
DCFH-DA	Dichlorodihydrofluorescein
DEFINE	Determination of the efficacy and safety of oral fumarate in relapsing-remitting multiple sclerosis
Dexlipotam	Alpha-Lipoic acid
DGR	Double glycine repeats
DIKI	Drug induced kidney injury
DILI	Drug-induced liver injury
DMSO	Dimethylsulfoxide
DOX	Doxycycline
ECH	Erythroid cell-derived protein with CNC homology domains
EDTA	Ethylenediaminetetraacetic acid
EFC	Enzyme fragment complementation

EPR Electron paramagnetic resonance  
 ERKs Extracellular signal-regulated kinases  
 ESR Electron spin resonance  
 F2RL2 Coagulation factor II receptor-like 2  
 FAD Flavin adenine dinucleotide  
 FCR1 Flavin coumarin redox sensor 1  
 FRET Forster resonance energy transfer  
 GCL Glutamate cysteine ligase  
 GCMS gas chromatography-mass spectrometry  
 GFR Glomerular filtration rate  
 GLuc Gaussia luciferase  
 GS Glutathione synthetase  
 GSH Glutathione  
 GSK-3 $\beta$  Glycogen synthase kinase 3 $\beta$   
 H&E Haematoxylin and eosin  
 H2O2 Hydrogen peroxide  
 hCG Human chorionic gonadotrophin  
 Het Heterozygote  
 Hmox1 Haem oxygenase 1  
 HNE 4-hydroxynonenal  
 hPAP Human placental alkaline phosphatase  
 HSP Heat shock protein  
 HTP High through put  
 IP Intraperitoneal  
 IRPs Iron regulatory proteins  
 IVIS In vivo imaging system  
 IVR Intervening linker region  
 JNK Jun N-terminal kinase  
 KEAP1 Kelch-like ECH-associated protein 1  
 KO Knock out  
 LacZ  $\beta$ -galactosidase  
 LDH Lactate dehydrogenase  
 LOC344887 NmrA-like family domain containing 1 pseudogene  
 LPS Lipopolysaccharide  
 Maf Masculoaponeurotic fibrosarcoma  
 MAPK Mitogen activated protein kinase  
 MARE Maf recognition element  
 MCLA Methyl-cypridine-luciferin analogue  
 MDA Malondialdehyde  
 MEF Mouse embryonic fibroblast  
 MIE Molecular initiating event  
 miRNA microRNA  
 MMF Monomethyl fumarate  
 MS Multiple sclerosis  
 MTT 3-(4,5-dimethylthiazol-2-yl)-2,5-diphenyltetrazolium bromide  
 NAC N-acetylcysteine  
 NADH Nicotinamide adenine dinucleotide  
 NAPQI N-acetyl-parabenzquinoneimine  
 Neh Nrf2-ECH homologous  
 NF-E2 AP1-nuclear factor erythroid 2  
 NF- $\kappa$ B Nuclear factor-KappaB

NHPA 3-nitro-4-hydroxyphenylacetate  
 NO Nitric oxide  
 Nphs2 Podocin  
 NQO1 NAD(P)H dehydrogenase quinone 1  
 NRF2 Nuclear factor erythroid 2-related factor 2  
 Nrf2-Luc Nrf2-Luciferase  
 NSCLC Non-small cell lung cancer  
 O2- Superoxide radical  
 OD Optical density  
 OECD Organisation for Economic Co-operation and Development  
 ONOO- Peroxynitrite  
 p62/SQSTM1 Sequestosome 1  
 PBMCs Peripheral blood mononuclear cells  
 PBN N-tert-butyl-a-phenylnitron  
 PBS Phosphate buffered saline  
 PCL-1 Peroxy caged luciferin-1  
 Pdrx5 Peroxiredoxin 5  
 PHH Primary human hepatocytes  
 PI3K-Akt Phosphatidylinositol-3-kinase/Protein kinase B  
 PKC Protein kinase C  
 PROSPECTIVE Probuco Trial for Secondary Prevention of Atherosclerotic Events in Patients with Prior Coronary Heart Disease  
 Prx Peroxiredoxins  
 PTEN PI3K-regulator phosphatase and tensin homologue  
 qPCR Quantitative (real-time) polymerase chain reaction  
 QSAR Quantitative structure-activity relationship  
 REF-1 Redox factor 1  
 RFL-6 Rat foetal lung cells  
 ROI Region of interest  
 ROS Reactive oxygen species  
 SAPKs Stress-activated protein kinases  
 SDS-PAGE sodium dodecyl sulfate poly acrylamide gel electrophoresis  
 SFX-01 Sulforadex®  
 -SH Sulfhydryl group  
 SNP Single nucleotide polymorphism  
 SOD Superoxide dismutase  
 Srx Sulfiredoxin  
 SRXN1 Sulfiredoxin 1  
 TAC Total antioxidant capacity  
 TBARS Thiobarbituric acid reactive substances  
 tBHQ Tert-butylhydroquinone  
 TBS Tris-buffered saline  
 TBST TBS-Tween  
 TNF $\alpha$  Tumour necrosis factor alpha  
 TRIM16L Tripartite Motif Containing 16 Like  
 Ub Ubiquitination  
 WT Wild-type  
 $\beta$ -TrCp  $\beta$ -transducin repeat containing E3 ubiquitin protein ligase

## **Chapter 1**

### **General introduction**

## Contents

1.1.	<b>Introduction</b> .....	15
1.2.	<b>Oxidative stress</b> .....	16
1.2.1.	Oxidative stress and disease .....	17
1.2.2.	Drug-induced chemical and oxidative stress .....	18
1.2.3.	Cell defence mechanisms.....	20
1.2.4.	Therapeutic potential of antioxidants .....	21
1.3.	<b>Nrf2 and the antioxidant response</b> .....	22
1.3.1.	Regulation by Keap1 .....	26
1.3.2.	Phosphorylation of Nrf2.....	27
1.3.3.	Antioxidant response element-regulated genes .....	28
1.3.4.	Nrf2 activation in response to drug toxicity .....	34
1.4.	<b>Identifying oxidative and chemical stressors</b> .....	35
1.4.1.	Detection of oxidative stress .....	35
1.4.2.	Measurement of antioxidant levels.....	36
1.4.3.	Identifying potential chemical stressors.....	39
1.5.	<b>Monitoring activity of the Nrf2 pathway</b> .....	40
1.5.1.	In vitro models .....	40
1.5.2.	In vivo models .....	43
1.6.	<b>Therapeutic potential of Nrf2 modulators</b> .....	46
1.6.1.	Compounds in the clinic.....	46
1.6.2.	Identification of Novel Nrf2 modulators.....	50
1.7.	<b>Thesis aims</b> .....	51

## 1.1. Introduction

Adverse drug reactions (ADRs) are a substantial burden to clinical practice and drug development. Defined as an unintended, noxious response to a drug at a dose normally used in humans, ADRs may be due to single, prolonged or synergistic effects of a drug (Board, 1973) and can be fatal. For instance the most common cause of acute liver failure is drug-induced liver injury (DILI) (Lee, 2012). Mortality due to serious ADRs in the US is approximately 100,000 deaths/year (Lazarou et al., 1998) while it is the seventh most common cause of death in Sweden (Wester et al., 2008). In the UK, up to 6.5% of all hospital admissions and approximately 5,000 deaths per year are associated with ADRs (Pirmohamed et al., 2004).

Current preclinical testing identifies less than 25-55% of drugs associated with DILI (Olson et al., 2000; Xu et al., 2004). A recent systematic review identified hepatotoxicity as the most common reason for medicinal products being withdrawn from the market between 1953 to 2013 (Onakpoya et al., 2016). Indeed, toxicity is accountable for the attrition of 30% of all drug candidates during development (Kola and Landis, 2004). Cessation of candidate drugs late in development, due to lack of efficacy and unexpected adverse effects, incurs substantial costs. Many of these novel agents can provoke deleterious effects in cells via the induction of chemical stress (direct or indirect chemical interaction with one or more critical macromolecules) or oxidative stress (accumulation of reactive oxygen species (ROS) due to mitochondrial dysfunction, perturbation of cellular oxidase enzymes, or the redox cycling of the chemical entity). Both chemical and oxidative stress can inhibit the physiological function of specific target proteins, cause damage to DNA and/or provoke lipid peroxidation and disruption of cell membrane integrity, ultimately leading to cellular dysfunction or death (Finkel, 2011). Therefore, it is imperative that the ability of a chemical entity to provoke chemical and/or oxidative stress can be determined prior to human exposure, in order to minimise the risk of clinical toxicity and aid the design of safer alternatives.

In addition to drug-induced toxicity, oxidative stress has been linked to the pathophysiology of cardiovascular diseases such as atherosclerosis and hypertension (Griendling and FitzGerald, 2003); inflammatory diseases including arthritis and diabetes (García-González et al., 2015; Giacco and Brownlee, 2010); neurodegenerative diseases and depression (Black et al., 2015; Browne et al., 1999; Nakabeppu et al., 2007; Nunomura et al., 2001). Chronic accumulation of free radicals may be linked to the natural aging process (Harman, 1956) and ROS-mediated mutagenic damage to DNA and enhanced proliferation contribute to



carcinogenesis (Ishikawa et al., 2008; Kumar et al., 2008). As a result, there is much interest in the potential therapeutic value of antioxidants in these and other disease contexts.

Mammalian cells can withstand moderate increases in local concentrations of electrophiles and ROS due to the concerted actions of numerous antioxidant proteins. The expression of most genes encoding these proteins is regulated by the ubiquitously expressed transcription factor Nuclear factor erythroid 2-related factor 2 (Nrf2) (Bryan et al., 2013). Further insight into its therapeutic role may aid the development of treatments for diseases with an underlying oxidative stress component. In addition, there is evidence to suggest activation of the Nrf2 pathway precedes some forms of toxicity and therefore may serve as a marker for the screening of compounds with toxic liabilities. This thesis evaluates novel Nrf2 activity measures to assess the toxicological and pharmacological effects of drugs. Specifically, this work explores the use of Nrf2-Luc mice for the non-invasive measurement of Nrf2-pathway activity in response to toxicants; investigates regulation of the Nrf2-pathway in human liver cells; characterises the expression of Nrf2-regulated genes in whole-blood following toxicological and pharmacological stimulation of the transcription factor and assesses the value of luciferase reporter genes for evaluating potencies of novel therapeutic inducers of Nrf2.

## **1.2. Oxidative stress**

Exposure to high or sustained levels of reactive oxygen species (ROS) disrupt the normal intracellular redox state causing oxidative stress. Defined as an imbalance between antioxidant defence molecules and ROS (Sies, 2015), oxidative stress can damage DNA, lipids and protein by the formation of adducts. ROS include peroxides, singlet oxygen, superoxide and hydroxyl radicals ( $\cdot\text{OH}$ ). The unpaired valence electrons within these free radicals facilitate oxidation of surrounding lipids, proteins and DNA. Low levels of ROS are generated during normal metabolism mostly by oxidative phosphorylation. ROS are also generated by phagocytes during the 'Oxidative burst' (Babior et al., 1973) and act as both inter and intra cellular messengers. Mittal and Murad were the first to discover that  $\cdot\text{OH}$  activates the second messenger cyclic guanosine monophosphate (cGMP) (Mittal and Murad, 1977). Redox signalling has also been implicated in a number of physiological functions including regulation of vascular tone, cell adhesion, inflammatory response and apoptosis (Bulua et al., 2011; Chiarugi et al., 2003; Matoba et al., 2000). Maintenance of 'steady state'

concentrations of ROS is determined by the rate of generation and removal by antioxidants. When redox-buffering capacity is overwhelmed, oxidative stress occurs.

### **1.2.1. Oxidative stress and disease**

Oxidative damage has been implicated in the aetiology of many diseases due to deviation from redox homeostasis. For instance, oxidative stress is a facet of many cardiovascular diseases; excessive generation of ROS in vascular cells results in the oxidation of low-density lipoproteins that promote atherosclerosis (Chen et al., 2003; Kunsch and Medford, 1999). Release of large amounts of ROS including superoxide and hydroxyl radicals, following myocardial ischemia implicates oxidative stress in heart failure and reperfusion injury (Arroyo et al., 1987; Zweier et al., 1988). Many antioxidant therapies have proved cardioprotective in the clinic (Kurian et al., 2016).

Inflammation and oxidative stress are closely linked. Inflammatory cells generate and secrete ROS while oxidative stress can activate pro-inflammatory responses (Mittal et al., 2014; Morgan and Liu, 2011). During carcinogenesis, reactive species enhance cell proliferation, tumour invasiveness and mutagenic DNA damage (Franco et al., 2008; Barry Halliwell, 2007). Progression of gastric cancer is aided by the generation of reactive species from commensals within the gut (Handa et al., 2011). Additionally, patients with type 2 diabetes mellitus exhibit reduced antioxidant capacity (Bruce et al., 2003) and over-production of superoxide by the mitochondrial electron transport chain is the common cause of hyperglycaemic damage (Nishikawa et al., 2000). Perturbation of the mitochondrial respiratory chain is also apparent in patients with chronic kidney disease (Gamboa et al., 2016).

Multiple neurodegenerative diseases have an underlying oxidative stress component. For instance, patients with multiple sclerosis exhibit elevated DNA and lipid oxidation in the brain (Haider et al., 2011). One source of reactive species during Alzheimer's disease is the incorporation of amyloid beta peptides within neuronal membranes, resulting in free fatty acid release associated with Tau polymerisation (Butterfield et al., 2001; Lauderback et al., 2001). This is accompanied by an increase in oxidised macromolecules and a reduction in antioxidant activity. Additionally, diminished antioxidant capacity and increased protein oxidation are associated with aging (Harman, 1956).

### 1.2.2. Drug-induced chemical and oxidative stress

Formation of reactive intermediates capable of generating ROS underpins a plethora of drug toxicities. Perhaps the most well-known hepatotoxin, paracetamol is one such example. Also known as acetaminophen (APAP), paracetamol is metabolised by the liver to generate unreactive glucuronide and sulfate moieties alongside the reactive metabolite *N*-acetylparabenzquinoneimine (NAPQI) (Fig 1.1). This is conjugated to the reduced form of glutathione (GSH) to be excreted as mercapturic acid (Dahlin and Nelson, 1982). At therapeutic doses, depleted GSH is recoverable. However, the extent of GSH depletion associated with APAP overdose allows excess NAPQI to form DNA and protein adducts within the liver (Hinson et al., 2010). Increased mitochondrial membrane permeability causes cytochrome C release and loss of ATP synthesis (Kon et al., 2004). Ultimately, this results in centrilobular hepatic necrosis.

Aside from bioactivation of drugs to entities that induce oxidative stress, chemical stress is induced directly by drugs that undergo covalent binding and the formation of adducts. One such example is nephrotoxicity associated with the chemotherapeutic agent cisplatin (cis-diamminedichloroplatinum). High doses of the cisplatin are limited due to damage within the proximal tubules of the kidney (Aleksunes et al., 2010). Indeed, one third of patients suffer from nephrotoxicity when prescribed the drug (Shord et al., 2006). Direct chemical stress is caused by cisplatin-DNA crosslinks that result in cell cycle arrest. Cisplatin induces intra-strand crosslinks (between adjacent guanines or adenine and guanine), inter-strand DNA crosslinks and irreversible DNA-protein crosslinks (Eastman, 1983; Fichtinger-Schepman et al., 1985). As the kidneys are the major excretory route of cisplatin, apoptosis of renal tubular cells initiates reduced glomerular filtration rate (GFR), and acute renal failure (Gonzales-Vitale et al., 1977).

Further investigation into the underlying mechanisms of bioactivation and covalent binding are needed to identify chemical entities capable of inducing oxidative and/or chemical stress and improve the sensitivity of current pre-clinical drug safety assessment.

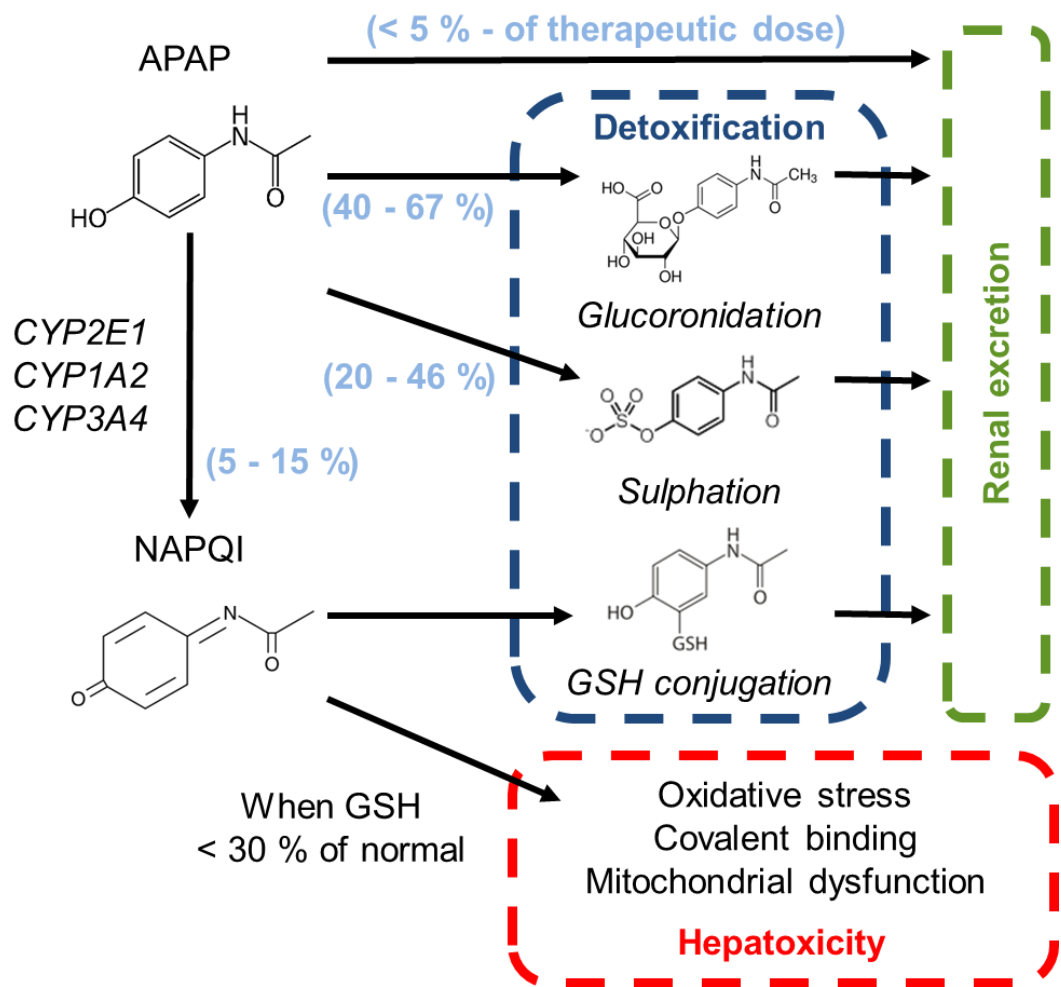


**Figure 1.1 Bioactivation of paracetamol**

Paracetamol (APAP) is metabolised by the liver to generate unreactive glucuronide and sulphate moieties before producing the reactive metabolite *N*-acetyl-parabenzoquinoneimine (NAPQI). This forms glutathione conjugates (GSH) and is excreted as mercapturic acid. However, the extent of GSH depletion associated with APAP overdose, allows excess NAPQI to form DNA and protein adducts within hepatic and renal tissues. Following a therapeutic dose of APAP, average percentage of APAP metabolised by the liver highlighted in light-blue. Adapted from (Jaeschke and Bajt, 2010).

### 1.2.3. Cell defence mechanisms

Following induction of oxidative stress, numerous stress response cascades are activated that coordinate the adaptive response to the insult or, when overwhelmed, lead to cell death. Enzymatic scavengers of ROS include glutathione reductase, superoxide dismutase and catalase. Non-enzymatic scavengers include flavonoids and vitamins A, C and E. Multiple signalling cascades are activated, including: mitogen activated protein kinase (MAPK) signalling, phosphatidylinositol-3-kinase/Protein kinase B (PI3K-Akt), Protein kinase C (PKC), Heat shock protein response, P53 and nuclear factor-KappaB (NF-κB). Localised accumulation of ROS may aid specificity of these signals. For example, Woo et al highlighted the specific accumulation of hydrogen peroxide (H<sub>2</sub>O<sub>2</sub>) around membranes following inactivation of the antioxidant peroxiredoxin, facilitating redox-dependent signalling but not toxic ROS damage (Woo et al., 2010). Modification of small molecules within these pathways affects a diverse range of cellular processes including proliferation, metabolism, differentiation and survival.

Upregulation of cytoprotective genes is also triggered in response to oxidative stress. Redox factor 1 (Ref-1) regulates activity of basic leucine zipper (bZIP) transcription factors such as Nrf2, DNA lesion and base excision repair, and ultimately activates multiple cell survival pathways (Thakur et al., 2014; Xanthoudakis et al., 1992). Cysteine residues within the N-terminus of Ref-1 are liable to redox modification that facilitates DNA binding (Luo et al., 2012). The transcription factor nuclear factor kappa b (NF-κB) mediates immune and inflammatory responses. Its activation by ROS is debated. Inhibitors of NF-κB such as N-acetyl-L-cysteine (NAC), were thought to inactivate NF-κB through their antioxidant activity but they in fact exert their effects by other mechanisms (Hayakawa et al., 2003). In the case of NAC, the compound reduced tumour necrosis factor alpha (TNFα)-mediated NF-κB-activation. However, exposure to H<sub>2</sub>O<sub>2</sub> inhibits phosphorylation of the NF-κB suppressor IκBα in some cell lines (Schoonbroodt et al., 2000). NF-κB is also activated following exposure to high levels of ROS via the protein kinase C pathway (Imran and Lim, 2013).

If survival mechanisms are overwhelmed, cell death programs such as apoptosis, necrosis, pyroptosis and autophagy are activated. ROS can directly modulate cell death effectors: caspases, B-cell lymphoma 2 (Bcl-2) and cytochrome C. Caspases are cysteine-dependent proteases that mediate apoptosis via DNA fragmentation, membrane permeabilisation and cleavage of a range of substrates. Low doses of H<sub>2</sub>O<sub>2</sub> induce caspases while high doses induce necrosis (Cai et al., 1999). Bcl-2 is an anti-apoptotic regulatory protein that is antagonised by

nitric oxide (NO) mediated oxidation (Cahuana et al., 2004). Excessive ROS trigger the peroxidase activity of cytochrome C leading to its release into the cytosol and subsequent permeabilization of the mitochondrial membrane (Kagan et al., 2005).

#### **1.2.4. Therapeutic potential of antioxidants**

Antioxidants are defined as 'any substance that delays, prevents or removes oxidative damage to a target molecule' (B. Halliwell, 2007). This defence network comprises of non-enzymatic compounds (including Vitamin A, C and E, uric acid) and enzymes (such as glutathione peroxidase, superoxide dismutase (SOD) and catalase). Catalase facilitates H<sub>2</sub>O<sub>2</sub> detoxification to water and oxygen. Superoxide dismutase, originally identified by McCord and Fridovich, catalyses the detoxification of superoxide radicals (O<sub>2</sub><sup>-</sup>) (McCord and Fridovich, 1969). The therapeutic value of antioxidants in the clinic is debated. Large epidemiological cohort studies show higher intake of antioxidants reduces risk of coronary heart disease (CHD) (Correa et al., 2000; Hirvonen et al., 2001), cancer (Greenlee et al., 2012) and neurodegenerative diseases (Ascherio et al., 2005; Engelhart et al., 2002). However, as an adjuvant therapy, clinical trials highlight mixed results. For instance, one meta-analysis of randomised trials of vitamin E (7 studies) and beta carotene (8 studies) over the course of 1.4 to 12 years showed the dietary supplementation was ineffective at reducing long-term cardiovascular mortality (Vivekananthan et al., 2003). A systematic review in 2008, found antioxidant therapy ineffective at reducing cognitive decline in aging populations (Jia et al., 2008). Under certain conditions, antioxidants may act as pro-oxidants and unrelated harmful effects of antioxidant therapy must not be overlooked (Bjelakovic et al., 2007). Additional reasons why antioxidants may have proven ineffective in human trials include the lack of stratification, as the extent of oxidative stress is likely to vary between patients. Oxidative damage may not be reduced by a single antioxidant and pathology may be localised to a specific area such as an arthritic joint that the therapy does not reach. It may be more suitable for antioxidant therapy to be applied as a prophylactic measure and not for treatment of established pathology.

Despite this, a plethora of anti-oxidant drugs have been approved for clinical use including N-acetylcysteine (NAC, Acetadote®) as an antidote for paracetamol overdose (Aitio, 2006). Edaravone (3-methyl-1-phenyl-pyrazolin-5-on) is routinely used clinically for the reduction of neuronal damage after stroke (Watanabe et al., 2008). It reacts strongly with free radicals to produce stable products. Alpha-Lipoic acid (Dexlipotam) has been approved for the

treatment of diabetic neuropathy (Ziegler et al., 2004). In its reduced form, the compound is a potent antioxidant and has been recently introduced as a part of a cocktail of antioxidants known as Zycose for the treatment of diabetes (Stirban, 2008). The antioxidant drug Probuco1 is currently undergoing the PROSPECTIVE (Probuco1 Trial for Secondary Prevention of Atherosclerotic Events in Patients with Prior Coronary Heart Disease) trial in patients with a history of CHD as an antioxidant therapy in combination with statins (Yamashita et al., 2016).

### 1.3. Nrf2 and the antioxidant response

Nrf2 is a bZIP transcription factor of the cap'n'collar subfamily first identified by Moi *et al.* (1994) for its ability to bind to the AP1-nuclear factor erythroid 2 (NF-E2) promoter sequence during a screen of a cDNA library from a hemin-induced erythroleukemia cell line (Moi et al., 1994). Encoded by *NFE2L2* gene, Nrf2 is expressed ubiquitously in humans and mice (Chan et al., 1996; McMahon et al., 2001; Moi et al., 1994). It is highly expressed in organs exposed to the external environment, such as the skin and lungs, and those implicated in detoxification, including the liver and kidneys. It is thought that the role of Nrf2 evolved from the need to survive in an oxygen-rich environment (Gacesa et al., 2016). Venugopal *et al.* showed similarity between Nrf1 and Nrf2 binding motifs similar to the antioxidant response element (ARE) in human NAD(P)H dehydrogenase quinone 1 (NQO1) and that this cis-element responded to transfection with Nrf1 and Nrf2 in HepG2 cells (Venugopal and Jaiswal, 1996). They proposed Nrf2 may be a key transcription factor in regulating the genetic response to xenobiotic metabolism (Itoh et al., 1997; Venugopal and Jaiswal, 1996). The Yamamoto group also observed inducible expression of enzymes like GSTs and NQO1 were lost in liver of Nrf2 knock out (KO) mice (Itoh et al., 1997). The transcription factor has since been established as the master regulator of the response to chemical and oxidative stress (Fig 1.2). Despite the viability of Nrf2 null mice indicating its redundancy during growth and development (Chan et al., 1996), Nrf2 is also implicated in proliferation, differentiation, cellular growth and apoptosis (Hinoi et al., 2006; Homma et al., 2009; Niture and Jaiswal, 2012; Zhao et al., 2009).

The 2.2 kb transcript of Nrf2 was predicted to translate to a protein approximately 66 kDa (Moi et al., 1994). However, sodium dodecyl sulfate poly acrylamide gel electrophoresis (SDS-PAGE) analysis of cellular Nrf2 produces bands at approximately 90 kDa (Lau et al., 2013). This is thought to be due to the abundance of acidic residues within Nrf2. Nrf2 consists of six highly conserved Neh (Nrf2-ECH homologous) (ECH = erythroid cell-derived protein with CNC

homology domains) (Fig 1.2) (Itoh et al., 1995). The Neh1 domain contains a CNC-bZIP sequence with the cysteine residue (506) that is essential for Nrf2 binding to the ARE and facilitates heterodimerization with small musculoaponeurotic fibrosarcoma (Maf) proteins to bind to DNA (Bloom and Jaiswal, 2003). The Neh2 domain contains two motifs (DLG and ETGE) to which the cytosolic inhibitor of Nrf2, Kelch-like ECH-associated protein 1 (Keap1) binds (Itoh et al., 1999; Katoh et al., 2005). Deletion of the Neh3 domain resulted in a 'transcriptionally silent' Nrf2 protein, despite maintaining the ability to translocate to the nucleus and bind to DNA (Nioi et al., 2005). This implicates the final residues of the C terminus are involved transactivation and recruitment of co-activator proteins. The Neh4 and Neh5 domains are also regarded as transactivation domains that interact with cAMP response element binding protein (CREB) independently (Katoh et al., 2001). The Neh6 domain ensures turnover of Nrf2 during stressed conditions and interacts with  $\beta$ -transducin repeat containing E3 ubiquitin protein ligase ( $\beta$ -TrCp) (Fig 1.2) (Chowdhry et al., 2013; McMahon et al., 2004).



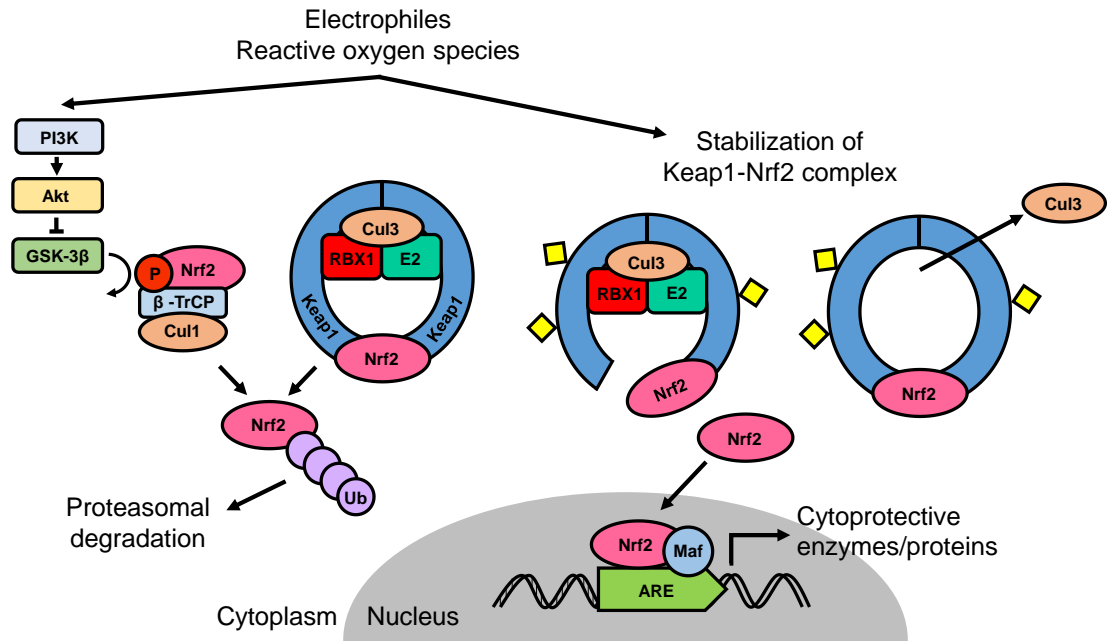


**Figure 1.2 Overview of the Nrf2-Keap1 pathway**

Under basal conditions, the cellular abundance and activity of Nrf2 is repressed through ubiquitination (Ub) via the Cullin-dependent E3 ubiquitin ligase Cul3 bound to Keap1 homodimers, or Cul1 bound to  $\beta$ -TrCP. The latter interaction is promoted via GSK-3 $\beta$  - mediated phosphorylation of Nrf2. Chemical and oxidative stressors activate Nrf2 signalling via stimulation of the PI3K pathway, or chemical/oxidative modifications of cysteine-containing pockets (diamonds) in Keap1. The latter process stabilises the Keap1-Nrf2 complex, by inactivating Keap1 or stimulating the dissociation of Cul3, allowing newly-synthesised Nrf2 to accumulate in the cell and translocate to the nucleus, where it forms heterodimers with Maf proteins and transactivates ARE-regulated genes to coordinate an adaptive response to chemical/oxidative stress.

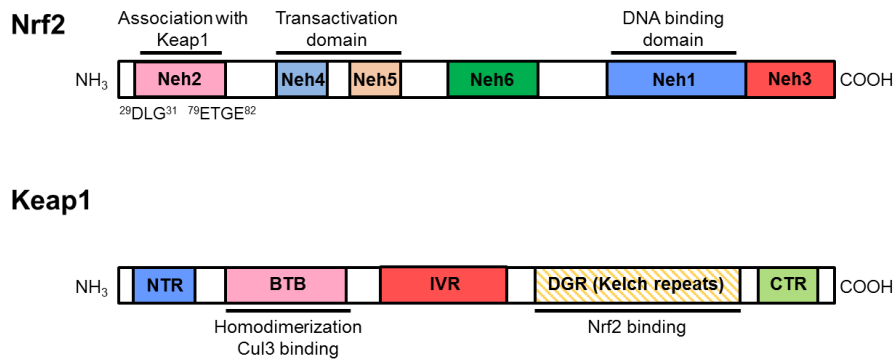


**Figure 1.3 Functional domains of Nrf2 and Keap1**

Nrf2 includes six highly conserved Neh (Nrf2-ECH homologous) domains. Neh2 is responsible for interactions with Kelch-like ECH-associated protein 1 (Keap1). Neh4 and Neh5 interact with co-activator proteins for transactivation, as does Neh3. Neh6 interacts with  $\beta$ -TrCp and is phosphorylated by GSK3 $\beta$ . Neh1 contains the DNA binding domain to which small Maf proteins bind. Keap1 consists of the bric-a-brac/tram-track/broad complex (BTB), intervening linker region (IVR) which interact with Cullin3 and other Keap1 molecules to form homodimers. The double glycine repeats (DGR) and C-terminal region (CTR), also known as the DC domain, bind with Nrf2.

### 1.3.1. Regulation by Keap1

Under basal conditions, Nrf2 is repressed via cytoplasmic tethering and ubiquitination mediated by the redox-sensitive Kelch-like ECH-associated protein 1 (Keap1) (Itoh et al., 1999). Keap1<sup>-/-</sup> mice do not survive to adulthood due to hyperkeratosis of the gastrointestinal tract and ulceration of the stomach (Wakabayashi et al., 2003). Mouse embryonic fibroblasts (MEFs) from the knock out mice exhibited constitutive Nrf2 activation. Yeast two hybrid analysis identified the strong interaction between Keap1 and the Neh 2 binding domain of Nrf2 (Itoh et al., 1999) (Fig 1.3). Co-immunoprecipitation of Keap1 with anti-actin antibody highlighted direct binding of Keap1 to the actin-cytoskeleton via the Kelch domain facilitating cytoplasmic tethering of Nrf2 under basal conditions (Kang et al., 2004). The cullin-dependent E3 ubiquitin ligase complex associates with a Keap1 homodimer to facilitate proteasomal degradation of Nrf2 (Cullinan et al., 2004; Zhang et al., 2004) (Fig 1.2). Inhibition of the proteasome results in accumulation of Nrf2 protein and induction of Nrf2-regulated genes (Nguyen et al., 2003; Sekhar et al., 2000; Stewart et al., 2003).

Keap1 is endowed with a relatively high number of cysteine residues (27) (Miseta and Csutora, 2000). These residues are incorporated into the functional domains of the protein and are sensitive to changes in cellular redox state. The 'cysteine code' hypothesis was first proposed by Kobayashi *et al.* (2009) following the discovery of distinct sets of cysteine residues are altered when exposed to a range of Nrf2 activating compounds (Kobayashi et al., 2009). This enables plasticity of the Nrf2 mediated response to a plethora of stimuli.

The hinge latch hypothesis is based on differential affinity of Keap1 homodimers to the ETGE and DLG motifs within Neh 2 domain of Nrf2 (Tong et al., 2006). Only when both sites are bound to the Keap1-Cullin ligase complex, can lysine residues within Nrf2 be ubiquitinated facilitating its proteasomal degradation. Under conditions of chemical and oxidative stress, modification of thiols within Keap1 inhibit its ability to bind to the DLG motif of Nrf2 and efficiently target it for ubiquitination, thus inhibiting its proteasomal degradation. Keap1 molecules become saturated and *de novo* synthesised Nrf2 translocates to the nucleus. However, the mechanism by which Nrf2 is able to move freely within the cell is debated. Partial and complete dissociation of Nrf2 from Keap1 was observed following exposure to electrophiles (Levonen et al., 2004; Niture et al., 2009). Exposure to electrophiles also resulted in the loss of Cullin3 from Keap1-Nrf2 complexes (Gao et al., 2013; Rachakonda et al., 2008). In some instances, exposure to Nrf2 activators including *tert*-butylhydroquinone (tBHQ), facilitate ubiquitination of Keap1 (Zhang et al., 2005). Others postulate transient

nuclear shuttling of Keap1 suppresses Nrf2 (Nguyen et al., 2005). However, this is contested; Watai *et al.* observed no change in the cytoplasmic localisation of Keap1 in MEFs following exposure to diethyl malate or the nuclear export inhibitor Leptomycin B (Watai et al., 2007). Additionally, proteins with motifs comparable to the ETGE sequence, compete with NRF2 for binding with KEAP1, thus indirectly activating the transcription factor. These include P62 and DPP3 (Dipeptidyl Peptidase 3) (Lau et al., 2010).

### 1.3.2. Phosphorylation of Nrf2

Nrf2 contains many serine, threonine and tyrosine residues. Phosphorylation of Nrf2 has been reported by a myriad of kinases including protein kinase C, tyrosine kinase Fyn, JNK, ERK, PERK and MAP kinases (Bryan et al., 2013). In particular, MAP kinase P38 phosphorylates Nrf2 improving its association with Keap1 (Keum et al., 2006). Recent evidence also implicates phosphorylation of Nrf2, mediated by glycogen synthase kinase 3 $\beta$  (GSK-3 $\beta$ ), as a Keap1-independent regulatory mechanism, (Fig 1.2). Salazar *et al.* highlighted phosphorylation of Nrf2 by GSK-3 $\beta$  resulted in nuclear exclusion of the transcription factor (Salazar et al., 2006). This acts independently of Keap1 regulation. Rada *et al.* demonstrated GSK-3 $\beta$  inhibitor SB216367 stabilized Nrf2 expression in Keap1<sup>-/-</sup> MEFs while an Nrf2 ETGE motif mutant, impervious to Keap1 degradation, accumulated following GSK-3 $\beta$  inhibition in HEK293T cells (Rada et al., 2011). Knock down of GSK-3 $\beta$  also resulted in accumulation of Nrf2 protein. Phosphorylated Nrf2 binds to the adaptor protein  $\beta$ -TrCp ( $\beta$ -transducin repeat-containing protein) that recruits Cullin-1 to form an E3 ligase. Both McMahon and Rada groups identified a redox independent degron within Neh 6 of Nrf2 (McMahon et al., 2004; Rada et al., 2011). The former by analysing deletion mutants in the fibroblast-like kidney cell line COS1 following exposure to sulforaphane. The latter via bioinformatic analysis of the  $\beta$ -TrCp consensus motif in both mouse and human Nrf2. GSK-3 $\beta$  mediated phosphorylation of the Ser<sup>344</sup> and Ser<sup>347</sup> residues within Neh 6 of human Nrf2 allows  $\beta$ -TrCP to bind and facilitate E3 ligase mediated degradation (Rada et al., 2012).

A second Neh6-based degron, identified by Chowdhry *et al.*, has the amino acid sequence DSAPGS and can bind to  $\beta$ -TrCp (Chowdhry et al., 2013). However, the phosphorylated binding site described by Rada et al. (amino acid sequence: DSGIS) has a stronger affinity to the adaptor protein (Rada et al., 2011). Nrf2 target gene expression and GSH levels increased in the hippocampus of neuron-specific GSK-3 $\beta$  knock out mice and those treated with GSK-3 $\beta$  inhibitor (Rada et al., 2012). GSK-3 $\beta$  is downstream of multiple kinase cascades: PI3K, AKT,

mTOR signalling (Maurer et al., 2014). The serine-threonine kinase has been implicated in glycogen metabolism, Wnt signalling, microtubule stability and apoptosis (Anderton et al., 2001; Ding et al., 2000; Hoeflich et al., 2000; Yoshino and Ishioka, 2015).

### **1.3.3. Antioxidant response element-regulated genes**

Increases in intracellular concentrations of electrophiles and ROS interfere with the ability of Keap1 to repress Nrf2, and PI3K signalling inhibits phosphorylation of Nrf2 (Salazar et al., 2006). This facilitates accumulation of the transcription factor in the nucleus and upregulation of cell defence genes that contain the cis-acting antioxidant response element (ARE) within their promoter regions (Fig 1.2). Nrf2 forms heterodimers with Jun and small Maf proteins for high affinity binding to DNA (Itoh et al., 1997). Originally identified by Rushmore *et al.* from rat GSTY<sub>a1</sub> and NQO<sub>1</sub>, the ARE consensus sequence has since been revised (Erickson et al., 2002; Nioi et al., 2003; Rushmore et al., 1991; Wyeth W. Wasserman and Fahl, 1997). Kuosmanen *et al.* define the core sequence into three motifs: n-‘TGA’-n-‘TCA’-n-‘GC’ after comparing variation in Nrf2 ChIP-seq datasets (Kuosmanen et al., 2016). The Nrf2 interactome is thought to include around 7469 transcription factor-DNA interactions (Papp et al., 2012) Single nucleotide polymorphisms (SNPs) within ARE sequences can alter Nrf2 binding. Also, SNPs within the Nrf2 promotor are associated with increased incidence of acute lung injury (Marzec et al., 2007). The first genome-wide study of Nrf2 binding via ChIP-seq identified 242 high confidence binding sites in the genome of human lymphoblastoid cells following sulforaphane exposure (Chorley et al., 2012). Common functions of Nrf2-regulated genes include xenobiotic metabolism, antioxidant defence systems, the immune response, regulation of the proteasome, haem, lipid and carbohydrate metabolism (Table 1.1).

The Nrf2 promotor contains two ARE sequences and the transcription factor has been shown, by chromatin immunoprecipitation, to bind directly to its own promoter region (Kwak et al., 2002). Autoregulation of Nrf2 by Nrf2-dependant Keap1 expression also occurs, via an ARE within the Keap1 promoter (Chorley et al., 2012). This negative feedback loop ensures sustained levels of Nrf2 induces Nrf2-dependent production of Keap1 causing suppression of Nrf2. Nrf2 also regulates expression of Cul3-Rbx1 (Kaspar and Jaiswal, 2010) and its heterodimeric partner MafG (Yamamoto et al., 2006). Some ARE-regulated genes, such as sequestosome 1 (p62/SQSTM1), act as both an Nrf2 target and inducer (Copples et al., 2010, 2010). p62 binds to Keap1 directly, competing with Nrf2 and forming a positive feedback loop.

Conserved Nrf2 target genes include NAD(P)H dehydrogenase (quinone) 1 (NQO1), sulfiredoxin 1 (SRXN1) and haem oxygenase 1 (HMOX1) (Table 1.1). Mutation analysis of the ARE sequence within the promoter region of NQO1 led to revision of the accepted ARE consensus sequence of the time (Nioi et al., 2003). Nrf2<sup>-/-</sup> mice had reduced basal expression and impaired induction of NQO1 (Nioi et al., 2003). NQO1 is a cytosolic phase 1 drug-metabolising enzyme (introduces functional groups to xenobiotics) that forms homodimers with the cofactor Flavin adenine dinucleotide (FAD). It catalyses the two or four- electron reduction of quinones to hydroquinones (Lars Ernster, 1958). Detoxification of quinones is essential to avoid 'redox cycling' and production of reactive semi-quinones. NQO1<sup>-/-</sup> mice were indistinguishable from wild-type mice aside from increased susceptibility to quinone toxicity when exposed to the drug menadione (Radjendirane et al., 1998). The enzyme is also negatively regulated by the transcription factor BACH1 (BTB and CNC homolog 1) (Dhakshinamoorthy et al., 2005). CHIP analysis of BACH1 overexpression in HepG2 cells revealed competitive binding to the ARE site with Nrf2 suggesting a balance between the two transcription factors is needed to regulate ARE-driven genes.

Srxn1 catalyses the ATP-dependent reduction of hyperoxidized peroxiredoxins (Prx) (Biteau et al., 2003). Also known as thioredoxin peroxidases, Prx contain cysteine residues that enable them to catalyse the reduction of ROS (Chae et al., 1994). Overexpression of Srxn1 prevents hyperoxidation of Prx following oxidative insult (Woo et al., 2005). *SRXN1* expression is abolished in Nrf2 knockout mice (Soriano et al., 2008). Hmox1, also known as Heat shock protein (HSP) 32, is regarded as a typical Nrf2-regulated gene. Haem oxygenases catalyse the rate limiting step during haem catabolism, cleaving haem to form biliverdin, carbon monoxide and iron (Eisenstein et al., 1991; Tenhunen et al., 1968). Three isoforms of haem oxygenase have been identified: the inducible isoform Hmox1 (32 kDa), the constitutively active isoform Hmox2 (36 kDa) and Hmox3 that lacks catalytic activity. Hmox1 null mice developed iron retention disorders and displayed significant serum iron deficiency (Poss and Tonegawa, 1997). However, Hmox1 may have additional functions. Nuclear translocation of Hmox1 was stimulated in rat foetal lung cells (RFL-6) following hypoxic stress (Suttner et al., 1999) and elevated Hmox1 in hypoxic conditions is associated with increased activation of antioxidant responsive promoter (Lin et al., 2007). Localisation of Hmox1 to the mitochondria may indicate a role in the turnover of mitochondrial haem proteins (Converso et al., 2006). *Hmox1* expression is regulated by a plethora of stress-response transcription factors: HSF, AP-1 and NF-κB (Alam and Cook, 2007a). Inactivation of Bach1 is also required to induce *Hmox1* (Reichard et al., 2007). This occurs independently

from nuclear accumulation of Nrf2 as removal of the repressor facilitates the low basal levels of nuclear Nrf2 to induce *Hmox1* transcription. Hmox1 is therefore seen as an early indicator and potential biomarker of general chemical stress.

**Table 1.1 Human genes positively regulated by Nrf2**

Evidence for direct binding of Nrf2 to ARE in genes highlighted green. Adapted from (Chorley et al., 2012; Hayes and Dinkova-Kostova, 2014).

Function	Gene symbol	Gene	Validated ARE	References
Phase 1 - drug oxidation, reduction and hydrolysis	AKR1B1	Aldo-keto reductase family 1, member B1 (and 1BB and 1B10)		(Agyeman et al., 2012; Jung et al., 2013; MacLeod et al., 2009)
	AKR1C1	Aldo-keto reductase family 1, member C1 (and 1C2 and 1C3)	TCAGGGTGACTCAGC AGCTTG	(Agyeman et al., 2012; Lou et al., 2006)
	AKR1C2	Aldo-keto reductase family 1 member C2	TCAGGGTGACTCAGC AGCTTG	(Lou et al., 2006; MacLeod et al., 2009)
	ALDH3A1	Aldehyde dehydrogenase 3 family, member A1 (and 3A2)		(Agyeman et al., 2012; Paek et al., 2012)
	CBR1	Carbonyl reductase 1 (and 3)		(Agyeman et al., 2012)
	EPHX1	Epoxide hydrolase 1 microsomal		(Jung et al., 2013)
	PTGR1	Prostaglandin reductase 1 (also called LTB4DH)		(MacLeod et al., 2009)
	NQO1	NAD(P)H dehydrogenase [quinone] 1	TCACAGTGACTCAGC AGAATC	(Dhakshinamoorthy et al., 2005; Li and Jaiswal, 1992)
	NQO2	NQO2 (NAD(P)H Quinone Dehydrogenase 2)	AGGTGGTGATGTTG CATCACA	(Wang and Jaiswal, 2006)
	Phase 2 - drug conjugation	CES1A1	Carboxylesterase 1	AGATCGTGAGACAG CATTAAAT
MGST1		Microsomal glutathione S-transferase 1 (and 2)		(Agyeman et al., 2012; Jung et al., 2013)
SULT1A1		Sulfotransferase family cytosolic 1A member 1		(Agyeman et al., 2012)
UGT1A1		UDP Glucuronosyltransferase1 family polypeptide 1A	AAACCCGGACTTGGC GCTTGG	(Yueh and Tukey, 2007)
UGT1A6		UDP Glucuronosyltransferase Family 1 Member A6	GAAAGCTGACACGG CCATAGT	(Münzel et al., 2003)
UGT1A6		UDP Glucuronosyltransferase Family 1 Member A6	TCTGTCTGACTTGGC AAAAAT	(Münzel et al., 2003)
UGT2B7		UDP Glucuronosyltransferase 2 family polypeptide B7	AACTACTGACTCGGC TGGTCT	(Nakamura et al., 2008)
Phase 3 - drug transport	ABCB6	ATP-binding cassette subfamily B (MDR/TAP) member 6		(Chorley et al., 2012)
	ABCC1	ATP Binding Cassette Subfamily C Member 1	TCTGTGTGACTCAGC TTTGGA	(Kurz et al., 2001)
	ABCC2	ATP-binding cassette subfamily C (CFTR/MRP) member 2		(Agyeman et al., 2012)
	ABCC3	ATP-binding cassette subfamily C (CFTR/MRP) member 3		(Jung et al., 2013)
	ABCB11	ATP-binding cassette, sub-family B member 11	CCAAGGTGAATCAG CAATTTTC	(Weerachayaphorn et al., 2009)
Antioxidant enzymes	SAT	Sulfate adenylyltransferase	CCGCTATGACTAAGC GCTAGT	(Wang et al., 1998)
	SOD1	Superoxide dismutase	AACTAATGACATTTTC TAGACA	(Dreger et al., 2009; Park and Rho, 2002)



Antioxidant (GSH-based)	GCLC	Glutamate-cysteine ligase catalytic subunit	TCCCCGTGACTCAGC GCTTTG	(Mulcahy et al., 1997)
	GCLM	Glutamate-cysteine ligase modifier subunit	TAACGGTTACGAAGC ACTTTC and AGACAATGACTAAGC AGAAAT	(Erickson et al., 2002)
	GGT1	Gamma-glutamyltransferase 1		(Agyeman et al., 2012)
	GLRX	Glutaredoxin 1		(Agyeman et al., 2012)
	GLS	Glutaminase		(Agyeman et al., 2012)
	GPX2	Glutathione peroxidase 2	CCAGGATGACTTAGC AAAAAC	(Banning et al., 2005; Paek et al., 2012)
	GSR1	Glutathione reductase		(MacLeod et al., 2009)
	GSTP1	Glutathione S-Transferase Pi 1	GCGCCGTGACTCAGC ACTGGG	(Montano et al., 2004)
	SLC7A11	Cysteine/glutamate transporter		(MacLeod et al., 2009)
Antioxidant (TXN-based)	PRDX1	Peroxiredoxin 1	TGTAAGTGAATCAGC ATCAGC	(Chorley et al., 2012; Kim et al., 2007)
	PRDX6	Peroxiredoxin 6	GCAACGTGACCGAG CCCCGCA	(Chowdhury et al., 2009)
	SRXN1	Sulfiredoxin 1	CCAGGGTGAGTCGG CAAAGCC	(Soriano et al., 2008)
	TXN	Thioredoxin	TCACCGTTACTCAGC ACTTTG	(Kim et al., 2003)
	TXNRD1	Thioredoxin reductase 1	TCATTCTGACTCTGG CAGTTA and TCAGAATGACAAAGC AGAAAT	(Hintze et al., 2003)
	Carbohydrate metabolism and NADPH regeneration	G6PD	Glucose-6-phosphate 1-dehydrogenase	
HDK1		Hexokinase domain containing 1		(Agyeman et al., 2012)
ME1		Malic enzyme 1, NADP dependent cytosolic	CTGCCATGACTCAGC GCTTCT	(Chorley et al., 2012)
PGD		6-phosphogluconate dehydrogenase		(Paek et al., 2012)
TALDO1		Transaldolase		(Agyeman et al., 2012; Chorley et al., 2012)
TKT		Transketolase isoform 1		(Agyeman et al., 2012)
UGDH		UDP-glucose dehydrogenase		(Agyeman et al., 2012)
Haem and iron metabolism	BLVRA	Biliverdin reductase A		(Agyeman et al., 2012)
	BLVRB	Biliverdin reductase B (flavin reductase (NADPH))		(Agyeman et al., 2012)
	FECH	Ferrochelatase		(MacLeod et al., 2009)

	FTH1	Ferritin heavy polypeptide 1	CCTCCATGACAAAGC ACTTTT and CCACCGTGACTCAGC ACTCCG	(Tsuji, 2005)
	FTHL12	Ferritin heavy polypeptide-like 12		(MacLeod et al., 2009)
	FTHL17	Ferritin heavy polypeptide-like 17		(Agyeman et al., 2012)
	FTL1	Ferritin light polypeptide	TCAGCATGACTCAGC AGTCGC GGACCGTGACTCAG CAGGAAA and GGACCGTGACTCAG CGAAAAC and AGACCGTGACTCAGC GAAAAC	(Hintze and Theil, 2005)
	HMOX1	Haem oxygenase (decycling) 1		(Keum et al., 2006; MacLeod et al., 2009)
Lipid metabolism	APOA1	Apolipoprotein A1	CAGCTCTGTCCTGG GGCTGG	(Mooradian et al., 2004)
	TBXAS1	Thromboxane A synthase 1 (Converts prostaglandins to thromboxane)	AAGGAATGAATCAG CAACTTT	(Yaekashiwa and Wang, 2003)
Transcription factors and associated proteins /signal transduction	ATF3	Activating Transcription Factor 3	TTAAGGTGACACAGC ATCTAA	(Kim et al., 2010)
	GNAI2	Guanine Nucleotide Binding Protein (G Protein), Alpha Inhibiting Activity Polypeptide 2	AGCCTGTGACTGGG CCGGGGC	(Arinze and Kawai, 2005)
	MAFG	MafG protein	TCACGCTGACTCAGC ACATTG	(Chorley et al., 2012; MacLeod et al., 2009)
	PPARG	Peroxisome proliferator-activated receptor gamma (PPAR $\gamma$ )		(Chorley et al., 2012)
	PPARGC1B	Peroxisome proliferator-activated receptor gamma coactivator 1-beta		(Chorley et al., 2012)
	RXRA	Retinoid X receptor alpha		(Chorley et al., 2012)
	S100A6	S100 calcium binding protein A6 (cell cycle progression and differentiation)	GACACGTGACTCGG CAAGGGG	(Leśniak et al., 2005)
Ubiquitin - proteasome	KEAP1	Kelch-like ECH-associated protein 1		(Chorley et al., 2012)
	PSMA3	Proteasome (Prosome, Macropain) Subunit, Alpha Type, 3	AGCCAATGAGCGGG CCTGTTA	(Takabe et al., 2006)
Cytoskeleton	Keratin 16	KRT16	GAACCTGGAGTCAG CAGTTAG	(Endo et al., 2008)
Immune response	ETS1	Protein C-ets-1 – expression of cytokine and chemokine genes	AGCGGGTGACCAAG CCCTCAA	(Wilson et al., 2005, p. 200)
	PTGS2	Prostaglandin-Endoperoxide Synthase 2 (inflammatory prostaglandin production)	TTTTAGTGACGACGC TTAATA	(Sherratt et al., 2003)

#### 1.3.4. Nrf2 activation in response to drug toxicity

While Nrf2<sup>-/-</sup> mice survive to adulthood, they exhibit lowered basal and inducible levels of ARE-regulated genes in multiple tissues (Enomoto et al., 2001). They are highly susceptible to pathologies associated with exposure to chemical toxicants, such as acetaminophen hepatotoxicity (Chan et al., 2001; Enomoto et al., 2001), cisplatin nephrotoxicity (Aleksunes et al., 2010) and bleomycin lung fibrosis (Cho et al., 2004). Conversely, tissue-specific ablation of the *KEAP1* gene confers resistance to acute drug toxicity *in vivo* (Okawa et al., 2006). Based on these observations, and evidence that Nrf2 pathway activity is perturbed in diseases with an oxidative stress component, there is an increasing interest in the therapeutic value of targeting Nrf2 with small molecules (Mutter et al., 2015).

A number of toxic chemicals and drugs have also been shown to induce Nrf2-mediated adaptive responses in cell and animal models. For example, the bioactivation of acetaminophen to the reactive metabolite NAPQI has been associated with the rapid accumulation of Nrf2 and induction of target genes in mouse liver (Goldring et al., 2004). Importantly, dose-dependent activation of the Nrf2 pathway was evident in animals receiving non-toxic and toxic doses of acetaminophen (Goldring et al., 2004), highlighting the ability of Nrf2 to report early chemical stress associated with drug-induced liver injury. Consistent with these findings, direct application of NAPQI to mouse hepatoma cells has been shown to cause chemical adduction of selected cysteine residues in Keap1 and the activation of Nrf2 signalling (Copple et al., 2008a). Accumulation of Nrf2 and/or induction of its target genes have been observed in response to other model hepatotoxins, including diclofenac (Fredriksson et al., 2014) and carbon tetrachloride (Randle et al., 2008). It has also been observed in response to nephrotoxins such as cisplatin (Aleksunes et al., 2010) and cyclosporin A (Wilmes et al., 2011), and the neurotoxins 1-methyl-4-phenyl-1,2,3,6-tetrahydropyridine (Chen et al., 2009) and 6-hydroxydopamine (Tobón-Velasco et al., 2013).

In addition, many electrophilic skin sensitisers appear to be capable of stimulating Nrf2 signalling; this is the rationale for use of the *in vitro* Keratinosens™ assay, in which a human HaCaT keratinocyte cell line equipped with an ARE-regulated luciferase reporter transgene is used to classify the skin sensitisation hazard associated with new chemical entities (Emter et al., 2010). The above evidence demonstrates that Nrf2 can respond to diverse chemical toxins in multiple cell types, both *in vitro* and *in vivo*.

#### 1.4. Identifying oxidative and chemical stressors

Identification of compounds liable to bioactivation and subsequent induction of oxidative stress is vital for the prevention of drug-induced toxicity. However, monitoring oxidative stress is hampered by the ephemeral nature of free radicals. A multitude of fluorescent and chemiluminescent probes have been developed for the indirect quantification of ROS generation. Oxidative damage to proteins lipids and DNA can be readily assayed. However, in order to avoid drug-induced oxidative damage, computational platforms to predict a chemical's propensity for bioactivation have been established. While these *in silico* methods can identify chemical liability, they are not capable of predicting the biological consequences of metabolic bioactivation *in vivo*. Therefore, better detection and prediction systems are needed to avoid drug-induced oxidative stress.

##### 1.4.1. Detection of oxidative stress

Direct measurement of ROS is difficult due to their transient nature and low abundance. For instance, nitric oxide ( $\cdot\text{NO}$ ) has a half-life of only 4 seconds (Hakim et al., 1996). Electron spin resonance (ESR) and paramagnetic resonance (EPR) identifies the unpaired spins of free radicals but with limited sensitivity. In order to increase signal strength, spin traps are employed to measure free radicals indirectly. Spin trapping involves the addition of nitroxyl probes that react with free radicals to generate more stable radical adducts. However the half-life of the detectable products remains short, for instance, the hydroxyl adduct of PBN (N-tert-butyl- $\alpha$ -phenylnitron) has a half-life of 38 s (Janzen et al., 1992). Lack of signal penetration and potential toxicity of the probes limits their application in human imaging.

Fluorescent and chemiluminescent probes offer a more sensitive and versatile method of ROS detection. One of the most commonly used probes, dichlorodihydrofluorescein (DCFH-DA) is oxidised to the fluorescent compound 2',7'-dichlorofluorescein (DCF). DCFH-DA reacts readily with carbon trioxide ( $\text{CO}_3^{\cdot-}$ ) and nitrogen dioxide ( $\text{NO}_2^{\cdot}$ ) but has low reactivity to the more abundant  $\text{H}_2\text{O}_2$  and  $\text{O}_2^{\cdot-}$  radicals (Wrona et al., 2005). However, DCFH-DA can react with oxygen to generate free radicals itself (Yazdani, 2015) and generates artifactual fluorescence when oxidised by cytochrome C and haem peroxidases (Burkitt and Wardman, 2001). Chemiluminescent reactions emit light without excessive heat production. The most widely used probe Lucigenin (bis-N-methylacrydinium nitrate) is oxidised by superoxide to the intermediate dioxetane, which cleaves spontaneously to the excited product N-

methylacridone that emits a photon of light (Peters et al., 1990). Other luciferin-based probes such as Luminol and methyl-cypridine-luciferin analogue (MCLA), also lack specificity.

Genetically encoded fluorescent and chemiluminescent protein reporters facilitate measurement of ROS activity *in vivo* and *ex vivo*. HyPer was the first genetically encoded fluorescent sensor specific for H<sub>2</sub>O<sub>2</sub> activity (Belousov et al., 2006). It consists of cpYFP (circulatory permuted yellow fluorescent protein) inserted into the regulatory region of OxyR, a prokaryotic H<sub>2</sub>O<sub>2</sub>-sensing protein. Subsequent HyPer mutants offer increased dynamic range and faster redox kinetics (Bilan et al., 2013; Markvicheva et al., 2011). However, in order to achieve reversible fluorescence quenching many fluorescent probes are pH sensitive, which could lead to erroneous signal (Schwarzländer et al., 2014; X. Wang et al., 2013). Many genetically encoded sensors employ the luciferase-dependent catalytic conversion of luciferin to oxyluciferin and bioluminescence for the detection of ROS. Luciferase genes have been derived from a plethora of species including firefly, clickbeetle, sea pansy (*Renilla reniformis*), and Copepod (Huh et al., 2009; Shimomura, 1985; Steghens et al., 1998). Gaussia luciferase (GLuc) is the smallest known secretory luciferase (Szent-Gyorgyi et al., 1999). Subsequent variants such as fLuc8 exhibit increased stability to changes in pH and temperature and extend the half-life of the probe. Peroxy caged luciferin-1 (PCL-1), a chemoselective bioluminescent probe, facilitates real-time detection of H<sub>2</sub>O<sub>2</sub> in mice (Bittner et al., 2010). Expressed in all tissues, the reporter is sensitive to both inducible and basal levels of H<sub>2</sub>O<sub>2</sub> *in vivo*. While numerous probes exist for the enhancement of ROS detection, they are limited by their stability, signal strength, and specificity. Probes may perturb the system being studied producing artefactual signal. The probe signal may be stimulated or quenched by off target reactions, such as changes to pH, while specific measurement of individual ROS is hampered by a probes sensitivity to other ROS and antioxidants such as the case with DCFH-DA. The recently established chemiluminescent probes offer an alternative to fluorescent indicators but further optimization is needed to improve signal strength and stability.

#### **1.4.2. Measurement of antioxidant levels**

Measurement of individual antioxidant activity such as GSH can give insight into the extent of cellular oxidative stress. GSH is a tripeptide thiol present in all tissues that neutralizes free radicals in combination with many detoxifying enzymes such as glutathione peroxidases and glutathione-S-transferases (Fig 1.5). Quantification of the ratio between reduced GSH and its

oxidised state (GSSG) or total GSH levels is possible via a rapid colorimetric assay (Rahman et al., 2007). Measurement of individual antioxidants are also influenced by bioavailability, metabolism, location, distribution, fate of anti-oxidant derived radicals and interaction with other antioxidants/ combinations of radicals.

Wayner *et al* developed the first assay to quantify 'total antioxidant capacity' (TAC) by measuring oxygen consumption after adding peroxy radicals to a biological fluid (Wayner et al., 1985). Low total antioxidant capacity of serum may indicate oxidative stress or increased susceptibility to oxidative damage. Contrary to their name, TAC assays do not measure the entire antioxidant capacity, instead the low molecular weight antioxidants such as urate, ascorbate and thiols, thus correlate poorly with other assays that include quantification of enzymes such as catalase and superoxide dismutase (Costantini and Verhulst, 2009). Individual expression patterns of antioxidant molecules give more insight than TAC assessment (Pompella et al., 2014).

Currently no single biomarker has the specificity, sensitivity and potency to monitor the response to oxidative stress. While markers of oxidative damage are more stable than reactive species themselves, these cannot provide predictive insight. In addition, the variable extent and onset of oxidative damage leads to poor correlation between markers of damage and levels in healthy tissue. Artificial oxidation from sample handling and oxidised protein/lipids from dietary sources may also lead to false positives.

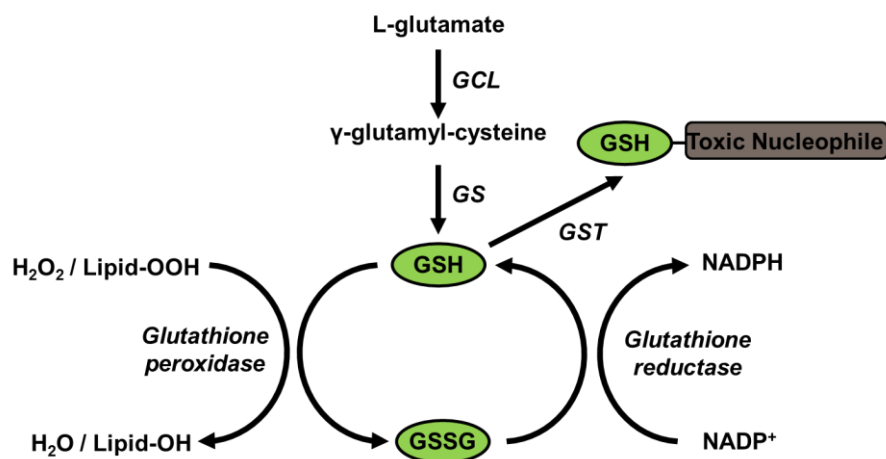


**Figure 1.5 The Glutathione system**

The reduced form of glutathione (GSH) is generated by glutamate cysteine ligase (GCL) which converts L-glutamate to  $\gamma$ -glutamyl-cysteine in an ATP-dependent reaction. Glutathione synthetase (GS) converts this product with glycine to GSH (comprised of the amino acids cysteine, glutamate and glycine). Glutathione-S-transferases (GST) catalyse the formation of GSH conjugates that facilitate detoxification of xenobiotics. GSH is oxidised (GSSG) by lipid peroxides and ROS such as hydrogen peroxide ( $H_2O_2$ ). Glutathione reductase catalyses the NADPH-dependent reduction of GSSG. Adapted from (Lehane et al., 2012).

### 1.4.3. Identifying potential chemical stressors

Identification of chemicals liable to metabolise into covalently reactive species early in the drug development process reduces costs and avoids post-market withdrawal. Idiosyncratic adverse drug reactions, though low in incidence, can be fatal (Uetrecht and Naisbitt, 2013). Currently, no consensus exists for the reactive metabolite risk assessment strategies because of the challenges faced when quantifying reactive metabolites and the complex mechanisms of toxicity (Thompson et al., 2016). A number of *in silico* techniques have been developed to predict the reactive nature of drug-candidates. Identifying structural motifs with propensity to form reactive metabolites is a useful tool to guide drug design. For instance, quantitative structure-activity relationship (QSAR) modelling predicted candidate drugs with the propensity to form reactive metabolites based on structures previously associated with that risk (Liew et al., 2012). Hsiao *et al.*, used density functional theory calculations to predict sites of metabolism in lead compounds by cytochrome P450 enzymes (Hsiao et al., 2012). While predictive tools can provide insight into potential formation of reactive species, this does not imply actual formation nor does it inform on biological consequences of bioactivation. Relying solely on this approach may rule out or overlook potentially effective compounds.

The majority of *in vitro* assays for the detection of reactive metabolites assess covalent binding of a drug-candidate via 'trapping' agents or radiolabelling of the compound. Nucleophilic trapping agents such as GSH are employed to analyse a compound's liability for bioactivation. Srivastava *et al.*, highlighted the propensity of lead compounds to form reactive intermediates using trapping agents GSH and NAC when incubated with human and rat liver microsomes (Srivastava et al., 2014). Structural modification in succeeding analogues negated this risk. However, within the body, the metabolite is expected to be trapped by protective molecules such as GSH and therefore this approach may not accurately identify compounds liable to bind covalently with proteins *in vivo*.

Integrated risk assessments incorporate other chemical insults occurring during drug toxicity in order to reflect more accurately events *in vivo*. For instance, DILI mechanisms of initial injury include immune responses, direct cell and mitochondrial stress (Rusmann et al., 2009). It is therefore important to incorporate assessment of actual metabolic activation of the compound and not exclusively its chemical propensity to form reactive metabolites. The generation of increasingly sophisticated co-cultures aids physiologically relevant risk assessment. Recently, microphysiological systems have been designed to include immune



component 3D cultures (Choucha Snouber et al., 2013; Tsamandouras et al., 2017). This information aids the expansion of adverse outcome pathways (AOPs). Developed by the Organisation for Economic Co-operation and Development (OECD), AOPs aim to delineate the underlying mechanisms of toxicity from molecular initiating events (MIEs) and toxicological endpoints (Ankley et al., 2010; Vinken, 2013). Combining this data along with structural information about a drug-candidate may increase the specificity and sensitivity of current methods to detect chemical stressors.

### **1.5. Monitoring activity of the Nrf2 pathway**

While established toxicological endpoints, such as decreases in cellular adenosine triphosphate levels and leakage of lactate dehydrogenase into cell culture media, unquestionably demonstrate the ability of a compound to provoke cell death, their sensitivity is generally not sufficient to identify sub-lethal chemical insults that initiate adaptive stress responses but do not culminate in overt cytotoxicity. These stress responses encompass the Nrf2-driven antioxidant response, but also the DNA damage response (effected by the tumour suppressor p53), the unfolded protein response (effected by activating transcription factor 4/X-box binding protein 1, in response to endoplasmic reticulum stress), and the heat shock response (effected by heat shock factors), amongst others (Jennings et al., 2013). Such responses encapsulate some of the earliest biochemical signals that precede the initiation of toxic cascades, and can thus provide sensitive and mechanistic insights into the deleterious effects of a chemical entity (Wink et al., 2014). In this regard, stress responses represent important components of AOPs. There is much interest in the value of monitoring stress responses and other components of AOPs to minimise reliance on animal models and improve the mechanism-based identification of hazardous chemical entities (Vinken, 2013).

#### **1.5.1. *In vitro* models**

To overcome some of the technical barriers of measuring Nrf2 directly (including a historic lack of sensitive antibodies for the detection of the low-abundance Nrf2 protein and relative stability of Nrf2 mRNA during activation of the pathway), researchers have developed novel strategies for monitoring Nrf2 pathway activity. These include the use of stable ARE-driven reporters, fluorescent-tagged Nrf2 or target genes and, transcriptomic analysis of dynamic

changes in gene signatures that have been shown (for example, in CHIP data) to be representative of the battery of Nrf2-regulated genes.

One example of a stable reporter is 8AREL, established in H4IIE and HEK293 cell lines (Kratschmar et al., 2012). 8AREL contains an eight times repeated ARE sequence from the promoters of rat GSTA2 and mouse GSTa1 controlling a luciferase reporter gene (Wang et al., 2006). This cell line was used to assess the *in vitro* therapeutic index of Nrf2 activators (CDDO-Me, sulforaphane and DMF) (Copple et al., 2014). In addition, the keratinosens<sup>TM</sup> assay utilizes a luciferase reporter gene directed by Aldo-Keto reductase family 1, member C2 (AKR1C2) ARE sequence in HaCaT cells to identify the skin sensitization hazard of novel chemicals (Emter et al., 2010). It has been adopted as an OECD test guideline.

Many other ARE reporters have been constructed. The AREc32 cell line also contains eight copies of the ARE sequence in human mammary cell line MCF7 (Wang et al., 2006). The Nrf2 CALUX assay utilizes an ARE-luciferase construct consisting of a 4 x ARE sequence: consensus ARE, NQO1 ARE, hGCLM ARE and hGCLC ARE transfected into the human bone-derived cell line U2OS (van der Linden et al., 2014). The reporter responded to compounds whose toxicity was due to oxidative stress but failed to respond to drugs that needed bioactivation. This is one limitation of test systems utilising a homogenous cell culture. Motahari *et al.* were the first to generate an ARE-luciferase base reporter driven by a construct containing one copy of an extended consensus response element (from the NQO1 promotor) (Motahari et al., 2015). Transfected human hepatoma cells (Huh7) respond as early as 4 h following exposure to hydroquinone and p-benzoquinone and the antioxidant curcumin. While incorporating a single ARE element into a reporter provides specificity, multiple ARE elements may increase the sensitivity of the reporter and better reflect activity of the Nrf2 pathway.

As part of the Tox21 initiative to identify better *in vitro* models of toxicity assessment, Kim *et al.* employed an ARE-*bla* ( $\beta$ -lactamase) reporter to assess Nrf2 pathway activation following exposure to a library of 10,000 compounds (Kim et al., 2016). This reporter was part of a panel designed to assess activation of stress responses prior to cell death that were consistent with the structure or class of compound. Broad relationships identified in this study would inform the development of AOPs. Identifying compounds that provoke toxicity in the early stages of an AOP instead of reaching the toxicological endpoint will aid the development of assays that avoid toxicity in animals. Aside from ARE-based reporters, Smirnova *et al.* highlight the ability of a Neh2-luc reporter to be recognised, ubiquitinated and degraded by the proteasome (Smirnova et al., 2011). The reporter successfully identified

Nrf2 activators from a library of 2000 compounds, including a novel activator Genunin. ARE-based reporter signal follows the stabilization of Nrf2-target gene expression whereas the Neh based system allows immediate monitoring of drug induced Nrf2 accumulation.

Automated, high-content imaging of cell lines expressing fluorescent-tagged Nrf2 or target gene products provide insight into subcellular localization of constituents of the Nrf2 pathway in real time. For instance, an SRXN1-GFP reporter has been incorporated in the novel (geno)toxicity assay: ToxTracker (Hendriks et al., 2012). ToxTracker incorporates mouse embryonic stem cell lines with either Bcl2-GFP (ATR-Chk1 signalling pathway), Btg2-GFP (P53 pathway) or SRXN1-GFP reporters and provides mechanistic insight into oxidative/genotoxic manifestations of toxicity. In order to distinguish DILI compounds that initiate either Nrf2 or NF- $\kappa$ B defence pathways, Herpers *et al.* established a novel GFP-reporter, GFP-SRXN1, expressed in the immortalised human hepatoma cell line HepG2 (Herpers et al., 2016). Through high quality live cell imaging, they also observed altered nuclear translocation of NF- $\kappa$ B subunit via the reporter GFP-P65.

Holistic profiling of transcriptional changes following oxidative insult has shown substantial involvement of the battery of Nrf2-regulated genes. For instance, following exposure to cyclosporine A (CsA) in the human proximal tubule cell line RPTEC/TERT1, the resulting transcriptomic, metabolomic and proteomic response was integrated to elucidate cell stress-induced signalling cascades (Wilmes et al., 2013). This was the first study to highlight 'CsA-induced stress not linked to primary pharmacology'. Gene expression alone does not give insight into alternative splicing, post-translational modifications or protein expression. By employing all three 'omics' approaches, Wilmes *et al.* identified Nrf2 pathway activation alongside mitochondrial dysfunction and the unfolded protein response in CsA-exposed cells. NQO1 and Hmox1 were induced at early time points. Transcriptomic analysis of long-term repeat dose toxicity studies in the RPTEC/TERT1 cell line revealed global and compound specific responses to particular nephrotoxins (Aschauer et al., 2014). The majority of the compounds induced a strong Nrf2 response (most prominent: CsA chloroacetaldehyde and cadmium chloride).

Whilst the cytoprotective genes regulated by Nrf2 are relatively well conserved amongst mammals (Table 1), the majority of these genes are also regulated by other transcription factors, including those that govern the activity of discrete stress responses (Limonciel et al., 2015). Therefore, the consolidation of these gene signatures is vital to unravelling the roles of different molecular pathways in the cellular response to chemicals that have diverse

pharmacological and toxicological effects. These efforts will be enhanced by detailed assessments of the gene networks that are regulated by Nrf2 in human primary cells. As the toxicological phenotypes associated with activation of the Nrf2 stress response become clearer, it is envisaged that monitoring the activity of this pathway will contribute to the continuing drive toward *in vitro* and *in silico* approaches for predicting the human hazard posed by chemicals and new drugs.

### 1.5.2. *In vivo* models

An important limitation of the above cell-based models is their lack of key physiological traits, which can limit their predictive value. For example, in the case of drug-induced liver injury, the current lack of stable hepatocyte cell models that retain the capacity to metabolise many drugs, and the dedifferentiation of primary hepatocytes following their isolation from liver tissue (Elaut et al., 2006), renders such systems more suitable for identifying direct, metabolism-independent hepatotoxins. Whilst recent advances in stem cell technology are increasingly being used to address these shortcomings, state-of-the-art protocols currently generate only hepatocyte-like cells, given that their complement of cytochrome P450 enzymes and ability to metabolise drugs remains inferior to their primary counterparts (Takayama et al., 2014). At least until these barriers are overcome, animal models will continue to provide a unique opportunity to consider aspects of drug disposition in the toxicological effects of a given compound.

Several lines of transgenic mice have been established with a reporter construct under the transcriptional control of an ARE. For instance, the ARE-hPAP reporter mice contain the human placental alkaline phosphatase (hPAP) reporter gene under the control of an ARE from the promoter of NQO1 (Johnson et al., 2002). Primary cortical cultures from ARE-hPAP mice exhibited dose-dependent induction of hPAP activity following exposure to tBHQ alongside induction of endogenous Nqo1. Treatment with the antioxidant GSHEE (cell-permeable GSH) blocked DEM-mediated ARE activation; while LY 294002 (a selective PI3-kinase inhibitor) blocked tBHQ-mediated ARE activation. Following exposure to the excitotoxin kainate, as a model of neurodegeneration, the ARE-hPAP reporter mice showed ARE activation within damaged hippocampus (Kraft et al., 2006). ARE-hPAP mice have been used as a model of the neurodegenerative disorder Alexander disease that is due to mutated intermediate filament protein (GFAP) forming Rosenthal fibres. ARE-hPAP mice crossed with transgenic mice over-expressing hGFAP were more susceptible to kainate-induced seizures

with alkaline phosphatase activity localised to white matter within the murine brain, implicating the Nrf2-pathway in progression of this disease (Hagemann et al., 2005).

Hmox1-Luc reporter mice established by Zang *et al.* facilitates non-invasive imaging of Hmox1 activity (Zhang et al., 2001a). The transgene consists of the Hmox1 promoter sequence fused to firefly luciferase. The transgenic line have since been used to analyse Hmox1 induction to known toxicants including cadmium chloride (CdCl<sub>2</sub>), doxorubicin and thioacetamide (Malstrom et al., 2004a). Tissue damage, predominantly in the liver, kidney and intestines, was more pronounced than luciferase expression. This may be because the reporter acts downstream of Nrf2. While these transgenic lines hold potential for the *in vivo* screening of compounds that induce luciferase signal as a marker of toxicity, a reporter capable of responding to earlier activation of the Nrf2 pathway may avoid toxic damage.

Oikawa *et al.* recently established the OKD48-luc mouse model that expresses a transcriptionally inactive luciferase-tagged human Nrf2, under the transcriptional control of endogenous Nrf2, mediated through an ARE sequence repeated three times, from the promoter of GSTY<sub>a</sub> (Oikawa et al., 2012) (Fig 1.6). Microinjection of the transgene into fertilised embryos facilitated random integration of the reporter gene into the C57BL/6J background. Whilst the transgene product is able to interact with Keap1, and is therefore repressed in the absence of an Nrf2-inducing stimulus, general or oxidative stressors such as sodium arsenite cause the accumulation of luciferase-tagged Nrf2 via inhibition of Keap1-mediated turnover and transcriptional induction of the transgene by endogenous Nrf2. This dual-regulating mechanism produces a bioluminescent signal, detectable via whole animal and *ex vivo* organ imaging, upon activation of the Nrf2 response. By facilitating non-invasive, real-time measurement of Nrf2 activity *in vivo*, this model provides a platform to examine the relationship between drug disposition, activation of Nrf2 stress response signalling and organ-specific drug toxicity.

### OKD48 Reporter

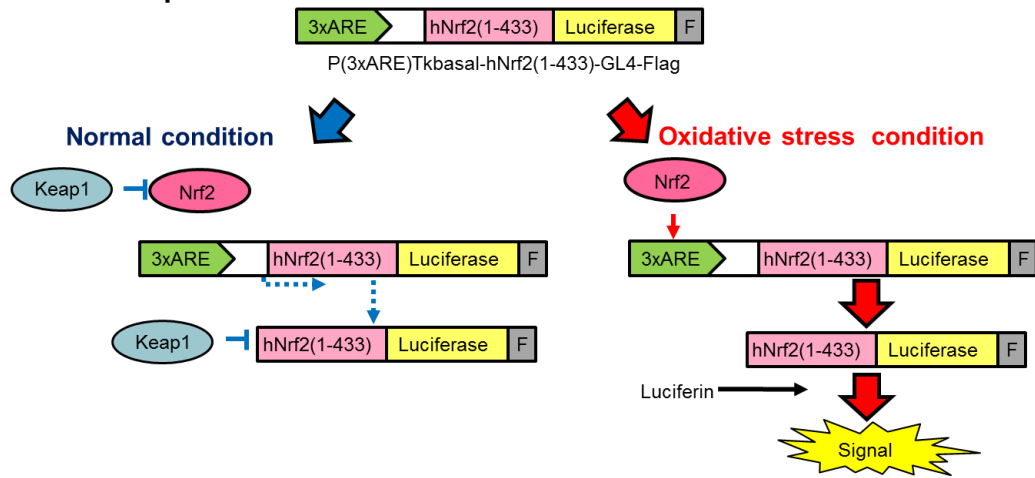


**Figure 1.6 Overview of the OKD48 reporter**

The OKD48 transgene consists of the Neh2 domain of human Nrf2 bound to flag-tagged Luciferase, driven by 3xARE promoter. Dual regulation of construct expression under normal conditions limits background signal and increases specificity via Keap1-mediated degradation of endogenous Nrf2 and leaked expression of the fusion protein. In response to oxidative stress, endogenous Nrf2 transactivates expression of the construct, which evades repression following inactivation of Keap1. This induces a luminescent signal in the presence of the substrate luciferin.

## 1.6. Therapeutic potential of Nrf2 modulators

The diverse, protective role of Nrf2 makes it an attractive candidate for therapeutic modulation. A myriad of small-molecule inducers of Nrf2 have been established for clinical use. Application of *in vitro* systems to monitor the Nrf2 pathway facilitate high through put (HTP) screening of potential inducers and provides insight into the chemical structures and motifs of compounds capable of preventing oxidative stress. Further investigation may aid the establishment of treatment for a range of diseases with an underlying oxidative stress component.

### 1.6.1. Compounds in the clinic

Aside from toxic compounds, a range of small-molecules have been shown to induce Nrf2 therapeutically and are currently undergoing pre/clinical trials (Fig 1.7). The most potent of these is the triterpenoid CDDO-Me, a methylated variant of CDDO (2-cyano-3,12-dioxooleana-1,9(11)-dien-28-oic acid), a synthetic triterpenoid. Derived from oleanolic acid, triterpenoids have been associated with a plethora of therapeutic properties including anti-tumour, anti-inflammatory, anti-microbial, cardio protective, wound healing, and hepato-protective effects (Liby and Sporn, 2012). CDDO-Me appears to activate Nrf2 via covalent modification of cysteine residues in Keap1 to stimulate Nrf2 mediated cytoprotective gene expression (Cleasby et al., 2014; Wong et al., 2016). A 5-fold increase in the mRNA level of *NQO1* has been reported in peripheral blood mononuclear cells (PBMCs) obtained from patients with advanced solid tumours or lymphomas who received a daily dose of CDDO-Me for three weeks (Hong et al., 2012). Also known as Bardoxolone methyl, CDDO-Me was a leading candidate for the treatment of Type 2 diabetes mellitus and chronic kidney disease in the Phase 3 BEACON trial. Early phase 1 trials indicated and improved eGFR in patients (Hong et al., 2012). However, the daily 20 mg dose increased the number of heart failure events via fluid overload resulting in termination of the study (de Zeeuw et al., 2013). Following reassessment of the cohort, it was clear that only patients with increased risk factors for heart failure (elevated D-type natriuretic peptide and prior hospitalisation for cardiac injury) experienced fluid overload (Chin et al., 2014). Therefore, clinical trials excluding at-risk patients are currently ongoing to assess CDDO-Me for the treatment of Alport syndrome (CARDINAL, NCT03019185) and CKD patients with comorbidities such as diabetes mellitus (TSUBAKI, NCT02316821). The compound is also undergoing trials for the treatment of pulmonary hypertension and associated connective tissue disease in the CATALYST (NCT02657356), and LARIAT trials (NCT02036970). Another synthetic triterpenoid RTA 408 (Reata Pharmaceuticals Inc.) is currently undergoing phase 2 trials (PRIMROSE) for

protection against dermatitis, a common side effect of radiation therapy during the treatment of breast cancer (NCT02142959). Preclinical data in mice highlighted its dose-dependent reduction of epidermal thickening and skin ulcers after irradiation (Reisman et al., 2014).

Dimethyl fumarate (Tecfidera® or BG-12) is an oral therapy prescribed for multiple sclerosis (MS). Derived from fumaric acid, the compound was originally used as a radiosensitizer and later as an oral treatment for psoriasis (Fumaderm) (Held et al., 1988; Mrowietz et al., 2007). Two randomised phase 3 clinical trials DEFINE (Determination of the efficacy and safety of oral fumarate in relapsing-remitting multiple sclerosis) and CONFIRM (Comparator and an oral fumarate in relapsing-remitting multiple sclerosis) highlighted the reduced risk of MS progression by 34-38% after 2 years and 44 - 55 % reduction of the annual relapse rate (Fox et al., 2012; Gold et al., 2012). Adverse events associated with dimethyl fumarate include gastrointestinal disturbances, elevated aminotransferases and decreased lymphocyte counts. The electrophilic compound and its metabolite monomethyl fumarate (MMF) modify cysteine residues within Keap1, including Cys151, resulting in the activation of Nrf2 (Linker et al., 2011). However, the compounds anti-inflammatory effects may be modulated by Nrf2-independent mechanisms. Dimethyl fumarate reduces the number of pro-inflammatory T-cells, resulting in many patients developing lymphopenia (Longbrake et al., 2016).

Isolated from broccoli, the isothiocyanate sulforaphane is a potent inducer of the Nrf2 pathway (Zhang et al., 1992). This is achieved by reacting with cysteine residues within Keap1 to disrupt Nrf2-Keap1 binding (Dinkova-Kostova et al., 2002). Sulforaphane is absorbed, conjugated to GSH and metabolised through the mercapturic acid pathway in humans. The anti-apoptotic and anti-inflammatory activity of sulforaphane are independent of Nrf2 activation (Greaney et al., 2016; Kallifatidis et al., 2009). In a randomised double-blind clinical trial in males suffering from autism spectrum disorder, daily doses of sulforaphane improved behaviour and verbal communication over an 18 week period (Singh et al., 2014). Phase 1 trials for sulforaphane as a treatment of autism spectrum disorder are currently ongoing (NCT02561481). Many analogues of sulforaphane have been produced for use in the clinic. Sulforadex® (SFX-01) is a sulforaphane-cyclodextrin compound with a longer shelf life than its parent compound. It has completed a randomised, double-blind trial assessing the safety, pharmacodynamics and pharmacokinetics of Sulforadex in healthy male subjects (NCT02055716) and is now part of the SAS (SFX01 after subarachnoid haemorrhage) trial,



currently investigating the efficacy of Sulforadex as a treatment for haemorrhage (NCT02614742). The compound has also been proposed as a combination therapy with tamoxifen for the treatment of breast cancer following evidence in primary cell culture that the combination therapy reverses cancer stem-cell like cell mediated resistance greater than tamoxifen alone (Simões et al., 2015).

Veda-1209, developed by Cureveda (USA), is another Nrf2 activator currently undergoing preclinical testing for the treatment of ulcerative colitis (Gao et al., 2014). The dithiolethione Oltipraz (4-methyl-5-(2-pyrazinyl)-1,2-dithiole-3-thione) induces many antioxidant and phase 2 enzymes that may account for its anti-carcinogenic effects (Ramos-Gomez et al., 2003; Sharma et al., 2006) and inhibits liver cirrhosis in rodents (Kim et al., 2013). The compound has completed phase 3 trials for the treatment of liver fat reduction in patients with non-alcoholic fatty liver disease (NCT02068339). However, in a phase 2 trial, weekly doses of Oltipraz failed to reduce the number of DNA adducts in the blood or lung epithelial cells of smokers (Kelley et al., 2005). The compound is also capable of generating superoxide radicals in human kidney cell culture (Velayutham et al., 2005).

While a number of promising Nrf2-activating compounds have been developed, the consequences of acute/chronic activation of Nrf2 and underlying mechanisms of action are unknown. Constitutive activation of Nrf2 occurs in many cancers, generating a favourable environment for tumour cell survival (DeNicola et al., 2011). In addition, Nrf2 deletion in ApoE<sup>-/-</sup> mice resulted in a reduction of atherosclerotic lesions, indicating Nrf2 has a pro-atherosclerotic role (Barajas et al., 2011), whereas overexpression of Nrf2 increased liver lipogenic gene expression and levels of hepatic cholesterol that may play a role in increased atherosclerosis (Jiansheng Huang et al., 2010). Keap1 knockout mice are also not viable due to constitutive activation of Nrf2 in the upper digestive tract (Wakabayashi et al., 2003). Further understanding of the consequences of pharmacologically targeting Nrf2 is needed to ensure adverse effects do not outweigh the transcription factors protective effects.

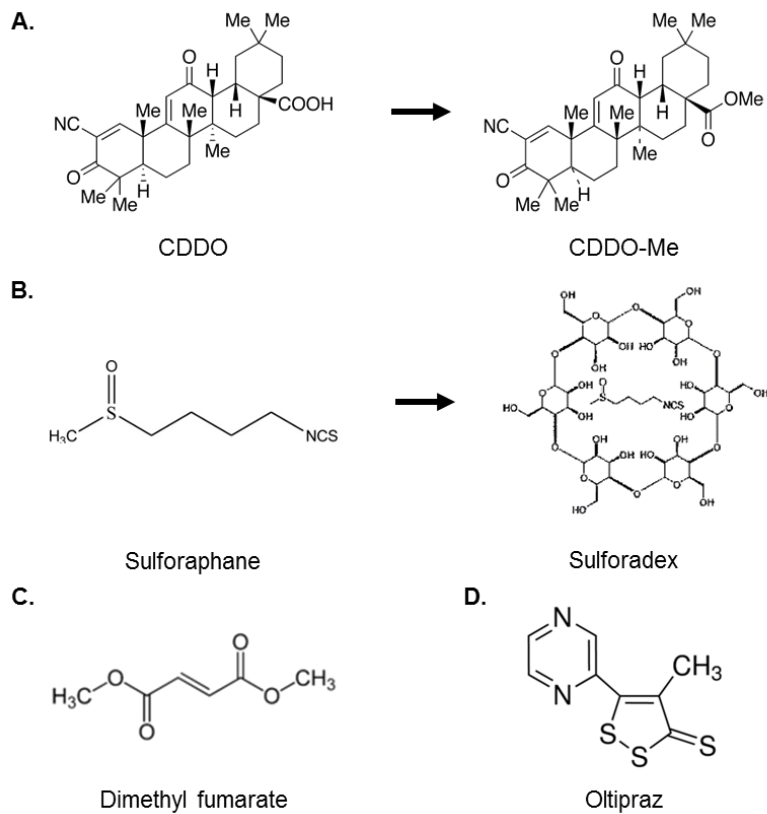


**Figure 1.7 Nrf2 inducing compounds**

(A) CDDO-Me, a synthetic triterpenoid, is derived from the potent Nrf2 inducer CDDO. (B) The isothiocyanate Sulforadex is an analogue of sulforaphane bound to cyclodextrin (Evgen). (C) Dimethyl fumarate is a derivative of fumaric acid and (c) Oltipraz is a dithiolethione.

### 1.6.2. Identification of Novel Nrf2 modulators

The HTP detection of Nrf2 inducers, via the screening of compound libraries, holds promise for the identification of novel drug candidates. Many screening platforms utilise *in vitro* ARE based reporters and bioinformatics to identify compounds liable to prevent oxidative stress. For instance, 47,000 compounds were screened using the AREc32 cell line described earlier (Wu et al., 2012). Chemical structure relationship analysis of hits (238 compounds) inducing the strongest luminescent signal highlighted the enrichment of four structural motifs. Insight into the structure of potent Nrf2 activators will aid the design of analogues. Shukla *et al.* utilized ARE-*bla* and ARE-Luc based assays in HepG2 cells to screen a US National toxicology program library of 1,408 compounds (Shukla et al., 2012). The ARE-*bla* reporter consisted of a three times repeat of the ARE from the promotor of NQO1 while the ARE-*luc* construct contained a seven times repeat of the consensus ARE sequence (Simmons et al., 2011). Both reporter systems were employed as the ARE-*luc* reporter identified Nrf2-specific activity in response to stress, while the ARE-*bla* assay identified compounds inducing ARE through complex interactions. It also aided the identification of false positives.

*In silico* screening offers a cost effective, fast method to identify compounds for drug development. The quantum model established by Williamson *et al.*, screened over 18 million commercially available compounds for structures predicted to activate the Nrf2-pathway (Williamson et al., 2012). The computational process predicts significant potency against targets based on the structure of known Nrf2 inducers. Top hits were validated in primary cell culture using an ARE-hPAP reporter. This process identified a novel family of activating structures with comparable potency of tBHQ.

While primary cell cultures are more physiologically relevant than immortalised cell lines, prolonged culture conditions and accessibility are limited. Stem cells derived from accessible tissues and reprogrammed, offer a viable alternative culture system. Höing *et al.*, developed a stem cell-based phenotypic assay for the screening of neuroprotective compounds in microglia (Höing et al., 2012). Initial *in silico* analysis identified compounds that were metabolically stable and able to cross the blood-brain barrier. Co-culture of stem cell-derived motor neurons and astrocytes expressing GFP were used to screen over 10,000 small molecules and identify 'hits' increasing cell survival. Expression profiling of these cells implicated many of the hits as Nrf2 activators. Inducers of Nrf2 were also identified using a cell-based luciferase enzyme fragment complementation (EFC) assay whereby N and C terminal domains of firefly luciferase fused to respective interacting proteins in the HEK293T

cell line (Ramkumar et al., 2013). NLuc-Keap1 and CLuc-Nrf2 complexes dissociated following Nrf2 activation facilitating non-invasive imaging of Nrf2 activation. The most potent compound identified in the screen, Pterostilbene, reduced luciferase activity significantly in tumour xenografts of the HEK293T cells in mice following a daily dosing regimen. The search for Nrf2 inducing compounds has been accelerated, thanks to HTP screening systems establishing direct evidence for Nrf2 activation or Keap1 modification. *In silico* and *in vitro* systems, prioritise chemicals for further detailed mechanism-based higher content studies. Insight into the compounds activity in relevant cell types and involvement in other stress response pathways such as DNA damage and inflammation is needed prior to therapeutic application.

### 1.7. Thesis aims

Currently, the lack of predictive biomarkers for drug-induced injury hinders the ability to screen novel compounds for toxicity. Nrf2 is the master regulator of the response to oxidative stress stimulated by bioactivation of drugs to form chemically reactive metabolites. Insight into the Nrf2 pathway may aid the analysis of novel or repurposed drug's propensity to induced oxidative stress linked to drug toxicity. Additionally, identifying clinically relevant markers of Nrf2-pathway activity may aid the early identification or status of patients suffering from drug-induced injury. As DILI is the most common form of drug-induced injury, the regulation and function of the Nrf2-pathway in liver cell culture is of particular importance. Therapeutic manipulation of the Nrf2 pathway is becoming more common in the treatment of diseases with an underlying oxidative stress component. Understanding the pharmacodynamics of novel Nrf2 activators may aid future generation of effective Nrf2-inducing compounds. Therefore, this thesis focuses on monitoring the Nrf2 pathway with the ultimate aim to improve testing strategies to identify chemicals and drugs that are likely to provoke toxicity in humans. The principle aims of this thesis were to investigate novel ways to measure activation of the Nrf2 pathway:

1. To characterise the response of Nrf2-Luc mice to organ-specific toxicants APAP and cisplatin.
2. To assess Nrf2 pathway activity in whole blood as a means of monitoring Nrf2 pathway status *in vivo*.
3. To characterise putative novel Nrf2-regulated genes in human liver cells.
4. To develop and use novel Nrf2-responsive reporter platforms to evaluate the potencies of novel analogues of the Nrf2-activating compound, Sulforaphane.

Chapter 2

**Bioluminescent imaging of Nrf2 reveals localised chemical stress associated with drug-induced organ toxicity**

**Contents**

2.1.	<b>Introduction</b> .....	54
2.2.	<b>Materials and Methods</b> .....	55
2.2.1.	Animals.....	55
2.2.1.1.	Wild-type mice.....	55
2.2.1.2.	Nrf2-Luc reporter mice .....	55
2.2.2.	Bioluminescence imaging .....	56
2.2.3.	Alanine transaminase quantification .....	59
2.2.4.	Glutathione quantification.....	59
2.2.5.	Blood urea nitrogen quantification.....	60
2.2.6.	Histological examinations .....	61
2.2.6.1.	Immunohistochemistry.....	63
2.2.7.	Total protein quantification .....	63
2.2.8.	Western blotting .....	64
2.2.9.	Gene expression analysis .....	66
2.2.9.1.	RNA extraction .....	66
2.2.9.2.	cDNA synthesis .....	66
2.2.9.3.	qPCR.....	67
2.2.10.	Statistical analysis .....	68
2.3.	<b>Results</b> .....	69
2.3.1.	Nrf2-Luc mice characterization.....	69
2.3.2.	Response to APAP toxicity in wild type C57BL/6J mice .....	72
2.3.3.	Nrf2-Luc respond to APAP toxicity.....	75
2.3.4.	Nrf2-Luc mice respond to cisplatin toxicity .....	90
2.4.	<b>Discussion</b> .....	100

### 2.1. Introduction

Nrf2 activation has been implicated in the early stages of drug-induced toxicity. A myriad of toxic drugs are associated with activation of Nrf2, including APAP and cisplatin (Cho et al., 2008; Goldring et al., 2004). There is increasing interest in the transcription factor's ability to differentiate between drugs likely to produce oxidative or chemical stress and those which are not toxic. For instance, predictive, Nrf2-based assays such as the ARE-*bla* reporter from the Tox21 initiative and Keratinosens<sup>TM</sup> assay have been developed (Emter et al., 2010; Kim et al., 2016).

Previous work from this laboratory has shown that the Nrf2 pathway is elevated in the murine liver following exposure to APAP (Copple et al., 2008b; Eakins et al., 2015; Goldring et al., 2004). This entailed endpoint analysis of a large number of liver tissues from wild-type mice, limiting the scope of examination. The recently established OKD48-Luc (hereafter referred to as Nrf2-Luc) mice provide the ability to monitor the Nrf2-mediated response to oxidative and chemical stress non-invasively and in real-time (Oikawa et al., 2012). This gives greater insight into the activity of Nrf2 over time, in the same individual and simultaneously reduces the number of animals needed in a study. This is in line with current 3R's guidelines (Russell and Burch, 1959; Tannenbaum and Bennett, 2015).

Nrf2-Luc mice respond to oxidative stress induced by sodium arsenite, UV radiation (Oikawa et al., 2012) and, more recently, during the onset of cerebral malaria (Imai et al., 2014). However, the value of these mice for investigating drug-induced organ toxicity has not been determined. I hypothesised that the Nrf2-Luc mice would respond to drug-induced organ toxicity and produce a localised bioluminescent signal to organ-specific forms of chemical stress. In order to test this hypothesis, Nrf2-Luc mice were exposed to the hepatotoxin APAP or the nephrotoxin cisplatin and their bioluminescent response quantified alongside classical markers of toxicity such as alanine transaminase and blood urea nitrogen. The results of these investigations are presented here and as part of the recent publication 'Real-time in vivo imaging reveals localised Nrf2 stress responses associated with direct and metabolism-dependent drug toxicity' (Forootan et al., 2017).

## **2.2. Materials and Methods**

All reagents were purchased from Sigma Aldrich unless otherwise stated.

### **2.2.1. Animals**

All animal experiments were conducted according to the Animals (Scientific Procedures) Act 1986 guidelines under the Home Office project licence PPL 40/3678 and approved by the University of Liverpool Animal Welfare Committee.

#### **2.2.1.1. Wild-type mice**

Male, wild-type C57BL/6J mice between 8-10 weeks old, were purchased from Charles River and had a 5 day acclimatisation period prior to experimentation. Animals were maintained in a 12 hour light/dark cycle in a temperature and humidity controlled, specific pathogen-free environment. Mice were fed CRM (P) diet (Special Diets Services) ad-libitum. Mice were administered APAP (300 mg/kg) or 0.9 % saline via intraperitoneal (IP) injection in groups of five mice per experimental time point. Mice were fasted for 16 h prior to administration of APAP. Mice were culled at 0, 2, 6 and 24 h with a rising concentration of CO<sub>2</sub>.

Blood was collected via cardiac puncture using a 25 G needle and 1 ml syringe to collect blood directly from the heart. The needle was removed from the syringe before decanting the blood into eppendorfs in order to avoid haemolysis. Freshly isolated blood was left to clot at room temperature for 30 min and centrifuged at 2000 *g* for 10 min. Serum was decanted and stored at -80 °C.

#### **2.2.1.2. Nrf2-Luc reporter mice**

A breeding colony of Nrf2-Luc C57BL/6J mice were established in Liverpool from founder mice kindly donated by Dr Takao Iwawaki, Gunma, Japan. Initial attempts to generate homozygous Nrf2-Luc mice were unsuccessful therefore all studies were performed with heterozygous mice. Litters of 4 week old Nrf2-Luc mice were genotyped by Transnetyx, using ear snips. Heterozygous Nrf2-Luc were identified using the primers specific for firefly luciferase. Four separate studies using Nrf2-Luc mice are described in this chapter: one study using female mice exposed to a single dose of sulforaphane; one male and one female time course study following a single dose of APAP and one female time course study following the administration of cisplatin. Mice were selected for each study with similar genotyping scores.

Firstly, wild-type and heterozygote male Nrf2-Luc mice were administered sodium arsenite as a positive control for the holistic induction of the Nrf2-Luc transgene. Wild-type and heterozygote Nrf2-Luc mice were administered either 13 mg/kg sodium arsenite via IP



injection (n=1). Injections were administered using a 1 ml syringe and short (16 mm) 25 G needle or insulin needle. Mice were anaesthetised and bioluminescence was quantified after 6 h (see section 2.2.2 for protocol). Mice were culled after 6 h by a lethal dose of pentobarbital (100 mg/kg), a Schedule 1 method. Organs were removed for *ex vivo* bioluminescence quantification.

During the APAP studies, male or female Nrf2-Luc mice were fasted for 16 h and given a single dose of either 0.9 % saline or 300 mg/kg APAP (n=5).. At 2, 6 and 24 h mice were anaesthetised and bioluminescence quantified. Mice were culled after 24 h by a lethal dose of pentobarbital and blood was collected by cardiac puncture. Organs were removed for *ex vivo* imaging. Following bioluminescence quantification, half of the hepatic central lobe was fixed and the rest of the liver was snap frozen.

In the cisplatin study, female mice were exposed to 0.9 % saline and 5 mice to 20 mg/kg cisplatin, administered via IP injection (n=4). At 24, 48, 72 and 96 h the mice were anaesthetised and bioluminescence quantified. Mice were culled after 96 h with an overdose of pentobarbital via IP injection and blood collected by cardiac puncture. The kidneys and livers were removed for *ex vivo* imaging. From each mouse, one kidney was fixed in formalin and one kidney was snap frozen.

### **2.2.2. Bioluminescence imaging**

Bioluminescence was quantified using the *in vivo* imaging system (IVIS) spectrum (Perkin Elmer, Waltham USA). This machine facilitates non-invasive imaging of live mice and produces a topographical image of the bioluminescent signal. Firefly luciferase, generated by the OKD48 transgene, produces light in an ATP dependent reaction with luciferin (Fig 1.6). In order to visualise the bioluminescent signal, mice were anaesthetised with isoflurane and either their torsos or backs were shaved with electric clippers. Mice were weighed and administered 150 mg/kg luciferin via IP injection using short 25 G needles. After 5 min, bioluminescence was quantified using the IVIS. Up to five mice were placed in the chamber in nose cones connected to anaesthetic supply. The mice were orientated either on their front or back, and images were taken using Living Image® Software. Exposure times was set to 'Auto', binning was set to 'medium' and F/stop kept at 1 with the excitation filter closed and emission filter open.

Bioluminescence of organs were also quantified *ex vivo*. After the animal had been culled, the organs were dissected and rinsed in phosphate buffered saline (PBS). These were

subsequently incubated in 150  $\mu\text{g/ml}$  *in vivo* grade luciferin in PBS for 2 min at room temperature. The organs were transferred to small petri-dishes and imaged using the IVIS. Bioluminescence in the region of interest (ROI) was calculated using Living Image<sup>®</sup> Software (Fig 2.1).

Organs were rinsed in PBS after imaging and either fixed in 4 % paraformaldehyde or snap frozen in liquid nitrogen.

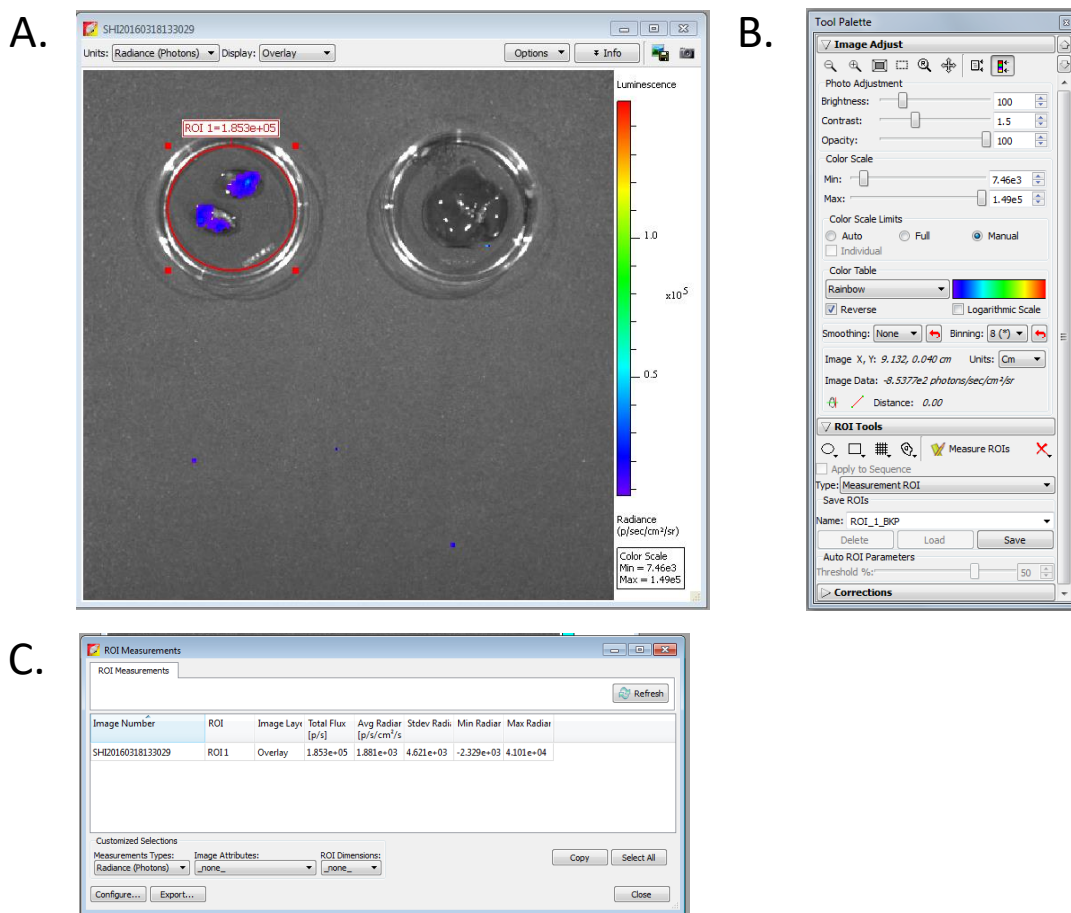


**Figure 2.1 Calculation of region of interest**

(A) Within the living image software, images were quantified in radiance ( $\text{p/sec/cm}^2/\text{sr}$ ). (B) Using the image adjust settings, min and max colour scales were set to the same range for all images of one experiment. The region of interest (ROI) was defined (red circle) and quantified (C).

### 2.2.3. Alanine transaminase quantification

Alanine transaminase (ALT) catalyses the conversion of  $\alpha$ -ketoglutarate and alanine to glutamate and pyruvate. Clinically, measurement of ALT reflects liver function and is used to diagnose liver pathophysiology. ALT quantification using lactate dehydrogenase (LDH) and nicotinamide adenine dinucleotide (NADH) was initially described by Wroblewski and LaDue (WRÓBLEWSKI *et al.*, 1956). Here I used the Infinity ALT Kit TR71121 (Thermo Scientific). This assay utilizes the production of pyruvate to convert a nearly colourless probe to a colourful product. This signal is proportional to pyruvate quantity. The change in optical density (OD) is measured over time as this is a kinetic assay for the measurement of enzymatic activity.

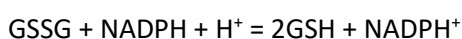
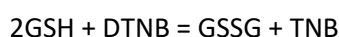
Murine serum was thawed only once to avoid ALT degradation and used immediately. Samples from APAP-treated mice were diluted 1:30 in 0.9 % saline and loaded in duplicate in a 96 well plate (30  $\mu$ l / well). Samples from saline-treated mice were loaded neat. Blank wells were loaded with 0.9 % Saline. Undiluted normal and abnormal control serum (Data Trol™) were included on the plate as negative and positive controls respectively. The plate reader and ALT reagent were heated to 37 °C, prior to the addition of 300  $\mu$ l ALT reagent to the samples. The OD was measured at 340 nm using a Varioscanner Flash (Thermo Scientific). ALT activity was expressed in U/L:

$$\text{ALT activity (U/L): Abs/min} \times 1746$$

$$1746 = [\text{Total reaction volume (ml)} \times 1000] / [\text{Absorption coefficient of NADH at 340 nm} \times \text{sample volume (ml)} \times \text{cuvette pathlength (cm)}]$$

### 2.2.4. Glutathione quantification

Total GSH content can be quantified by the 5-5'-Dithiobis(2-nitrobenzoic acid) (DTNB)-based 'recycling' method described by Vandeputte *et al.* (Vandeputte *et al.*, 1994). The assay utilises the following reactions, the latter catalysed by GSH reductase to generate the 5'thio-2-nitrobenzoic acid (TNB) chromophore:



Glutathione stock buffer was generated (11.15 g sodium dihydrogen phosphate monohydrate  $\text{NaH}_2\text{PO}_4 \cdot 2\text{H}_2\text{O}$  and 1.17 g Ethylenediaminetetraacetic acid (EDTA) in 500 ml

dH<sub>2</sub>O) at pH 7.4. 100 mg of liver tissue was homogenised in 400 µl GSH stock buffer and 200 µl 6.5 % sulfosalicylic acid using an oscillating mill (Retsch) and magnetic ball bearings, for 3 min at 30 s<sup>-1</sup>. Samples were left on ice for 10 min, then centrifuged at 18000 g for 5 min. The supernatant was snap frozen and stored at -80 °C. 1 ml of 1 M NaOH was added to the pellet and incubated at 60 °C for 1 h. Pellets were resuspended and frozen at -80 °C. Total protein content was quantified by Bradford assay (see section 2.2.7).

1 mM glutathione (in glutathione stock buffer) was prepared. This was diluted 1:10 to a 0.1 mM glutathione solution and used to make solutions for the standard curve (1, 2, 5, 10, 20, 40 and 80 nM glutathione in GSH stock buffer). Supernatant samples were defrosted on ice and diluted 1 in 10 in GSH stock buffer, vortexed and 20 µl added to wells of a 96 well plate in duplicate. Standard curve samples were loaded in a similar manner. 20 µl GSH stock buffer was added to each well, to neutralise the pH. The plate was left on ice.

The Daily assay reagent was generated (9.908 mg Ellman's reagent (DTNB), 7.08 mg NADPH in 25 ml GSH stock buffer). 10 ml of diluted GSH reductase was generated (in GSH stock buffer) and kept on ice. The quantity of enzyme to be diluted was based on the following reaction:

$$\text{Volume } (\mu\text{l}) = [(6.96 \text{ units/ml} \times 10 \text{ ml}) / (\text{Units/ml of stock reductase})] \times 1000$$

200 µl daily assay reagent was added to each well. After 5 min, 50 µl GSH reductase was added to each well. The OD was read at 405 nM using the Varioskanner Flash (Thermofisher).

### 2.2.5. Blood urea nitrogen quantification

Secreted by the kidneys, urea is the product of protein catabolism. Increased levels of circulating urea are associated with renal pathology, congestive heart failure and diabetes. Blood urea nitrogen (BUN) levels indicate the amount of nitrogen in the blood from urea. Developed by Jung *et al.* quantification of BUN consists of two steps (Jung *et al.*, 1975). Firstly ortho-phthaldialdehyde reacts with urea. The product undergoes a rapid reaction with primaquine diphosphate that yields red coloured product proportional to concentration of urea in the sample.

Serum was thawed once only, to avoid degradation. BUN levels were quantified using QuantiChrom™ Urea Assay Kit DIUR-500 (BioAssay Systems), following the kit instructions. Samples were diluted 1 in 50, in dH<sub>2</sub>O. Samples and standard were loaded in duplicate into a 96 well plate (5 µl / well). The kit standard contained 50 mg/dL Urea. Distilled H<sub>2</sub>O was used

as a blank sample. Samples were incubated with working reagent (Reagent A and B in equal volumes) for 20 min at room temperature. OD was measured at 520 nm using the Varioscanner Flash. Urea concentration was calculated in the following manner:

Urea concentration (mg/dL) = [ (OD sample – OD blank) / (OD standard – OD blank) ] x dilution factor (50) x 50 mg/dL

As blood urea nitrogen is the mass of nitrogen within urea, BUN levels were calculated using the following calculation:

BUN (mg/dL) = Urea concentration (mg/dL) / 2.14 (MW of urea (60)/ MW of urea nitrogen (28) = 2.14)

#### **2.2.6. Histological examinations**

For the histological and immunohistological examinations, liver sections from the central lobe, and kidney cross sections were fixed in 10 % buffered formalin for 48 h, trimmed and routinely paraffin wax embedded. Sections (3-5  $\mu$ m) were prepared and routinely stained with haematoxylin-eosin (HE). Processing and staining for histology was performed by Dr. Julie Haigh, Histology Laboratories, Department of Veterinary Pathology and Public Health, Institute of Veterinary Sciences, University of Liverpool.

The HE-stained sections were examined for any pathological alterations and the changes consistent with DILI were scored according to a previously applied scoring system (Table 2.2) (Antoine et al., 2009), whereas changes consistent with drug induced kidney injury (DIKI) were scored according to a previously published system by Zhang *et al.* (Table 2.3) (Zhang et al., 2009) by Prof. Anja Kipar, Laboratory for Animal Model Pathology, Vetsuisse Faculty, University of Zurich and Institute of Global Health, University of Liverpool.

**Table 2.2 Drug-induced liver injury scoring criteria**

From (Antoine et al., 2009)

Score	Description
0	Tissues are normal with no hepatic necrosis.
1	Hepatocyte loss and necrosis – minimal to mild Focal Limited to centrilobular region Less than ¼ of affected lobules are necrotic Associated with vacuolar degeneration or haemorrhages
2	Hepatocyte loss and necrosis – mild to moderate Focal and multifocal Extends from central to midzonal lobular region ½ of affected lobules are necrotic Associated with vacuolar degeneration or haemorrhages
3	Hepatocyte loss and necrosis – moderate to severe Multifocal May extends from centrilobular to portal region More than ½ to ¾ of affected lobules are necrotic Associated with vacuolar degeneration or haemorrhages
4	Hepatocyte loss and necrosis – severe Multifocal More than ¾ of affected lobules are necrotic Associated with vacuolar degeneration or haemorrhages
5	Massive hepatocyte loss and necrosis – severe, involving entire lobules Hepatocytes loss extends from central vein to portal area Hepatocytes loss extends o adjacent lobules (multilobular necrosis) Associated with vacuolar degeneration or haemorrhages

**Table 2.3 Drug-induced kidney injury score criteria**

From (Zhang et al., 2009)

Score	Description
0	Normal tubules, glomerulus, interstitium and vessels
1	Scant number of tubular epithelial cells showing minimal degeneration, mild tubular dilatation, small number of proteinaceous casts, no regeneration, no definitely significant necrosis or apoptosis. No changes in the glomerulus, interstitium and vessels
2	<25% of tubular epithelial cells showing mild degeneration (large cytoplasmic vacuoles, few hyaline droplets in the cytoplasm), mild degree of tubular dilation and proteinaceous casts, slight change in tubular brush border loss, acute tubular necrosis in individual cell or small group of cells, a few apoptotic cells, no regeneration. No changes in the glomerulus, interstitium and vessels
3	25-50% of tubular cells showing moderate degeneration (multiple large-sized cytoplasmic vacuoles, multiple foci of hyaline droplets), mild regeneration, moderate tubular brush border loss, moderate tubular necrosis in small groups of tubule and increased number of apoptotic cells. Little involvement of mild glomerular vacuolization. No changes in interstitium and vessels
4	51-75% of tubular epithelial cells showing extensive moderate degeneration; moderate regeneration; severe tubular brush border loss; severe acute tubular necrosis; large number of apoptotic cells with apoptotic bodies in clusters of tubules. Little involvement of mild glomerular vacuolization and interstitial lymphocytic infiltration
5	>75% of tubular epithelial cells showing severe degeneration, regeneration, severe tubular brush border loss, acute tubular necrosis, large number of apoptotic cells with numerous apoptotic bodies. Mild involvement of glomerular injury (vacuolization, mesangial cell proliferation, increase in mesangial matrix) and interstitial lymphocyte infiltration. No significant changes in the vessels

### 2.2.6.1. Immunohistochemistry

Consecutive sections (3-5  $\mu\text{m}$ ) from the paraffin blocks were stained by immunohistochemistry to detect luciferase and Hmox1 expression. Briefly after deparaffination, sections were pre-treated with EDTA buffer (1mM EDTA, 0.05% Tween 20) at pH 9, for 20 min at 98 °C (Staining for luciferase) and citrate buffer (10 mM sodium citrate and 0.05 % Tween 20) at pH 6, for 20 min at 98 °C (Staining for Hmox1), respectively. To avoid endogenous peroxidase activity, all sections were incubated for 10 min with Peroxidase blocking reagent (Dako, S2023) at room temperature. All following incubations were conducted at room temperature. Between each incubation sections are washed with TBS-Tween (Buffer described in section 2.2.8) for 10 min at room temperature. Sections were incubated with the primary antibodies: mouse anti-luciferase (Clone Luci17) ab16466 abcam, or mouse anti-Hmox1 (clone MA1-112) Thermo Fischer Scientific, diluted 1:100 in Dilution buffer (Dako) for 1 h. To detect the antibody binding, sections were incubated in Envision Mouse HRP reagent (Dako) for 30 min. The reaction was visualised by incubating the sections for 10 min with DAB (3,3'-diaminobenzidine), and counterstained with Gills haematoxylin (1:20 in dH<sub>2</sub>O) for approximately 2 sec. Sections from a mouse spleen were used as a positive control for Hmox1 staining and sections from a mouse tumour exhibiting a luciferase expressing protein served as positive controls for luciferase. Sections incubated with a non-reactive mouse monoclonal antibody instead of the primary antibodies served as negative controls.

### 2.2.7. Total protein quantification

Protein concentration was determined via Bradford assay (Bradford, 1976). The assay utilises the coomassie brilliant blue G-250 dye reagent that binds to amino acids facilitating the colour change from brown to blue which is proportional to protein content. Liver lysates were defrosted on ice. 15 mg liver tissue was added to 500  $\mu\text{g}$  RIPA buffer and lysed using an oscillating mill for 3 min at 30 s<sup>-1</sup> (Retsch).

A standard curve was generated with known concentrations of bovine serum albumin (BSA). A 500  $\mu\text{g}/\text{ml}$  BSA stock solution was generated in dH<sub>2</sub>O and diluted to the following concentrations: 0.25, 0.2, 0.15, 0.1, 0.05 and 0.025 mg/ml. Tissue lysates were diluted 1 in 300 in dH<sub>2</sub>O. 20  $\mu\text{l}$  of standards or samples were loaded in duplicate in to the wells of a 96 well plate. Distilled H<sub>2</sub>O was loaded as a blank sample. Protein Assay Dye Reagent Concentrate (BioRad) was diluted 1 in 4 with dH<sub>2</sub>O. The diluted reagent was added to the



plate (200  $\mu$ l / well) and the plate was incubated at room temperature for 5 min. Absorbance was measured at 595 nm using the Varioskanner Flash.

### 2.2.8. Western blotting

Western blotting facilitates the semi-quantitative detection of specific proteins via gel-based separation and antibody staining (Burnette, 1981). NuPAGE 4x LDS Sample Buffer (Invitrogen) and NuPAGE 10x Sample Reducing Agent (Invitrogen) were added together in a ratio 7:3 to generate loading buffer. 5  $\mu$ l loading buffer was added to 20  $\mu$ g liver lysate and incubated at 90 °C for 10 min to denature the protein. Samples were centrifuged briefly and loaded into wells of NuPAGE Novex 4-12 % Bis-tris Polyacrylamide Gels (Invitrogen). Precision-Plus Kaleidoscope Protein Standards (BioRad) were included as reference markers. A 20x 3-(N-morpholino)propanesulfonic acid (MOPS) buffer was generated (209.2 g MOPs, 121.2 g Tris base, 20 g, SDS and 6 g EDTA in 1 L dH<sub>2</sub>O). Gels were resolved for 1 h at 170 V in 1 x MOPs buffer.

Once resolved, proteins were transferred to Nitrocellulose Membranes (GE Healthcare, Amersham). A 10 x Transfer buffer was generated (150.2 g Glycine, 30.3 g Tris base in 1 L dH<sub>2</sub>O). The transfer was conducted in Transfer Tanks (BioRad) filled with 1x Transfer buffer (100 ml 10x Transfer buffer, 200 ml Methanol and 700 ml dH<sub>2</sub>O) for 1 h at 230 mA. Confirmation of successful transfer was obtained by incubating membranes for 3 min in ponceau S solution.

A 20x Tris-buffered saline (TBS) stock solution was generated (175.2 g NaCl, 4.48 g KCl and 60.6 g Tris base in 1 L dH<sub>2</sub>O) at pH 7. Membranes were blocked with 10 % (w/v) Blotting grade blocker (BioRad) in TBS-Tween (TBST) (50 ml 20x TBS, 10 ml 10 % (v/v) Tween20 and 940 ml dH<sub>2</sub>O) for 2 h or overnight at 4 °C. Blots were incubated with antibodies listed in Table 2.4 in 2 % (w/v) Blotting grade blocker in TBST. Following secondary antibody incubation, blots were washed for 30 min with TBST.

Blots were developed with ECL reagent (Perkin-Elmer) and exposed to Hyperfilm™ (GE Healthcare) in a dark room for 1 – 120 sec. Photographic film was incubated in Developer (Carestream Health Inc.) diluted 1 in 5 with H<sub>2</sub>O for 1 min. The film was then incubated in Fixer (Carestream Health Inc.) diluted 1:5 with H<sub>2</sub>O for 1 min and rinsed with H<sub>2</sub>O. Once dry, films were scanned and densitometry performed using ImageJ (Schneider et al., 2012). Density of bands were normalised to  $\beta$  actin intensity as a loading control.

**Table 2.4 Antibody concentration and conditions for Western blot**

Primary Antibody	Dilution (in 2 % Milk in TBST)	Incubation time	Washing steps (using TBST)	Secondary antibody	Dilution (in 2 % Milk in TBST)	Incubation time (h)
$\beta$ Actin (ab6276) Monoclonal	1:20,000	10 min	4 x 5 min	Anti-Mouse-HRP (A9044, Sigma) Polyclonal	1:10,000	1
Hmox1 (ab13243) Polyclonal	1:5,000	Overnight	3 x 10 min	Anti-Rabbit-HRP (A9169, Sigma) Polyclonal	1:5,000	1
Keap1 (1050-3-2-AP, Proteintech) Polyclonal	1:2,000	Overnight	3 x 10 min	Anti-Rabbit-HRP (A9169, Sigma) Polyclonal	1:5,000	1
Txnrd1 (ab124954) Monoclonal	1:5,000	Overnight	4 x 5 min	Anti-Rabbit-HRP (A9169, Sigma) Polyclonal	1:5,000	1
Nqo1 (ab2346) Polyclonal	1:2,000	Overnight	4 x 5 min	Anti-Goat-HRP (P0449, Dako) Polyclonal	1:5,000	1
Nrf2 (16396-1-AP, Proteintech) Polyclonal	1:1,000	Overnight	6 x 10 min	Anti-Rabbit-HRP (A9169, Sigma) Polyclonal	1:5,000	1

### 2.2.9. Gene expression analysis

Expression of Nrf2 target genes was determined using quantitative (real-time) polymerase chain reaction (qPCR). Isolated RNA was converted to cDNA and quantified using the fluorescent dye SYBR green. This dye intercalates with double stranded DNA to produce a fluorescent signal (Ponchel et al., 2003).

#### 2.2.9.1. RNA extraction

In this chapter, RNA was isolated using the spin column-based purification RNeasy Mini Kit (Qiagen, Hilden Germany). Guanidium thiocyanate is used to facilitate binding of nucleic acids to silica (Boom et al., 1990). The mini kit spin columns contain silica-membranes and tissues were lysed in a guanidine-thiocyanate containing buffer. This lysis buffer also inhibits RNase activity within the sample.

Liver tissue was weighed and 20 mg lysed in 350  $\mu$ l of buffer RLT using the oscillating mill. Lysates were centrifuged for 3 min at 18,000  $g$  and the supernatant transferred to new eppendorfs. Samples were vortexed after the addition of 350  $\mu$ l of 70 % (v/v) ethanol in dH<sub>2</sub>O and loaded onto the spin column above a 2 ml collection tube. Spin columns were centrifuged for 15 sec at 8,000  $g$  and the flow-through discarded. The silica membranes were subsequently washed with 700  $\mu$ l buffer RW1 and 500  $\mu$ l buffer RPE two times. After loading the buffer, spin columns were centrifuged and flow through discarded. The spin column was spun at 8,000  $g$  a final time to dry the membrane and RNA eluted in 30  $\mu$ l RNase-free dH<sub>2</sub>O. The eluate was loaded back onto the spin column and centrifuged a second time to ensure a high RNA yield. The yield was quantified using the Nanodrop Spectrophotometer ND-1000 (Labtech International, Heathfield UK). Purity of the samples were based on the 260/280 ratio. Only those with a ratio between 1.9 and 2.1 were used. All RNA samples were stored at -80 °C.

#### 2.2.9.2. cDNA synthesis

RNA samples were reverse transcribed to cDNA using the GoScript™ Reverse Transcription System (Promega, Madison USA). In a semi-skirted 96 well plate (Starlab, Hamburg Germany), between 0.1 - 0.5  $\mu$ g RNA was added per well, along with 0.5  $\mu$ l random A primer (500  $\mu$ g/ml) and 0.5  $\mu$ l oligo dt primer (500  $\mu$ g/ml). Reactions were made up to 10  $\mu$ l with dH<sub>2</sub>O. Reactions included both sets of primers to increase cDNA yield. The plate was sealed and incubated at 70 °C for 5 min and cooled on ice for 2 min. A master mix was generated (8  $\mu$ l 5x reaction buffer, 4  $\mu$ l 25 mM MgCl<sub>2</sub>, 2  $\mu$ l 10 mM dNTPs, 2  $\mu$ l reverse transcriptase and 14  $\mu$ l dH<sub>2</sub>O per reaction) in excess of the total number of reactions and 30  $\mu$ l added to each

well. The plate was then incubated at an annealing temperature of 25 °C for 5 min, an extension temperature of 42 °C for 1 h and inactivation of the enzyme was achieved by incubating at 70 °C for 15 min. cDNA samples were stored at -20 °C.

### 2.2.9.3. qPCR

qPCR analysis was conducted using the Via7 qPCR machine (Life technologies, Carlsbad USA). Reactions were loaded into wells of a semi-skirted 96 well plate. cDNA was diluted 1 in 3 with nuclease free dH<sub>2</sub>O and 6 µl loaded per well. 5 µM primer pair solutions were generated by diluting the 100 µM stocks and combining both forward and reverse primers (Table 2.5). Master mixes were generated for each primer combination (10 µl Power SYBR green master mix (Life technologies, Carlsbad USA) and 4 µl 5 µM primer pair solution per well). 14 µl of Master Mix were added to each well of a 96 well plate. This made each reaction a final volume of 20 µl. Each sample was run in duplicate alongside wells with 6 µl Nuclease free water, substituting cDNA as a negative control. The plate was heated using the Via7 (program listed in Table 2.6) and fluorescence quantified at 60 °C. Ct threshold was set using Via7™ software v1.2.2. Ct values for each sample were averaged and fold changes generated using the following equation:

$$\text{Ct (Gene of interest)} - \text{Ct (Housekeeping gene)} = \Delta\text{Ct}$$

$$\Delta\text{Ct (Experimental sample)} - \Delta\text{Ct (Control sample)} = \Delta\Delta\text{Ct}$$

$$(2^{-\Delta\Delta\text{Ct}}) \times 100 = \text{mRNA level (\% control)}$$

**Table 2.5 Mouse qPCR primer sequences**

Gene	Primer	Sequence
Mouse <i>Nqo1</i>	Fwd	5'- TTT AGG GTC GTC TTG GCA AC -3'
	Rev	5'- GTC TTC TCT GAA TGG GCC AG -3'
Mouse <i>Gsta1</i>	Fwd	5'-CAG CCT GGC AGC CAG AGA -3'
	Rev	5'-TCT GTG GCT CCA TCA ATG CA -3'
Mouse <i>Srxn1</i>	Fwd	5'- AAA GTG CAG AGC CTG GTG -3'
	Rev	5'- CTT TGA TCC AGA GGA CGT CG -3'
Mouse <i>Nrf2</i>	Fwd	5'- CAT GAT GGA CTT GGA GTT GC -3'
	Rev	5'- CCT CCA AAG GAT GTC AAT CAA -3'
Mouse <i>Keap1</i>	Fwd	5'- CAC AGC AGC GTG GAG AGA -3'
	Rev	5'- CAA CAT TGG CGC GAC TAG A -3'
Mouse <i>Hmox1</i>	Fwd	5'- GTC AAG CAC AGG GTG ACA GA -3'
	Rev	5'- ATC ACC TGC AGC TCC TCA AA -3'
Mouse <i>Gapdh</i>	Fwd	5'- TGT CCG TCG TGG ATC TGA C -3'
	Rev	5'- CCT GCT TCA CCA CCT TCT TG -3'

**Table 2.6 qPCR Program**

Number of cycles	Temperature (°C)	Time
1	95	10 min
40	95	15 sec
	60	1 min

**2.2.10. Statistical analysis**

Standard deviation (SD) was calculated using Graphpad Prism7. All bar graphs shown as mean  $\pm$  SD. Normality was assessed by Shapiro Wilk test. Statistical significance of unpaired data was assessed by Student's T test, for parametric data, or Mann Whitney U test, for data with a non-parametric distribution. Where F values relating to variance were significant, Welch's correction was employed. For multiple comparisons, one-way ANOVA with Tukey's post-hoc analysis or Kruskal Wallis with Dunn's multiple comparisons tests, were used. Correlations were calculated either by Pearson's or Spearman's R test. P value notations are as follows: \*/@ P  $\leq$  0.05, \*\*/@@ P  $\leq$  0.01 and \*\*\*/@@@ P  $\leq$  0.001.

## 2.3. Results

### 2.3.1. Nrf2-Luc mice characterization

Initial characterization of Nrf2-Luc mice was conducted to identify basal activity of the Nrf2 pathway and GSH levels. This was vital to ensure the transgene did not interfere with gene expression or the major detoxification pathway of APAP, making the Nrf2-Luc mice more sensitive or more tolerant to chemical stress.

Untreated male and female wild type and heterozygote Nrf2-Luc mice were culled with a rising concentration of CO<sub>2</sub> and hepatic GSH levels quantified (Fig 2.2 A). No significant difference was observed between genotypes of male and female by unpaired t-test ( $P = 0.154$  and  $0.786$  respectively). Basal activity of hepatic Nrf2-regulated transcriptome revealed no significant difference between WT and Het female mice (Fig 2.2 B).

Oikawa *et al.* demonstrated the sensitivity of the Nrf2-Luc mice to sodium arsenite (ASN) as a systemic inducer of oxidative stress (Oikawa et al., 2012). To show mice from our breeding colony were also sensitive to Nrf2 induction in this manner, one wild-type and one heterozygous Nrf2-Luc mouse were exposed to 13 mg/kg ASN for 6 h. *In vivo* bioluminescence imaging following 6 h exposure revealed a strong signal in the lower abdominal region (Fig 2.3 A). *Ex vivo* analysis identified a hepatic luminescent signal specific to the heterozygous mouse.

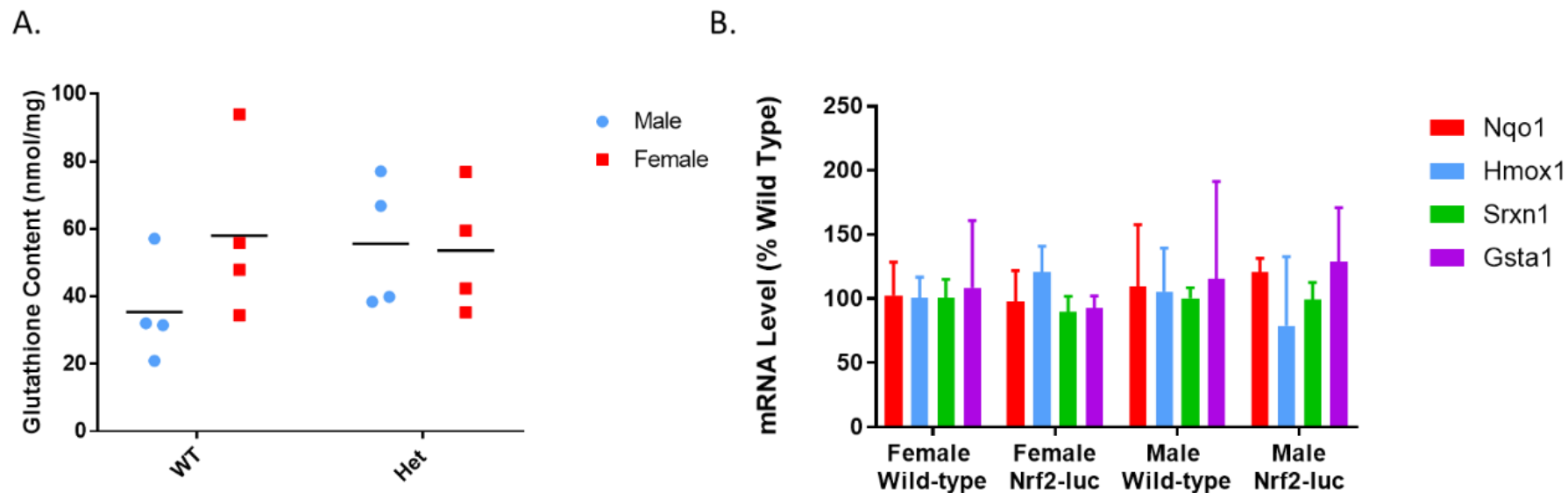


**Figure 2.2 Basal expression of glutathione and Nrf2 pathway activity in Nrf2-Luc mice.**

Wild type (WT) and heterozygote (Het) Nrf2-Luc mice were culled with a rising concentration of CO<sub>2</sub> (n=4) (A) Hepatic glutathione (GSH) levels were quantified and showed no significant difference between genotypes and sex via unpaired t-test. (B) Basal hepatic activity of the Nrf2-pathway was quantified by qPCR. No significant differences between WT and Het mice for each gender were calculated by one-way ANOVA.

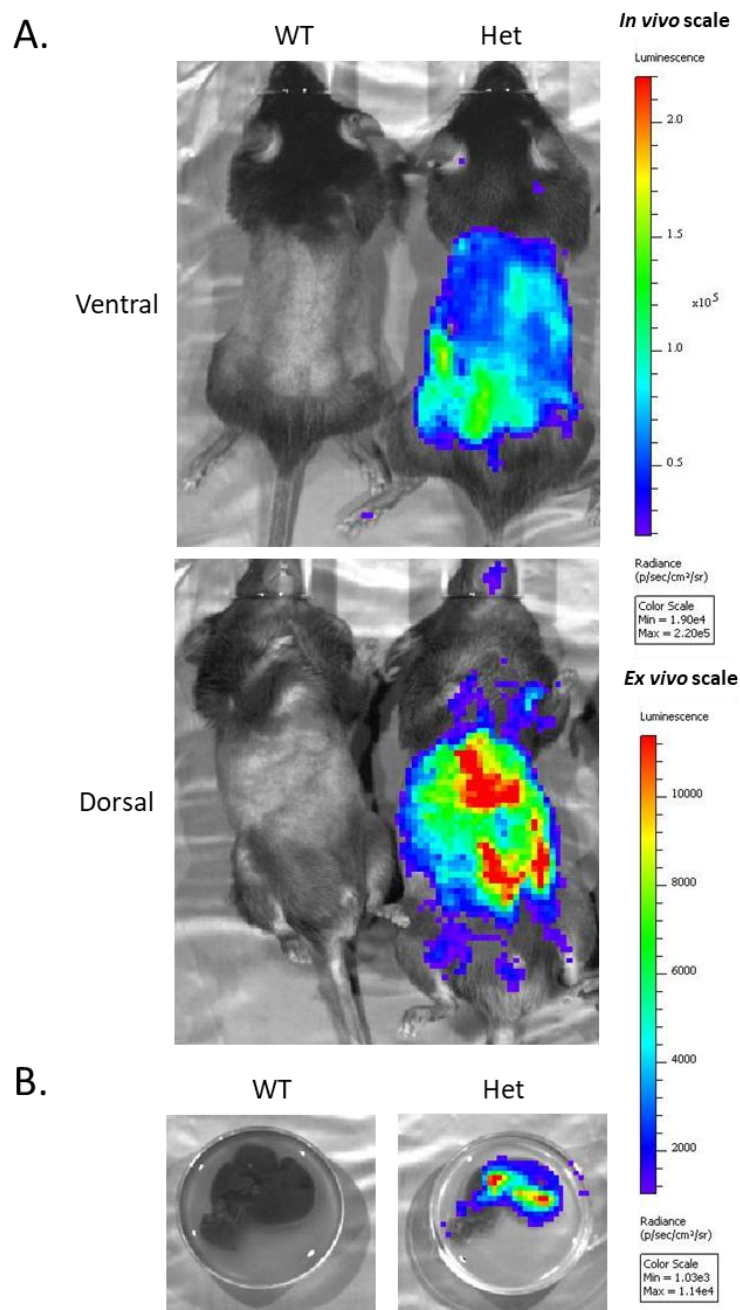


**Figure 2.3 *In* and *ex vivo* bioluminescence of Nrf2-Luc mice exposed to Sodium Arsenite (13 mg/kg).**

(A) Male wild-type (WT) and heterozygous Nrf2-Luc mice (Het) ( $n=1$ ) were exposed to 13 mg/kg sodium arsenite (ASN) by IP injection and their bioluminescence observed after 6 h using the IVIS spectrum. The liver from each mouse was excised and incubated in luciferin solution (150  $\mu\text{g/ml}$  in PBS) for 2 min. (B) *Ex vivo* signal was quantified.



### 2.3.2. Response to APAP toxicity in wild type C57BL/6J mice

Firstly, the dose and time needed to induce APAP toxicity in wild type mice of a similar background to the Nrf2-Luc mice (C57BL/6J) were determined. Male wild type mice were treated with a single dose of APAP (300 mg/kg) or with 0.9 % saline and five mice culled at either 2, 6, 24 or 48 h. One mouse, within the 48 h treatment group had to be culled at 8 h due to surpassing the severity threshold of the procedure. Data from this mouse was excluded from further analysis. Classical biomarkers of liver injury were monitored including serum ALT and hepatic GSH levels.

In APAP-treated mice, serum ALT peaked after 24 h exposure to APAP and had decreased by 48 h (Fig 2.4). ALT levels were significantly different to the 0 h treatment group at 6 and 24 h after exposure to APAP (both  $p < 0.0001$ ). Serum ALT levels in the 6 h saline treatment group were not elevated.

Glutathione content in the liver was rapidly depleted 2 h following exposure to APAP (Fig 2.5). Subsequent recovery of hepatic GSH content was observed between 6 and 48 h to levels similar to the saline 6 h treatment group. The 0 h treatment group GSH content significantly differed from the 2, 24 and 48 h APAP-treatment groups ( $P = 0.027$ ,  $0.033$  and  $0.026$  respectively). The 6 h saline-treatment group was also significantly different to the 0 h group ( $P = 0.0032$ ).

Gene and protein expression in the livers of wild-type mice were assessed for Nrf2 pathway activity. Upregulation of Nrf2-regulated were evident after as little as 2 h exposure to APAP (Fig 2.6 A). *Hmox1*, *Gsta1*, *Srxn1* and *Nqo1* activity peaked at 6h though extent of induction varied between genes. *Hmox1* induction at 2 and 6 h was significantly different to *Hmox1* activity in the 0 h treatment group (both  $p < 0.0001$ ). *Gsta1* and *Srxn1* activity was significantly increased at all time-points when compared to the gene activity at 0 h. Gene activity in the 6 h Saline-treated group did not differ from 0 h. However, all genes measured at 6 h were significantly elevated compared to the 6 h saline treatment group (*Hmox1* =  $p < 0.0001$ , *Gsta1* =  $p 0.0025$ , *Srxn1* =  $p < 0.0001$ , and *Nqo1* =  $p < 0.0001$ ). *Hmox1* protein expression peaked at 24 h and was significantly different at 6, 24 and 48 h compared to the 0 h treatment group (All  $p < 0.0001$ ) (Fig 2.6 B and C). When compared to the 6 h saline group, *Hmox1* protein expression was significantly greater in the 6 h APAP treatment group ( $P = 0.0051$ ).

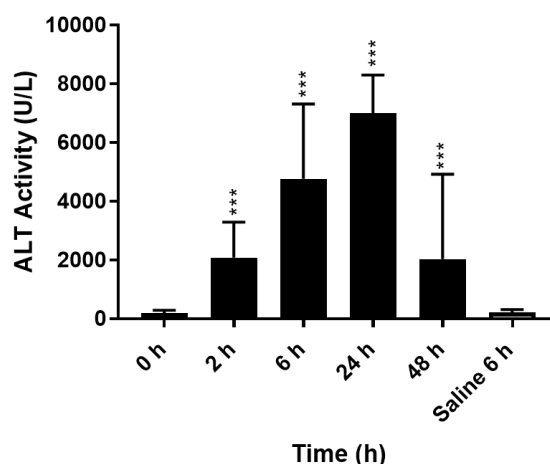


**Figure 2.4 Elevated serum alanine transaminase in wild-type mice exposed to a single dose of APAP (300 mg/kg).**

C57BL/6J wild-type mice (n=4) were exposed to a single dose of APAP or 0.9 % saline via IP injection. Blood was collected at 0, 2, 6, 24 and 48 h by cardiac puncture. ALT levels were significantly different at 2, 6 and 24 h compared to the 0 h treatment group, using Kruskal Wallis (\*\*P  $\leq$  0.01 and \*\*\* P  $\leq$  0.001).

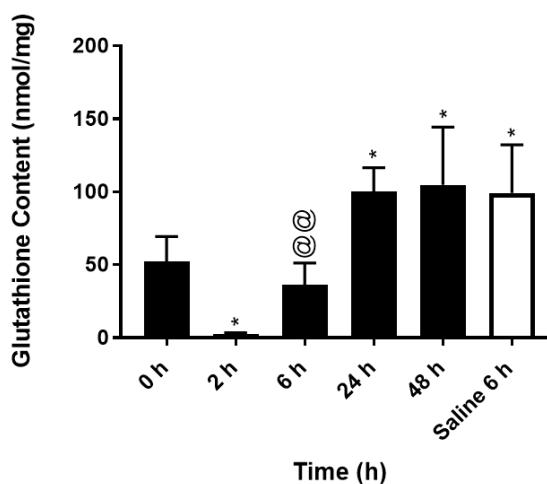


**Figure 2.5 Glutathione depletion in wild-type mice exposed to a single dose of paracetamol (300 mg/kg).** C57BL/6J wild-type mice (n=4) were exposed to a single dose of APAP or 0.9 % saline via IP injection. Mice were culled at either 0, 2, 6 24 or 48 h. GSH was quantified from liver lysates. GSH levels were significantly different when compared to 0 h treatment group, using one-way ANOVA (\* P  $\leq$  0.05).

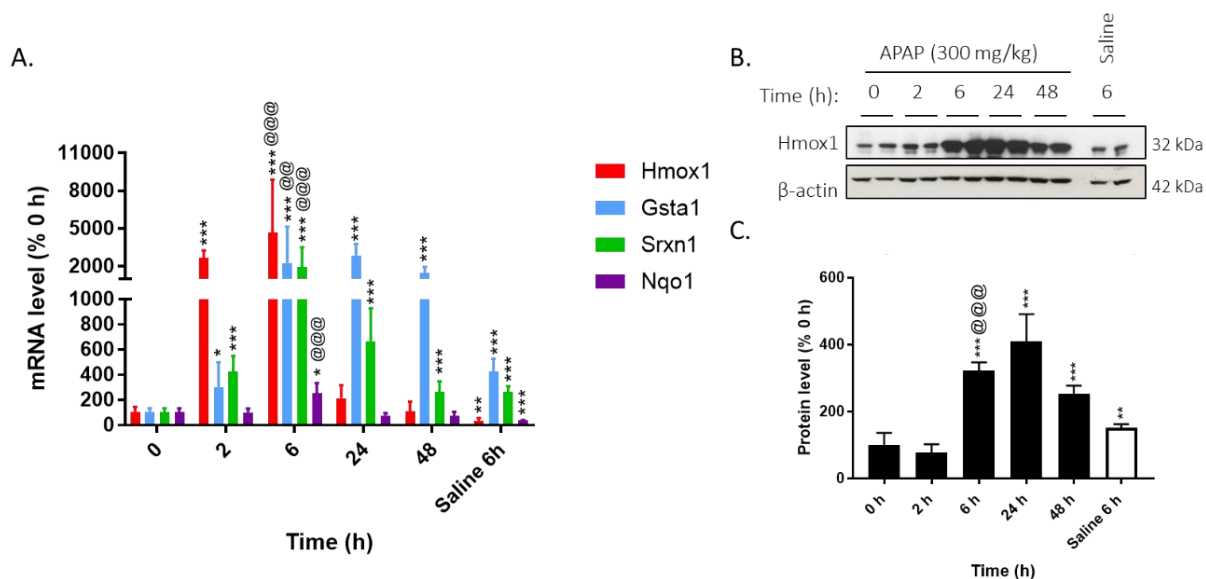


**Figure 2.6 Upregulation of the Nrf2-pathway in wild-type mice exposed to a single dose of paracetamol (300 mg/kg).**

(A) qPCR analysis of expression of Nrf2-target genes in the livers of wild-type C57BL/6J mice (n=4) exposed to APAP (300 mg/kg) or 0.9 % saline via IP injection (n=4). (B) Western blot for Haem oxygenase 1 (Hmox1) of **representative liver lysates** from 0, 2, 6, 24 and 48 h exposure. (C) Densitometry of immunoblotting from **all liver lysates (n=4)**. Significant difference in gene and protein expression 6h compared to 0 h treatment group was calculated by Kruskal Wallis (\*  $P \leq 0.05$ , \*\* $P \leq 0.01$  and \*\*\*  $P \leq 0.001$ ) or compared to the 6 h saline treatment group (@@  $P \leq 0.01$  and @@@  $P \leq 0.001$ ).

### 2.3.3. Nrf2-Luc respond to APAP toxicity

Nrf2-Luc mice were exposed to the hepatotoxin APAP as a model of drug induced liver injury. A dose of 300 mg/kg had been shown to induce toxicity and activate Nrf2 signalling over 24 h (See 2.3.2). Therefore, a similar dose and time course was used with male and female Nrf2-Luc mice. In both cases, serum ALT levels were significantly higher than in the saline treatment group after 24 h exposure to APAP ( $P = 0.0079$  and  $0.0002$  respectively) (Fig 2.7).

*In vivo* bioluminescence was quantified at 2, 6 and 24 h following exposure to 300 mg/kg APAP or 0.9 % Saline. In males, a strong bioluminescent signal within the region of the liver was seen after 6 h (Fig 2.8). However, the signal strength varied between individuals. Two of the APAP treated-mice had a strong signal in the liver region that peaked at 6 h and had reduced by 24 h. In one mouse the signal peaked in the liver region at 24 h, while two mice failed to show strong luminescence for the duration of the study. Additionally, low levels of bioluminescence were present in two saline-treated mice. This signal localised to the lungs and lymph node areas and was not present in the liver region.

*Ex vivo* analysis highlighted the liver-specific signal of the male APAP treated mice after 24 h exposure (Fig 2.9 A). Significantly different bioluminescence between saline and APAP – treated mice was observed in the liver ( $P = 0.0079$ ) but not the liver or kidneys (Fig 2.9 B). In three of the mice treated with APAP, there was low bioluminescence in the lungs. This signal was also present in one of the saline-treated mice suggesting that this may be caused by the anaesthetic.

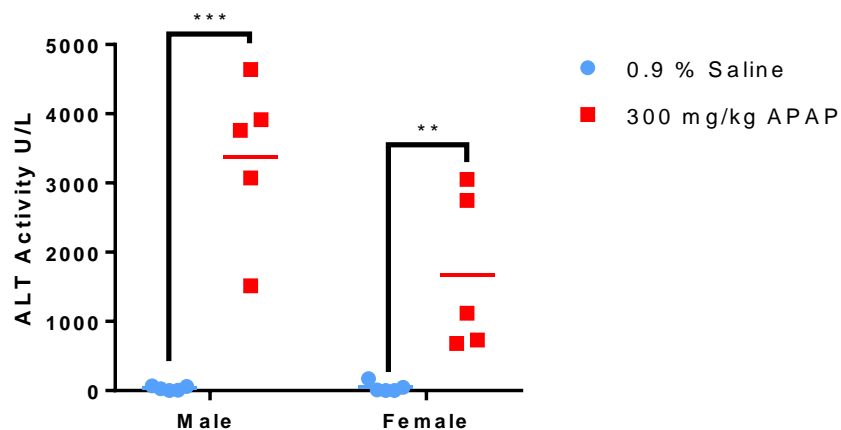


**Figure 2.7 Serum alanine transaminase significantly elevated in male and female Nrf2-Luc mice exposed to paracetamol (300 mg/kg)**

Serum ALT levels were significantly increased in both male and female heterozygous Nrf2-Luc mice 24 h after exposure to a single dose of APAP (300 mg/kg) compared to the saline treatment group (\*\*P  $\leq$  0.01 and \*\*\* P  $\leq$  0.001). Significance was calculated by Mann-Whitney U-test.

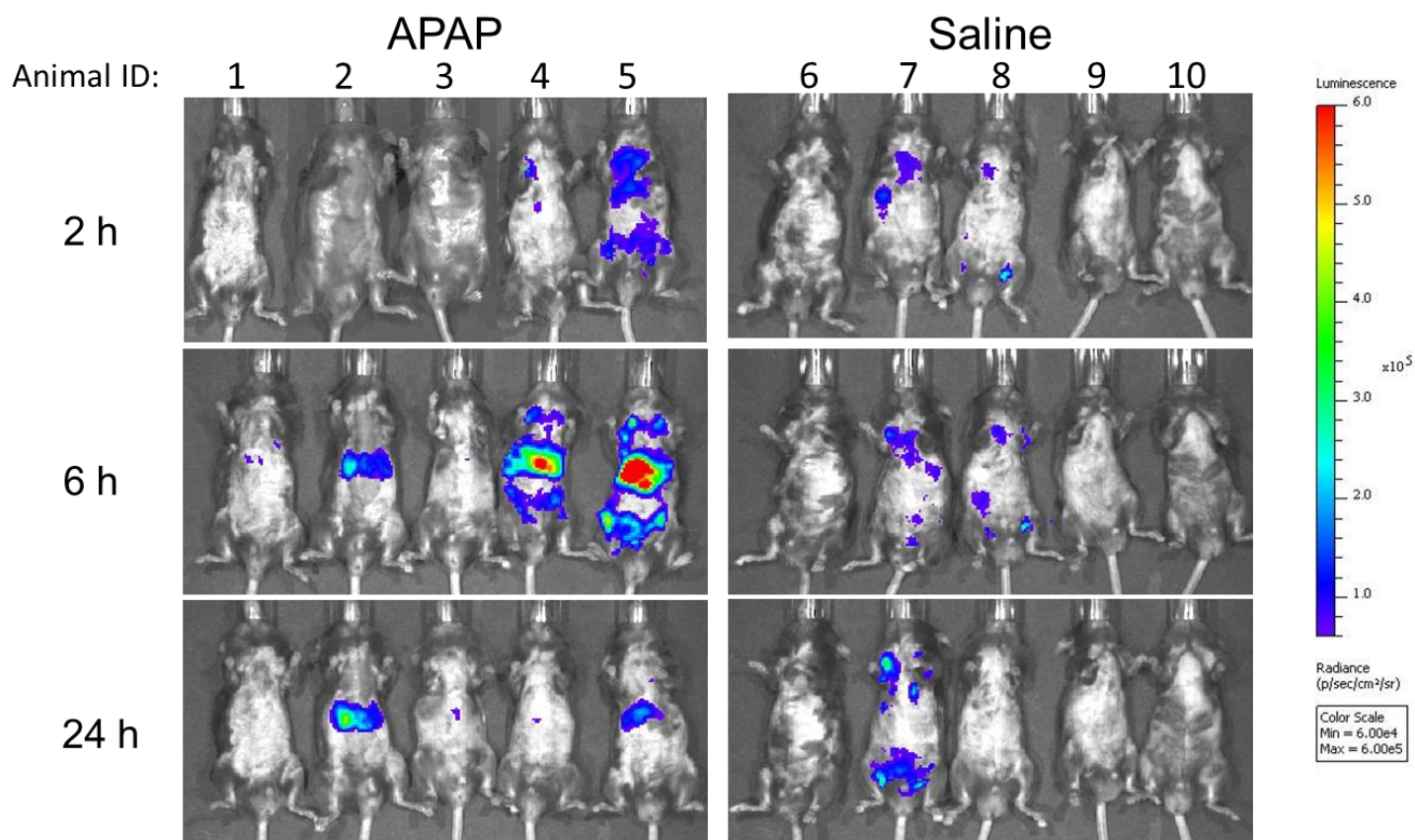


**Figure 2.8 In vivo bioluminescence induced in male Nrf2-Luc mice exposed to paracetamol (300 mg/kg)**

Male heterozygous mice (n=5) were exposed to a single dose of APAP (300 mg/kg) or 0.9 % Saline via IP injection and their bioluminescence observed at 2, 6 and 24 h using the IVIS spectrum.

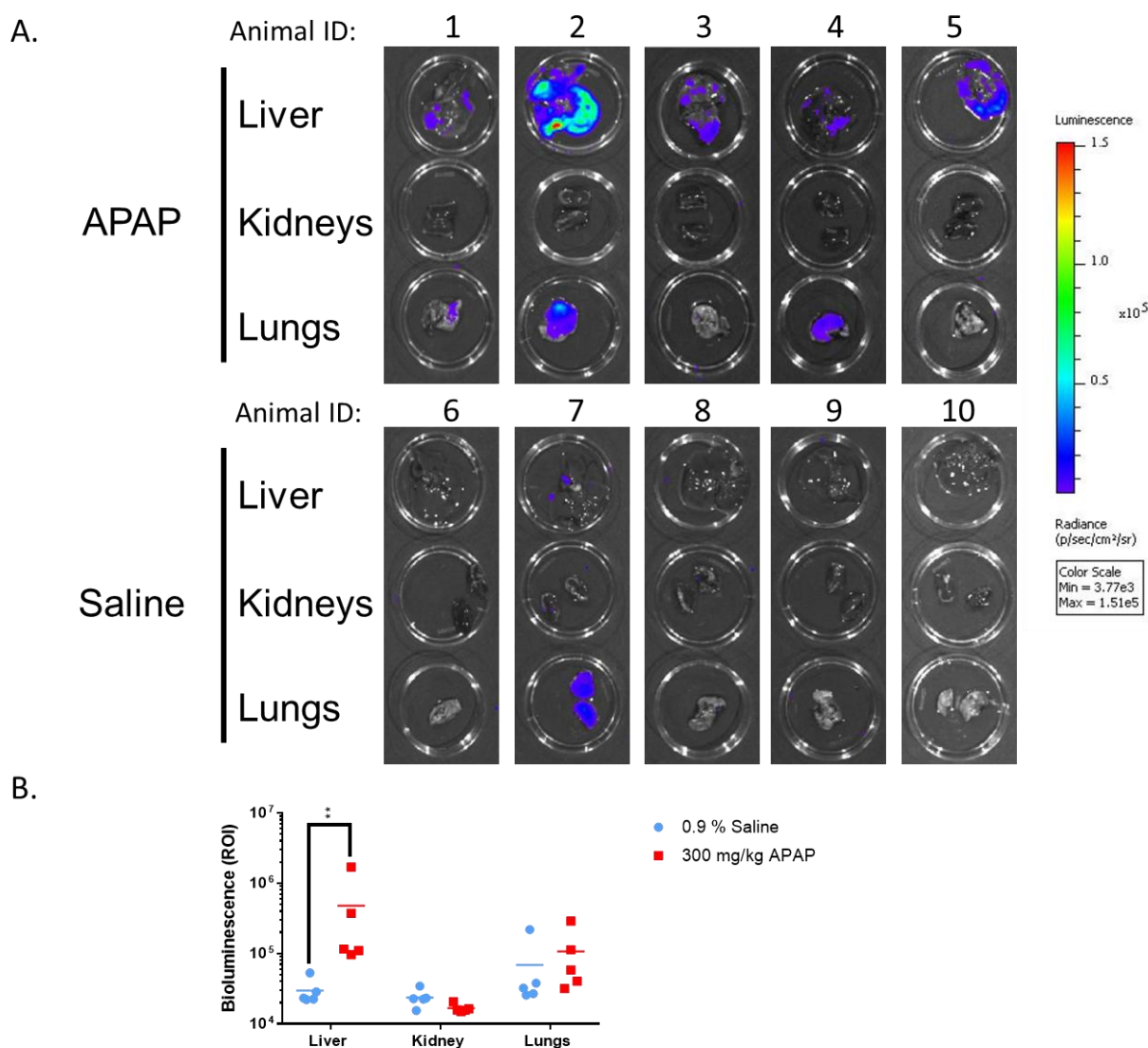


**Figure 2.9 *Ex vivo* bioluminescence induced in male *Nrf2*-Luc mice exposed to paracetamol (300 mg/kg)**

Male heterozygous mice exposed to a single dose of APAP (300 mg/kg) or 0.9 % saline via IP injection were culled after 24 h (n=5). The liver, kidney and lung from each mouse was excised and incubated in luciferin solution (150  $\mu$ g/ml in PBS) for 2 min. (A) Bioluminescence was quantified using the IVIS spectrum. (B) Region of interest (ROI) values were calculated within each petri dish, with significantly greater bioluminescence in the livers from the APAP treatment group when compared to the saline treatment group (\*\*  $P \leq 0.01$ ). This was calculated by Mann Whitney U test.

Females exhibited a more consistent and stronger bioluminescent signal following exposure to APAP, compared to the male mice (Fig 2.10). Bioluminescence almost exclusively from the liver region was evident after 6 h and in most mice peaked at 24 h, though a substantial signal in one mouse peaked at 6 h. No bioluminescence was present in the saline treatment group for the duration of the experiment.

A stronger *ex vivo* signal was detected in female APAP-treated mice, than in males (Fig 2.11 A). Bioluminescence was present in all livers of the APAP treatment group and was significantly greater than those from the saline-treated mice (Fig 2.11 B) ( $P = 0.0079$ ). The lungs of two APAP-treated mice also had signal resulting in significantly greater bioluminescence in the lungs from the APAP treatment group when compared to mice treated with saline ( $P = 0.317$ ). No bioluminescence was present in the organs of the saline treatment group similar to the *in vivo* analysis.

Significant correlation between ALT and bioluminescence was observed in both male (Fig 2.12 A) and female (Fig 2.12 B) APAP-exposure studies. However, ALT values were higher and more variable in the APAP-treated male mice when compared to their female counterparts.



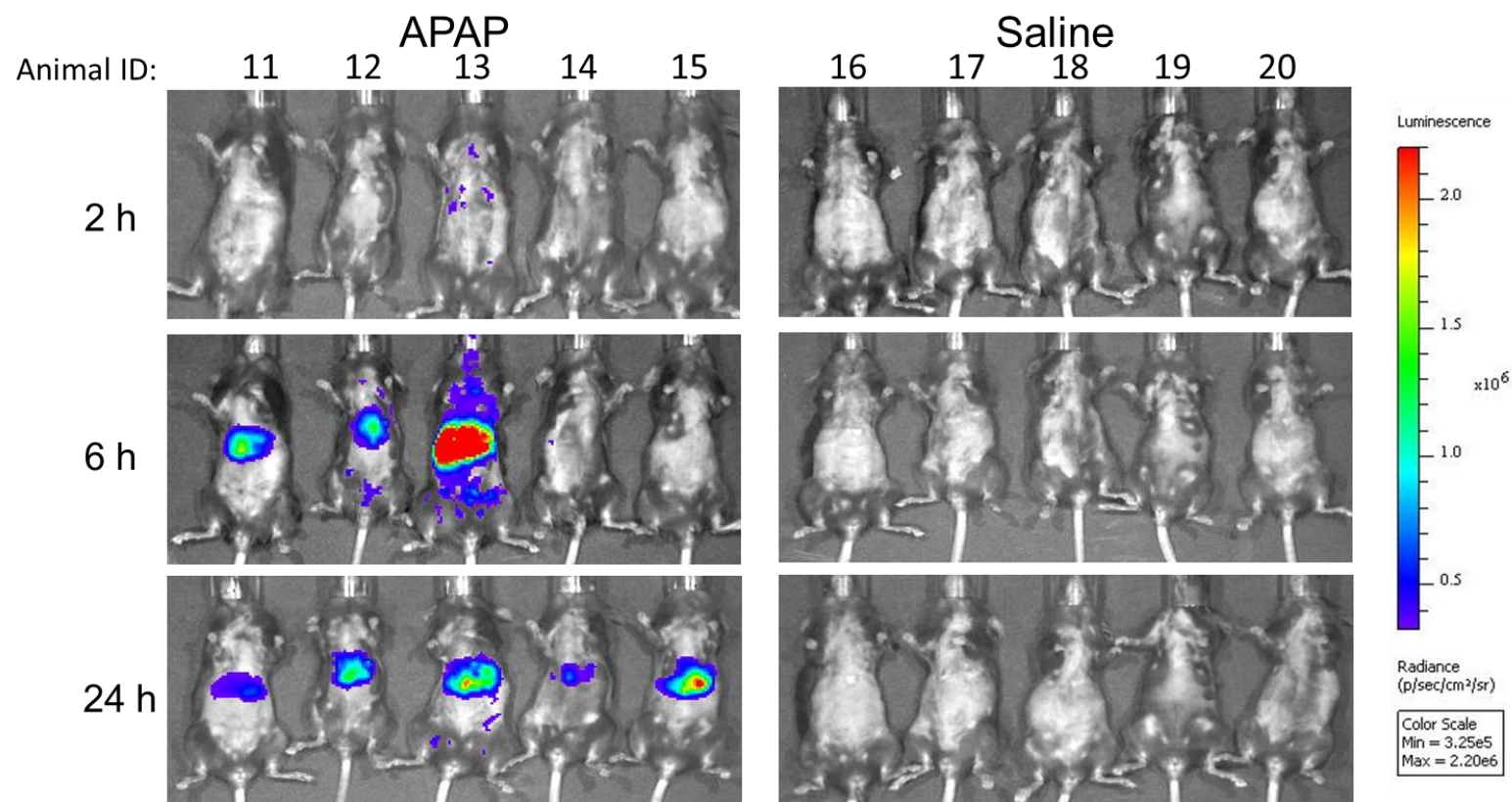


**Figure 2.10 *In vivo* bioluminescence induced in female Nrf2-Luc mice exposed to paracetamol (300 mg/kg)**

Female heterozygous mice were exposed to a single dose of acetaminophen (APAP) (300 mg/kg) or 0.9 % Saline via IP injection (n=5). (A) Bioluminescence was observed at 2, 6 and 24 h using the IVIS spectrum.

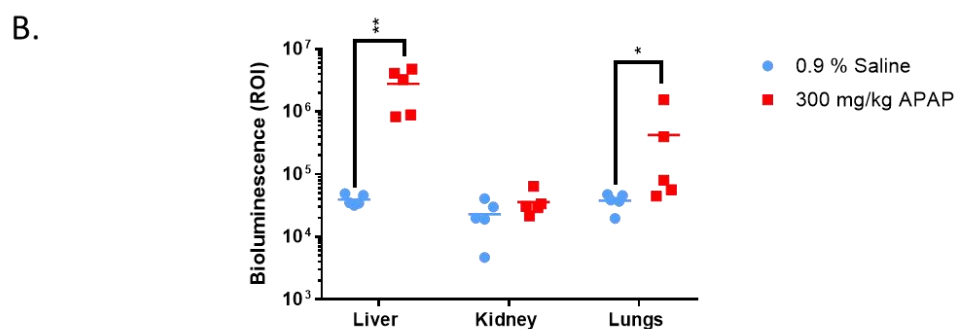
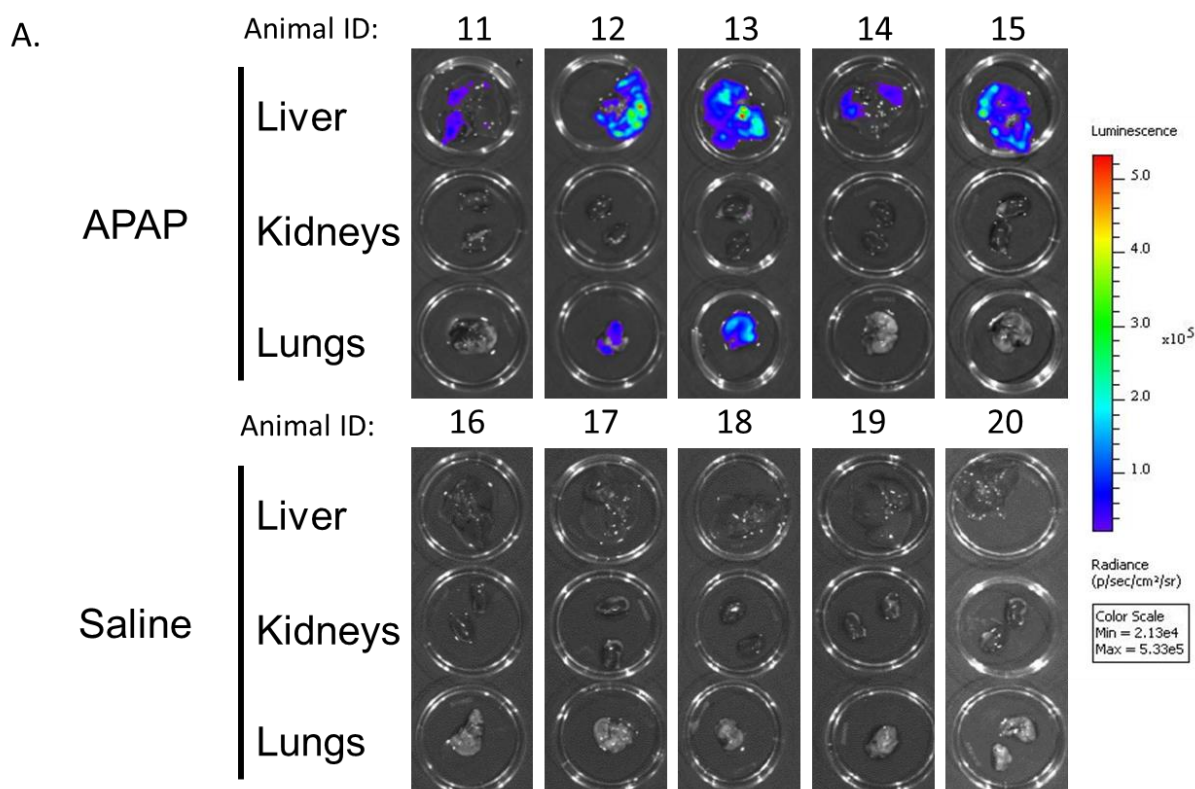


**Figure 2.11 *Ex vivo* bioluminescence induced in female *Nrf2*-Luc mice exposed to paracetamol (300 mg/kg)**

Female heterozygous mice exposed to a single dose of acetaminophen (APAP) (300 mg/kg) or 0.9 % saline via IP injection were culled after 24 h. The liver and kidney from each mouse was dissected and incubated in luciferin solution (150  $\mu$ g/ml in PBS) for 2 min. Bioluminescence was quantified using the IVIS spectrum (n=5). (A) Bioluminescence was observed using the IVIS spectrum. (B) Region of interest (ROI) values were calculated with no significant difference between bioluminescence in livers from the APAP and Saline treatment groups (\*  $p \leq 0.05$  and \*\*  $P \leq 0.01$ ). This was calculated by Mann Whitney U test.

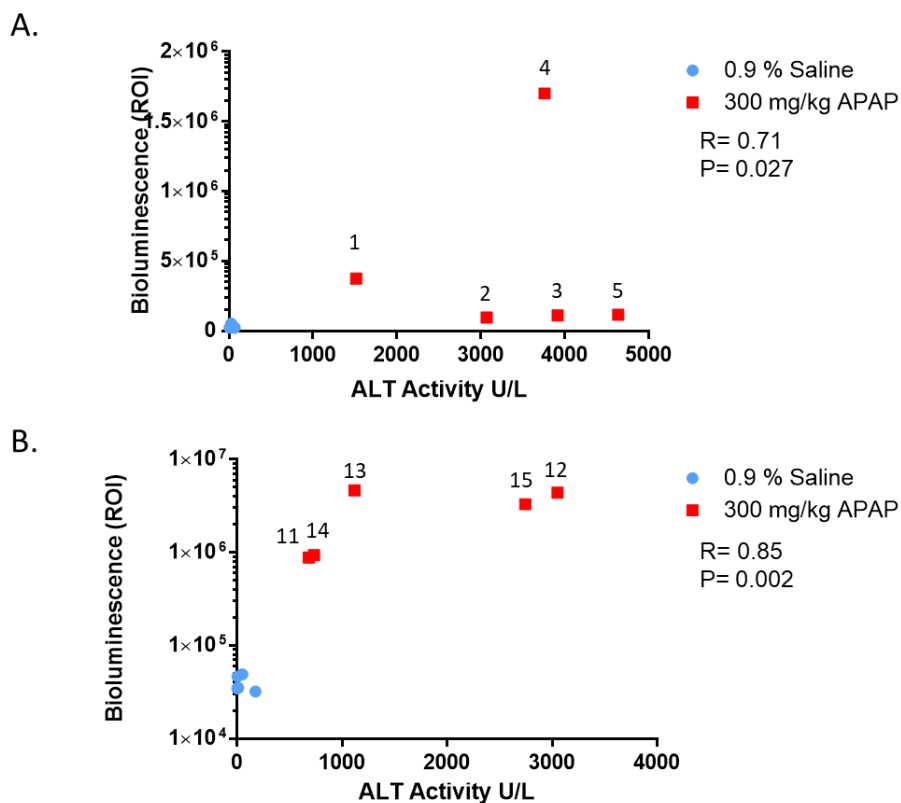


**Figure 2.12 Serum alanine transaminase and *ex vivo* bioluminescence in male and female Nrf2-Luc mice exposed to paracetamol (300 mg/kg)**

(A) *Ex vivo* bioluminescence in the region of interest (ROI) of the livers from the male mice compared to serum ALT levels at 24 h. (B) ROI and ALT values from female mice (n=5). APAP treatment groups labelled with animal ID numbers. Statistical analysis was performed using Pearson's R test (\*  $p \leq 0.05$  and \*\*  $P \leq 0.01$ ).

Extensive liver damage was also evident following histological analysis of the APAP-treated mice. In males, large areas of necrosis were present around the portal vein (Fig 2.13 A). Luciferase and Hmox1 staining also localised to this pericentral area. Four out of the five APAP-treated mice had a DILI score of 2 (Fig 2.13 B) indicative of moderate hepatocyte loss from the central to midzonal region (Table 2.2). Luciferase and Hmox1 staining was not present in the male saline-treated mice. Matched ALT scores were between 1627.7 – 3797.7 U/L.

In comparison to males, necrosis was muted in the female APAP-treated mice (Fig 2.14 A). Although, Luciferase and Hmox1 staining followed a similar pattern to the male APAP-treated mice. DILI scores were lower than males with three out of the five mice assigned a DILI score of 1 (Fig 2.14 B). This is indicative of mild necrosis restricted to the pericentral region in less than 25 % of the hepatic lobules. One female APAP-treated mouse had a DILI score of 0, despite exhibiting the greatest bioluminescent signal at 6 h (Fig 2.10 A). Consistent with the DILI scores, ALT levels were lower in the female mice compared to the male APAP-treated mice, ranging between 682.4 – 3055 U/L.

As the females responded in a more consistent manner, they were used for further analysis of endogenous Nrf2 pathway responses to APAP. In female mice, all the Nrf2-regulated genes measured in the livers of the mice from the APAP treatment group were significantly elevated compared to the saline treatment group after 24 h (Fig 2.15 A). At the protein level, Hmox1 was significantly induced in the APAP group ( $P = 0.0079$ ) but not Nqo1 ( $P = 0.54$ ) (Fig 2.15 B and C).

Finally, assessment of renal and hepatic Nrf2 pathway activation in wild-type mice highlighted the significantly greater perturbation of endogenous Nrf2-regulated genes in the liver, compared to the kidneys of APAP-treated mice (Fig 2.16). This data consolidates the liver-specific induction of the endogenous Nrf2 pathway alongside the bioluminescent reporter in response to a hepatotoxic dose of APAP.

A. Saline

APAP

Animal ID: 7

1

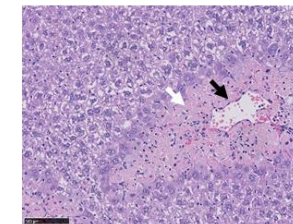
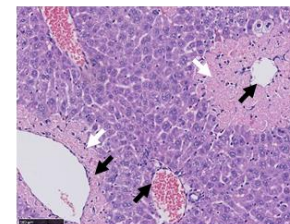
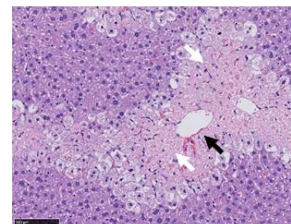
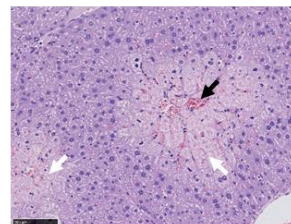
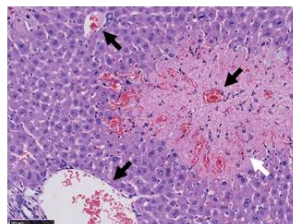
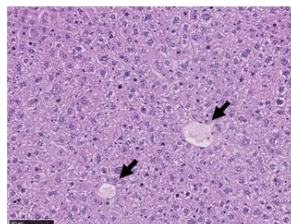
2

3

4

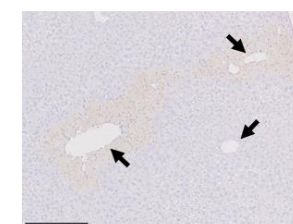
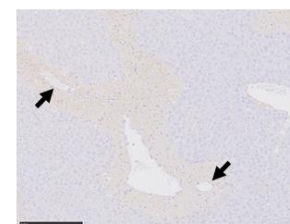
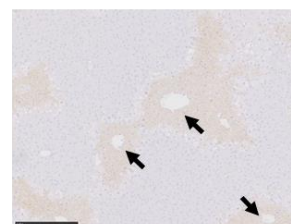
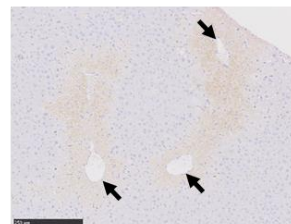
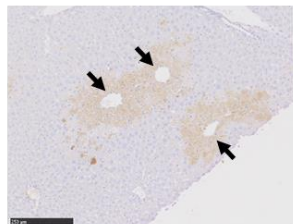
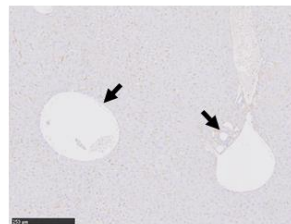
5

H&E



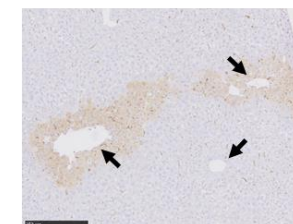
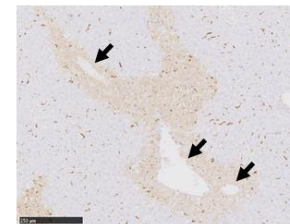
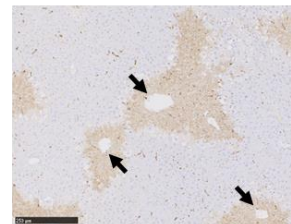
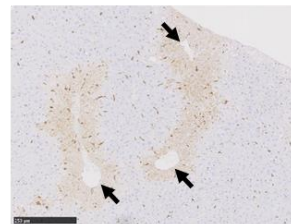
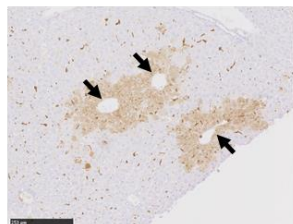
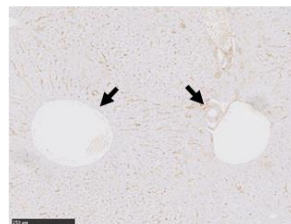
(scale = 100 μm)

Luciferase



(scale = 250 μm)

Hmox1



(scale = 250 μm)

**B.**

	Saline	APAP				
DILI Score	0	2	2	2	2	1-3
ALT (U/L)	0.8	2937.6	3247.2	3797.7	3446.7	1627.7

**Figure 2.13 Immunohistochemistry of livers from male Nrf2-Luc mice exposed to paracetamol (300 mg/kg)**

(A) Sections of liver tissue from male mice exposed to a single dose of 300 mg/kg APAP or 0.9 % Saline for 24 h were stained with H&E and probed for Luciferase and Hmox1 (n=5). Substantial necrosis surrounding the portal vein (black arrow) is shown in the light pink staining of the H&E treated sections (white arrow) from livers exposed to APAP but not saline. (B) Extent of necrosis is proportional to drug induced liver injury (DILI) score and alanine transaminase (ALT) levels.



**B.**

	Saline	APAP				
DILI Score	0	1	2(-3)	0	1	1(-2)
ALT (U/L)	10.3	682.4	3053.0	1117.9	732.8	2746.2

**Figure 2.12 Immunohistochemistry of livers from female Nrf2-Luc mice exposed to paracetamol (300 mg/kg)**

(A) Sections of liver tissue from female mice exposed to a single dose of 300 mg/kg APAP or 0.9 % Saline for 24 h were stained with H&E and probed for Luciferase and Hmox1 (n=5). Substantial necrosis surrounding the portal vein (black arrow) is shown in the light pink staining of the H&E treated sections (white arrow) from livers exposed to APAP but not saline. (B) Extent of necrosis is proportional to drug induced liver injury (DILI) score and alanine transaminase (ALT) levels.



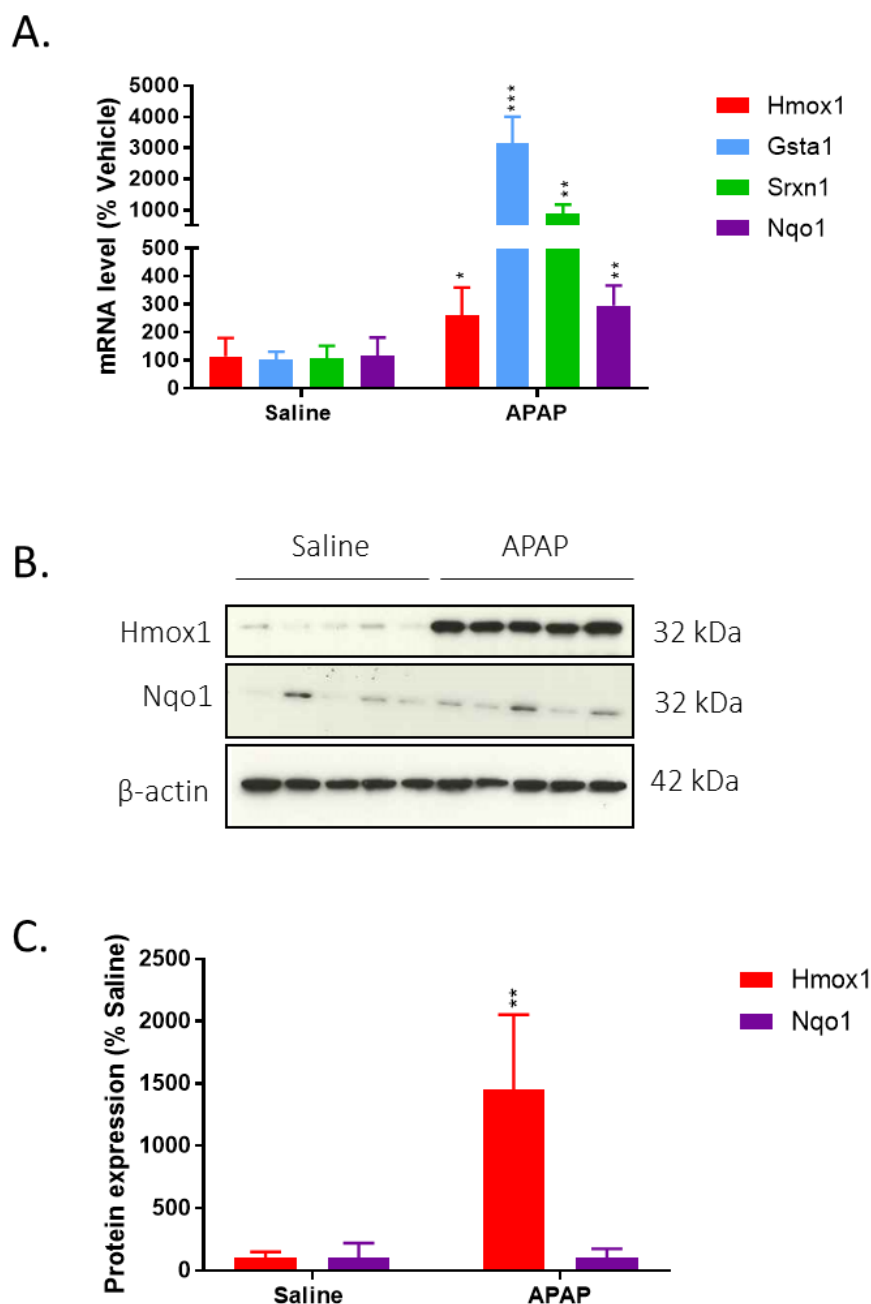


**Figure 2.15 Nrf2-Luc signal corresponds with upregulation of the Nrf2 pathway in livers of female Nrf2-Luc mice exposed to paracetamol (300 mg/kg)**

(A) qPCR analysis of the livers from female mice exposed to either 0.9 % Saline or 300 mg/kg APAP for 24 h highlighted induction of Nrf2-regulated genes (n=5). Significant induction compared to saline treatment group was calculated by Unpaired T test. (B) Western blots of Nrf2-regulated protein expression and (C) densitometry in these livers also highlighted significant induction of Hmox1 but not Nqo1, calculated by Mann Whitney U test (\*  $p \leq 0.05$ , \*\* $P \leq 0.01$  and \*\*\*  $P \leq 0.001$ ).

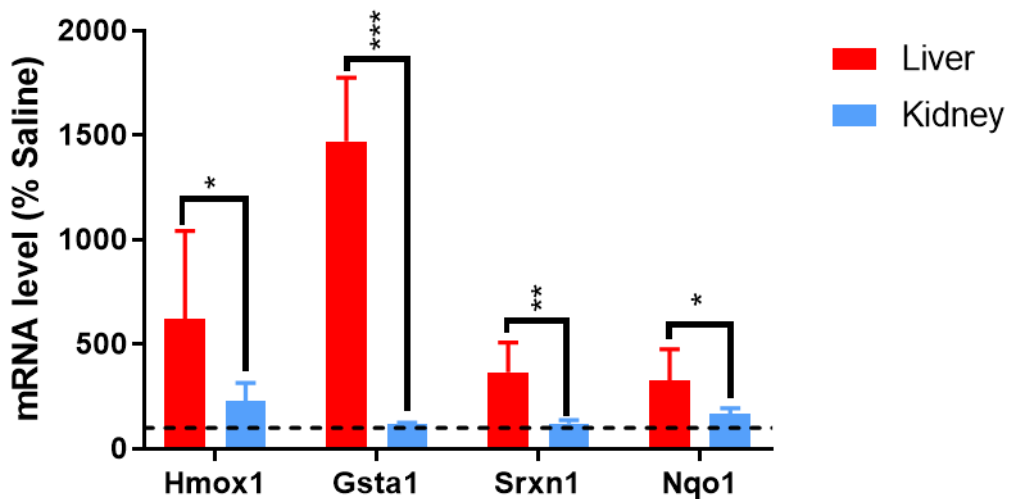


**Figure 2.16 Endogenous Nrf2 pathway activity in the livers and kidneys of wild-type mice exposed to paracetamol (300 mg/kg)**

qPCR analysis of the liver and kidneys from male wild-type mice (n=5) exposed to either 0.9 % Saline or 300 mg/kg APAP for 24 h. Significant induction of hepatic Nrf2 pathway compared to renal gene expression was calculated by Unpaired T test (\*  $p \leq 0.05$ , \*\*  $P \leq 0.01$  and \*\*\*  $P \leq 0.001$ ) (Dotted line = 100 %).

#### 2.3.4. Nrf2-Luc mice respond to cisplatin toxicity

In order to assess the response to other forms of drug-induced organ toxicity, the Nrf2-Luc mice were exposed to the nephrotoxin cisplatin under conditions previously shown to activate Nrf2 signalling in renal tissue (Miyagi et al., 2014). Female Nrf2-Luc mice were used due to the stronger bioluminescent response they displayed to paracetamol toxicity. Following 96 h exposure to cisplatin, serum BUN levels were significantly elevated when compared to their saline-treated counterparts ( $P = 0.0007$ ) (Fig 2.17).

Bioluminescence in the cisplatin-treated mice localised to the kidney region after 72 h (Fig 2.18). The strength of the signal varied between individuals and was also hampered by the skin pigmentation of the mice. Large black 'moles', typically observed in C57BL/6J mice (Curtis et al., 2011), inhibited the signal resulting in partial luminescence in some mice. In the saline treatment group, no signal was observed in the kidney region. However, low levels of luminescence were present at the base of the neck in two of the four mice. This signal intensity faded through the course of the experiment.

In light of the interference from skin pigmentation in some mice, it was particularly important to perform *ex vivo* imaging of relevant organs. *Ex vivo* signal was specific to the kidneys in all four mice treated with cisplatin (Fig 2.19 A). No signal was present in the livers of the mice from either treatment group. There was a significant difference between the kidney bioluminescence in cisplatin and saline treated mice, at 96 h ( $P = 0.023$ ) (Fig. 2.19 B). In comparison with matched BUN levels, *ex vivo* bioluminescence at 96 h significantly differed between the cisplatin and saline treatment groups (Fig 2.20).

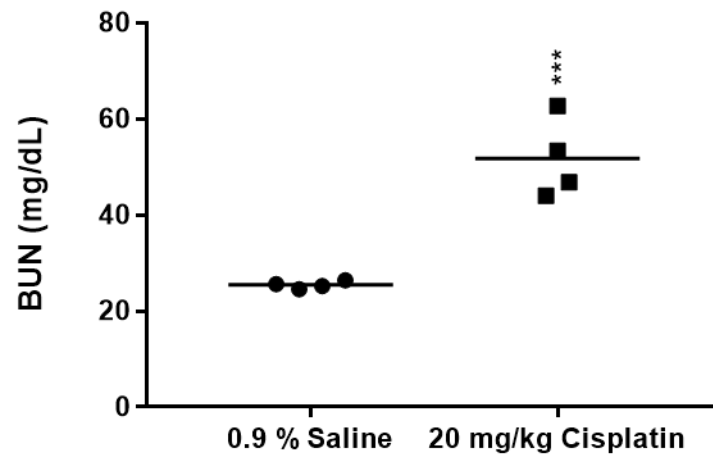


**Figure 2.17 Serum blood urea nitrogen significantly elevated in female Nrf2-Luc mice exposed to cisplatin (20 mg/kg)**

Serum blood urea nitrogen (BUN) levels were significantly higher in the Nrf2-Luc mice treated with a single dose of cisplatin (20 mg/kg) than those treated with 0.9 % saline after 96 h (n=4) (\*\*\*)  $P \leq 0.001$ ), by Unpaired T test.

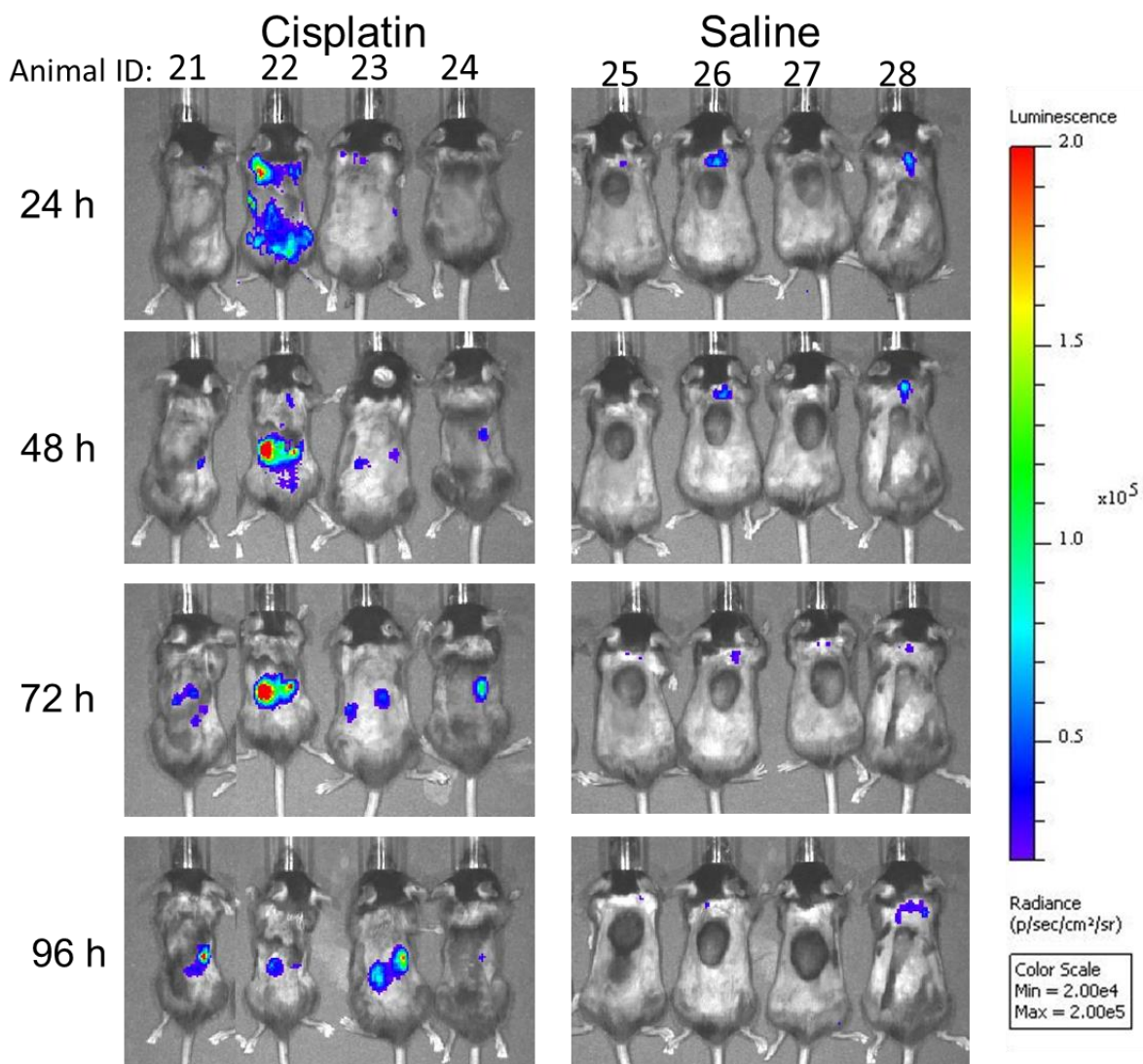


**Figure 2.18 *In vivo* bioluminescence induced in female Nrf2-Luc mice exposed to Cisplatin (20 mg/kg)**

Female heterozygous Nrf2-Luc mice were exposed to a single dose of Cisplatin (20 mg/kg) or 0.9 % Saline via IP injection and their bioluminescence observed at 24, 48, 72 and 96 h using the IVIS spectrum (n=4).

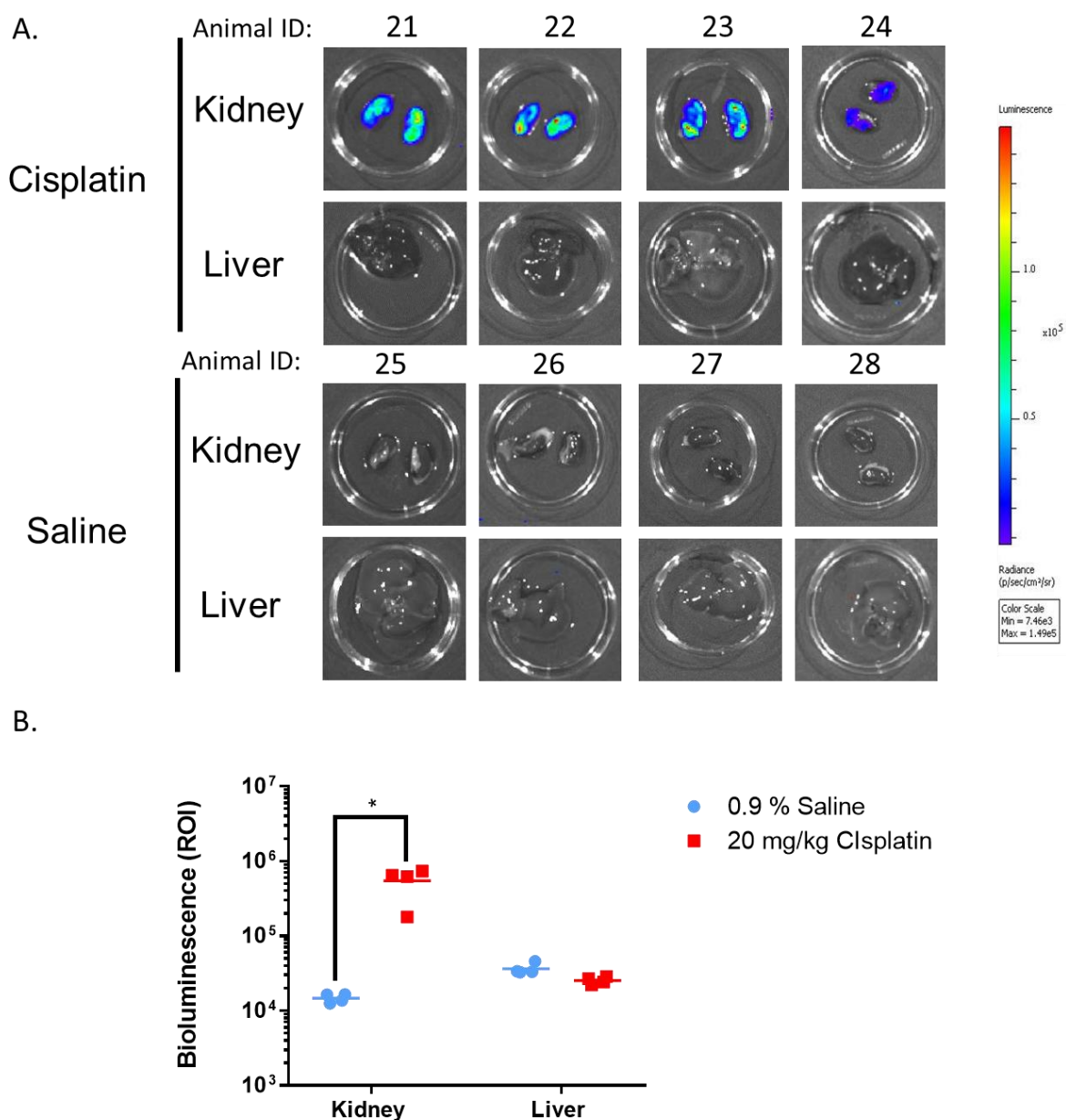


**Figure 2.19 Ex vivo bioluminescence induced in female Nrf2-Luc mice exposed to Cisplatin (20 mg/kg)**

Female heterozygous mice exposed to a single dose of Cisplatin (20 mg/kg) or 0.9 % saline via IP injection were culled after 96 h. The liver and kidney from each mouse was dissected and incubated in luciferin solution (150  $\mu$ g/ml in PBS) for 2 min. (A) Ex vivo bioluminescence was quantified using the IVIS spectrum (n=4). (B) Bioluminescence of the kidneys were significantly increased in the cisplatin treatment group when compared to the saline-treated group (\*  $p \leq 0.05$ ) via Mann Whitney U test.

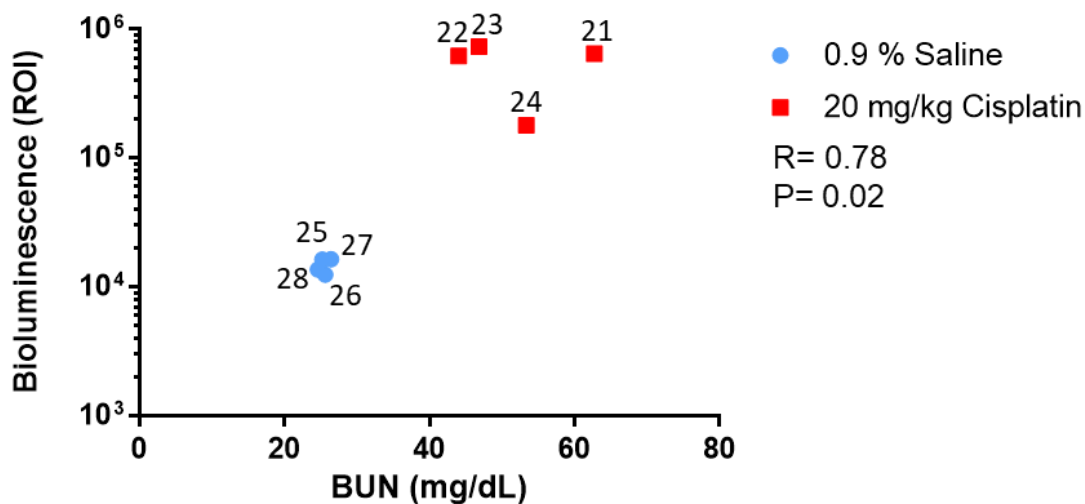


**Figure 2.20 Serum BUN and ex vivo bioluminescence in female Nrf2-Luc mice exposed to cisplatin (20 mg/kg)**

Comparison of serum BUN (blood urea nitrogen) levels obtained at 96 h with ex vivo bioluminescence in region of interest (ROI) of kidneys from female heterozygous mice ( $n=4$ ). Data points labelled with animal ID numbers. Statistical analysis was performed using Pearson's R test ( $* p \leq 0.05$ ).

Necrosis was evident in the proximal tubule region of kidneys from the cisplatin-treated mice (Fig 2.21 A). Hmox1 and luciferase staining co-localised to this region also. The extent of staining was proportional to the DIKI score and BUN values (Fig 2.21 B).

qPCR analysis of the kidneys from cisplatin-treated mice revealed only *Gsta1* expression was significantly upregulated in the cisplatin treatment group, when compared to the vehicle control group (Fig 2.22 A) ( $P = 0.28$ ). Renal Hmox1 was elevated at the protein level in kidneys of mice treated with cisplatin for 96 h although not significantly different to the saline treatment group (Fig 2.22 B and C) ( $P = 0.091$ ). Analysis of Nrf2-pathway activation in the livers of cisplatin-treated mice revealed no significant induction of Nrf2-regulated genes (Fig 2.23).





**B.**

	Saline	Cisplatin			
DIKI Score	0	2	2	3	2
BUN	25.2	62.7	44.0	46.8	53.4

**Figure 2.21 Immunohistochemistry of female Nrf2-Luc mice exposed to Cisplatin (20 mg/kg)**

Mice were culled after 96 h (n=4). (A) Sections of renal tissue were stained with H&E and probed for Luciferase and Hmox1. Luciferase and Hmox1 staining localised to the proximal tubule (black arrow). H&E staining shows significant damage in this region also. (B) Extent of necrosis is proportional to drug induced kidney injury (DIKI) score and blood urea nitrogen (BUN) levels.

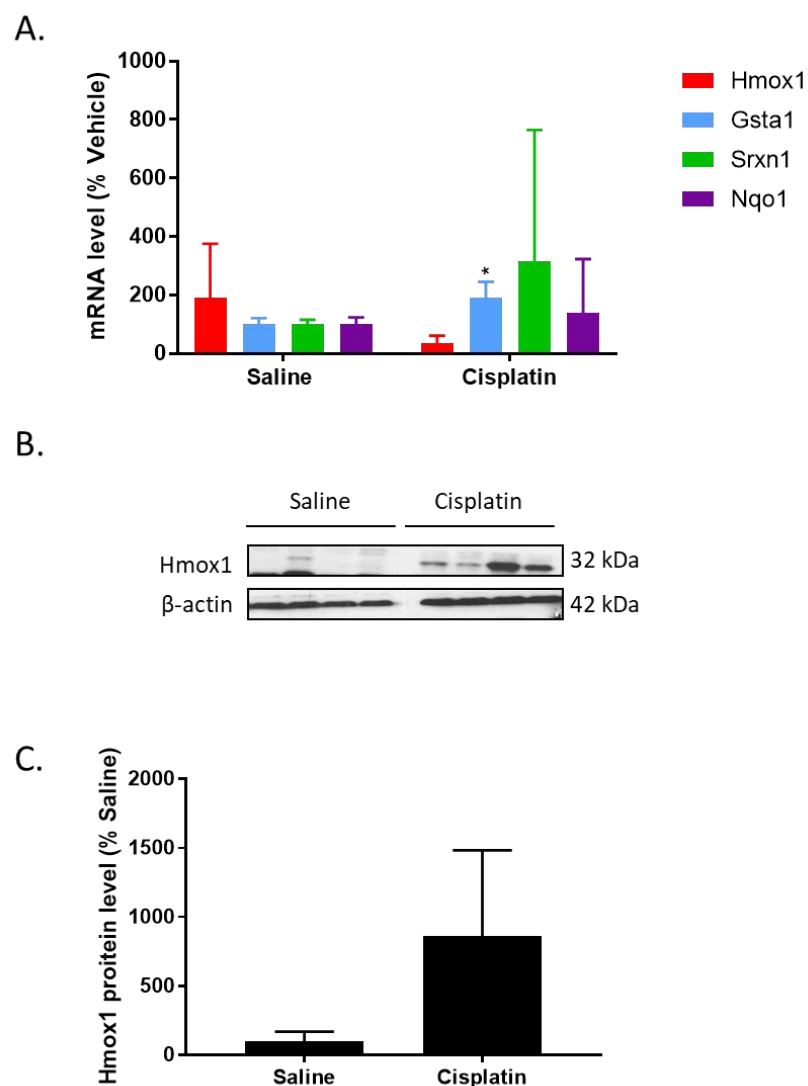


**Figure 2.22 Gene and protein expression in kidneys of female Nrf2-Luc mice exposed to Cisplatin (20 mg/kg)**

(A) qPCR analysis of the kidneys from female mice exposed to either 0.9 % saline or 20 mg/kg cisplatin for 96 h (n=4). Significant differences between saline and cisplatin treatment groups calculated by Mann Whitney U test (\*  $p \leq 0.05$ ). (B) Western blot for Haem oxygenase 1 (Hmox1) in liver lysates from 96 h exposure. (C) Densitometry of the Hmox1 protein expression was not significantly increased compared to saline-treated mice. This was calculated by Unpaired T Test.

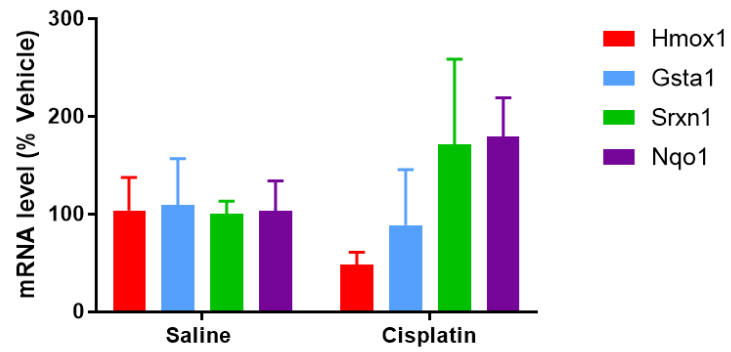


**Figure 2.23 Gene expression in livers of female Nrf2-Luc mice exposed to Cisplatin (20 mg/kg)**

qPCR analysis of the kidneys from female mice exposed to either 0.9 % saline or 20 mg/kg cisplatin for 96 h highlighted no significant induction of Nrf2-regulated genes by Student T-Test (n=4).

## 2.4. Discussion

Here, I have performed real-time, *in vivo* bioluminescence imaging of transgenic Nrf2-Luc mice to test the hypothesis that localised activation of Nrf2 represents a marker of chemical stress associated with organ-specific drug toxicity. Following exposure to APAP, upregulation of the hepatic Nrf2 pathway alongside classical markers of toxicity was observed in wild-type mice. A similar response was seen in Nrf2-Luc mice exposed to APAP, accompanied by liver-specific bioluminescence *in vivo* and *ex vivo*. The bioluminescent signal intensity correlated with serum ALT and degree of hepatic tissue damage. In response to cisplatin, Nrf2-Luc mice exhibited a kidney-specific bioluminescent signal *in vivo* and *ex vivo*, proportional to renal tissue damage that coincided with activation of the renal Nrf2 pathway. These findings further support the use of Nrf2 as a marker of chemical stress associated with drug toxicity and demonstrate the value of Nrf2-Luc mice for identifying localised stress responses through real-time *in vivo* bioluminescence imaging.

There is increasing interest in the value of stress response pathways as indicators of cellular perturbation that could lead to overt toxicity. This is emphasised by the integration of adaptive stress response pathways as vital components of adverse outcome pathways (AOPs) to clarify the underlying mechanisms of toxicity rather than rely on toxicological endpoints to identify chemical liabilities (Vinken et al., 2013). Current *in vitro* platforms include a plethora of cell-based reporters established in primary hepatocytes and cell lines for the detection of Nrf2 pathway activation associated with DILI (Kim et al., 2016; Wink et al., 2017). However, these *in vitro* platforms cannot inform *in vivo* distribution of a compound. While cisplatin induced an ARE-driven fluorescent reporter in HepG2 cells, observed by Wink *et al.*, no hepatic bioluminescent signal was present in the Nrf2-Luc mice exposed to the drug in this chapter. Whole-body distribution is therefore important to consider in the analysis of *in vitro* data. The Nrf2-Luc mouse model reflects organ-specific insult. However, a delayed response was observed when compared to the endogenous pathway induction seen in the WT time-course study. This may be due to the requirement for accumulation of endogenous Nrf2, to upregulate the transgene at the protein level prior to luminescent signal generation. Despite this, endogenous protein matched transgene bioluminescent signal, therefore allowing chemical/oxidative stress responses detected in cell-based models to be placed in a whole-body context, with consideration of drug distribution and pharmacokinetics. Further analysis of compounds identified in these screens for extra-hepatic activity using the Nrf2-Luc model would also be of interest.

In response to APAP and cisplatin, the intensity of the Nrf2-Luc bioluminescent signal reflected the extent of drug-induced tissue insult. Indeed, on a cellular level, exposure to a single hepatotoxic dose of APAP resulted in the co-localisation of Hmox1 and luciferase staining in centrilobular hepatocytes specifically, consistent with the known pathology of APAP (Hinson et al., 2010). However, the bioluminescent signal varied greatly between mice. For instance, one female mouse with the strongest bioluminescent signal, had a DILI score of 0 and moderate increase in serum ALT, perhaps due to the protective response of Nrf2 pathway activation. Additionally, the response to APAP differed greatly between genders. Males exhibited, on average, higher serum ALT levels, DILI scores and lower Nrf2-Luc bioluminescent signal when compared to APAP-treated females. It is widely accepted that male C57BL/6J mice are more susceptible than females to APAP-induced liver damage (Dai et al., 2006; McConnachie et al., 2007; Mohar et al., 2014). This is thought to be due to excessive GSH depletion and preferential adduction of mitochondrial Prdx6 in males (Mohar et al., 2014). While similar levels of NAPQI-mediated covalent binding were recorded between genders, female C57BL6-129/Sv mice exhibited slower metabolism of APAP, lower basal expression of CYP1a2 and lower induction of *cyp1a2* and *3a11*, along with GSTpi mRNA levels significantly lower than in males (Dai et al., 2006). Female Nrf2-Luc mice, on average, had stronger *ex vivo* liver bioluminescence than APAP-treated males. Rohrer *et al.* observed lower induction of hepatic Nrf2 in female mice compared to male mice following exposure to APAP (Rohrer et al., 2014). This may be due to the extensive damage seen in male liver tissue, resulting in depleted transgene activity.

In response to cisplatin, renal bioluminescence was induced in female Nrf2-Luc mice. This was clearly evident in *ex vivo* analysis despite the muted *in vivo* signal due to skin pigmentation. Significantly elevated BUN levels confirmed nephrotoxicity in the cisplatin-treatment group. This was proportional to the amount of luciferase and Hmox1 staining around the proximal tubules. As a chemotherapeutic, intercalation of cisplatin with DNA halts cellular proliferation, however, it primarily targets the S3 segment of the proximal tubule due to basolateral drug-transporters such as OCT2 which facilitate the accumulation of the drug within these cells (Hu et al., 2017). In order to avoid dark skin pigmentation, it would be necessary to cross the Nrf2-Luc strain into C57BL/6J albino mice. This would also reduce the duration of anaesthesia suffered by the mice as the signal may penetrate through the white hair, removing the need for shaving the mice prior to imaging.

While activation of renal Hmox1 was observed at the protein level, the Nrf2-regulated transcriptome did not significantly differ between cisplatin and saline treatment groups at 96 h. Microarray analysis of WT C57BL6 mice exposed to 20 mg/kg cisplatin at 0, 24, 48 and 72 h by Pellegrini *et al* revealed Nrf2 pathway activation peaked at 24 h (Pellegrini *et al.*, 2014). BUN levels peak at 96 h post-cisplatin exposure, in many strains of mice, including C57BL6 (Parrish *et al.*, 2009; Sharkey, 2013). Yet it is possible that 96 h is too late a time point to observe upregulation of Nrf2-regulated genes at the mRNA level, whereas protein levels such as Hmox1 remained significantly higher than in the vehicle control group.

Further assessment in more detailed dose and time-course studies are required to reveal the sensitivity of the Nrf2-Luc reporter to subtle chemical/oxidative stress that are not associated with overt organ injury. Other applications of the OKD48 mouse model to study cerebral malaria (Imai *et al.*, 2014) and periodontitis (Kataoka *et al.*, 2016) highlight the tissue-specific expression of Hmox1 coincides with bioluminescent signal. This is similar to our findings. The latter study assessed luminescence over seven days. The ability of the Nrf2-Luc model to monitor chronic exposure to oxidative insult may render it useful for monitoring adaptation in the context of chronic dosing.

Many probes exist for the real-time, *in vivo* detection of ROS during hepatocellular injury from APAP. Shuhender *et al.* utilize CF-SPN nano-probes, for the detection of ROS and OONO<sup>-</sup>s, to show in real-time the inhibition of APAP associated hepatotoxicity by ABT, GSH and the CYP2E1 inhibitor trans-1,2-dichloroethylene (Shuhendler *et al.*, 2014). Vasquez *et al.* generated near-infra red imaging probes to monitor cell death (Annexin-Vivo 750), inflammation (MMPSense-750-FAST) and metabolism (Transferrin-Vivo 750) which were stimulated following 18-22 hours exposure to 300 mg/kg APAP in C57BL6 mice (Vasquez and Peterson, 2017). These probes are administered to mice prior to imaging and react either with ROS entities themselves or downstream pathways induced by oxidative damage. Advantages of the use of probes compared to transgenic mice include the use of WT mice, avoiding the necessity of extensive breeding programs that require large numbers of animals. Probes are also more sensitive to temporal changes in ROS than the delayed transcription of the Nrf2-Luc transgene. However, redox-sensitive probes cannot inform on the biological response to ROS, only their presence.

Other bioluminescent Nrf2-based reporter models have been utilised for measuring responses to drug toxicity, including the Hmox1-Luc mice (Malstrom *et al.*, 2004b). This transgenic reporter consists of the Hmox1 promoter region controlling the expression of

firefly luciferase and responded to toxic exposure to cadmium chloride, doxorubicin and thioacetamide (Malstrom et al., 2004b). Bioluminescence correlated with endogenous Hmox1 induction. However, Hmox1 expression is repressed by Bach1 and regulated by many other transcription factors (Alam and Cook, 2007b; Fuse et al., 2015; Sun et al., 2014). Therefore, activation of the pathway may be missed when relying solely on the Hmox1 promoter or produce false positives when activation is driven by other transcription factors.

McMahon *et al.* generated a Hmox1 reporter model consisting of multiple reporter molecules including a  $\beta$  galactosidase, human chorionic gonadotrophin (hCG) and firefly luciferase, all under the control of the endogenous Hmox1 promoter (McMahon et al., 2018). Exposure of heterozygous reporter mice to BHA activated hepatic Nqo1, Gsta1 and Gstm1 at the protein level but not Hmox1 or the luminescent reporter after 96 h exposure. Dissimilar to our findings, treatment with APAP did not produce a significantly different luminescent response compared to the saline treatment group after 24 h. This is likely due to the lack of repeated ARE sequence, facilitating amplification of the endogenous transcription factor activation.

Unlike other lines of transgenic mice established with a reporter construct under the transcriptional control of an ARE (Johnson et al., 2002; Zhang et al., 2001b), the Nrf2-Luc model offers insight into the induction of Nrf2 in response to toxicity in a non-invasive manner. As such, our studies entailed a detailed analysis of Nrf2 activity in real time and a substantial reduction in number of animals required, complying with the current 3R's guidelines. This allows multiple measurements to be collected throughout a study instead of relying on end-point analysis, directed at specific tissues. I propose the utility of this model would be best served within the latter stages of pre-clinical testing rather than as an initial screening tool. Further assessment is needed to identify the sensitivity of the model to other DILI training compounds. The apparent embryo lethality of the homozygote Nrf2-Luc mice is a substantial limitation of the model as half to a third of each litter is wild-type and unusable. This lethal recessive phenotype may be due to the location of the transgene, disrupting vital gene function and further characterisation of the transgene locus within the Nrf2-Luc mice genome is needed.

In conclusion, Nrf2-Luc mice offer a novel insight into the activation of Nrf2 during the early stages of chemical stress associated with organ-specific drug toxicity. In response to acute hepato- and renal-toxicity, bioluminescent signal coincided with the cell-specific response to insult. This model provides holistic visualisation of chemical/oxidative stress resulting in the



evocation of the Nrf2-mediated stress response. Incorporation of the model into pre-clinical testing may aid the identification of toxic liabilities. In light of the emerging role of Nrf2 as a therapeutic target by drugs such as CDDO-Me, the utility of the Nrf2-Luc mice to screen therapeutic compounds would also be of interest.

**Chapter 3**

**Blood-based analysis of Nrf2 pathway activity**

**Contents**

<b>3.1. Introduction</b> .....	107
<b>3.2. Methods</b> .....	108
3.2.1. Animals.....	108
3.2.1.1. Whole blood analysis studies .....	108
3.2.2. Histology .....	108
3.2.3. RNA extraction, cDNA synthesis and qPCR.....	109
3.2.4. ALT quantification .....	110
3.2.5. Statistical analysis .....	110
<b>3.3. Results</b> .....	111
3.3.1. Validation of organ-specific qPCR primers.....	111
3.3.2. Blood-based analysis of Nrf2-pathway response to APAP.....	115
3.3.3. Blood-based analysis of Nrf2-pathway following intervention of APAP Toxicity ....	119
3.3.4. Blood-based analysis of Nrf2-pathway response to therapeutic Nrf2 stimulation .	125
<b>3.4. Discussion</b> .....	131

### 3.1. Introduction

The emerging role of Nrf2 as a therapeutic target and in the response to drug toxicity have resulted in the establishment of numerous approaches to monitor activation of the Nrf2 pathway in cells and tissues. The work in Chapter 2 demonstrates the use of transgenic Nrf2-Luc mice for monitoring *in vivo* Nrf2 response in real-time, through bioluminescent imaging. However, at present there is a lack of non-invasive methods for measuring Nrf2 activity in wild-type animals *in vivo* or in patients.

Recently, interest in the circulating transcriptome as a source of potential medical biomarkers has grown. For example, cell-free mRNA has provided a wealth of biomarkers for the diagnosis and prognosis of cancer therapies (García et al., 2008; Silva et al., 2007). Albumin mRNA can be used to assess hepatic complications in patients following liver transplant (Chan et al., 2013) and hepatocellular carcinoma recurrence (Cheung et al., 2008). Small, regulatory molecules known as microRNAs (miRNAs) are also detectable in plasma (Mitchell et al., 2008) and hold potential as non-invasive biomarkers for a range of diseases (Chen et al., 2008; Nielsen et al., 2012; Wang et al., 2010). Following DILI, miR-122 has been shown to be more sensitive to hepatotoxicity than ALT and AST (Antoine et al., 2013; Starkey Lewis et al., 2011). Toxicogenomic profiling following DILI highlighted the rapid gene expression changes in blood compared with classical markers of liver injury (Bushel et al., 2007). However, analysis of blood-based mRNA expression is limited, mostly to studies in rats (Bushel et al., 2007; Lobenhofer et al., 2008). Moreover, a specific investigation of the response of the blood mRNA complement to stimulation of the Nrf2 pathway has not been performed.

The ability to monitor Nrf2 activity in the blood may provide insight to the pharmacodynamics of Nrf2 modulating compounds and evidence for the role of Nrf2 in response to drug toxicity in humans. In this chapter, I assess the utility of murine whole blood to monitor Nrf2 activation. Following, exposure to APAP, APAP and N-acetyl cysteine (NAC), or the Nrf2 activator CDDO-Me, I ask whether whole blood can reflect toxicological and pharmacological changes in the Nrf2-pathway *in vivo*.

## 3.2. Materials and Methods

### 3.2.1. Animals

All mice used in these studies were wild-type male C57BL6 mice aged 8- to 10-week-old or 8-week-old BALB/c mice purchased from Charles River (Wilmington, USA). These were maintained under the same conditions described in section 2.2.1.

#### 3.2.1.1. Whole blood analysis studies

Firstly, mice were fasted for 16 h and exposed to 300 mg/kg APAP or 0.9 % saline by IP injection (See section 2.2.1). At 6 and 24 h the mice were culled with a rising concentration of CO<sub>2</sub>. Blood was collected by cardiac puncture and 100 µl added to RNAprotect tubes (Qiagen, Hilden, Germany). Each tube was inverted 8 times before being stored in the fridge. The rest of the blood was placed in a separate Eppendorf and left to clot at room temperature for 30 min. Serum was isolated by centrifugation at 2000 g for 10 min and stored at -80 °C. The liver and kidneys were snap frozen in liquid nitrogen and stored at -80 °C.

In the second study, fasted mice were exposed to either APAP or saline at 0 h, using the same method applied in the first study. Subsequent IP injections of either 500 mg/kg NAC or 0.9 % Saline were administered at 1 and 12 h post-APAP dosing. NAC at this dosage abrogates APAP hepatotoxicity in the short term (Lundbäck et al., 2016). Mice were culled at 24 h with a rising concentration of CO<sub>2</sub> and blood and tissue were collected, as above.

The third study comprised of mice exposed to 10 mg/kg CDDO-Me or 100 % DMSO via IP injection. This dose was shown previously to be tolerable and activate the Nrf2 pathway (Shelton et al., 2015; Walsh et al., 2014). Mice were culled with a rising concentration of CO<sub>2</sub> at 6 and 24 h. Blood and tissue were collected as above.

As repeated exposure is more likely in the clinic (Hong et al., 2012), in the fourth study, mice were exposed to three doses of DMSO or CDDO-Me. At 0, 72 h and 144 h (day 3 and 6), Balb/c mice were administered either 3 mg/kg CDDO-Me or 100 % DMSO via IP injection. At this dose, CDDO-Me has been shown to activate the Nrf2 pathway after 24 h by ITRAQ analysis in C57BL6 mice (Walsh et al., 2014). Mice were culled with a rising concentration of CO<sub>2</sub> at 150 and 172 h (6 and 28 h after the final dose).

### 3.2.2. Histology

See section 2.2.6. DILI scoring criteria listed in Table 2.2.

### 3.2.3. RNA extraction, cDNA synthesis and qPCR

RNA was extracted from the whole blood using the RNeasy Protect Animal Blood Kit (Qiagen, Hilden, Germany). RNAprotect tubes, containing 100  $\mu$ l whole blood, were left at room temperature overnight to increase RNA yield. The blood was centrifuged at 5000 g for 3 min and the supernatant was discarded. The pellet was vortexed in 1 ml RNase-free water and pelleted at 5000 g for 3 min. The supernatant was discarded and the pellet was vortexed in 240  $\mu$ l buffer RSB until dissolved. This solution was added to 200  $\mu$ l RBT buffer and 20  $\mu$ l Proteinase K and incubated for 10 min at 55 °C in a shaker-incubator at 800 rpm. The solution was added to a QIAshredder column (Qiagen, Hilden, Germany) and centrifuged at 18 000 g for 3 min. The flow through was added to 240  $\mu$ l of 100 % ethanol and vortexed.

The solution was added to an RNeasy MinElute spin column, which was placed above a 2 ml collection tube and centrifuged for 1 min at 8000 g. The column was washed with 350  $\mu$ l buffer RW1 and centrifuged at 8000 g for 15 sec. On column DNase digestion was performed using 10  $\mu$ l DNase 1 stock solution and 70  $\mu$ l RDD buffer. The columns were incubated at room temperature for 15 min and 350  $\mu$ l RW1 buffer was added before being centrifuged at 8000 g for 15 sec. The column was centrifuged in a similar manner after the addition of Buffer RPE. A solution of 80 % (v/v) ethanol in dH<sub>2</sub>O was generated and 500  $\mu$ l added to the column before being centrifuged at 8000 g for 2 min. The column was placed in a new 2 ml collection tube and centrifuged at 18 000 g for 5 min with the lid of the column open to dry the membrane. RNA was eluted in 30  $\mu$ l REB buffer by centrifugation at 8000 g for 1 min and the yield was quantified using the Nanodrop.

RNA extraction from tissue was conducted in a similar manner to section 2.2.9.

For reverse transcription and SYBR green qPCR analysis see section 2.2.9. Additional qPCR primers for murine genes are detailed in Table 3.1. Gene expression quantified in 96 well-plate format normalising Ct values to GAPDH levels.

**Table 3.1 Additional Mouse qPCR primers**

<b>Gene</b>	<b>Primer</b>	<b>Sequence</b>
<i>Ambp</i>	Fwd	5' AAGAGAGTGAGGGGTCAG 3'
	Rev	5' CAGGGGCCTTCTGAGTAAT 3'
<i>Apoa2</i>	Fwd	5' CACAGAATCGCAGCACTGTTC 3'
	Rev	5' GTCCTTCCAGGCTACAGAT 3'
<i>Aqp2</i>	Fwd	5' GGTTGCCATGTCTCCTT 3'
	Rev	5' CGGATTCTACAGGGGTA 3'
<i>Nphs2</i>	Fwd	5' CGGTCCATAGCGTTCT 3'
	Rev	5' AGCCAAGGCCAAAGAA 3'

**3.2.4. ALT quantification**

See section 2.2.3.

**3.2.5. Statistical analysis**

See section 2.2.10.

### 3.3. Results

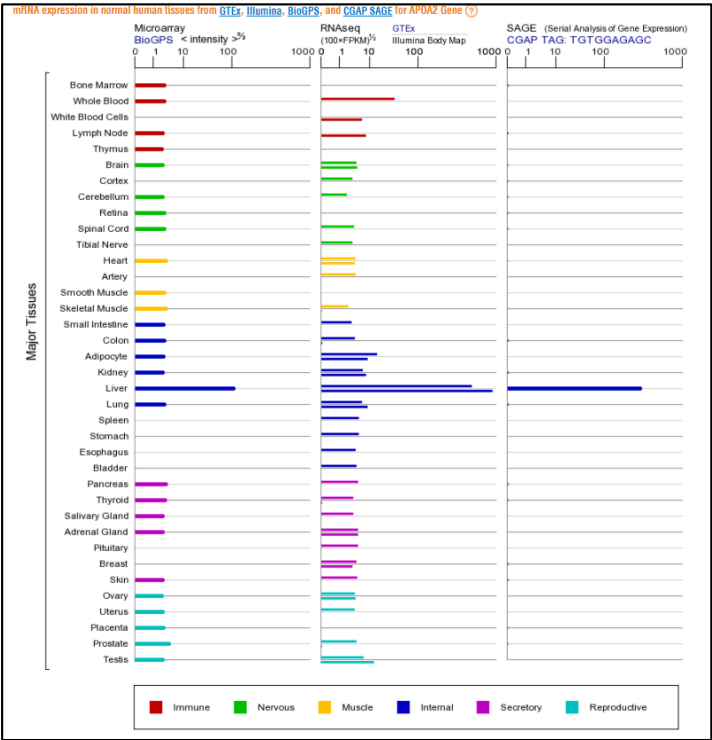
#### 3.3.1. Validation of organ-specific qPCR primers

Liver- and kidney- specific primers were designed to assess the levels of tissue-specific genes in whole blood following liver damage (Fig 3.1 A, B, C and D) (sequences listed in Table 3.1). The liver-specific  $\alpha$ -1-microglobulin/bikunin precursor (*Ambp*) has been shown to circulate in blood following APAP exposure and treatment with other hepatotoxic compounds in rats, concurrently with ALT (Miyamoto et al., 2008; Okubo et al., 2013). Additionally, elevated Apolipoprotein A2 (*Apoa2*) has been recorded in plasma of C57BL6 mice following APAP administration (K. Wang et al., 2013). GTEX, Illumina, BioGPS, and CGAP SAGE datasets, collated in the Genecards database, indicated tissue specific expression of these transcripts. Both Podocin (*Nphs2*) and aquaporin 2 (*Aqp2*) are exclusively expressed in the kidney. None of these genes have been reported to be regulated by Nrf2.

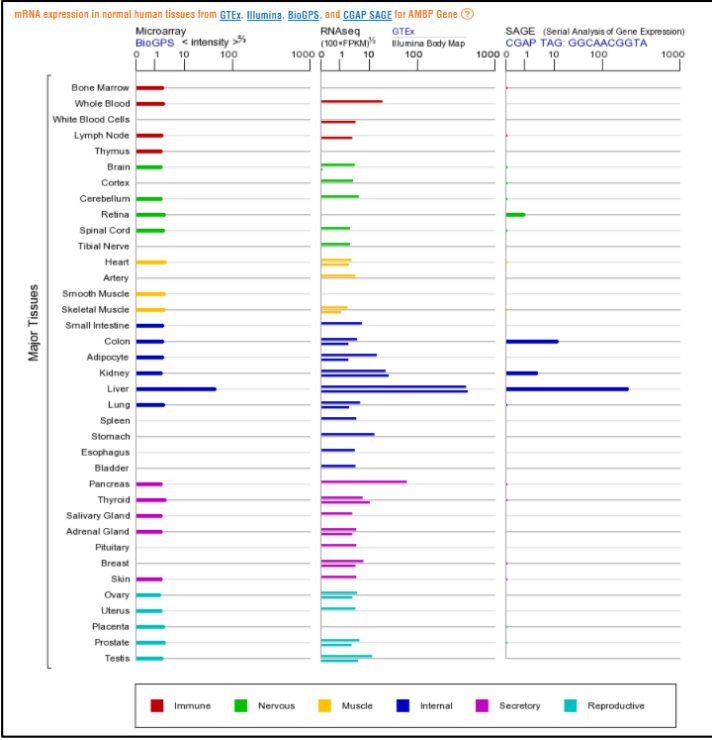
The tissue specificity of the genes was validated in livers and kidneys from mice exposed to 0.9 % saline for 24 h (Fig 3.1 E and F). In the livers, Ct values of liver-specific genes were much lower than kidney-specific genes. In the kidneys, Ct values of kidney-specific genes were lower than liver-specific Ct values. When normalised to housekeeping gene expression,  $\Delta$ Ct values of organ-specific primers were lower in the tissue of origin indicating higher expression and tissue specificity.



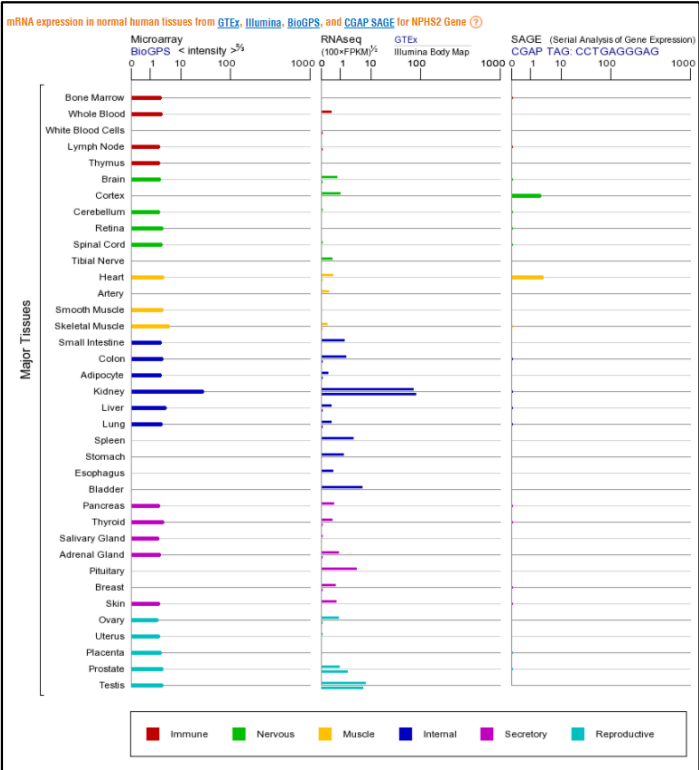
### A. Alpha-1-Microglobulin/Bikunin Precursor (AMBP)



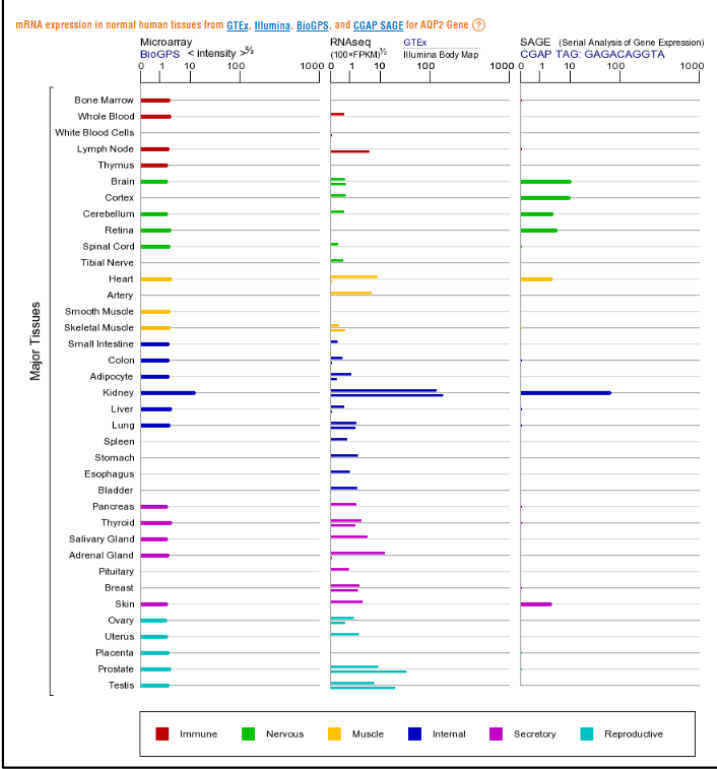
### B. Apolipoprotein A2 (APOA2)



### C. Podocin (NPHS2)



### D. Aquaporin 2 (AQP2)



E.	Liver (Saline 24 h)	House keeping	Liver-specific		Kidney specific	
	Gene	<i>Gapdh</i>	<i>Ambp</i>	<i>Apoa2</i>	<i>Nphs2</i>	<i>Aqp2</i>
	Average Ct	15.49 ± 0.39	15.46 ± 0.29	14.15 ± 0.54	27.80 ± 1.25	28.08 ± 1.85
	Average ΔCt	n/a	0.15 ± 0.09	-1.16 ± 0.46	12.12 ± 1.40	12.40 ± 1.93

F.	Kidney (Saline 24 h)	House keeping	Liver-specific		Kidney specific	
	Gene	<i>Gapdh</i>	<i>Ambp</i>	<i>Apoa2</i>	<i>Nphs2</i>	<i>Aqp2</i>
	Average Ct	15.32 ± 0.93	26.47 ± 0.41	25.52 ± 0.23	20.61 ± 0.41	20.00 ± 0.41
	Average ΔCt	n/a	11.28 ± 2.14	9.25 ± 2.24	4.44 ± 0.32	3.83 ± 0.31

**Figure 3.1 – Validation of organ specific primers**

Screenshots from <http://www.genecards.org> of liver-specific Alpha-1-Microglobulin/Bikunin Precursor (*Ambp*) (A) and Apolipoprotein A2 (*Apoa2*) (B), and kidney-specific Podocin (*Nphs2*) (C) and aquaporin 2 (*Aqp2*) (D) gene expression. Data based on GTEx, Illumina, BioGPS, and CGAP SAGE datasets. Cts and ΔCts from qPCR analysis of mouse liver (E) or kidney (F) lysates from animals exposed to 0.9 % saline for 24 h shown as mean ± SD (n=5).

### 3.3.2. Blood-based analysis of Nrf2-pathway response to APAP

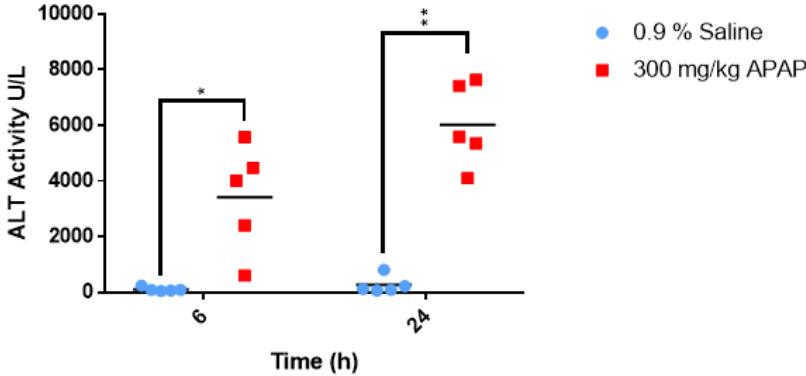
To investigate the response of the blood-based Nrf2 pathway following liver injury, whole blood samples were taken from mice exposed to a single dose of 300 mg/kg APAP. In these mice, serum ALT was significantly elevated at 6 and 24 h compared to their saline-treated counterparts (Fig 3.2 A) ( $P = 0.0343$  and  $0.0013$  respectively). This coincided with activation of the Nrf2 pathway in liver tissue (Fig 3.2 B). *Hmox1*, *Srxn1* and *Gsta1* expression were all significantly induced at 6 h (All  $p$  values  $<0.0001$ ) compared to the 6 h saline-treatment group. *Gsta1* expression remained significantly elevated at 24 h ( $P = 0.0002$ ). Liver-specific genes *AMBIP* and *APOA2* were not significantly induced at either time-point.

In the kidneys, activation of the Nrf2-pathway activity was evident at 6 h (Fig 3.2 C) with *Hmox1* and *Srxn1* significantly upregulated ( $P = <0.0001$  and  $0.0339$ ). However, these fold changes were lower than those observed in the liver at 6 and 24 h. Kidney-specific genes *Nphs2* and *Aqp2* were not induced at either time-point.

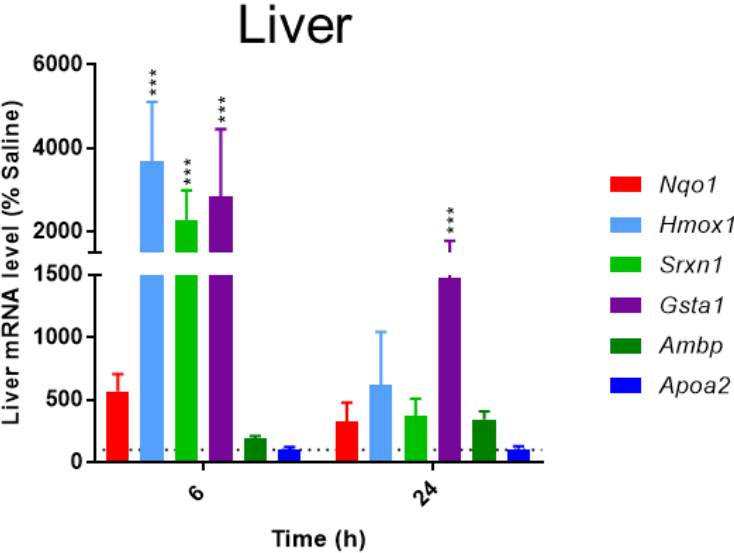
Whole blood qPCR analysis revealed significantly elevated *Gsta1* levels in the APAP-treated mice at 24 h compared to the saline treatment group (Fig 3.2 D) ( $P = <0.0001$ ). *Hmox1* expression increased after 24 h exposure, but varied considerably between mice.

To test the hypothesis that Nrf2-regulated mRNA was present in whole blood as a result of release into circulation following cell damage, liver- and kidney- specific gene expression was measured in the whole blood samples. At 24 h, liver-specific  $\Delta$ Cts in the APAP-treated mice were significantly lower than time-matched vehicle controls (Fig 3.3) (Both *Ambp* and *Apoa2*  $P$  values  $<0.001$ ). The expression levels of kidney-specific genes did not differ between treatment groups and  $\Delta$ Cts were large in all cases. However, there was considerable variability within groups. Therefore, elevated Nrf2-regulated gene expression in whole blood coincides with release of liver-specific mRNA into circulation, following APAP-induced liver damage.

A.



B.



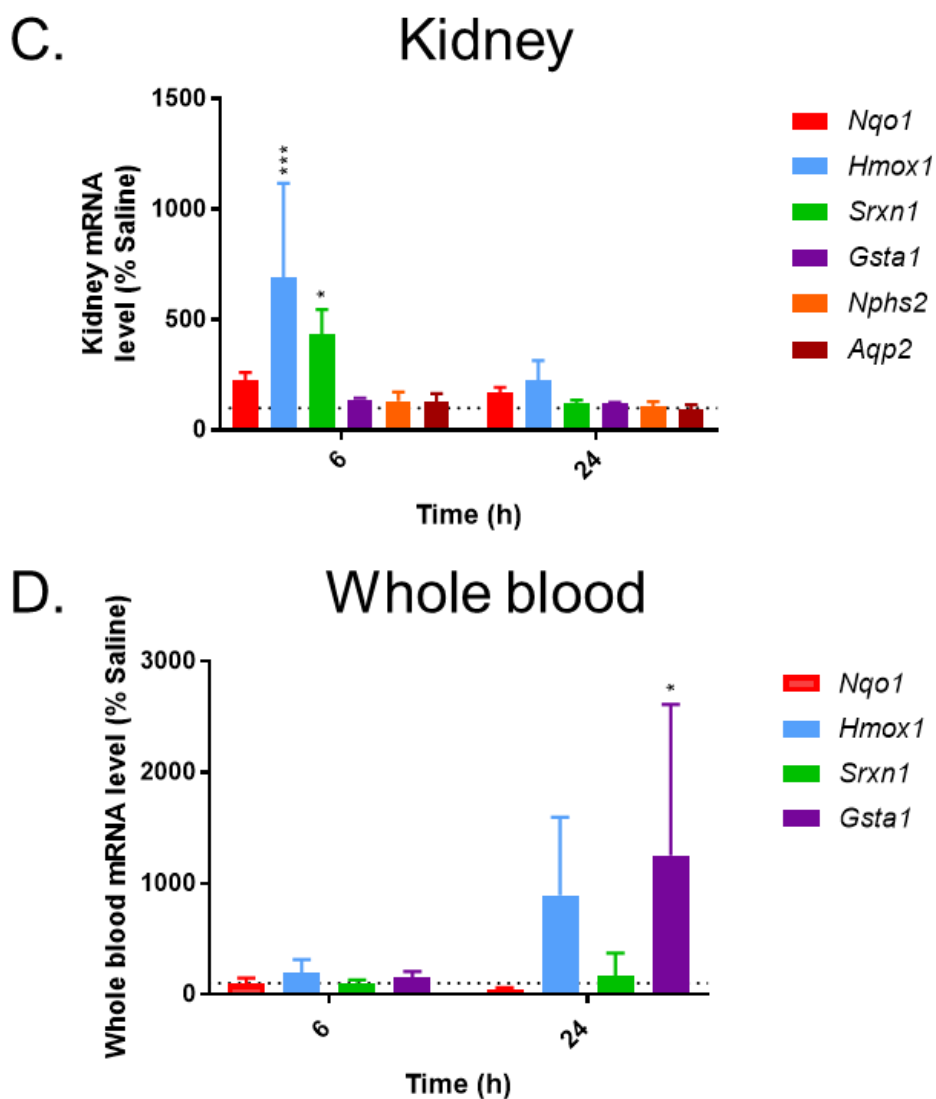


**Figure 3.2 Induction of Nrf2 pathway in whole blood following a toxic dose of paracetamol**  
 Male C57BL6 mice were administered either 0.9 % Saline or 300 mg/kg acetaminophen (APAP) by IP injection (n=5). Blood was collected by cardiac puncture at 6 and 24 h. (A) Serum ALT levels were significantly different between saline and APAP treatment groups. qPCR analysis of gene expression in murine livers (B), kidneys (C) and whole blood (D) showing activation of Nrf2-regulated genes. Significant difference in ALT levels and gene expression compared to time-matched saline treatment groups were calculated by one-way ANOVA and Kruskal Wallis (\*  $P \leq 0.05$ , \*\* $P \leq 0.01$  and \*\*\*  $P \leq 0.001$ ) (Dotted line = 100 %).

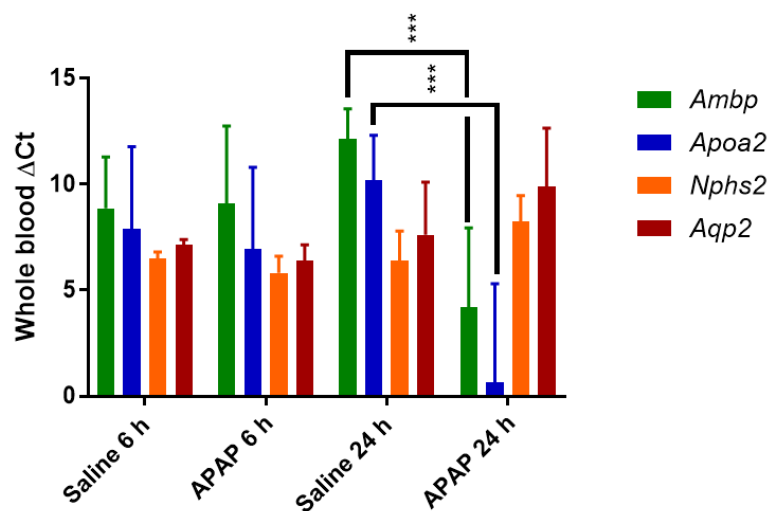


**Figure 3.3 – Increased liver-specific gene expression in whole blood of paracetamol-treated mice**

$\Delta$ Cts of liver-specific genes (*Ambp* and *Apoa2*) compared to kidney-specific gene (*Nphs2* and *Aqp2*) in whole blood for mice exposed to 0.9 % saline or 300 mg/kg acetaminophen (APAP) for 6 and 24 h. Mean  $\Delta$ Ct  $\pm$  SD shown. Significance between time-matched APAP and Saline treatment groups were calculated by one-way ANOVA (\*\*\*)  $P \leq 0.001$ ).

### 3.3.3. Blood-based analysis of Nrf2-pathway following intervention of APAP Toxicity

To ascertain whether changes in the whole blood levels of Nrf2-regulated genes were proportional to liver damage, APAP-treated mice were administered two doses of NAC at 1 and 12 h. In mice administered this intervention, there was significantly lower serum ALT activity (Fig. 3.4) ( $P = <0.0001$ ). Histological analysis revealed pericentral necrosis in the APAP-treated mice (Fig 3.5 A). *Hmox1* staining was also present in the region surrounding the portal vein. Compared to the APAP + Saline treatment group, necrosis and *Hmox1* staining was muted in the APAP + NAC treated tissues. DILI scoring of liver tissue was proportional to serum ALT (Fig 3.5 B). Four of the five livers of APAP + NAC treated mice had a DILI score of between 0-1, while one mouse exposed to APAP+NAC presented with higher serum ALT and a DILI score of 1-2. In the APAP + Saline treatment group, all mice scored between 1-2.

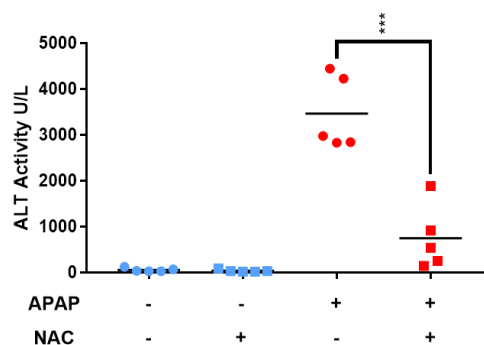
The hepatic Nrf2-pathway was upregulated in the APAP + Saline and the APAP + NAC treated mice (Fig 3.6 A). When compared to saline-treated mice, *Srxn1* and *Gsta1* were upregulated significantly in the livers of APAP-treated mice ( $P = 0.019$  and  $<0.0001$ ). *Gsta1* was also significantly elevated in the APAP + NAC treatment group ( $P = 0.216$ ). *Nqo1* was elevated in these groups but not significantly. *Hmox1* expression was elevated in the APAP-treated mice but not APAP + NAC treated mice. *Gsta1* expression was significantly reduced in the APAP + NAC treated livers compared to the APAP + Saline treatment group ( $P = <0.0001$ ). Expression of liver-specific genes *Ambp* and *Apoa2* did not differ significantly in APAP + Saline or APAP + NAC treatment-groups compared to controls.

In the kidneys, *Nqo1* and *Gsta1* were significantly induced in the APAP-treated mice when compared with the saline treatment group (Fig 3.6 B) ( $P = <0.0001$  and  $0.0493$  respectively). *Nqo1* expression was significantly reduced in the kidneys of APAP + NAC treated mice, when compared to the APAP + Saline treatment group ( $P = <0.0001$ ). There was little difference in expression of the other genes across treatment groups. Expression of kidney-specific genes *Nphs2* and *Aqp2* did not differ between groups.

Analysis of whole blood revealed significant induction of *Hmox1* in the APAP-treated mice compared to the vehicle control group (Fig 3.6 C) ( $P = 0.0002$ ) and APAP + NAC treatment group ( $P = 0.0108$ ). *Hmox1* was elevated in whole blood from the APAP + NAC treatment group but this was not significant when compared to expression in saline treated mice. *Gsta1* expression was very variable in the APAP + Saline treated mice and to a lesser extent in the APAP+NAC treated mice.

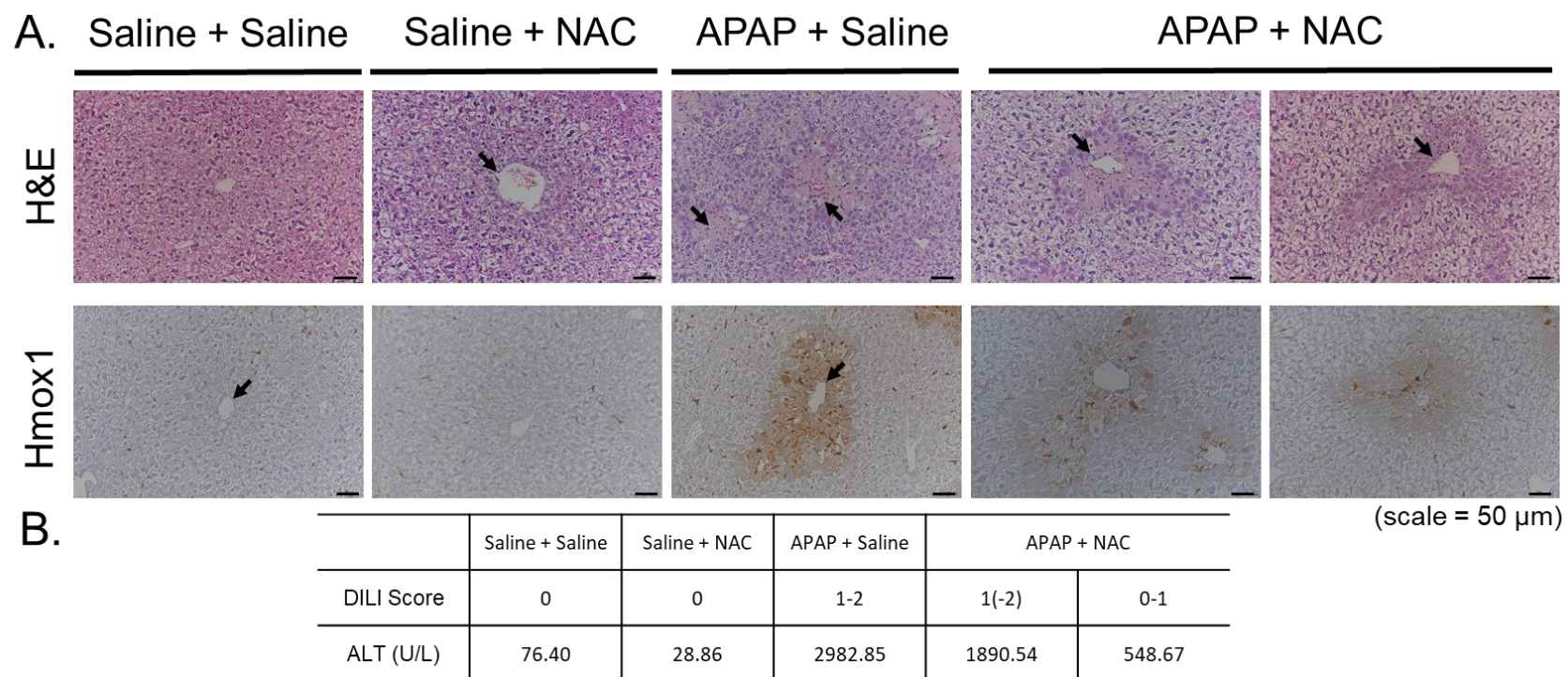


Organ-specific gene expression in whole blood from this study, again was extremely variable (Fig 3.6 D). However, the mean  $\Delta\text{Ct}$  values for liver-specific genes in the APAP + Saline group were lower (*AMBIP*: 5.55 and *APOA2*: 3.56) than the mean  $\Delta\text{Ct}$  in the APAP+NAC (*AMBIP*: 8.10 and *APOA2*: 5.86) and control treatment groups. While not significant, this indicates a trend towards lower  $\Delta\text{Ct}$ s in liver-specific gene expression in the APAP + Saline group indicative of the release of liver-specific genes into the circulation being proportional to the degree of liver injury. Kidney-specific  $\Delta\text{Ct}$ s did not vary between groups. Therefore, damaged hepatocytes remain a potential source of the Nrf2-regulated mRNA in whole blood, as expression levels were relative to the extent of perturbation.



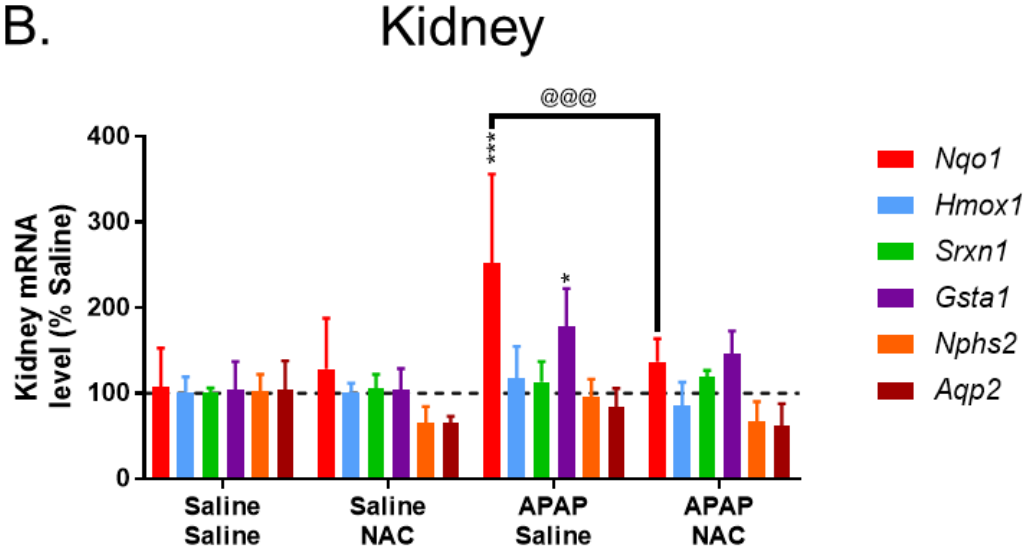
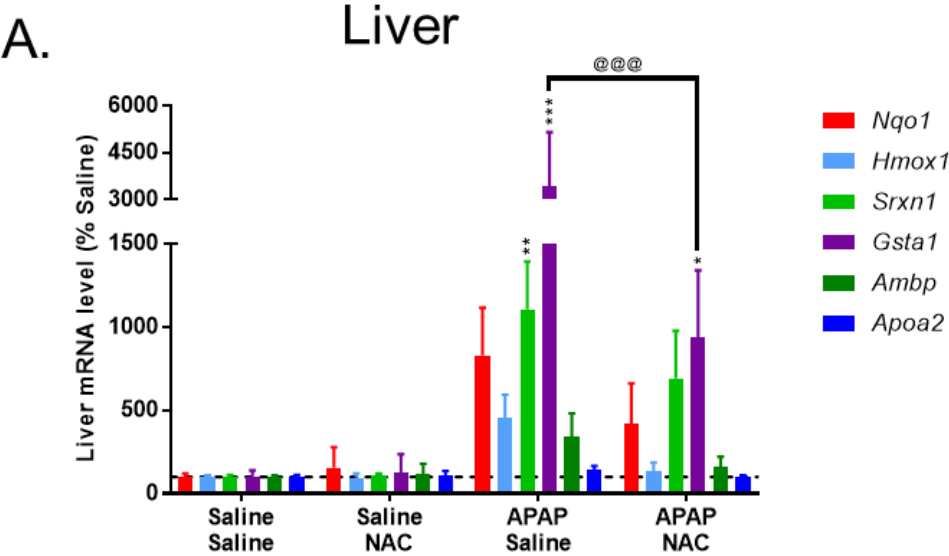
**Figure 3.4 – Muted elevation of serum alanine transaminase in response to N-acetylcysteine exposure following paracetamol toxicity**

Male C57BL6 mice were administered either 0.9 % Saline or 300 mg/kg acetaminophen (APAP) by IP injection (n=5) at 0 h. At 1 and 12 h exposure, mice were administered 500 mg/kg N-acetylcysteine (NAC) or 0.9 % Saline. Blood was collected by cardiac puncture at 24 h and serum ALT levels quantified. Significant difference between treatment groups were calculated by one-way ANOVA (\*\*\*) P ≤ 0.001).



**Figure 3.5 – Muted necrosis and Hmox1 staining in mice administered N-acetylcysteine in response to paracetamol toxicity**

Male C57BL6 mice were administered either 0.9 % Saline or 300 mg/kg acetaminophen (APAP) by IP injection (n=5) at 0 h. At 1 and 12 h post-APAP exposure, mice were administered 500 mg/kg N-acetylcysteine (NAC) or 0.9 % Saline. All groups were culled after 24 h. (A) Sections of the central hepatic lobule were stained with H&E and probed for Hmox1. Necrosis surrounding the central vein (black arrow) is shown in the light pink staining of the H&E treated sections. Hmox1 staining was also present in the pericentral region. (B) Extent of necrosis is proportional to drug induced liver injury (DILI) score and alanine transaminase (ALT) levels.



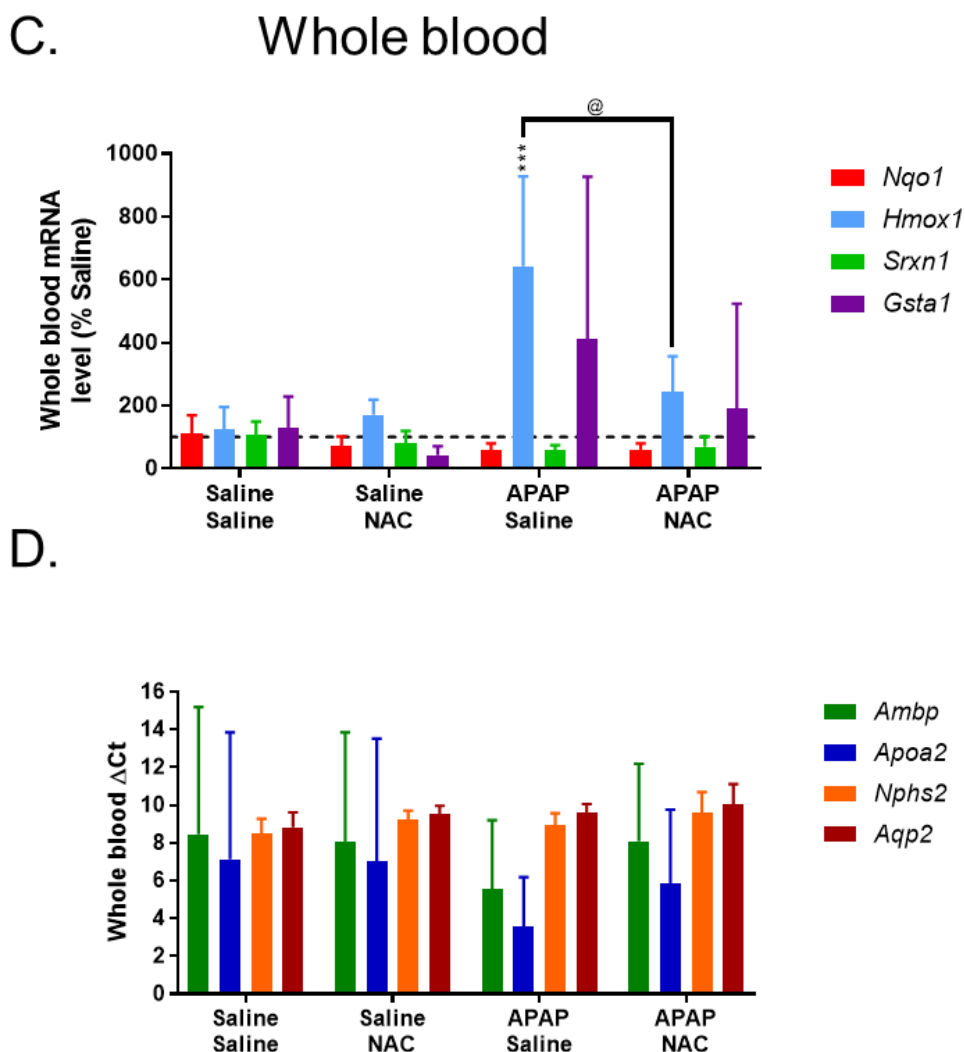


**Figure 3.6 – Gene expression in tissues and whole blood from mice treated with paracetamol and N-acetylcysteine**

Male C57BL6 mice were administered either 0.9 % Saline or 300 mg/kg acetaminophen (APAP) by IP injection (n=5) at 0 h. At 1 and 12 h exposure, mice were administered 500 mg/kg N-acetylcysteine (NAC) or 0.9 % Saline. Blood was collected by cardiac puncture at 24 h. qPCR analysis of gene expression in murine livers (A), kidneys (B) and whole blood (C) highlighted activation of Nrf2-regulated genes (Dotted line = 100 %). (D)  $\Delta$ Cts of liver-specific gene (*Ambp* and *Apoa2*) compared to kidney-specific gene (*Nphs2* and *Aqp2*) expression in whole blood samples. Mean  $\Delta$ Ct  $\pm$  SD shown. Significant difference in gene expression compared to Saline + Saline group (\*  $p \leq 0.05$ , \*\*  $p \leq 0.01$  and \*\*\*  $p \leq 0.001$ ) or APAP + Saline compared to APAP + NAC (@  $p \leq 0.05$  and @@@  $p \leq 0.001$ ) were calculated by one-way ANOVA and Kruskal Wallis.

### 3.3.4. Blood-based analysis of Nrf2-pathway response to therapeutic Nrf2 stimulation

Following administration of CDDO-Me, hepatic *Srxn1* expression was significantly elevated after 6 and 24 h, when compared to time-matched DMSO-treated counterparts (Fig 3.7 A) ( $P = <0.0001$  and  $0.0066$  respectively). *Nqo1* and *Gsta1* were significantly elevated in the livers of CDDO-Me-treated mice after 24 h exposure, compared to the DMSO-treatment group (Both  $P$  values  $<0.0001$ ). Liver-specific gene expression did not differ between groups

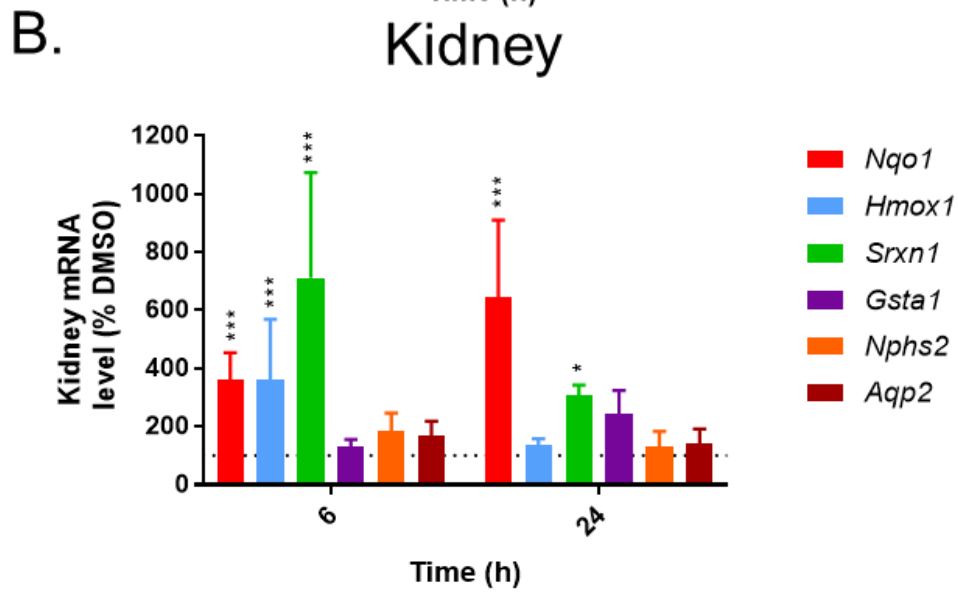
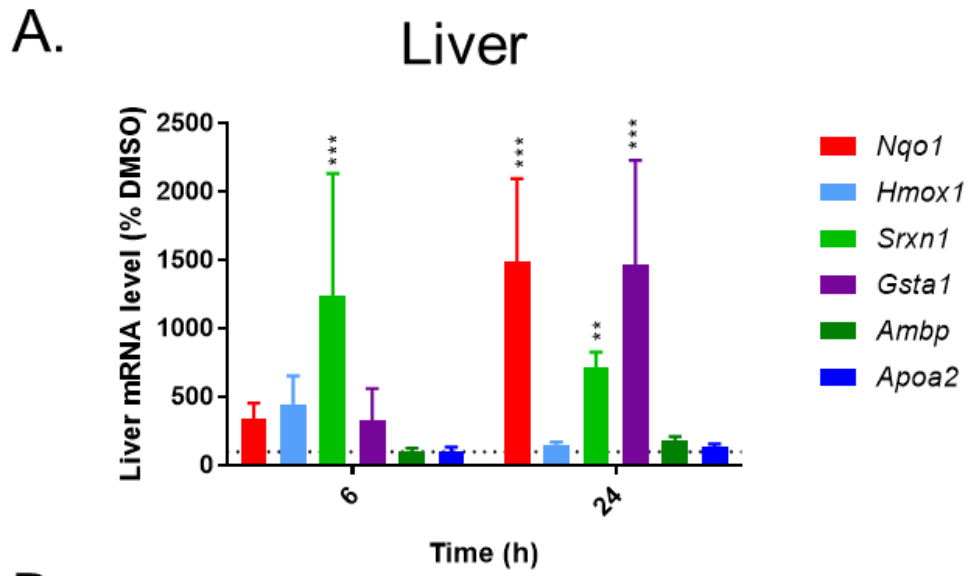
In the kidneys of CDDO-Me-treated mice, *Nqo1*, *Hmox1* and *Srxn1* were induced significantly at 6 h (Fig 3.7 B) ( $P = 0.0008$ ,  $0.0008$  and  $<0.0001$  respectively). *Nqo1* and *Srxn1* gene expression was also significantly greater than the DMSO-treated mice at 24 h ( $P = <0.0001$  and  $0.0154$ ). In general, the induction of Nrf2-regulated genes was lower in kidneys than in the liver. Expression of kidney specific genes *Nphs2* and *Aqp2* did not change at either time-point.

Whole blood qPCR analysis revealed significant elevation of *Srxn1* and *Gsta1* in CDDO-Me-treated mice after 24 h exposure compared to the DMSO-treatment group (Fig 3.7 C) ( $P = 0.0453$  and  $0.0001$  respectively). Consistent with a lack of tissue damage, liver- and kidney-specific  $\Delta Ct$  values in whole blood from mice exposed to CDDO-Me or DMSO showed no significant differences but varied greatly within treatment groups (Fig 3.7 D).

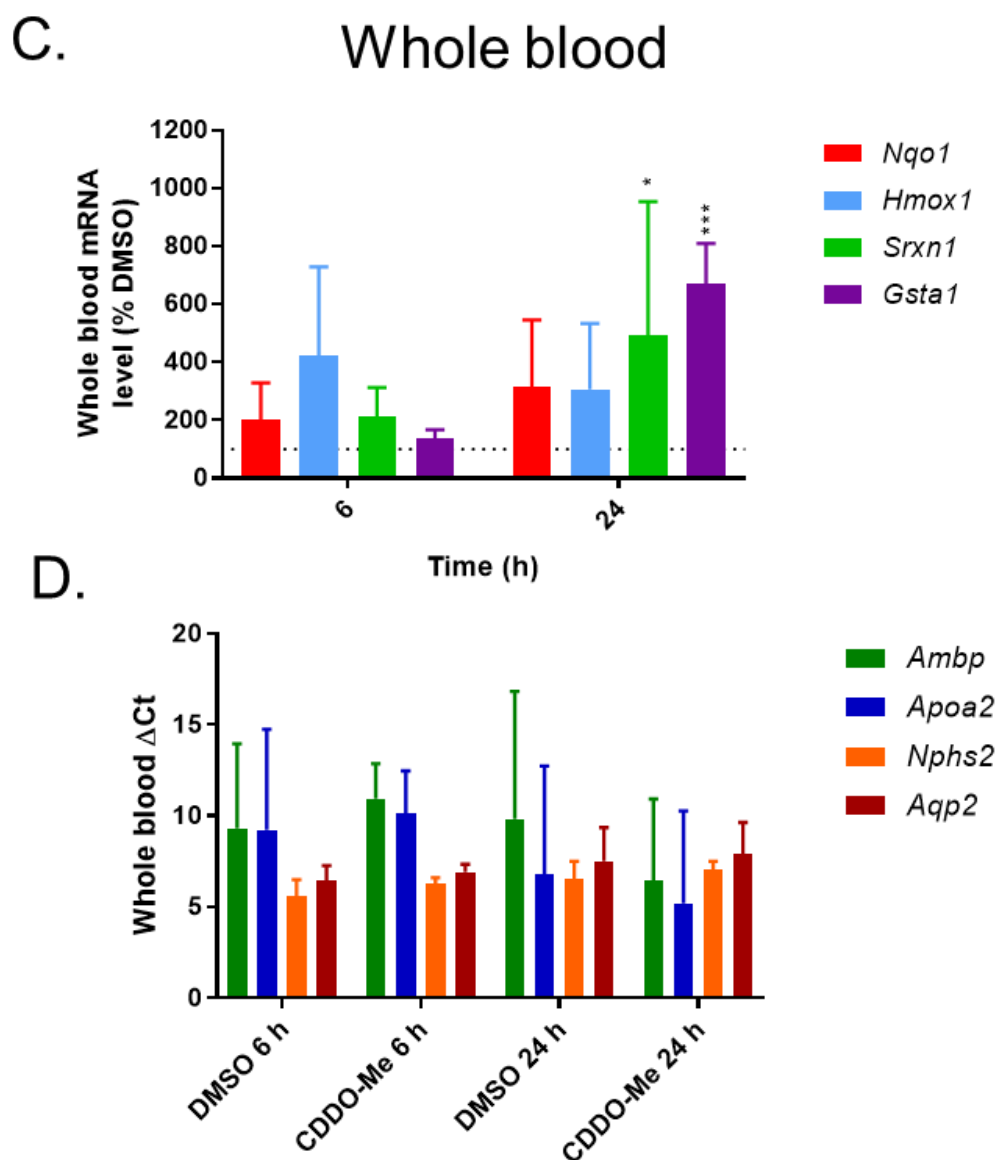
To recapitulate repeated exposure to CDDO-Me, as seen in the clinic (Ongoing trials include CATALYST (NCT02657356), and LARIAT (NCT02036970)), BALB/c male mice were exposed to three consecutive 3 mg/kg doses via IP injection. Hepatic Nrf2-pathway induction was evident at 6 h after the final dose of CDDO-Me (Fig 3.8 A), with significant induction of *Srxn1* and *Gsta1* compared to time-matched DMSO-treated mice ( $P = <0.0001$  and  $0.0193$  respectively). *Nqo1*, *Srxn1* and *Gsta1* were significantly upregulated 28 h after the final dose of CDDO-Me (All  $p <0.0001$ ). Induction of the Nrf2 pathway in livers following chronic exposure to CDDO-Me was less than the fold changes measured after a single dose of CDDO-Me (Fig 3.7 A). However, variability within treatment groups was reduced.

Renal Nrf2 pathway activity was induced at 6 h after the final dose of CDDO-Me (Fig 3.8 B), with significantly greater levels of expression of *Nqo1*, *Hmox1*, *Srxn1* and *Gsta1* compared to the time-matched DMSO-treatment group ( $P = 0.014$ ,  $<0.0001$ ,  $<0.0001$  and  $0.0175$  respectively). At 28 h after the final dose of CDDO-Me, both *Nqo1* and *Gsta1* were significantly induced (All  $P <0.0001$ ).

Whole blood qPCR analysis revealed variable changes in Nrf2-regulated genes within treatment groups (Fig 3.8 C). Elevations of Nrf2-regulated transcripts were observed after 6 h although variability within groups resulted in these changes not being significantly different from time-matched DMSO-treated controls.  $\Delta$ Cts of organ-specific genes were also extremely variable between individual mice (Fig 3.8 D). Aside from the variability within groups, this data highlights the activation of Nrf2-regulated gene expression in whole blood following therapeutic induction in mice exposed to CDDO-Me.

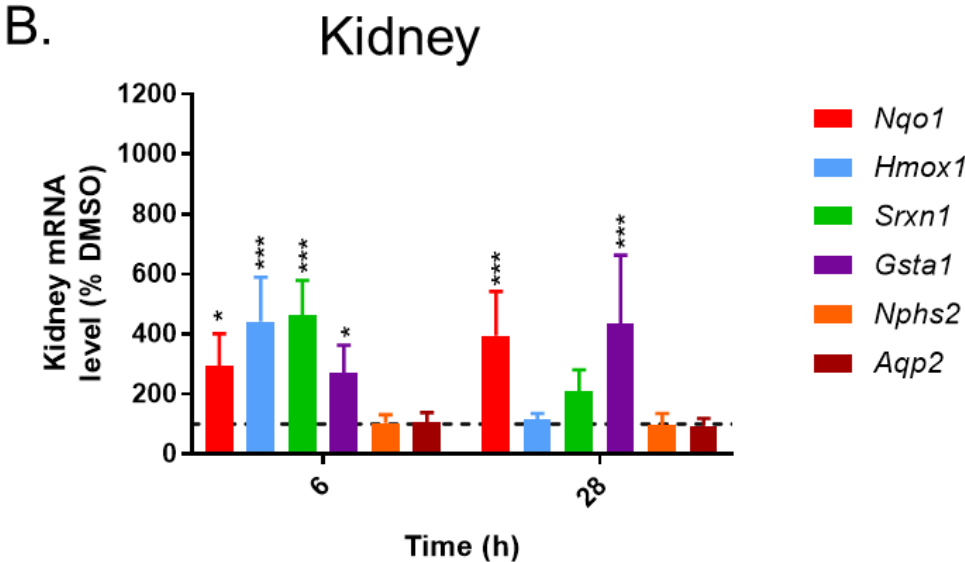
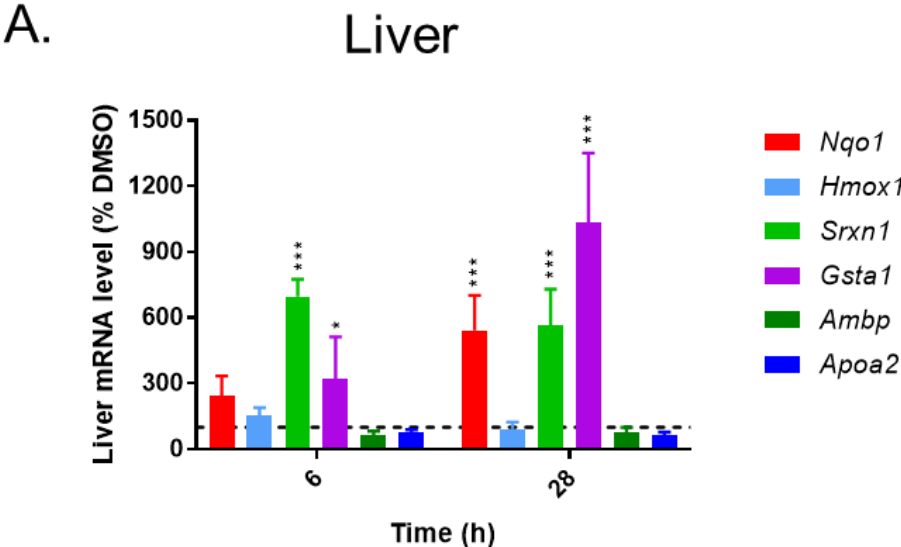






**Figure 3.7 Induction of Nrf2 pathway in tissues and whole blood by CDDO-Me**

qPCR analysis of gene expression in the livers (A), kidneys (B) and whole blood (C) of male C57BL6 mice, exposed to either 100 % DMSO or 10 mg/kg CDDO-Me by IP injection for 6 or 24 h (n=5 animals) (Dotted line = 100 %). (D)  $\Delta$ Cts of liver-specific gene (*Ambp* and *Apoa2*) compared to kidney-specific gene (*Nphs2* and *Aqp2*) in whole blood samples. Mean  $\Delta$ Ct  $\pm$  SD shown. Significant differences in gene expression compared to time-matched DMSO treatment groups were calculated by one-way ANOVA and Kruskal Wallis test (\*  $P \leq 0.05$  and \*\*\*  $P \leq 0.001$ )



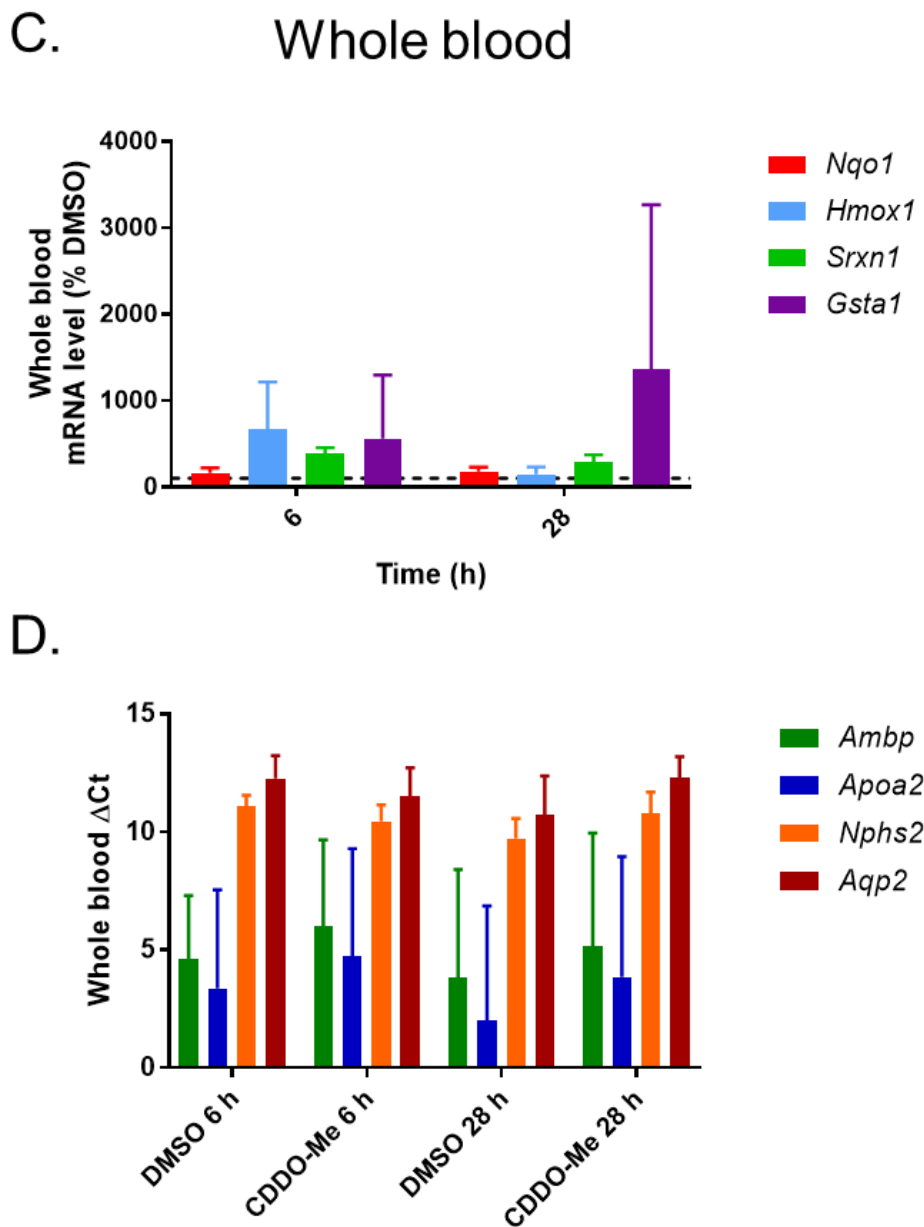


**Figure 3.8 Upregulation of the Nrf2 pathway in response to chronic exposure to CDDO-Me** qPCR analysis of gene expression in the livers (A), and kidneys (B) and whole blood (C) of male BALB/c mice, exposed to three doses of either 100 % DMSO or 3 mg/kg CDDO-Me by IP injection over the course of 6 days (n=5 animals). Tissues were collected 6 or 28 h after the final dose of CDDO-Me (Dotted line = 100 %). (D)  $\Delta$ Cts of liver-specific gene (*Ambp* and *Apoa2*) compared to kidney-specific gene (*Nphs2* and *Aqp2*) expression in whole blood samples. Mean  $\Delta$ Ct  $\pm$  SD shown. Significant differences in gene expression compared to time-matched DMSO treatment groups were calculated by one-way ANOVA (\*  $P \leq 0.05$  and \*\*\*  $P \leq 0.001$ ).

### 3.4. Discussion

In this chapter, I analysed activity of the Nrf2 pathway, *in vivo*, in whole blood following toxicological and pharmacological stimulation. Induction of Nrf2-regulated transcripts in response to APAP exposure, was muted in mice administered NAC, the antidote to APAP toxicity. This coincided with reduced liver-specific but not kidney-specific transcripts in whole blood. Following exposure to the therapeutic Nrf2-inducing compound CDDO-Me, murine whole blood exhibited variable induction of Nrf2-regulated mRNA. Further analysis into the expression patterns within the sub-components of whole blood may shed light on the source and potential function of these RNA molecules.

Previously, extensive toxicogenomic profiling of blood following DILI in rats has showed that gene expression changes in blood preceded elevation of classical markers of liver injury (Bushel et al., 2007; Lobenhofer et al., 2008) and that these transcripts can accurately predict extent of toxicity, mirroring ALT level (J. Huang et al., 2010; Zhang et al., 2012). In this chapter, APAP exposure resulted in significant induction of both the renal and hepatic Nrf2 pathway after 6 h. However, significant activation of the pathway in whole blood was only evident after 24 h exposure, alongside induction of liver-derived transcripts *Ambp* and *Apoa2*. This coincides with the findings of Umbricht *et al.* who showed that many genes upregulated in the rat liver following APAP-induced damage, were also upregulated in the blood (Umbricht et al., 2010). Microarray analysis of RNA from leukocytes, isolated from rats administered APAP, highlighted induction of Nrf2-regulated genes Thioredoxin reductase 1 (*Txnrd1*), Peroxiredoxin 5 (*Pdrx5*) and *Nqo1*. In an earlier study, *Prdx5* was induced over two-fold and *Srxn1* showed a 21-fold increase in plasma from rats following APAP-induced hepatotoxicity (Wetmore et al., 2010). In addition to elevated Nrf2-regulated mRNA, liver-specific transcripts were only increased with hepatotoxicant exposure, APAP or D-galactosamine, and not myotoxic doses of bupivacaine HCl. Next-generation sequencing of total RNA from plasma of female C57Bl6 mice exposed to 350 mg/kg APAP revealed changes in the levels of 1459 transcripts within plasma – the majority of which were increased following APAP overdose (K. Wang et al., 2013). Comparable to our findings, Wang *et al.* observed elevated *Gsta1* alongside glutathione reductases and synthetases in the liver at 24 h post-APAP administration. *Apoa2* was identified as one of the 5493 transcripts present in both liver and plasma.

Loss of hepatic GSH-dependent enzymes such as GSTA1 in Nrf2 KO mice result in the strain's sensitivity to chemical stressors (Chanas et al., 2002). In humans, liver necrosis associated

with hypertension resulted in elevated GSTA1 protein levels in plasma (Knapen et al., 1998). Omics profiling of blood and urine from healthy human volunteers after oral administration of 4 doses of APAP in the form of two 500 mg tablets every 6 h over 24 h (resulting in a total dose of 4 g) lead to upregulation of transcripts associated with the oxidative stress response 25 h after the first dose (Jetten et al., 2012). Glutathione-S-transferases such as *GSTM3* mRNA were elevated in whole blood compared to 0 h samples, although expression varied between donors. Fannin *et al.* also observed distinct transcriptional gene expression signatures in peripheral blood from six healthy volunteers exposed to a single dose of 4 g APAP compared to the placebo-treated control group (Fannin et al., 2010). After 48 h, down-regulation of genes associated with oxidative phosphorylation were observed in the APAP-treatment group. However, out of the 795 differentially expressed genes, Nrf2 pathway activity was not observed. The authors reported greater variability in gene expression patterns within the earlier 24 h time-point. Larger cohort analysis is needed to avoid skewed datasets from variable populations. Additionally, insight into expression patterns in the peripheral tissues of APAP-treated patients may inform mechanisms underlying toxicity.

Circulating RNA can originate from a variety of sources. Passive release of mRNA into circulation can occur during tissue necrosis (Wetmore et al., 2010). Active secretion of mRNA transcripts has been documented in association with exosomes, microvesicles and apoptotic bodies (Halicka et al., 2000; Skog et al., 2008; Valadi et al., 2007). In this chapter, qPCR analysis highlighted significantly increased levels of liver-specific genes (*Ambp* and *Apoa2*) in whole blood samples compared to time-matched, saline-treated controls. Kidney-specific gene expression (*Nphs2* and *Aqp2*) remained low across treatment groups. This highlights the presence of liver-specific and NRF2-regulated transcripts in whole blood after 24 h exposure to APAP that may be derived from damaged hepatocytes following DILI.

Bioactivation of APAP to NAPQI occurs in the liver, however reactive metabolites may migrate into circulation. Radioactively-labelled APAP exposure led to dose-dependent radioactive labelling of haemoglobin alongside hepatic and renal proteins in mice (Axworthy et al., 1988). The authors surmised that these effects were due to migration of reactive metabolites from the liver to erythrocytes, and not direct alkylation of haemoglobin by APAP within erythrocytes, due to the similarity of the dose-response curves of APAP binding to liver proteins and haemoglobin, and the fact that activation of cytochrome P450 enzymes, via IP administration of phenobarbital or 3-methylcholanthrene, did not alter the ratio of haemoglobin- to liver protein-adducts. Interestingly, APAP overdose in cats and dogs causes

haemolysis and methaemoglobinemia due to the generation of the deacetylation product of APAP: *p*-aminophenol by erythrocytes (McCONKEY et al., 2009). Inactive forms of NAPQI have been detected in circulation as cysteine conjugates (Muldrew et al., 2002) or bound covalently to proteins. For instance, NAPQI-albumin adducts have been detected at low levels in serum from mice exposed to APAP (Switzar et al., 2013). *In vitro*, increased protein content of culture medium has been observed following exposure of PHHs to NAPQI (McGill et al., 2013). This indicates the potential for NAPQI itself being released into circulation alongside APAP-protein adducts. Mass spectrometric analysis of NAPQI and its conjugated forms would shed light on the potential for the induction of the Nrf2 pathway in whole blood to be the result of effects in blood cell, themselves.

To assess the hypothesis that the increase of Nrf2-regulated genes within whole blood is proportional to extent of hepatotoxicity and thus more likely to be the result of mRNA leaking from damaged hepatocytes, mice were administered APAP and the antidote, NAC. Intervention of APAP toxicity, by repeated exposure to NAC, resulted in reduced pericentral necrosis and co-localised Hmox1 staining. In the liver, *GSTA1* and in the kidneys, *NQO1* expression was reduced significantly after 24 h. Interestingly, reduced Nrf2 pathway activity was also identified in the whole blood of mice exposed to both APAP and NAC. Circulating miRNA levels rapidly decline in APAP overdose patients receiving NAC therapy (Krauskopf et al., 2015; Ward et al., 2014). However, little is known about the modulation of circulating mRNA following exposure to NAC. Here, liver-specific mRNA transcripts were reduced in whole blood from mice exposed to APAP and NAC compared to mice treated with APAP and saline. Complete suppression of Nrf2-regulated gene induction was not expected due to the 1 h delay in NAC treatment, following exposure to APAP. However, further analysis is needed to confirm that the liver is the source of these Nrf2-regulated transcripts and to identify the mechanism of mRNA release in response to APAP toxicity.

Evidence suggests that exosomal shuttling of RNA can confer protection in recipient cells following oxidative stress (Eldh et al., 2010). Nrf2-regulating miRNAs have been detected within exosomes extracted from serum of rats experiencing chronic heart failure, that were not present in sham controls (Tian et al., 2017). Overexpression of these miRNAs in cardiomyocytes *in vitro* resulted in downregulation of Nrf2, consistent with observations of Nrf2 downregulation in murine models of heart failure. This raises the question of whether functional Nrf2-transcripts are actively secreted into circulation following liver injury. Without thorough characterization of exosomes derived from hepatocytes following DILI one

cannot confirm Nrf2 pathway activation was due to Nrf2-mRNA cargo within exosomes or other vesicles. Further analysis of exosomal content may confirm the presence of Nrf2-activating and/or Nrf2-regulated mRNA released in response to APAP toxicity.

Aside from liver-derived exosomes, Nrf2 transcripts can be actively expressed by cells circulating within whole blood. Hematopoietic cells, including lymphocytes, dendritic and mast cells secrete exosomes (Blanchard et al., 2002; Skokos et al., 2001; Théry et al., 2001). Additionally, platelet-derived extracellular vesicles are secreted in response to agonists such as thrombin and lipopolysaccharide (LPS) (Aatonen et al., 2014). *Ex vivo* analysis of peripheral blood mononuclear cells (PBMCs) in culture highlight their sensitivity to Nrf2 modulation. For example, during the first in human trial of CDDO-Me, PBMCs isolated from participants at both 2 and 22 days after exposure and cultured *ex vivo*, exhibited increased expression of *Nqo1* (Hong et al., 2012).

Here, in response to acute CDDO-Me exposure, both the renal and hepatic Nrf2 pathways were activated at 6 and 24 h. This was similar to previous analysis of the renal activation of Nrf2 pathway in wildtype mice, after 24 h exposure to CDDO-Me (Shelton et al., 2015). This coincided with significant induction of *Srxn1* and *Gsta1* in whole blood after 24 h exposure. A potential source of these Nrf2-regulated transcripts in whole blood are circulating blood cells themselves, as triterpenoids have been shown to influence PBMC gene expression. PBMCs and neutrophils isolated from healthy donors, exposed to CDDO-Im and CDDO-Me *ex vivo*, exhibited increased expression of antioxidant genes and were protected against LPS-induced oxidative damage (THIMMULAPPA et al., 2007). However, in PBMCs from patients with septic shock, treatment with CDDO-Me resulted in increased *Nqo1* and decreased *Hmox1* expression (Noel et al., 2014). Monocytes from healthy donors treated with 50 nM CDDO-Me *in vitro* exhibited induced *Nqo1* at 8 and 16 h post LPS stimulation (Noel et al., 2014). PBMCs from burn victims and healthy donors, treated with CDDO-Me exhibited induced *NQO1* and *HMOX1* (Eitas et al., 2017). Primary peripheral blood lymphocytes from C57BL6 mice, immunised with MOG 33-55 (Model of experimental autoimmune encephalomyelitis), and stimulated with repeated doses of CDDO-TFEA (a triterpenoid analogue of CDDO-Me) over 5 days and cultured *ex vivo*, exhibited induced *Nrf2* and *Hmox1* mRNA levels compared to vehicle-treated mice (Pareek et al., 2011).

Here, chronic exposure to CDDO-Me resulted in similar Nrf2-pathway activation in the liver and kidneys, with lower fold changes than the single dose study but less variability within groups. However, the Nrf2 pathway was not significantly induced in whole blood. This may

be due to time or dose not being sufficient to maintain maximal induction of the pathway. It is also important to note that this study was conducted in the BALB/c background and may not be directly comparable with the acute CDDO-Me study in C57BL6 mice.

A prominent finding, following the assessment of circulating mRNA in response to toxicant exposure is the chemical-specific gene expression profiles observed in blood samples. These expression profiles were capable of discerning organ-specific toxicities in rodents (Umbricht et al., 2010; Wetmore et al., 2010) and can differentiate toxic and non-toxic doses (Bushel et al., 2007). Lobenhofer *et al.* identified overt drug 'signatures' in transcriptional profiles of whole blood from rats exposed to a panel of eight acute hepatotoxicants (Lobenhofer et al., 2008). These transcriptomic markers, when applied to an independent study, were able to predict APAP-induced liver toxicity in rats with 92.1 % accuracy (J. Huang et al., 2010). While the results presented in this chapter show that Nrf2-regulated gene expression in whole blood was not evident until latter time points and therefore could not compete with current clinical markers of DILI, non-invasive sampling for Nrf2 pathway activation in blood may aid pre-clinical screening of drug candidates.

Throughout this chapter, whole blood analysis revealed variable gene responses within treatment groups that may be due the inter-individual variability. Future studies with larger cohorts may better take this variability into account in order to be identify outliers. Additionally, there is debate as to the length of transcripts in circulation. Many claim the concentration of mRNA in plasma is misrepresented due to the fact that most circulating RNAs are not full length (K. Wang et al., 2013; Zhong et al., 2008). However, one of the longest human mRNA transcripts recovered from the serum of patients suffering from oral squamous cell carcinoma, included 93.4 % of the full length GAPDH sequence indicating intact cell-free mRNAs are present in circulation (Li et al., 2006). These intact cell-free RNA molecules are likely to be protected within vesicles (El-Hefnawy et al., 2004). To be confident of the extent of induction of Nrf2-regulated genes in whole blood, optimisation of primers annealing across different regions of the transcripts are needed. Moreover, factors such as diet and exercise can significantly impact gene expression in peripheral blood cells (Radom-Aizik et al., 2008; van Erk et al., 2006). Further studies would need to control for these variables.

While the data in this chapter confirms the presence of Nrf2-regulated transcripts in whole blood in response to APAP toxicity and that induction of these mRNA are muted in mice receiving the antidote, NAC, further work is needed to identify the sources of these



transcripts. It is appealing to surmise that these transcripts are released into circulation from damaged liver cells. Other circulating RNA molecules such as miR122 have been shown to confer protective effects on peripheral tissues following acute kidney injury in rodents (Fan et al., 2016). Analysis of vesicles such as exosomes, released from hepatocytes following toxicity may identify a potential source of these transcripts. Alternatively, Nrf2-regulated transcripts may be derived directly from circulating blood cells. Another interesting question is the function of these transcripts within whole blood. Does Nrf2-regulated mRNA within whole blood retain functionality and does this provide protection to peripheral tissues? The increasing use of Nrf2 activating compounds in the clinic demands thorough characterisation of the response to drug exposure. Ultimately more detailed time course and whole blood fraction analysis is needed to fully characterise the response of the circulating Nrf2-pathway to pharmacological and toxic stimuli.

**Chapter 4**

**Investigation of putative Nrf2-regulated genes in human hepatocytes**

**Contents**

<b>4.1. Introduction</b> .....	139
<b>4.2. Materials and Methods</b> .....	140
4.2.1. Bioinformatic analysis .....	140
4.2.2. Antioxidant response element-reporter construction .....	141
4.2.2.1. Preparation of inserts for cloning.....	142
4.2.2.2. PCR amplification of inserts.....	142
4.2.2.3. Restriction enzyme digestion and gel extraction .....	143
4.2.2.4. Transformation of pGL4.20 ligations .....	144
4.2.2.5. Colony screening.....	144
4.2.3. Cell culture .....	145
4.2.3.1. Primary hepatocyte isolation.....	145
4.2.3.2. Drug treatment .....	146
4.2.3.3. Transfection .....	147
4.2.4. In vitro luciferase assays .....	147
4.2.5. qPCR and Western blotting.....	148
<b>4.3. Results</b> .....	149
4.3.1. Bioinformatic analysis reveals putative NRF2-regulated target genes.....	149
4.3.1.1. Comparison with other microarray datasets.....	150
4.3.1.2. Response to toxic stimuli.....	151
4.3.1.3. Sequence-based analysis .....	153
4.3.1.4. Gene shortlist.....	160
4.3.2. Putative NRF2-regulated gene activation in human liver cells.....	160
4.3.3. Clone construction .....	164
4.3.4. Assessment of SRXN1 antioxidant response elements.....	166
4.3.5. ARE-reporter construct response to pharmacological induction of NRF2 .....	167
4.3.6. ARE-reporter response to overexpression of NRF2.....	170
4.3.7. SRXN1 ARE assessment.....	173
<b>4.4. Discussion</b> .....	175

#### 4.1. Introduction

Activation of the NRF2-mediated protective response to chemical and oxidative stress, is an early event in adverse outcome pathways, following exposure to many compounds associated with DILI (Herpers et al., 2016). As a result, NRF2-regulated genes are increasingly being incorporated into assays for the assessment of compounds liable to provoke toxicity. Many ARE-based reporters incorporating single or repeated *cis*-elements of promoter regions from a particular NRF2-regulated gene have been reported for the detection of NRF2-activating compounds (Kim et al., 2016; Motahari et al., 2015; Shukla et al., 2012). Primary human hepatocytes (PHH) are considered the ‘gold standard’ of *in vitro* DILI assessment due to their maintenance of liver-specific functionality for up to 72 h post-isolation (Gómez-Lechón et al., 2014). Despite this, little is known about the molecular landscape of the NRF2 pathway in PHH. Therefore, thorough characterisation of the PHH NRF2 pathway is vital. Previous work from this laboratory included microarray analysis of PHHs transfected with siRNA targeting *NRF2* or *KEAP1* (Manuscript in preparation). This dataset can be used to identify putative novel NRF2-regulated genes that may act as useful molecular markers of the NRF2 pathway and potentially reflect perturbations associated with DILI. In this chapter, I aim to define the regulatory sites responsible for the NRF2-dependent activation of putative novel Nrf2-regulated. Additional insight into the regulation of NRF2-target gene induction may provide novel means of monitoring the NRF2 pathway in response to chemical and oxidative stress and improve predictive models for drug safety assessment.

## 4.2. Materials and Methods

All materials and reagents were sourced from Sigma (Poole, UK) unless otherwise stated.

### 4.2.1. Bioinformatic analysis

In response to small interfering RNA (siRNA), genes significantly downregulated by siNRF2 and significantly upregulated by siKEAP1 in PHH were collated.

Initial comparison of this shortlist of genes to other human microarray datasets was achieved using the publicly available datasets GSE28813 and GSE38332 (Agyeman *et al.*, 2012; Singh *et al.*, 2013). Singh *et al.* assessed NRF2 pathway activity following siRNA-mediated knockdown of NRF2. When multiple probes were included, the smallest value relating to the most downregulated probe, was used. Agyeman *et al.* compared NRF2 pathway activation following siKEAP1 or sulforaphane exposure. In this instance, where multiple probes were included, the highest upregulated probe following siKEAP1 and sulforaphane exposure was considered.

The response of the putative Nrf2-regulated genes to toxic stimuli known to activate NRF2 signalling via exposure of PHH to butylated hydroxyanisole (BHA) and diethyl maleate (DEM) was assessed using the TG-GATES dataset (Igarashi *et al.*, 2014). Data was accessed via Toxygates, a platform for accessing the TG-GATES database (Nyström-Persson *et al.*, 2013). The fold change of gene expression following 24 h exposure to low, medium and high doses were considered. Where multiple probes were used for a specific gene, the probe with the highest fold change was included in the analysis.

Assessment of ARE sequence location within and around the gene locus was achieved using data from the mathematical algorithm for ARE sequence identification developed by Kuosmanen *et al.* (Kuosmanen *et al.*, 2016). This model, based on chromatin immunoprecipitation (ChIP-Seq) data, scored potential ARE sites throughout the genome by their predicted propensity for NRF2 binding. Data kindly provided by Prof. Anna-Liisa Levonen, was uploaded to the human genome assembly GRCh37/hg19 in the University of California Santa Cruz (UCSC) Genome Browser and was categorised in individual 'tracks' based on predicted NRF2-binding strength: strong, medium-strong, medium, medium-weak and weak. Screen shots of binding regions within the gene or 5 kb upstream of the gene start site were collected.

We utilised data generated by Chorley *et al.* documenting the NRF2 binding following sulforaphane treatment in human lymphoblastoid cells (Chorley *et al.*, 2012). The publicly

available CHIP-Seq dataset, was uploaded to human genome assembly NCBI36/hg18 in the UCSC genome browser. Data from vehicle and sulforaphane treated cells were uploaded in separate 'tracks'. If either track included a 'peak' region, the data view scaling of both tracks were configured to the highest peak. Screen shots of 'peak' regions within and under 5 kb to the gene start site were compiled. The location of ARE sites from the Kuosmanen dataset was compared to the Chorley dataset to identify active ARE sites.

#### **4.2.2. Antioxidant response element-reporter construction**

Promoter regions spanning 1-2 Kb upstream of the gene start site ATG were synthesised (GeneMill, Liverpool, UK). *NQO1* and *SRXN1* ARE sites were included as positive controls. During analysis of the *SRXN1* promoter region, an ARE element was identified -274 to -193 bp from the transcriptional start site of *SRXN1* responsible for its regulation (Singh et al., 2009). However, this sequence contains two putative ARE sites. Constructs of both ARE sites were synthesised.

Johnson *et al.* identified the region within LOC344887 as the site responsible for activation and therefore the region 1kb around this ARE was included instead of the promoter region for synthesis (Johnson et al., 2016). Mutated ARE sequences within the inserts were designed by replacing the bases T with G and A with C and vice-versa (Table 4.1).

The OR5T3 promoter locus was included as a negative control as it contained no ARE sites and was not modulated by NRF2 in our analysis. These regions were sub-cloned into the pGL4.20 vector (Promega, Madison, USA) using Kpn1 and Nhe1 restriction sites.

**Table 4.1 Wild-type and mutated ARE sequences within synthesised constructs**

Wild type (WT) and mutated (MUT) ARE sequences. The SRXN1 promotor region contains two potential ARE sites, which were mutated individually or in combination.

Insert	ARE1	ARE2
F2RL2 WT	TGCTCTGTAC	n/a
F2RL2 MUT	GTAGAGTGACA	n/a
LOC344887 WT	GTGACAGAGCG	n/a
LOC344887 MUT	TGCTACTCTAT	n/a
NQO1 WT	GTGACACAGCT	n/a
NQO1 MUT	GTGACTCAGCA	n/a
TRIM16L WT	GTGACACAGCT	n/a
TRIM16L MUT	TGTCACACTAG	n/a
SRXN1 WT	TGCAAACAC	CTGAGTCAGCC
SRXN1 ARE1 MUT	GTACCCAGACA	CTGAGTCAGCC
SRXN1 ARE2 MUT	TGCAAACAC	AGTCTGACTAA
SRXN1 ARE 1+2 MUT	GTACCCAGACA	AGTCTGACTAA

#### 4.2.2.1. Preparation of inserts for cloning

Inserts from the synthesised construct were either isolated and purified following restriction digestion (Kpn1 and Nhe1) from MIDI prepped DNA (QIAGEN, Hilden, Germany) or, when these yields were low, amplified from these plasmids using PCR.

#### 4.2.2.2. PCR amplification of inserts

Inserts were amplified in reactions using an M13 forward primer (M13) 5'-GTTTTCCAGTCACGAC-3' and a vector-specific reverse primer (Promoter\_reverse) 5'-AGCGCCCAATACGCAAGG-3' (Table 4.2) and amplified for 35 cycles with 58 °C annealing and an extension stage of 1 min/Kb product. Following PCR, a small amount of the reactions were resolved on 1.5 % agarose gels to ensure amplification.

**Table 4.2 Q5 polymerase PCR reaction conditions**

Reagent	Volume ( $\mu$ l)
5x Q5 buffer	10
10 mM dNTPs	1
5 uM Forward Primer	2.5
5 uM Reverse Primer	2.5
Template (25 ng/ $\mu$ l)	1
DNase-free H <sub>2</sub> O	32.5
Q5 polymerase	0.5

**4.2.2.3. Restriction enzyme digestion and gel extraction**

Following amplification, inserts were incubated with 0.5  $\mu$ l *Dpn1* (NEB, Hitchin, UK) for 30 min at 37 °C to digest methylated DNA. Reactions were cleaned up using the Wizard® SV gel and PCR clean-up system following the kits instructions (Promega, Madison, USA).

Inserts and pGL4.20 plasmid were digested with *Kpn1*-HF and *Nhe1*-HF restriction enzymes (New England Biosciences, Ipswich, USA) in 80  $\mu$ l reactions (Table 4.3) for 2 h, at 37 °C. Reactions were subsequently resolved on a 1.5 % agarose gel for 1 h, at 135 V. Inserts were excised from the gel using a scalpel and purified using the Wizard® SV gel and PCR clean-up system. Inserts from MIDI prepped DNA were obtained by digestion as described above and purified from the remainder of the plasmid by gel extraction.

Digested pGL4.20 was resolved with uncut plasmid and the rest of the reaction cleaned up.

The concentration of all digest products was measured using the Nanodrop Spectrophotometer ND-1000 (Labtech International, Heathfield, UK) and inserts ligated into digested pGL4.20. Briefly, 50 ng pGL4.20 was ligated with increasing ratios of insert DNA (1:1, 1:2 and 1:4) and 50 ng/ $\mu$ l T4 ligase (NEB, Hitchin, UK). Ligation reactions were incubated overnight at 4 °C prior to transformation.



**Table 4.3 Insert digestion reaction**

Reagent	Volume ( $\mu$ l)
10 ug plasmid DNA	X
10x CutSmart buffer	8
Kpn1-HF	2
Nhe1-HF	2
DNase-free H <sub>2</sub> O	Up to 80

**4.2.2.4. Transformation of pGL4.20 ligations**

Ligation reactions were incubated with competent STBL3 *Escherichia coli* (Thermo Fischer Scientific, Waltham, USA) on ice for 30 min prior to heat shock at 42 °C for 1 min. Following recovery on ice for 2 min, super optimal broth with catabolite repression (SOC) medium was added to bacteria and incubated for 1 h at 37 °C with shaking. Bacteria were subsequently plated onto agar plates containing 100  $\mu$ g/ml Carbenicillin and cultured at 37 °C overnight.

**4.2.2.5. Colony screening**

Successful ligation into pGL4.20 was initially determined by screening transformed colonies. Screening PCR reactions consisted of an RV3 forward primer and an insert-specific reverse primer (Table 4.4 A), and were amplified with GoTaq Polymerase (NEB, Hitchin, UK) (Table 4.4 B). Colonies were picked using a pipette tip and added to the PCR reactions by pipetting up and down. Reactions were amplified over 35 cycles with 58 °C annealing temperature and extension stage of 1 min/Kb product. PCR products were resolved on a 1.5 % agarose gel. Plates were left at room temperature to allow colony regrowth and positive colonies were picked into 5 ml LB medium containing 0.1  $\mu$ g/ml Carbenicillin for overnight culture.

All positive clones were purified and sent for Sanger sequencing (Source-Biosciences, Rochdale, UK) to confirm correct integration and sequence of the insert using forward primer (RV3) 5' CTAGCAAATAGGCTGTCCC 3' and reverse primer 5' GGTGGCTTTACCAACAGTACCG 3'. Correct clones were MIDI prepped (Qiagen, Hilden, Germany). DNA was quantified using the Nanodrop. Purity of the samples were based on the 260/280 ratio. Only those with a ratio between 1.7 and 1.9 were used.

**Table 4.4 Colony screening reactions**

(A) Screening primers (B) PCR reactions to confirm successful transformation of plasmids.

A.

Primer	Sequence
F2RL2 Screening primer	5' – CACACAGATTTCTACCCAG – 3'
LOC344887 Screening primer	5' – CACCACATCCAGTTAATCAC – 3'
NQO1 Screening primer	5' – CTTCCCTATAACTGCTATCTC – 3'
TRIM16L Screening primer	5' – CTGTTTGGCTCTTGTGG – 3'
OR5T3 Screening primer	5' – GATAAACAAGGTACAGAGG – 3'
SRXN1 Screening primer	5' – GCTTGTCTTCGACCGAG – 3'
Forward primer RV3	5' – CTAGCAAAATAGGCTGTCCC – 3'

B.

Reagent	Volume ( $\mu$ l)
One Taq <sup>TM</sup> polymerase	5
10 $\mu$ M Screening primer pair	1
DNase-free H <sub>2</sub> O	4

**4.2.3. Cell culture**

All cells lines were maintained at 37 °C with 5 % CO<sub>2</sub>. HepG2 cells were cultured in media consisting of Dulbecco's Modified Eagle's medium (DMEM), supplemented with 10 % (v/v) heat-inactivated Foetal bovine serum (FBS) and 1 % (v/v) Penicillin / streptomycin.

Once confluent, cells were dissociated from culture flasks with trypsin. Briefly, the monolayer was washed with 5 ml 0.02 % (v/v) Ethylenediaminetetraacetic acid (EDTA) in PBS. This was then replaced with 2 ml 0.25 % Trypsin and incubated at room temperature for 1 min. Trypsin was removed and the flask incubated at 37 °C for 5 min. Cells were resuspended in media and counted using a haemocytometer. HepG2 cells were dissociated through a 21G needle prior to counting. Cells were passaged every 4 days up to 25 passages before being discarded. Cultures were regularly tested for mycoplasma using the 'eMyco kit' (Lonza, Slough, UK).

**4.2.3.1. Primary hepatocyte isolation**

Surgical excess tissue from hepatobiliary surgery performed at Aintree Hospital (Liverpool, UK) was obtained with informed consent. Ethical approval was granted by the NReS

committee Northwest Liverpool Central. Written consent was taken from all patients and the study protocol adhered to the 1975 Declaration of Helsinki. Liver parenchyma was taken from non-cancerous margins and ideally, with most of the outer capsule intact. Tissue was stored on ice in perfusion buffer (10 mM HEPES, 5 mM KCl, 136 mM NaCl and 0.5 % (w/v) glucose (Thermo-Fisher Scientific, Waltham, USA) in dH<sub>2</sub>O) for approximately 30 min during transport to the University laboratories.

PHH were isolated by Dr Amy Schofield, Dr Monday Ogese and Dr Laleh Kamalian via two-step collagenase digestion as previously described (LeCluyse et al., 2005). The tissue was weighed and transferred to a laminar flow cabinet for digestion. Firstly, the sample was perfused with perfusion buffer until the tissue appeared blanched in colour, indicating the removal of blood. This was achieved using a Heidolph Pump Drive 5006 (Thermo Fischer Scientific, Waltham, USA) at a flow-rate of between 15-30 ml/min, depending on tissue size and capsule integrity.

The tissue was then perfused with digestion buffer (0.5 mg/ml Collagenase IV (400-600 U/mg) and 700 µM CaCl<sub>2</sub> in perfusion buffer) at a similar flow rate, until the tissue appeared to crack and sag beneath the capsule. Perfusion with digestion buffer did not exceed 20 min. At this point, the capsule was minced with sterile scissors and the cell suspension passed through a 125 µm nylon mesh (Clarcor UK, Warrington, UK) to remove large undigested material. The suspension was centrifuged at 80 *g* for 5 min at 4 °C and gently resuspended in Williams E medium. Cells were counted, and viability assessed using Trypan blue. Only cell suspensions with ≥ 75 % viability were used for experiments. Cells were resuspended in complete medium (1 % (v/v) insulin-transferrin-selenium (Life Technologies, Carlsbad, USA), 2 mM L-glutamine, 100 nM dexamethasone and 1 % (v/v) penicillin/streptomycin in Williams E medium) and plated at 250 000 cells/cm<sup>2</sup> in collagen-coated plates (Corning Life Sciences, Amsterdam, Holland). After 3 h, culture medium was replaced to remove any unattached cells.

#### **4.2.3.2. Drug treatment**

Cells were seeded in a 6 well-plate at 1 million cells per well, per 2 ml media, 24 h prior to treatment to allow adherence. 100 or 200x stock solutions were generated for each drug concentration. Drug-treated media was generated by diluting the stock solutions 1 in 200 and used to replace existing media. The resulting concentration of DMSO was 1 or 0.5 % per well respectively. CDDO-Me and Doxycycline (DOX) was purchased from Sigma (Poole, UK).

#### 4.2.3.3. Transfection

Cells were reverse transfected using jetPEI™ (Polyplus, New York, USA). The pRL-SV40 construct was kindly donated by Johnathan Po, University of Liverpool and pSB-tet-NRF2 by Dr. Nick Harper, University of Liverpool. DNA was diluted to 12.5 ng/ul in 150 mM NaCl. jetPEI reagent was diluted 1 in 20, in 150 mM NaCl. All solutions were vortexed before adding 10 µl (125 ng) diluted DNA to 10 µl diluted jetPEI per well. These transfection reactions were vortexed and incubated at room temperature for 20 min while a cell suspension of 25 000 cells per 180 µl medium was generated for each transfection reaction. Cell suspension and transfection reactions were combined and 200 µl added dropwise to the wells of a 96 well plate.

For Western blotting, cells in 12 well-plates were reverse transfected in a similar manner. The ratio of reagents per well in this instance was 100 000 cells per 800 µl media with 200 µl transfection reaction. Transfection reactions consisted of 2 µl jetPEI™ in 100 µl 150 mM NaCl and 250-1000 ng plasmid DNA in 100 µl 150 mM NaCl.

Subsequent drug treatments were achieved by replacing the media 24 – 48 h post transfection with drug-treated media, as described previously.

#### 4.2.4. *In vitro* luciferase assays

All luminescence assays were performed in white-walled 96 well plates (Greiner Bio-one, Kremsmünster, Austria) to avoid signal interference between wells. To measure expression of Firefly luciferase, cells were incubated with *in vivo* grade D-luciferin (Promega, Madison, USA). Cells were washed with PBS and 100 µl 150 µg/ml luciferin in PBS was added to each well. Plates were incubated at room temperature for 5 min and luminescence quantified using the Varioskanner Flash.

To quantify both Firefly luciferase and Renilla luciferase expression, Bright-Glo and Renilla-Glo luciferase assay kits (Promega, Madison, USA) were used. Medium was removed, and Cell lysis was achieved by adding 200 µl 1x GloLysis buffer (Promega, Madison, USA) to each well, and shaking the plate for 5 min at 700 RPM on an Orbit™ plate shaker (Labnet, New Jersey, USA). 100 µl of the cell lysates were transferred to a second white-walled 96 well plate and placed on ice. The Bright-Glo assay was performed on the first plate. 20 µl Bright-Glo reagent was added to each well and the plate was shaken at 700 RPM for 15 sec. Luminescence was quantified using the Varioskanner Flash. To the second plate, 20 µl Renilla-Glo reagent was added. This plate was shaken for 15 sec at 700 RPM and incubated

at room temperature for 10 min. Renilla luciferase expression was then quantified in a similar manner.

#### 4.2.5. qPCR and Western blotting

qPCR analysis described in section 2.2.8. In this chapter, primers designed for human gene products were used (Table 4.5). Western blotting completed using the method described in section 2.2.9.

**Table 4.5 Human qPCR primers**

Gene	Primer	Sequence
<i>F2RL2</i>	Fwd	5'- ACT GAG GTG AAA TTG TGC TCC A -3'
	Rev	5'- TTT CCA TGC CAC TCT GAC AA -3'
<i>LOC344887</i>	Fwd	5'- CTG GAG AAC GTC AAG CGA CT -3'
	Rev	5'- GGG ATG CCA ATG GAC CAG AA -3'
<i>NQO1</i>	Fwd	5'- AGG ACC CTT CCG GAG TAA GAA -3'
	Rev	5'- TGG AAG CCA CAG AAA TGC AGA -3'
<i>NRF2</i>	Fwd	5'- GAG AGC CCA GTC TTC ATT GC -3'
	Rev	5'- TTG GCT TCT GGA CTT GGA AC -3'
<i>SRXN1</i>	Fwd	5'- GAT CCG GGA GGA CCC AGA CA -3'
	Rev	5'- CAA GGA GGC TGC TAC TGC AA -3'
<i>GAPDH</i>	Fwd	5'- GGC CTC CAA GGA GTA AGA CC -3'
	Rev	5'- AGG GGT CTA CAT GGC AAC TG -3'
<i>TRIM16L</i>	Fwd	5' – CCA ATG TAA GTT GTG AAC G - 3'
	Rev	5' – GAA ACC TAG ATG AGA GAT GG - 3'
<i>OR5T3</i>	Fwd	5' – GAC TCC ACT TTC ACA GG - 3'
	Rev	5' – CTT CAG TCT TGT TCT TCA GT - 3'

### 4.3. Results

#### 4.3.1. Bioinformatic analysis reveals putative NRF2-regulated target genes

Previous work from our laboratory identified genes modulated by NRF2 in PHH (Manuscript in preparation). To generate these data, PHH were transfected with either siRNA targeting either NRF2 or KEAP1 for 48 h. Gene expression in samples was assessed using the SurePrint G3 human gene 8x60K v2 microarray kit (Agilent technologies, Santa Clara, US). Transcripts that were both significantly up-regulated in response to KEAP1 knockdown and down-regulated following NRF2 silencing were selected as they exhibited proportional activity to NRF2 and therefore may be potential markers of NRF2 activity.

Initially, the list of genes most responsive to NRF2 pathway modulation in PHH was compared to the literature (See examples in Table 1.1) for prior evidence of direct regulation by NRF2. This resulted in a subgroup of 77 genes without previous direct association with NRF2 (Table A1).

To further refine this list of putative Nrf2-regulated genes, bioinformatic analysis was applied. Firstly, I compared similar siRNA microarray datasets for evidence of the responsiveness of the genes to NRF2 regulation (Fig 4.1 A). As many Nrf2-regulated are implicated in the response to chemical stress, genes were analysed for their sensitivity to activation by toxic stimuli known to induce NRF2 (Fig 4.1 B). Finally, potential ARE sites within the promoter regions of the remaining genes were identified and their activation in response to sulforaphane exposure assessed (Fig 4.1 C).

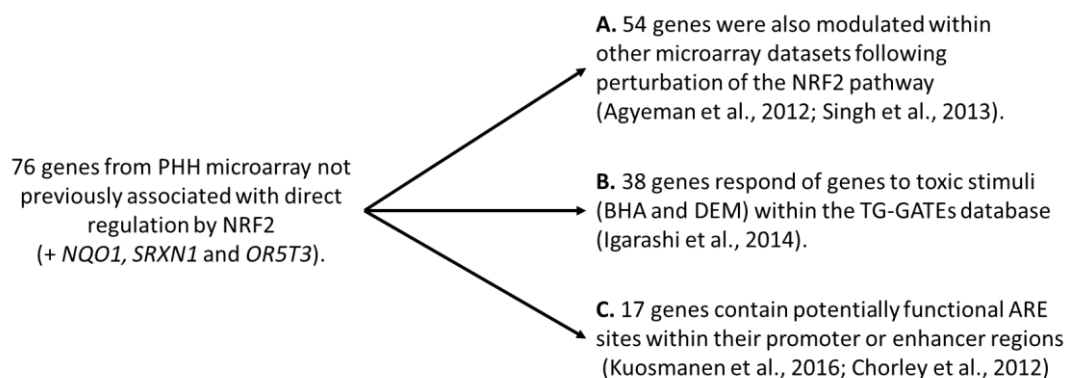


**Figure 4.1 Work flow of microarray hit comparison with existing datasets.**

The 76 potentially novel Nrf2-regulated genes were compared in turn with other microarray datasets in which cells were exposed to siNRF2 or siKEAP1 (A). Secondly, the dataset was compared to gene expression profiles of primary human hepatocytes (PHH) exposed to toxic compounds, known to stimulate Nrf2 activity (B). Finally, location of predicted ARE sites within gene promoter regions and evidence for the site's potential for activation were assessed using Kousmanen motif discovery algorithm and Chorley ChIP-Seq dataset within UCSC genome browser (C). Analysis included positive (*NQO1* and *SRXN1*) and negative (*OR5T3*) controls throughout.

#### 4.3.1.1. Comparison with other microarray datasets

Firstly, the responsiveness of the 76 potentially novel NRF2-regulated genes to siRNA modulation of the pathway in other human cell lines was assessed, utilising previously published microarray datasets (Table A1) (Agyeman et al., 2012; Singh et al., 2013).

Singh *et al.* (GSE38332) evaluated the transcriptomic response of A549 lung cancer cells to siNRF2 compared to non-targeting siRNA (luciferase siRNA) as a control. 266 transcripts were down-regulated to 50 % or lower, than control-treated cells (Singh et al., 2013). These repressed genes were mainly associated with carbohydrate and xenobiotic metabolism pathways. From the 76 genes modulated by NRF2 in PHH, 23 were not present in the Singh dataset. *OR5T3* expression was not assessed. Out of the 56 genes measured, 8 genes were expressed at a similar level to samples exposed to control siRNA, 35 were down regulated between 99 – 50 % of the control group and 13 genes were down regulated to <50 %

expression (Table A1). Within the top 10 most down-regulated genes included *NQO1* and *SRXN1*.

Agyeman *et al.* (GSE28813) assessed NRF2 induction following exposure to sulforaphane or *KEAP1* knockdown in MCF10A, a human breast epithelial cell line. Significant modulation of 1710 transcripts were observed in response to *KEAP1* knockdown while 6378 transcripts were up- or down-regulated more than 1.5-fold by sulforaphane. 879 transcripts were induced by both stimuli. From the 76 potentially novel NRF2-regulated genes in PHH, 24 genes were not measured in the Agyeman datasets, additionally *OR5T3* was not measured. However, 55 genes were measured in both Agyeman datasets (Table A1). In response to siKEAP1, 44 genes were induced, 18 of which were induced over 200 % compared to cells transfected with control siRNA. The 10 most upregulated genes included *NQO1* and *SRXN1* (Table A1). In response to sulforaphane exposure, 44 out of the 76 transcripts were induced alongside *NQO1* and *SRXN1* (Table A1). Over 200 % induction compared to vehicle treated controls were seen in 29 of these transcripts. Genes activated over two-fold by both siKEAP1 and sulforaphane exposure included: *LOC344887*, *MAP2*, *F2RL2*, *SPP1*, *ADHFE1*, *EID3*, *SRXN1*, *ABHD4*, *TRIM16L*, *SULT1A2*, *NQO1*, *KYNU*, *ALDH3A1*, *IKBKKG*, *PPARA*, and *MLLT11*.

In comparison with the Agyeman dataset, 12 genes were shared across datasets that were down-regulated by at least 50 % by siNRF2 treatment and upregulated over two-fold by both siKEAP1 and sulforaphane exposure, compared to vehicle controls. These genes were: *ALDH3A1*, *F2RL2*, *KYNU*, *LOC100506922*, *LOC344887*, *MAP2*, *MYEOV*, *NQO1*, *NRG1*, *SFN*, *SPP1*, and *SRXN1*. Therefore, comparison of putative Nrf2-regulated genes identified by this laboratory with other microarray datasets following modulation of NRF2, highlights similar gene expression patterns in other human cell lines. This further supports the hypothesis that these genes are indeed directly regulated by NRF2.

#### **4.3.1.2. Response to toxic stimuli**

To identify genes that responded to toxic stimuli, known to activate hepatic NRF2 signalling, I assessed the 77 genes (alongside positive and negative control genes) for modulation by the compounds butylated hydroxyanisole (BHA) and diethyl maleate (DEM) (Hiemstra *et al.*, 2017; Yuan *et al.*, 2006). The carcinogen BHA is bioactivated to electrophilic metabolites including *tert*-butylhydroquinone (tBHQ) capable of activating the NRF2 pathway via modification of KEAP1 cysteine residues (Abiko *et al.*, 2011). DEM depletes glutathione via



sulfhydryl group alkylation resulting in induction of oxidative stress and activation of NRF2-regulated genes (Katsuoka et al., 2005; Kaur et al., 2006). Here, I utilise the TG-GATES database, which consists of gene expression data from PHH exposed to a wide range of hepatotoxic compounds (Igarashi et al., 2014).

In response to a 200  $\mu\text{M}$  dose of BHA *in vitro*, 34 genes from our microarray dataset were included in the top 1000 hits collated in the TG-GATES database (Table A1). *SRXN1* and *NQO1* were induced over two-fold compared to vehicle-treated controls. Fold changes in response to BHA ranged from 116 – 402 % across the 36 genes. Likewise, PHH exposed to 1500  $\mu\text{M}$  DEM exhibited induction of 21 genes from the list of 76 and controls: *NQO1* and *SRXN1* (Table 4.8). Expression levels of these genes ranged from 133 – 1532 % in DEM-treated cells, compared to vehicle-treated controls. The most upregulated of which was *F2RL2*. Where multiple probes for the same target were used, the probe with the highest fold change was included only. The negative control gene *OR5T3* was not present in the top 1000 hits modulated by BHA or DEM.

Therefore, there is some homology between NRF2 pathway activity in response to siRNA and toxic stimuli in PHH. Putative NRF2-regulated genes that respond to both would make exciting candidates for novel markers of NRF2 pathway activation in response to chemical stress.

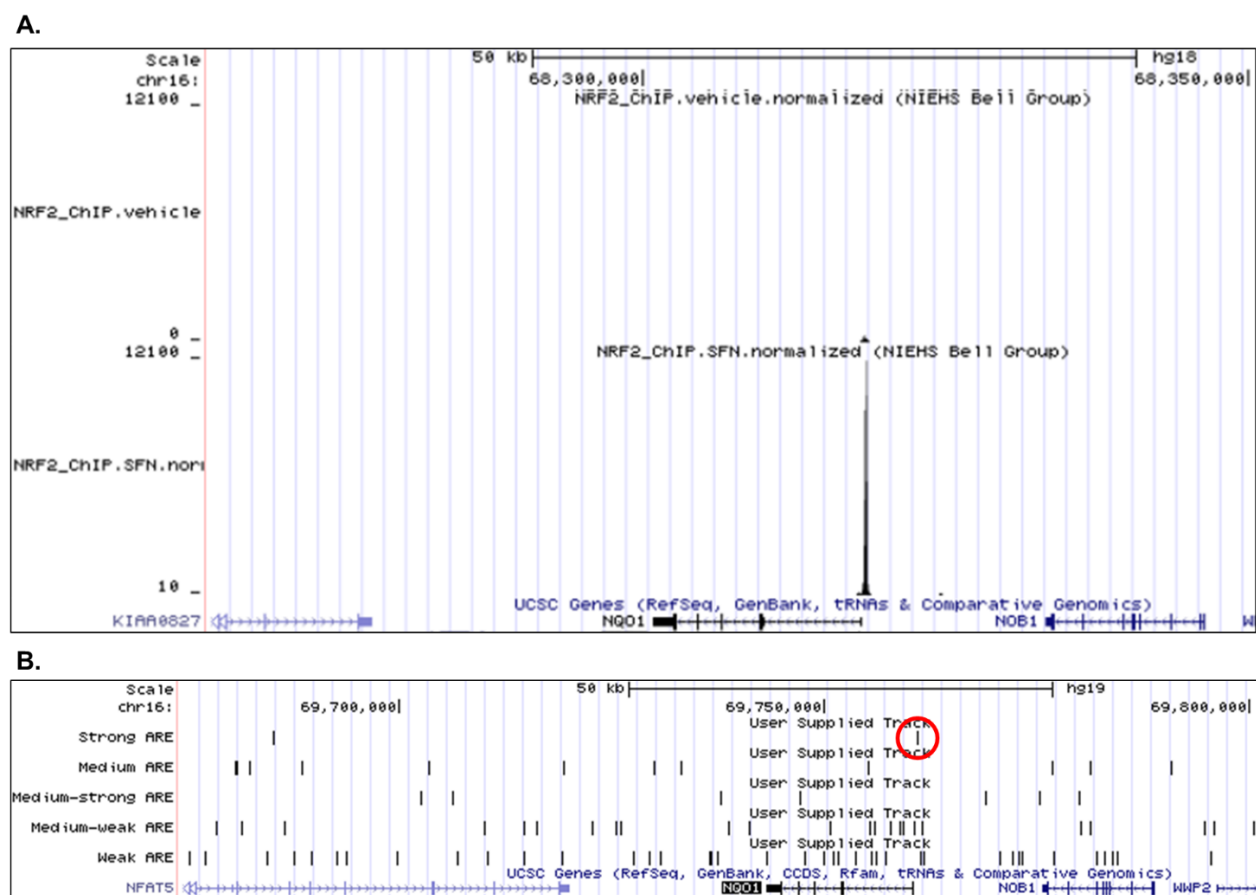
#### 4.3.1.3. Sequence-based analysis

To identify candidate ARE sites within and around the promotor of genes modulated by NRF2 in PHH, I utilised data from Kuosmanen *et al.* documenting ARE sequence variation in the human genome (GRCh37/hg19) (Kuosmanen *et al.*, 2016). In this study, AREs were categorised by the probability of NRF2-binding and given a strong to weak value. All 76 genes contained at least a weak ARE within, or 2 kb upstream of, the gene start site: ATG (Data not shown). *OR5T3*, a gene not modulated by NRF2 in PHH, was used as a negative control (Table 4.6).

To identify functional AREs, I compared these data to locations of NRF2-binding to the human genome (NCBI36/hg18) (Chorley *et al.*, 2012). The authors exposed six different human lymphoid cell lines to sulforaphane and NRF2-binding sites were identified by chromatin immunoprecipitation sequencing (ChIP-Seq). From the 242 high-confidence NRF2-binding sites identified by Chorley *et al.*, 17 were within or close to the promoters of the 76 genes not previously associated with direct regulation by NRF2 (Table 4.6). These genes contained 'peak' regions on the genome wide density plots exhibiting a density greater than 50 units. The negative control, *OR5T3* did not contain an NRF2-binding site within the Chorley dataset.

When compared with the Kuosmanen dataset, many ChIP-Seq 'peak' regions aligned with predicted ARE sites (For example see Fig 4.2). As both datasets were affiliated with different genomes, I compared the location of ARE from the Kuosmanen dataset with the ChIP-seq peaks of the Chorley dataset manually. Out of the 17 putative NRF2-regulated genes exhibiting a peak in response to sulforaphane exposure, 3 were aligned with Strong ARE, 6 with medium strong, 3 with medium, 4 with medium weak and 1 with weak AREs (Table 4.6). The positive control genes *NQO1* and *SRXN1* aligned with strong and medium strong sites respectively.

Therefore, I identified a subgroup of putative NRF2-regulated genes associated with functional ARE sites responsive to sulforaphane exposure, providing strong evidence for direct regulation by NRF2.

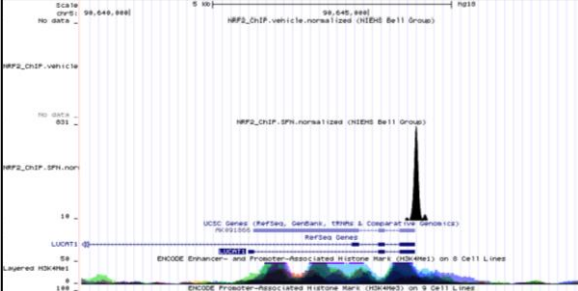
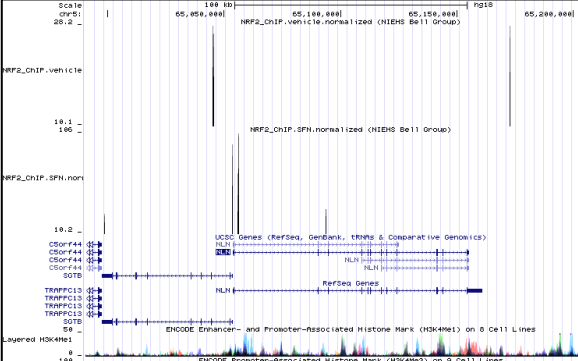
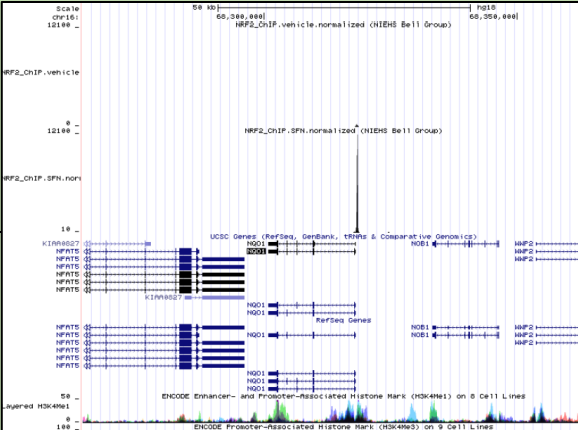
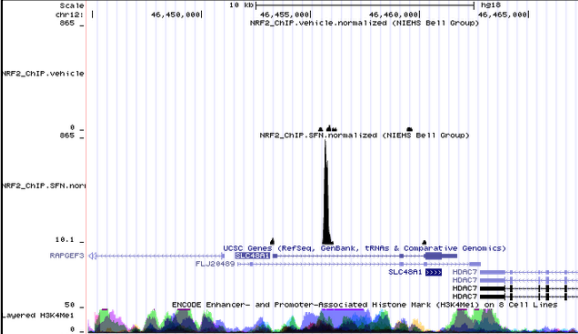


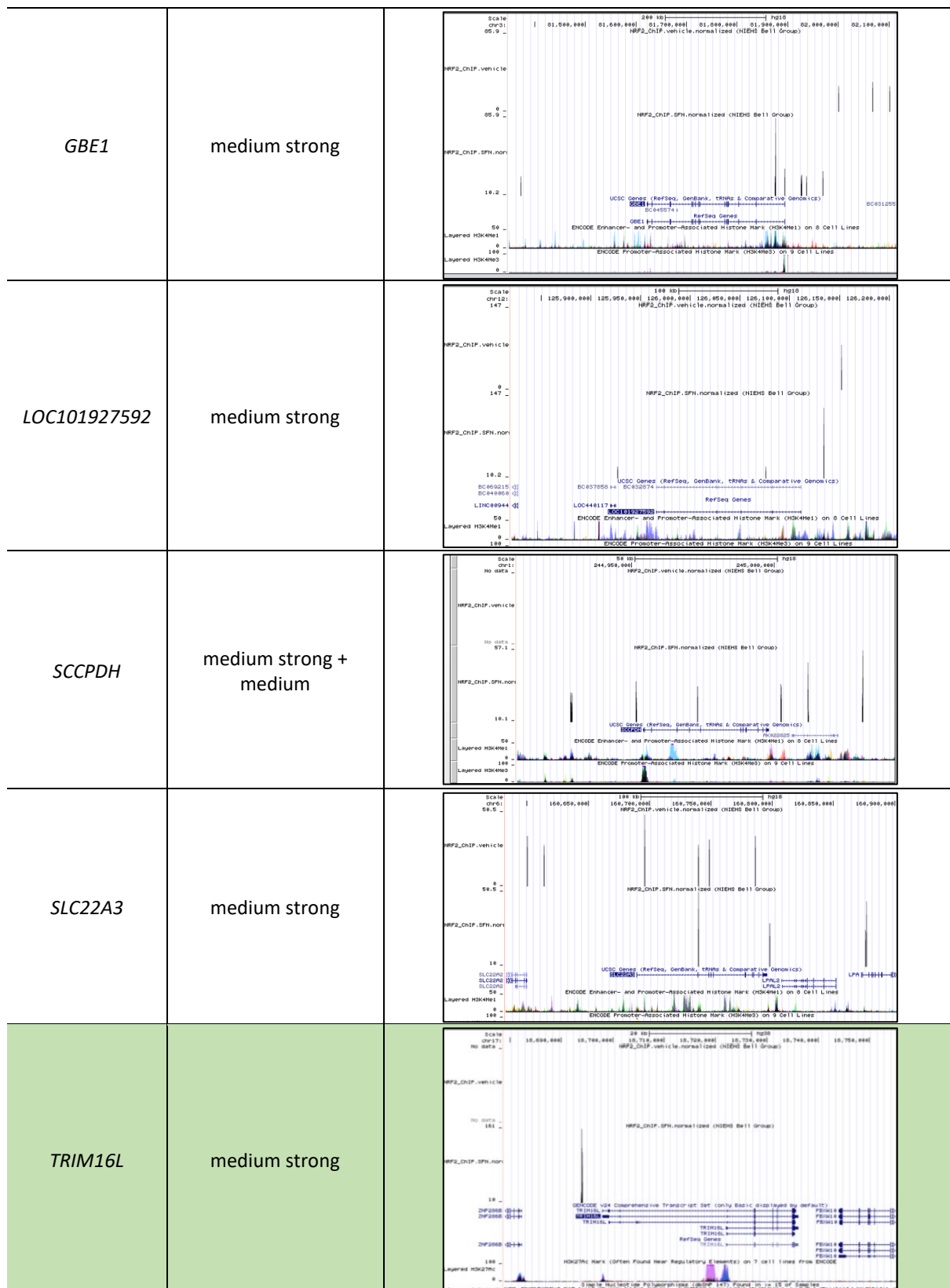
**Figure 4.2 Alignment of ChIP-Seq peaks with predicted antioxidant response elements**

ChIP-seq regions identified by Chorley *et al.* at the NQO1 locus to which NRF2 binds, in response to sulforaphane (SFN) exposure (A) and (B) corresponding predicted 'strong' ARE site, identified by Kuosmanen *et al.*, circled in red (Chorley *et al.*, 2012; Kuosmanen *et al.*, 2016).

**Table 4.6 Genes with antioxidant response elements responsive to sulforaphane**

Green = Genes included in further analysis

Genes with AREs responsive to sulforaphane (Chorley et al., 2012)	Predicted ARE category (Kuosmanen et al., 2016)	Overlapping ChIP-seq Peak (Chorley et al., 2012)
<i>LUCAT1</i>	strong	
<i>NLN</i>	strong	
<i>NQO1</i>	strong	
<i>SLC48A1</i>	strong	



<p><i>UGDH</i></p>	<p>medium strong + weak</p>	
<p><i>ABHD4</i></p>	<p>medium</p>	
<p><i>ALDH1L1</i></p>	<p>medium</p>	
<p><i>PANX2</i></p>	<p>medium</p>	
<p><i>SRXN1</i></p>	<p>medium</p>	

<p><i>ICK</i></p>	<p>medium weak</p>	
<p><i>LOC344887</i></p>	<p>medium weak + weak</p>	
<p><i>TCEB3</i></p>	<p>medium weak</p>	
<p><i>MPP3</i></p>	<p>medium weak</p>	
<p><i>ALDH3A1</i></p>	<p>weak</p>	





#### 4.3.1.4. Gene shortlist

Following comparison with similar microarray datasets based in alternative cell lines, expression analysis in response to chemical stress, and location of ARE sites around the promoter that respond to sulforaphane exposure, I decided to focus on a subgroup of putative NRF2-regulated genes for further analysis: *F2RL2*, *TRIM16L* and *LOC344887*.

Expression of *F2RL2* and *LOC344887* were significantly altered in other microarray datasets modulating the NRF2 pathway (Table 4.6). Additionally, all three genes were significantly upregulated by sulforaphane (Agyeman et al., 2012). While *TRIM16L* was not considerably down-regulated by siNRF2 exposure in the Singh dataset, the response to siKEAP1 and sulforaphane exposure in both the Agyeman and Chorley datasets provide strong evidence for its direct regulation by NRF2. In response to toxic stimuli, all three genes were induced by BHA but only *LOC344887* and *F2RL2* were activated by DEM. Despite significant activation by sulforaphane in the Agyeman dataset, *F2RL2* was not associated with a ChIP-seq peak (Chorley et al., 2012). Due to the gene's significant induction to toxic stimuli and modulation in Singh and Agyeman datasets, *F2RL2* was included for further analysis.

#### 4.3.2. Putative NRF2-regulated gene activation in human liver cells

To confirm the response of these potentially novel NRF2-regulated genes, PHH were exposed to NRF2-activating compounds: CDDO-Me and sulforaphane for 24 h. qPCR analysis revealed significant induction of *F2RL2* and *TRIM16L* by CDDO-Me, compared to gene expression in vehicle-treated cells ( $P = 0.0005$  and  $0.0021$  respectively) (Fig 4.3 A). Following sulforaphane exposure, *F2RL2* expression was also significantly elevated compared to the DMSO treatment group ( $P = < 0.0001$ ) (Fig 4.3 B). While changes in the other genes in response to both CDDO-Me and sulforaphane were not significant, expression levels in all four donors were clearly elevated compared to vehicle-treated cells. Variability between donors may be due to differences in pathology, age and weight (Fig 4.3 C). For instance, Donor 207 was the only patient suffering from COPD and taking a substantial list of medications, displayed the greatest induction of *NQO1* and *F2RL2* in response to NRF2 induction.

In HepG2 cells, exposure to CDDO-Me resulted in upregulation of *F2RL2* and *LOC344887* (Fig 4.4 A). *F2RL2* was significantly induced ( $P = < 0.0001$ ). This effect was NRF2 dependent as target gene activation by CDDO-Me was inhibited in HepG2 cells transfected with siNRF2. In these samples *NRF2* was significantly knocked down to between 29 -15 %, compared to cells

transfected with siCON and exposed to DMSO (Fig 4.4 B) ( $P = 0.0001$ ). In cells transfected with siNRF2 and exposed to CDDO-Me, *TRIM16L* expression was significantly reduced compared to cells transfected with control siRNA and exposed to CDDO-Me ( $P = <0.0001$ ). As a similar response was evident between PHH and HepG2 cells, the immortalised cell line was chosen for transfection with luciferase promotor-reporter constructs (the generation of which is described in 4.3.3).

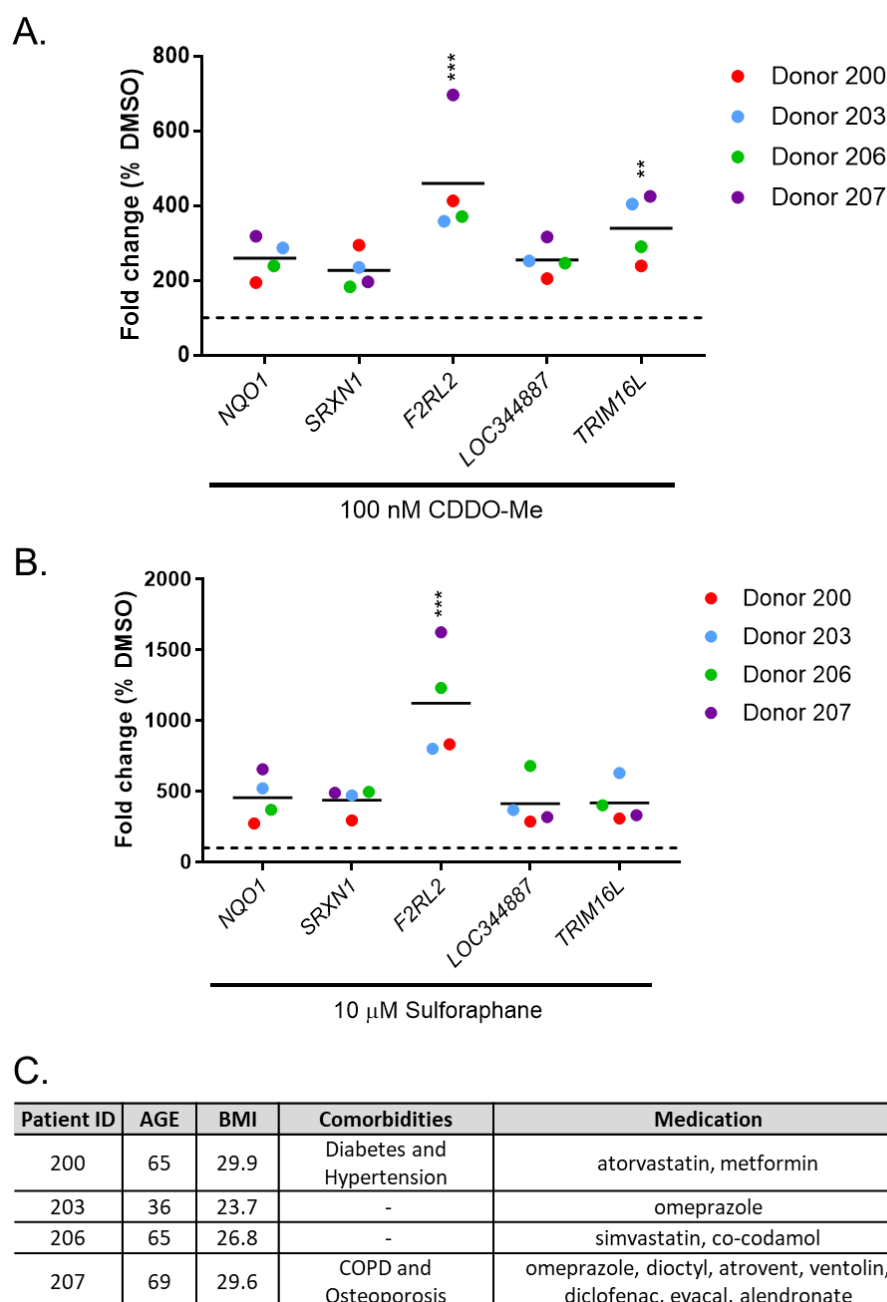


**Figure 4.3 Gene expression in primary human hepatocytes exposed to CDDO-Me**

Primary human hepatocytes (PHH) isolated from four donors were exposed to either 100 nM CDDO-Me (A) or 10  $\mu$ M sulforaphane (B) for 24 h. Gene expression normalised to cells treated with 0.5 % DMSO. Significant induction compared to vehicle-treated cells was assessed by one-way ANOVA or Kruskal Wallis (\*\*  $P \leq 0.01$  and \*\*\*  $p \leq 0.001$ ) (Dotted line = 100%). Age, body mass index (BMI,) comorbidities (such as chronic obstructive pulmonary disease (COPD)) and medication taken by the donors (C).

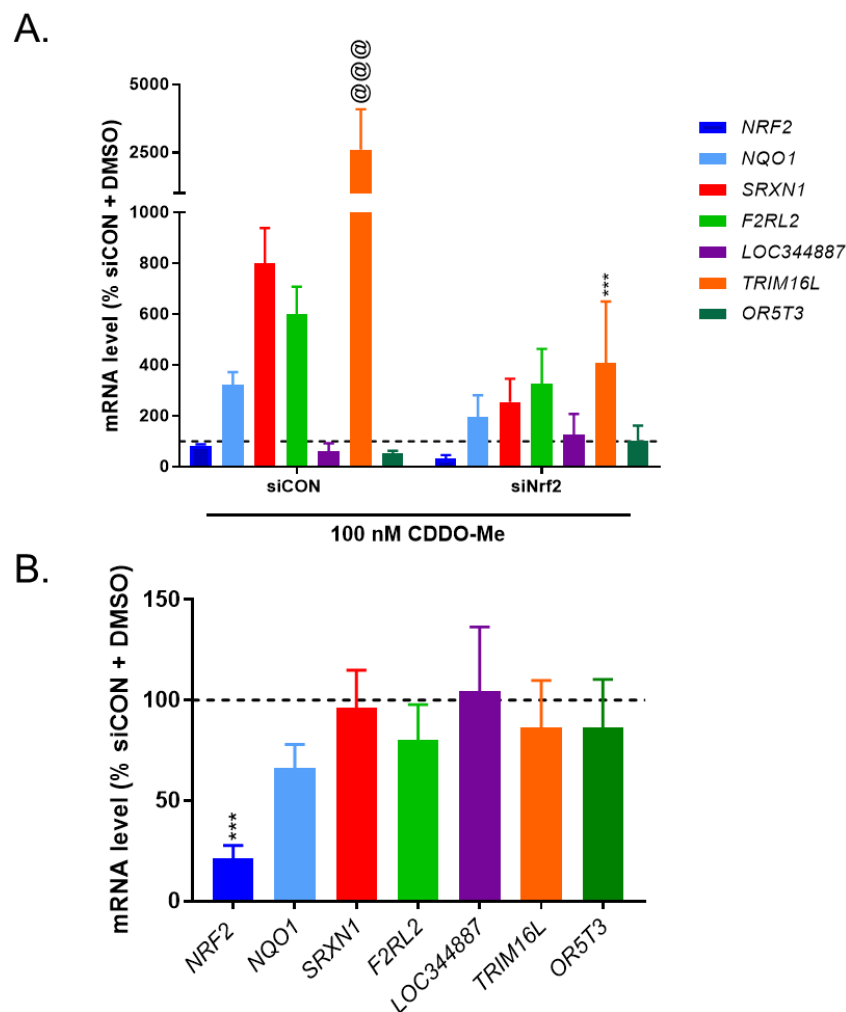


**Figure 4.4 Gene expression in HepG2 cells exposed to CDDO-Me**

HepG2 cells were transfected with siNrf2 or siCON for 24 h and exposed to 100 nM CDDO-Me or 0.5 % DMSO for a further 24 h (n=4). (A) qPCR analysis HepG2 cells transfected with siNrf2 and exposed to DMSO. (B) qPCR analysis of HepG2 cells exposed to siNRF2 or siCON and CDDO-Me. (Dotted line = 100 %) Significant differences in gene expression between siCON + CDDO-Me and siCON+ DMSO treated samples was calculated by one-way ANOVA (@@@  $p \leq 0.001$ ). Significant differences between siCON and siNrf2 + CDDO-Me treatment groups were also calculated by one-way ANOVA (\*\*\*)  $p \leq 0.001$ ).

### 4.3.3. Clone construction

In order to investigate potential ARE target sites through which Nrf2 mediates the expression of F2RL2, LOC344887 and TRIM16L, I next generated luciferase reporters under the control of the relevant gene promoter regions. Promotor regions were synthesised commercially by GeneMill, Liverpool (For example Fig A1). Mutated ARE sequences within the inserts were designed by replacing the bases T with G and A with C and visa-versa (Table 4.1). These inserts were sub-cloned into the pGL4.20 vector (Fig A2) utilising the restriction sites for Kpn1 and Nhe1 within the multiple cloning site of pGL4.20 (Fig A3 A). Successful linearization of the vector (Fig A3 B) and digestion of the WT and MUT inserts (Fig A3 C) were achieved using the restriction enzymes Kpn1 and Nhe1. The TRIM16L WT insert was amplified by PCR due to repeatedly low DNA yield by miniprep. DNA products were extracted from the agarose gels, cleaned up and ligated with the pGL4 vector (For example Fig A4).

Transformed bacteria were screened for successful clone integration and miniprepped DNA sequenced (Fig 4.5 A to D). Fidelity of the WT and MUT ARE sequences were maintained.

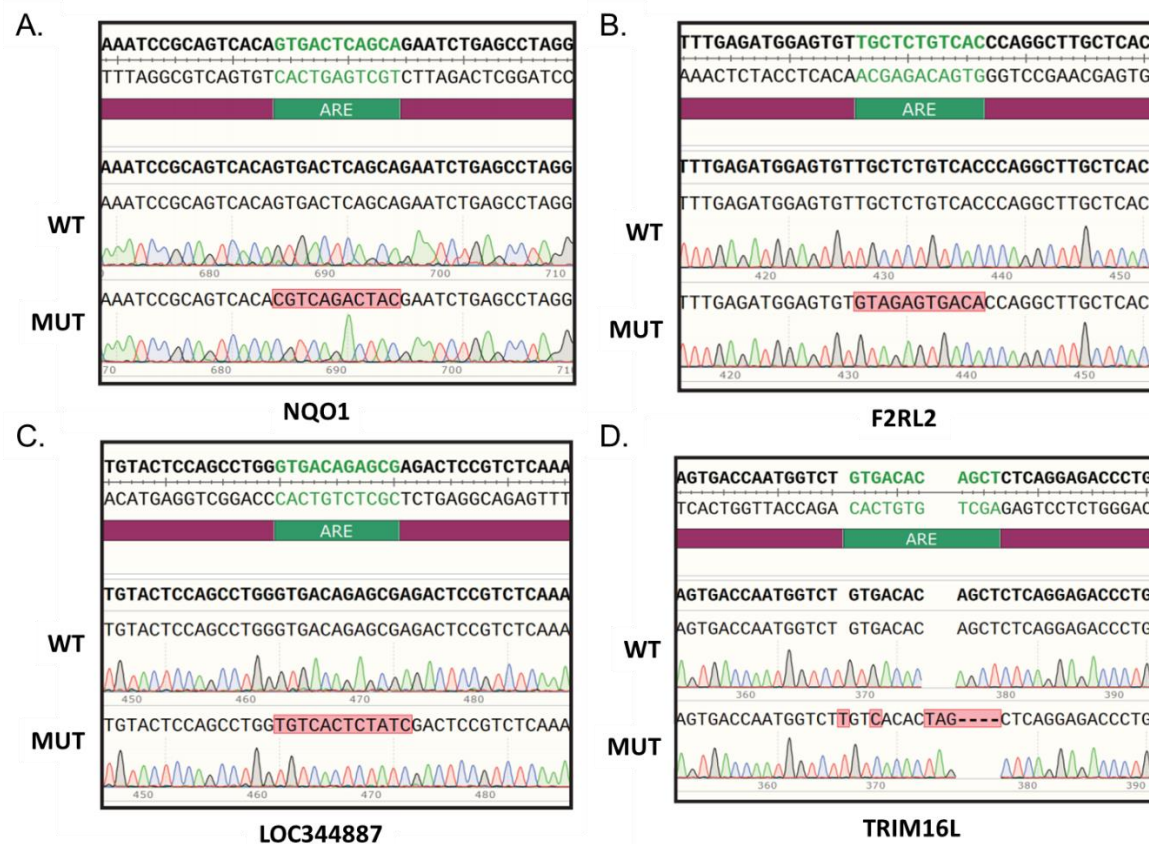


**Figure 4.5 Confirmation of pGL4 clones by Sanger sequencing**

Aligned sequences of wild type (WT) (Top) pGL4-WT (middle) and pGL4-MUT (bottom) sequences of NQO1 (A), F2RL2 (B), LOC344887 (C) and TRIM16L (D) promoter reporter constructs. ARE site highlighted green. Misaligned MUT ARE sequences highlighted red. Genomic WT sequence from UCSC genome Hg38.

#### 4.3.4. Assessment of *SRXN1* antioxidant response elements

Inclusion of AREs from both *NQO1* and *SRXN1* were considered as positive controls for the promoter-reporter assay. Utilising a similar luciferase-based promoter-reporter assay, Singh *et al.* identified an NRF2-responsive element -274 to -193 bp from the transcriptional start site of *SRXN1* (Singh *et al.*, 2009). However, I noticed this sequence contains two putative ARE sites (Fig 4.6). Both sequences fall within ChIP-Seq region of NRF2-binding identified by Chorley *et al.* (Chorley *et al.*, 2012) (Table 4.6). Further analysis is needed to identify the necessity of either/both of these ARE sites for NRF2-dependent activation and so WT and MUT constructs of both ARE sites were synthesised in a similar manner to section 4.3.3.

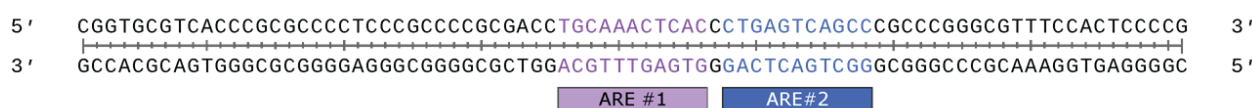


**Figure 4.6 Potential ARE sites within the *SRXN1* promoter**

The region -274 to -193 bp from the transcriptional start site of *SRXN1*, identified by Singh *et al.* as an NRF2-responsive element (Singh *et al.*, 2009). However, this sequence contains two putative ARE sites highlighted.

#### 4.3.5. ARE-reporter construct response to pharmacological induction of NRF2

Initial transfections were conducted in the readily transfectable HEK293T cell line. Following 24 h exposure to CDDO-Me, luminescence was quantified in the transiently transfected cells (Fig 4.7 A). Cells transfected with the empty pGL4 vector and the negative control construct pGL4-OR5T3 WT did not produce a luminescent response greater than their vehicle-treated counterparts. pGL4-NQO1 WT transfected cells produced significantly greater luminescence than those transfected with pGL4-NQO1 MUT, following CDDO-Me exposure ( $P = <0.0001$ ) (Fig 4.7 A). Amongst the novel gene reporters, only cells transfected with pGL4-Trim16L WT and pGL4-Trim16L MUT produced luminescence greater than DMSO-treated counterparts (Fig 4.7 B). Unexpectedly HEK293T cells transfected with pGL4-TRIM16L MUT produced more luminescence than those exposed to pGL4-TRIM16L WT. However, these data are only  $n=1$ .

Following successful transfection in HEK293T cells, the construct response to CDDO-Me was assessed in HepG2 cells. When transiently transfected with the pGL4-constructs and exposed to CDDO-Me for 24 h, a similar luminescent response to the HEK293T cells were observed (Fig 4.8 A). Following induction of NRF2 by CDDO-Me, pGL4-NQO1 WT produced a significantly stronger luminescent signal than the mutant construct ( $P = <0.0001$ ). Cells transfected with pGL4-TRIM16L MUT also produced significantly greater luminescence than cell transfected with pGL4-TRIM16L WT ( $P = <0.0001$ ), consistent with the findings in HEK293T cells.

Firefly luminescence (fLuc) induced by CDDO-Me was subsequently normalised to renilla luminescence (rLuc) expression to account for in-well transfection efficiency and potential discrepancies in cell viability (Fig 4.8 B and C). In this assay HepG2 cells were co-transfected with the constitutively active, rLuc-based, pRL-SV40 construct. Both fLuc and rLuc activity were normalised to DMSO-treated, equivalently transfected cells. fLuc activity was then expressed as a percentage of rLuc activity. When normalised to renilla luciferase expression, luminescence did not differ greatly from the initial analysis. HepG2 cells transfected with pGL4-NQO1 WT produced significantly more luminescence than the mutated construct ( $P = 0.0286$ ) (Fig 4.8 B). Cells transfected with pGL4-OR5T3 did not produce a luminescent response to CDDO-Me exposure. Therefore, while positive and negative control promotor-reporter constructs exhibited expected luminescence values, lack of induction of F2RL2 WT, LOC344887 WT and TRIM16L WT greater than their MUT counterparts (Fig 4.7 C), indicated potentially indirect mechanisms for NRF2 activation in response to CDDO-Me exposure.



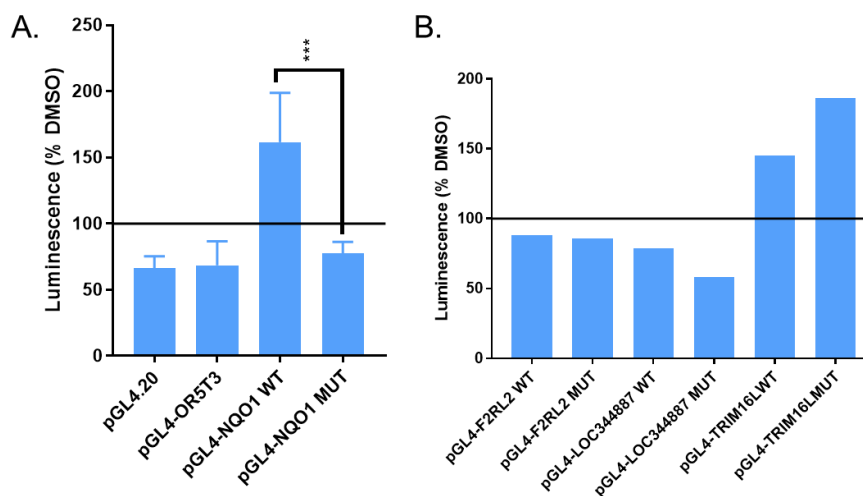


**Figure 4.7 pGL4-construct response to CDDO-Me in HEK293T cells**

Luminescence in HEK293T cells transiently transfected with promoter-reporter constructs and exposed to 100 nM CDDO-Me for 24 h. (A) Luminescent response of empty vector, positive and negative control plasmids (n=3). (B) Luminescent response of WT and MUT constructs (n=1). Luminescence normalised to DMSO-treated, transfected counterparts. Significant difference between WT and MUT construct luminescence calculated by Student's T test (\*\*\*)  $p \leq 0.001$ . Mean + SD shown.

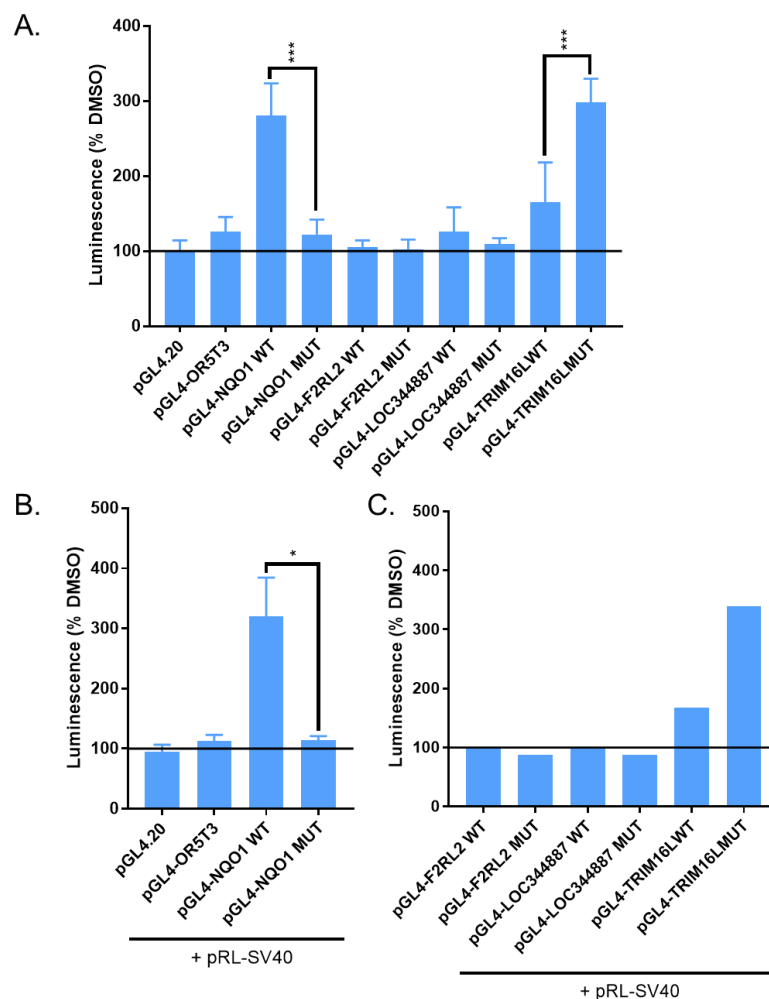


**Figure 4.8 pGL4-construct response to CDDO-Me in HepG2 cells**

(A) Luminescence in transiently transfected HepG2 cells following exposure to 100 nM CDDO-Me for 24 h (n=3). Luminescence normalised to 0.5 % DMSO-treated, transfected counterparts. Significant difference of wild-type (WT) and mutant (MUT) construct luminescence was calculated by one-way ANOVA. (B) Firefly (fLuc) and renilla (rLuc) luciferase expression was subsequently quantified in HepG2 cells co-transfected with either the empty vector, positive or negative control constructs and pRL-SV40, then treated with CDDO-Me in a similar manner (n=3). fLuc normalised to rLuc activity and expressed as a percentage of the DMSO-treatment groups. (C) fLuc expression of pGL4- WT and MUT constructs normalised to rLuc of pRL-SV40 vector in transiently transfected HepG2 cells stimulated with CDDO-Me (n=1). Significant difference between WT and MUT construct luminescence calculated by one-way ANOVA or Kruskal Wallis (\*  $p \leq 0.05$  and \*\*\*  $p \leq 0.001$ ). Mean + SD shown.

#### 4.3.6. ARE-reporter response to overexpression of NRF2

To minimise off target effects of pharmacological activation of the NRF2 pathway, construct luminescence in response to NRF2 overexpression was assessed. As similar luminescence expression was evident with and without normalisation to rLuc expression of the pRL-SV40 control plasmid, this control was not included in further experiments. Induction of NRF2 was achieved using the pSB-tet-NRF2 inducible construct (Fig A5). This plasmid utilises the 'tetracycline (Tet) on' system, established by Gossen *et al.*, whereby the constitutively active Tet repressor binds to the TRE promoter region, inhibiting transcription (Gossen *et al.*, 1995). In cells transfected with pSB-tet-NRF2, repression of the NRF2 sequence is relieved following exposure to the tetracycline analogue, Doxycycline (DOX). This results in NRF2 overexpression. Firstly, HEK293T cells were transfected with increasing amounts of pSB-tet-NRF2, and NRF2 expression was induced by treatment with 6 µg/ml DOX for 24 h (Fig 4.9 A). Similar levels of NRF2 protein expression, compared with 24 h exposure to 100 nM CDDO-Me and 2 h exposure to 10 µM MG132 were observed. To identify the optimal concentration of DOX for induction of the pGL4-reporter constructs in HepG2 cells, cells transfected with either pGL4-NQO1 WT or MUT constructs were exposed to increasing concentrations of DOX for 24 h (Fig.4.9 B). When normalised to DMSO-treated equivalents, doses of 5-8 µg/ml DOX induced the greatest difference between pGL4-NQO1 WT and MUT luciferase expression. Time course analysis revealed luminescence in HepG2 cells transfected with pGL4-NQO1 WT peaked at 12 h exposure to DOX (Fig 4.9 C).

Based on these preliminary experiments, HepG2 cells transfected with the pGL4 promoter constructs were exposed to 6 µg/ml DOX and luminescence quantified after 12 h (Fig 4.10). Luminescence was normalised to DMSO-treated equivalents. Cells transfected with pGL4-NQO1 WT produced significantly greater luminescent response to NRF2 overexpression compared to those transfected with pGL4-NQO1 MUT ( $P = 0.0026$ ). Cells transfected with the other pGL4 reporters exhibited a similar luminescent response to that induced by CDDO-Me (Fig 4.12 A). Therefore, despite testing alternative methods for NRF2-activation, the luminescence expression patterns of cells transfected with either WT or MUT constructs remained similar.

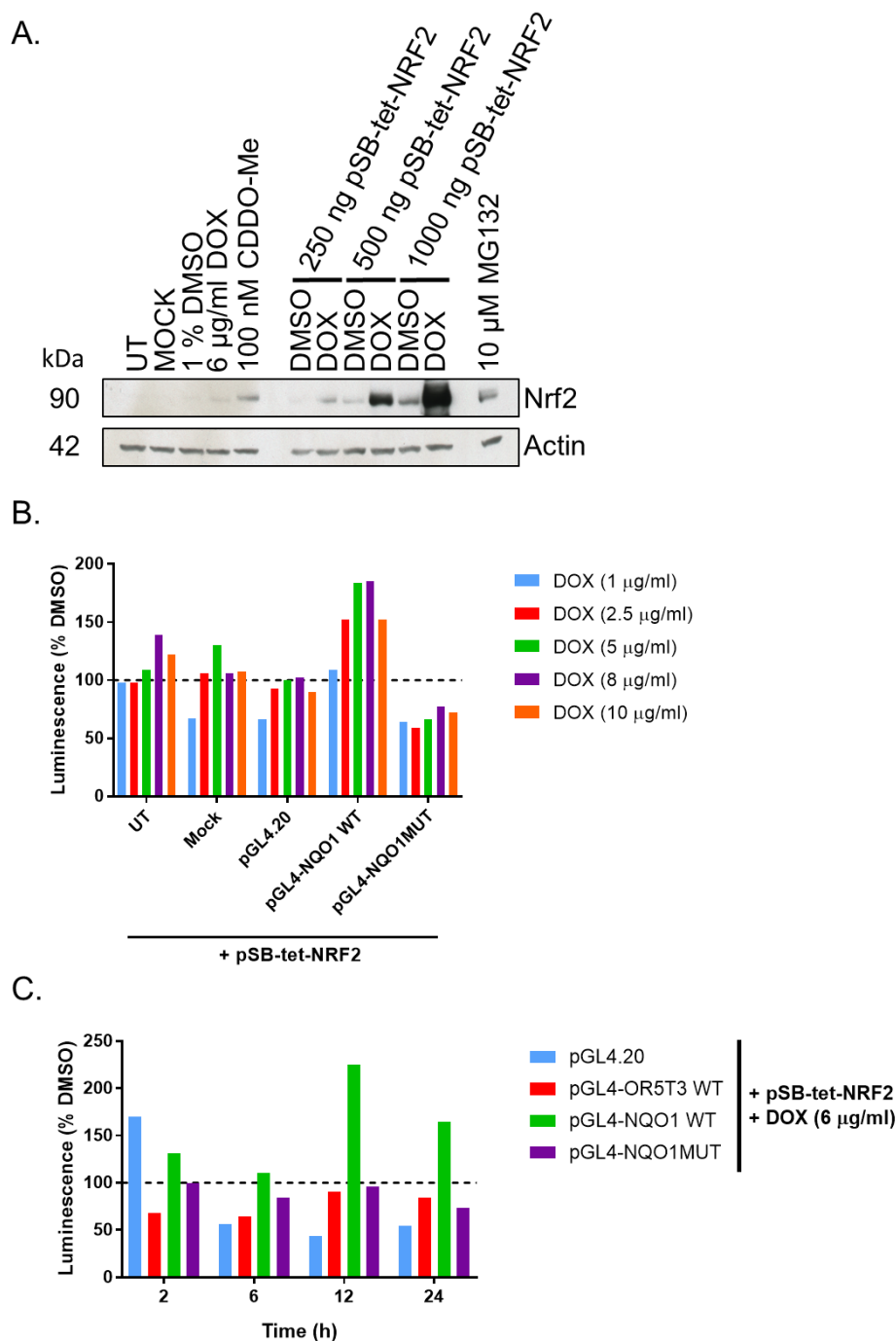


**Figure 4.9 Optimisation of NRF2 overexpression by pSB-tet-NRF2**

(A) Western blot of HEK293T cells transfected with increasing amounts of pSB-tet-NRF2 and exposed to either 1 % DMSO or 6 µg/ml Doxycycline (DOX) in comparison with untransfected HEK293T cells treated with 1 % DMSO, 6 µg/ml DOX or 100 nM CDDO-Me for 24 h or 10 µM MG132 for 2 h. (C) Luminescence in HepG2 cells co-transfected with pSB-tet-NRF2 and exposed to increasing concentrations of DOX. Luminescence was quantified after 24 h (n=1). (C) Time course analysis of pGL4-NQO1 induction at 2, 6, 12 and 24 h post DOX administration (n=1) (dotted line = 100 %).

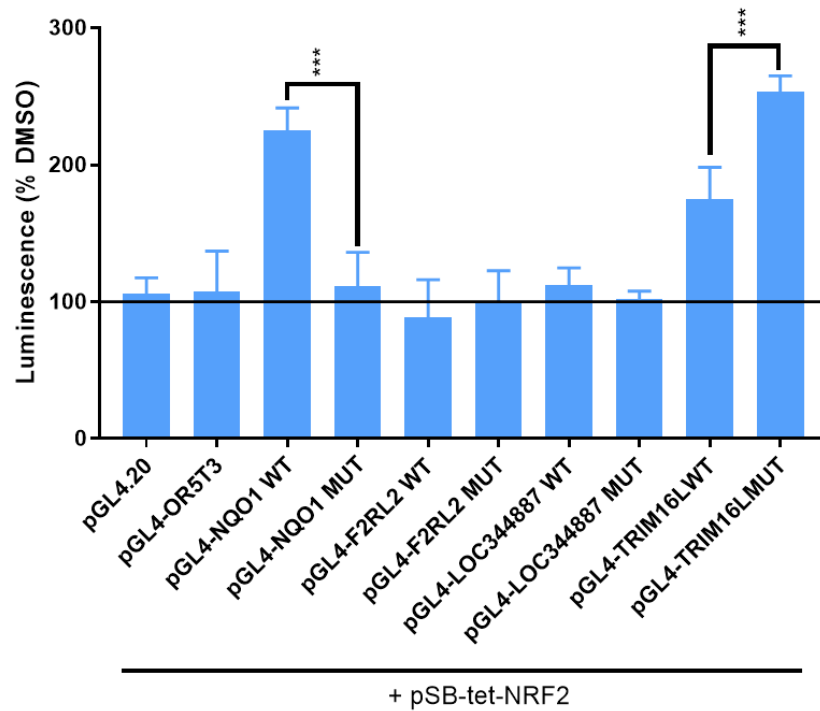


**Figure 4.10 pGL4-construct response to NRF2 overexpression in HepG2 cells**

HepG2 cells were co-transfected with a promoter-reporter construct and pSB-tet-NRF2. After 12 h, NRF2 overexpression was induced via exposure to 6  $\mu\text{g/ml}$  Doxycycline. Luminescence normalised to DMSO-treated, transfected counterparts ( $n=3$ ). Significant difference in WT compared to MUT construct induction was calculated by One-way ANOVA and Kruskal Wallis (\*\*\*)  $p \leq 0.001$ ). Mean + SD shown.

#### 4.3.7. SRXN1 ARE assessment

To assess the necessity of both ARE sites within the binding-region identified by Singh et al. as responsible for *SRXN1* activation, WT and MUT reporter constructs were generated. In CDDO-Me-treated, transiently transfected HepG2 cells, pGL4-SRXN1 WT luminescence was greater than the three mutant-ARE-constructs ( $P = <0.0001$  for all) (Fig 4.11 A). Interestingly, luminescence was not significantly different between the pGL4-SRXN1 ARE1, ARE2 or ARE 1+2 mutants. When normalised to rLuc expression of a constitutively active construct, a similar expression pattern was observed, indicating transfection with the pGL4-SRXN1 WT and MUT constructs did not affect cell viability and transfection efficiency varied little between wells (Fig 4.11 B).

In response to NRF2-overexpression, significantly greater luminescence was observed in HepG2 cells transfected with pGL4-SRXN1 WT compared to cells transfected with MUT constructs ( $P = <0.0001$  for all) (Fig 4.11 C). Again, the luminescence responses between the pGL4-SRXN1 ARE1, ARE2 and ARE 1+2 mutants did not significantly differ.

Therefore, while luminescence from cells transfected with the pGL4-SRXN1 WT construct was significantly greater than the other constructs in response to both CDDO-Me exposure and Nrf2 overexpression, luminescence of the pGL4-SRXN1 ARE1, ARE2 and ARE 1+2 mutants did not differ. Thus, highlighting the role both sites play in this extended ARE site during *SRXN1* activation by NRF2.

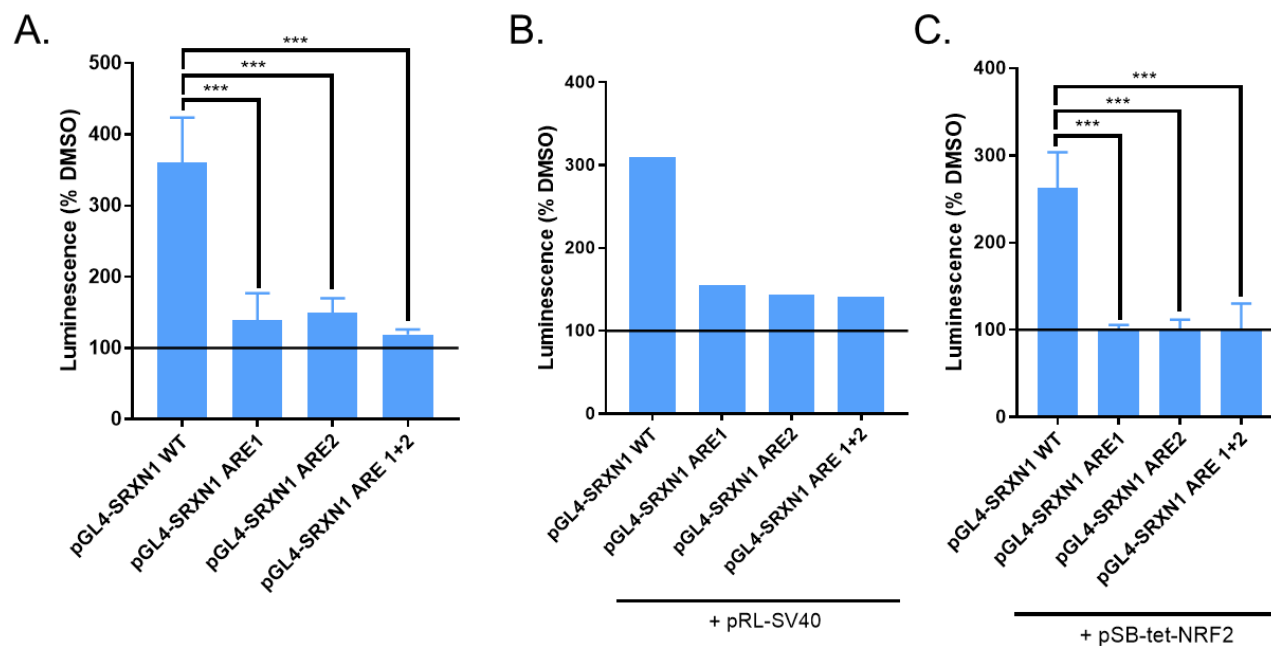


**Figure 4.11 Induction of wild-type but not mutant pGL4-SRXN1 constructs following NRF2 activation**

Luminescence of (A) HepG2 cells transiently transfected with promoter-reporter constructs and exposed to 100 nM CDDO-Me or 0.5 % DMSO for 24 h (n=3). Significance difference of wild-type (WT) and mutant (MUT) construct luminescence was calculated by one-way ANOVA. (B) Firefly (fLuc) and renilla (rLuc) luciferase activity was quantified in HepG2 cells co-transfected with pGL4-SRXN1 constructs and pRL-SV40, exposed to CDDO-Me or its vehicle control (n=1). fLuc was normalised to rLuc activity. (C) Luminescence of HepG2 cells co-transfected with pGL4-SRXN1 constructs and pSB-tet-NRF2, exposed to 6 µg/ml Doxycycline (DOX) or 1 % DMSO for 12 h. Significant difference in WT compared to MUT construct induction was calculated by one-way ANOVA (\*\*\*)  $p \leq 0.001$ ). Mean + SD shown.

#### 4.4. Discussion

Thorough understanding of the regulatory role of NRF2 in human hepatic cells may inform models of pathway activation for the identification hepatotoxic compounds. The aim of this chapter was to determine whether NRF2 directly regulates the expression of Coagulation factor II receptor-like 2 (*F2RL2*), NmrA-like family domain containing 1 pseudogene (*LOC344887*) and Tripartite Motif Containing 16 Like (*TRIM16L*), via specific ARE elements located in the promoter regions of these genes. Data mining publicly accessible datasets revealed these genes responded to NRF2 modulation by genetic and pharmacological stimuli (Agyeman et al., 2012; Igarashi et al., 2014; Singh et al., 2013). In particular, both *LOC344887* and *TRIM16L* exhibited responsive elements to sulforaphane exposure that aligned with ARE binding sites (Chorley et al., 2012; Kuosmanen et al., 2016). ARE sites identified via bioinformatic analysis were sub-cloned into the luminescent pGL4.20 vector. In response to NRF2 overexpression and pharmacological induction by CDDO-Me *in vitro*, the pGL4-Nqo1 WT and pGL4-SRXN1 WT constructs produced significantly stronger luminescent signals than their mutant counterparts. The negative control plasmid pGL4-OR5T3 was not induced under any conditions. However, the luminescent response of wild-type pGL4-F2RL2, -LOC344887 and -TRIM16L were never greater than cells transfected with their mutant counterparts, indicating the promoter regions included in this analysis may not be solely responsible for NRF2-mediated gene activation.

*LOC334887* is a transcriptionally active, duplicated pseudogene containing an RNA polymerase 2 and various transcription factor binding sites, identified by combining large-scale RT-PCR-Seq of pseudogenes with gene annotation datasets including HAVANA (Human and vertebrate analysis and annotation) (Pei et al., 2012). Located on chromosome 3, the pseudogene contains 10 introns and is associated with 8 mRNA splice variants (Thierry-Mieg and Thierry-Mieg, 2006). Initially described by Jacq *et al.*, pseudogenes share similar sequences to functional genes but lack protein-coding ability due to the accumulation of mutations, absence of transcriptional activity or ability to encode RNA (Jacq et al., 1977). They may arise from the incorporation of mRNA into the chromosome (processed pseudogenes) or the accumulation of mutations over time (unprocessed and unitary pseudogenes)(reviewed by Groen et al., 2014). The encyclopaedia of DNA elements (ENCODE) project identified 863 pseudogenes within the human genome that are transcriptionally active and related to active chromatin (Pei et al., 2012). Expression of non-coding RNA can act as endogenous siRNA or conversely compete with its functional paralog



for mRNA binding complexes resulting in enhanced stability and translation of mRNA associated with the parent gene of the pseudogene.

Induction of *LOC344887* *in vitro* has been demonstrated following exposure of cells to: 1,2,4-benzenetriol (A reactive metabolite of benzenoxide) (Miyahara et al., 2014), cigarette smoke (Boylston and Brenner, 2014), airborne free radicals (Sun et al., 2012), and sodium arsenate (Qiu et al., 2015). Johnson *et al.* describe *LOC344887* mediated co-activation of NRF2 resulting in induction of *NQO1* (Johnson et al., 2015). The authors treated colon cell lines with NRF2 inducers, sulforaphane, oltipraz and tert-butylhydroquinone, which resulted in induction of *LOC344887*. The pseudogene was also sensitive to knock down of NRF2. Chromatin immunoprecipitation identified potential NRF2 and MafK binding regions while RNA immunoprecipitation supplied evidence for direct binding to MafK. The authors hypothesized that *LOC344887* acts as a scaffold for MafK/NRF2 or other transcription factors on the promoter region of *NQO1*. Johnson *et al.* identify the 'TGACAGAGCCG' sequence (named ARE2) between exon1 and 2 as the location of NRF2 and MafK co-localisation. This ARE site was incorporated into our pGL4-*LOC344887* WT vector. However, the authors also note the binding of MafK to the ARE1 sequence (TGACACTGCA) in the pseudogene's promoter region. This ARE site was part of the 390 bp region deleted in the CRISPR/Cas9 knock out cell line. The ARE1 sequence was not included in our promoter reporter analysis and, if MafK is an essential cofactor for expression of *LOC344887* in hepatocytes stimulated with sulforaphane, may therefore be the reason for the lack of induction of the pGL4-*LOC344887* WT plasmid.

*F2RL2* encodes protease activated receptor 3 (PAR3), a member of the G protein coupled receptor family. The gene extends across two exons encoding the signal peptide and mature protein, seven transmembrane helices, a pro-domain, three intracellular loops, three extracellular loops and a carboxyl terminus (Kahn et al., 1998). PAR3 also contains a hirudin-like binding domain within the amino terminus, to which prothrombin binds. There are four PARs present in humans and mice which are activated following proteolysis of the N-terminus either by thrombin or other proteases including trypsin and coagulation factors (Reviewed by Coughlin, 2000). Originally identified by Ishihara *et al.*, there is little evidence to suggest PAR3 functions autonomously and is therefore classed as a non-signalling receptor (Ishihara et al., 1997). However, increasing evidence indicates its role as a cofactor for activation of other PARs including heterodimerization with PAR1 (McLaughlin et al.,

2007). X-ray crystallography highlighted the role of PAR3 as a cofactor for the activation of PAR4 via cleavage of prothrombin (Bah et al., 2007).

Knockdown of PAR3 in human pancreatic adenocarcinoma (PANC1) cells lead to: faster adhesion to plastic and madrigal-coated plates, slower 'wound closure' in a 2D assay, and increased expression of integrins and E-cadherin (Segal et al., 2014). While, knock down of PAR3 in human osteoarthritis synovial fibroblasts (OSAFs) significantly abolished thrombin mediated upregulation of *HMOX1* (Liu et al., 2012). Exposure to a PAR3 agonist, resulted in significant increases in *HMOX1*. It is thought that thrombin induces *HMOX1* via PAR1 and PAR3 interactions with NRF2 signalling in OSAFs. Other proteases have been shown to activate Nrf2-regulated: PAR2 activates *NQO1* in keratinocytes (HaCaT cells) by stabilizing NRF2 to facilitate its translocation (Kim et al., 2014).

Similar to *LOC344887*, increased expression of *F2RL2* alongside *HMOX1* was evident following treatment with 1% cigarette smoke extract in human bronchial epithelial cells (Boylston and Brenner, 2014). *F2RL2* is down-regulated in activating transcription factor 3 (*ATF3*) KO mice (Akram et al., 2010). *ATF3* has been shown to interact directly with NRF2 in order to repress NRF2 pathway activation (Brown et al., 2008). However, microarray analysis of global gene expression within the non-small cell lung cancer (NSCLC) cell line A549, revealed down-regulation of *F2RL2* in comparison to untreated cells, following 48 h of stimulation with 50  $\mu$ M quercitrin, a potent antioxidant and NRF2 activator (Cincin et al., 2014). This may be due to the 48 h time point or tissue specific *F2RL2* activity.

*TRIM16L*, also known as *TRIM70*, shares significant homology to the *TRIM16* sequence (Yu et al., 2016). As members of the tripartite motif-containing (TRIM) family, these genes contain a motif consisting of a ring domain, at least one B-box domain and an associated coiled-coil domain in the N-terminus (Hatakeyama, 2011). In response to laminar shear stress, microarray analysis of human umbilical vein endothelial cells (HUVECs) identified upregulation of *TRIM16* alongside NRF2-regulated genes including *HMOX1*, *NQO1* and *GCLM* (Warabi et al., 2004). Other members of the TRIM family, such as *TRIM21* have been shown to regulate NRF2 expression via direct ubiquitination of P62, inhibiting KEAP1 degradation, resulting in suppression of NRF2 pathway activity (Pan et al., 2016). In human non-small cell lung carcinoma tumours with mutations in *KEAP1* and exons within the KEAP1 binding sites of *NRF2*, both *TRIM16* and *TRIM16L* mRNA expression was elevated compared to tumours without these mutations (Goldstein et al., 2016). However, the role of *TRIM16L* and its place in the NRF2 pathway are yet to be discovered.

In this chapter, I utilised a luciferase-based promotor-reporter assay to determine the ARE sites responsible for NRF2-mediated activation. This technique, among others, has been used previously, to identify NRF2-regulation of genes. The electrophoretic mobility shift assay (EMSA) and super-shift assay document the slower migration of DNA-protein complexes through a gel compared to DNA alone (Fried and Crothers, 1981; Garner and Revzin, 1981). However, these 'peak' regions often span large areas, impeding identification of exact binding sequences. Here I applied mutational analysis of promotor regions of putative NRF2-regulated genes to provide direct evidence of NRF2 binding to putative ARE sites.

The consensus ARE sequence has undergone many revisions. Initial identification of the motif in rat *GSTA1* and *NQO1* revealed the sequence RGTGACnnnGC (R=A or G) (Rushmore et al., 1991). Assessment of mouse *Gsta2*, *Nqo1*, *Gstp1*, and *Ftl* indicated TMANNRTGAYNNNGCRWWWW (W=A/T M=A/C) was more representative (W. W. Wasserman and Fahl, 1997). Observation of two ARE sites within the human *GCLM* promoter revised the sequence to T,G/T,A,C/T,NNNGCA (Erickson et al., 2002). Comparison of well-established ARE motifs across human, mouse and rat genomes confirmed nucleotides TNANNNNGC were constant and TGACNNNGC as the most-likely core consensus sequence (Wang et al., 2007). However previous mutational analysis by Nioi *et al.* highlighted divergence between mouse and human ARE sequences, stating a universal ARE consensus sequence may not be possible (Nioi et al., 2003). In this chapter ARE sequences from *NQO1*, *F2RL2*, *LOC344887* and *TRIM16L*, included in our mutational analysis, all contained the TGACNNNGC motif (Table 4.1).

Despite using both genetic and pharmacological methods of NRF2 activation, luminescence in cells transfected with pGL4-LOC344887 and pGL4-F2RL2 WT and MUT constructs were not significantly different. Lack of differential activation of WT and MUT construct luminescence may suggest these genes are not regulated by NRF2. However, this is unlikely as bioinformatic analysis highlighted modulation in variety of cell types exposed to different stimuli known to modulate NRF2 (Agyeman et al., 2012; Igarashi et al., 2014; Singh et al., 2013). Expression may be indirectly regulated by the transcription factor. Nrf2 has been shown to modulate miRNAs that influence transcription of other genes (Chorley et al., 2012; Singh et al., 2013). In *Nrf2*<sup>-/-</sup> fibroblasts, rescue of *GCLC* promoter-reporter construct activation, in response to tBHQ via *Nrf2* overexpression was inhibited when activator protein 1 (AP-1) transcription factor binding sites within the *GCLC* promoter were mutated (Yang et al., 2005). Additionally there is cross-talk between NRF2-regulated genes and those containing xenobiotic response elements (XRE) sites regulated by the transcription factor

aryl hydrocarbon receptor (AHR) (Yeager et al., 2009). Many of the genes listed in Table A1 had XRE sites close to the gene start site (data not shown). NRF2 itself is regulated by AHR (Miao et al., 2005). Conversely NRF2<sup>-/-</sup> mice exhibited reduced expression of AHR and NRF2 has been shown to directly bind to an ARE site 250 bp upstream from the transcription start site of AHR (Shin et al., 2007). Alternatively, the promotor elements included in the reporter constructs may not contain the specific ARE sequence or additional enhancer sites necessary for activation. For instance, the ARE sites identified in the Kuosmanen dataset upstream of the *F2RL2* start site, do not align with a binding site within the Chorley dataset. One way to assess this would be to co-transfect promotor-reporter and trans-acting enhancer-reporter constructs similar to those utilized in massively parallel reporter assays (MPRAs) to identify sequences necessary for gene activation.

In response to different forms of NRF2 stimulation, pGL4-TRIM16L MUT luminescence was consistently significantly greater than in cells transfected with the WT construct. Introduction of another ARE site within the MUT construct may explain the additional luminescent activity however none were found. Interestingly, both 1 kb inserts contained the canonical AP-1 binding site, or TPA-responsive element (TRE): TGAGTCA, 52 base pairs from the transcription start site. This may be the reason for the substantial induction of luminescence observed in cells transfected with pGL4-TRIM16L WT and MUT constructs, compared to the other reporters. CDDO-Me is thought to activate AP-1 via induction of c-Jun expression (Zou et al., 2004). Additionally, c-JUN-Nrf2 heterodimers have been shown to activate Nrf2-regulated genes such as CYP2J2 (Lee and Murray, 2010). Generation of constructs with promotor regions of different lengths (i.e. 100/200/500 bp from transcription start site) would aid identification of the site responsible for pGL4-TRIM16L WT and MUT reporter construct activation. Diminished activation of luminescence following knock down of AP-1 expression, in cells transfected with the pGL4-TRIM16L constructs would also highlight the role the TRE site plays in the reporter activation. Additionally, sequential base changes to the ARE within the TRIM16L promotor would highlight the region responsible for increased luminescence seen in the pGL4-TRIM16L MUT construct.

The ARE region identified by Singh *et al.* as the NRF2 binding site in A549 lung cells, when stimulated by tBHQ, contains two ARE sites (Singh et al., 2009). Mutation of one or both ARE sites in the promotor region of *SRXN1*, identified by Singh *et al.*, showed no difference in luminescent response (Singh et al., 2009). This lack of significant induction of luminescence in cells transfected with MUT constructs with either or both ARE sites compromised,

compared to pGL4-SRXN1 WT, indicates potential for the extended ARE site to be essential for NRF2-mediated regulation. Consistent with our findings, Soriano *et al.* mutated bases within the ARE2 region (mutations highlighted in bold: **CTGCAA**ACTCAC**CTGAGTCAGCCC**) that lead to diminished activation of luciferase-based reporter constructs exposed to CDDO-TFEA in neuronal cells (Soriano *et al.*, 2008). One possibility is that the active ARE site bridges the two mutant constructs. Point mutational analysis across the entire extended sequence would highlight the exact region required for NRF2 binding.

In this chapter, mining of publicly available transcriptomic datasets corroborated our microarray analysis of genes sensitive to NRF2-pathway modulation in PHH. Activation of potentially novel NRF2-regulated genes *F2RL2*, *TRIM16L* and *LOC344887* were assessed by promoter-reporter assay. Further assessment of the promoter and potential enhancer elements of these genes, either by CHIP or EMSA of PHH lysates, is needed to confirm the direct or indirect NRF2-mediated induction of these transcripts. Assessment of multiple ARE sites in the promoter region of *SRXN1*, highlighted, for the first time, the necessity of both to facilitate transcription in response to NRF2 stimulation. Ultimately, delineation of the Nrf2-regulated transcriptome will shed light on the role of the pathway within the cell and provide markers to improve assessment of NRF2 pathway activity.

Chapter 5

**Use of Nrf2 reporter genes to assess the potencies of novel sulforaphane analogues**

**Contents**

5.1. <b>Introduction</b> .....	183
5.2. <b>Materials and Methods</b> .....	185
5.2.1. Cell culture, drug treatment and reverse transfection.....	185
5.2.2. Annealed Oligo cloning.....	185
5.2.3. ATP quantification.....	186
5.2.4. <i>In vitro</i> luciferase assays.....	186
5.2.5. Statistical analysis.....	186
5.3. <b>Results</b> .....	187
5.3.1. Sulforaphane analogues produce a bioluminescent response in H4IIE-8AREL cells .....	187
5.3.2. Construction and validation of pGL4-5xARE reporter.....	190
5.3.3. pGL4-5xARE reporter activated by sulforaphane analogues in HepG2 cells.....	194
5.4. <b>Discussion</b> .....	196

### 5.1. Introduction

The dietary isothiocyanate sulforaphane is currently undergoing clinical trials for the treatment of a range of different diseases including schizophrenia (NCT02880462), autism (NCT02909959), lung cancer (NCT03232138), skin aging following UV exposure (NCT03126539), prostate cancer (NCT01950143), colon cancer (NCT01344330) and type 2 diabetes (NCT02801448). The electrophilicity of isothiocyanates facilitates the formation of covalent bonds with cysteine residues (Lewis et al., 2017). Dinkova-Kostova *et al.* recorded cysteine modifications of murine Keap1 in the presence of sulforaphane using UV-VIS and mass-spectroscopy (Dinkova-Kostova et al., 2002). In particular, the cysteine residue C151 in the BTB domain of KEAP1 mediates NRF2 activation as expression of a mutant KEAP1-C151 protein repressed NRF2 pathway activation by sulforaphane (Zhang and Hannink, 2003). This was confirmed using biotin-switch technique whereby unstable cysteine adducts were biotinylated and precipitated using streptavidin beads (McMahon et al., 2010). Additionally, sulforaphane has also been shown to augment NRF2 synthesis by promoting ribosomal internalization of *NRF2* mRNA for protein synthesis (Li et al., 2010). Recently, Clulow *et al.* identified over 500 proteins potentially liable to modification by sulforaphane (A. Clulow et al., 2017). Sulforadex® (SFX-01), the  $\alpha$ -cyclodextrin coated sulforaphane produced by Evgen pharma, is currently undergoing clinical trials for the treatment of sub arachnoid haemorrhage (NCT02614742) and metastatic breast cancer (NCT02970682).

Regulatory authorities such as the OECD have endorsed the integration of cell-based reporters for screening compounds in a medium- to high-throughput manner for NRF2 pathway activation linked to certain forms of drug toxicity (Emter and Natsch, 2015; Mutter et al., 2015). Initiatives such as ToxCast and Tox21 demonstrate the utility of *in vitro* high-throughput screening to identify activation of NRF2 (Huang et al., 2016; Richard et al., 2016). The latter employed fluorescent reporters such as SRXN1-GFP to inform on the mechanisms of toxicity in human cell lines. Conversely, a number of ARE-driven reporter cell models have been used to screen for the therapeutic activation of NRF2 (Ramkumar et al., 2013; Wu et al., 2012). For instance, the luminescent AREc32 cell line established by Wang *et al.*, identified NRF2-inducers from a panel of 54 natural dietary compounds such as curcumin and quercetin (Wang et al., 2006; K. C. Wu et al., 2014).

Here, I exemplify the use of a rat liver cell line, H4Ile-8AREL, stably transfected with a luciferase reporter driven by an eight times repeated ARE sequence from the promotor of rat *Gsta2* (Kratschmar et al., 2012), to assess the potencies of a sulforaphane analogue series



to guide the selection of back up compounds for the SFX-01 development program. To improve the human relevance of this approach, I also describe the generation of a luciferase reporter under the control of a quintupled ARE sequence and demonstrate its use as a screening tool for NRF2 activators in human HepG2 liver cells.

## 5.2. Materials and Methods

All reagents were purchased from Sigma unless otherwise stated.

### 5.2.1. Cell culture, drug treatment and reverse transfection

H4Ile-8AREL cells, kindly donated by Prof. Alex Odermatt (Basel University, Switzerland), were cultured in conditions similar to those previously described in section 4.2.3. Culture media consisted of DMEM supplemented with 1x Non-essential amino acids (Life Technologies, Carlsbad, USA), 10 mM HEPES (Life Technologies, Carlsbad, USA), 1 % (v/v) Penicillin/streptomycin and 10 % heat-inactivated FBS. Cells were seeded 25,000 cells per well of a 96 well plate.

Sulforaphane and its analogues were produced by Dr. Noureddine Khier (Consejo Superior de Investigaciones Cientificas, Seville, Spain) with support from EVGEN pharma (Liverpool, UK). Drug treatments were conducted in a similar manner to those described in section 4.2.3.2, in a 96 well-plate format. Concentrations at which there is 200 % luciferase activity, proportional to NRF2 activity (CD values) were calculated using Graph-pad prism previously described (Copple et al., 2014). Briefly, non-linear regression of the concentration-response curves facilitates interpolation of the CD concentration.

HepG2 cells were transiently transfected with plasmids as previously described in section 4.2.3.3. Induction of the pSB-tet-NRF2 plasmid was achieved upon exposure of HepG2 cells to 6 µg/ml Doxycycline (DOX) in comparison with vehicle-treated cells (1 % DMSO).

### 5.2.2. Annealed Oligo cloning

Annealed oligonucleotides provide a fast, cost-effective method of generating short double-stranded DNA sequences. Primers are first heated to break any hydrogen bonds and generate single-stranded DNA sequences. Subsequent slow cooling facilitates hybridisation of the complementary sequences. The following primers were annealed and ligated into the linearized pGL4 plasmid (Table 5.1). Forward and reverse primers were incubated at 94 °C for 10 min in 10 µl reactions consisting of: 1 µl 100 µM Fwd primer, 1 µl 100 µM Rev primer, 1 µl 10x ligase buffer and 7 µl dH<sub>2</sub>O. Reactions were left to cool slowly to room temperature for 1 h. Inserts were diluted 1 in 12.5 with dH<sub>2</sub>O. Ligation reactions consisted of: 0.5 µl 50 ng linearized pGL4.20, 4 µl of diluted insert, 1 µl 10x ligase buffer, 0.5 µl T4 ligase and 4 µl dH<sub>2</sub>O. These were incubated at 16 °C overnight. Bacteria were transformed, and successful ligations screened and sequenced in a similar manner to section 4.2.2.3. HepG2 cells were reverse transfected with either the pGL4-5xARE WT, MUT or empty vector.

**Table 5.1 Annealed oligo cloning primers**

WT and MUT ARE sequences underlined.

Insert	Primer	Sequence
NQO1 ARE 5x WT	Fwd	5' – CCCC <u>GTGACTCAGCACCCGTGACTCAGCACC</u> CGTGACTCAGCACCC <u>GTGACTCAGCACCCGTGACT</u> <u>CAGCACCCG</u> – 3'
	Rev	5' – CTAGCGGGT <u>GCTGAGTCACGGGTGCTGAGTC</u> <u>ACGGGTGCTGAGTCACGGGTGCTGAGTCACGGGT</u> <u>GCTGAGTCACGGGGTAC</u> – 3'
NQO1 ARE 5x MUT	Fwd	5' – CCCCCGTCAGACTACCCCGTCAGACTACCC CGTCAGACTACCCCGTCAGACTACCCCGTCAGACT <u>ACCCCG</u> – 3'
	Rev	5' – CTAGCGGGTAGTCTGACGGGGTAGTCTGA <u>CGGGTAGTCTGACGGGGTAGTCTGACGGGGTA</u> <u>GTCTGACGGGGTAC</u> – 3'

### 5.2.3. ATP quantification

ATP was quantified using the Cell-Titer-Glo kit (Promega, Madison, USA). 20 µl ATP reagent was added per well of a 96 well-plate. The plate was shaken for 1 min at 700 RPM. 100 µl of cell lysate was transferred from each well to a white-walled 96-well plate (Greiner Bio-one, Kremsmünster, Austria) and incubated for 5 min at room temperature. Luminescence was quantified using the Varioscan Flash.

### 5.2.4. *In vitro* luciferase assays

See section 4.2.4.

### 5.2.5. Statistical analysis

See section 2.2.10. Non-Linear regression was calculated using Prism.

### 5.3. Results

#### 5.3.1. Sulforaphane analogues produce a bioluminescent response in H4IIE-8AREL cells

Firstly, concentration-dependent activation of the 8AREL reporter was assessed in response to established and clinically used NRF2 activators (Fig 5.1 A and B). At toxic concentrations of CDDO-Me and sulforaphane, both luminescence and cellular ATP content decreased. CD values associated with these compounds were 0.001 and 0.829  $\mu\text{M}$  respectively. SFX-01 is sulforaphane coated in  $\alpha$ -cyclodextrin. No induction of luminescence or loss of cell viability was observed following treatment with the coating substrate alone (Fig 5.1 C). However, SFX-01-treatment resulted in a CD value of 1.468  $\mu\text{M}$  comparable to that of sulforaphane (Fig 5.1 D). The resulting rank order of potency as inducers of the 8AREL reporter was CDDO-Me>>sulforaphane>SFX-01 (Fig 5.1 E).

Subsequently, I applied this screening technique to determine the potency of NRF2-activating compounds on a larger scale. The H4IIE cell line was subsequently exposed to 42 sulforaphane analogues, as part of the SFX-01 development program in collaboration with EVGEN Pharma (Liverpool, UK). CD values were calculated, and compounds ranked for their NRF2 activating potencies (Table A2). These ranged from 1.45 to 89.33  $\mu\text{M}$ . The sulforaphane parent compound (EVG01) was assessed as a positive control and, out of all the compounds included in the SFX-01 program, produced a CD value much lower than the experimental compounds (1.45  $\mu\text{M}$ ).

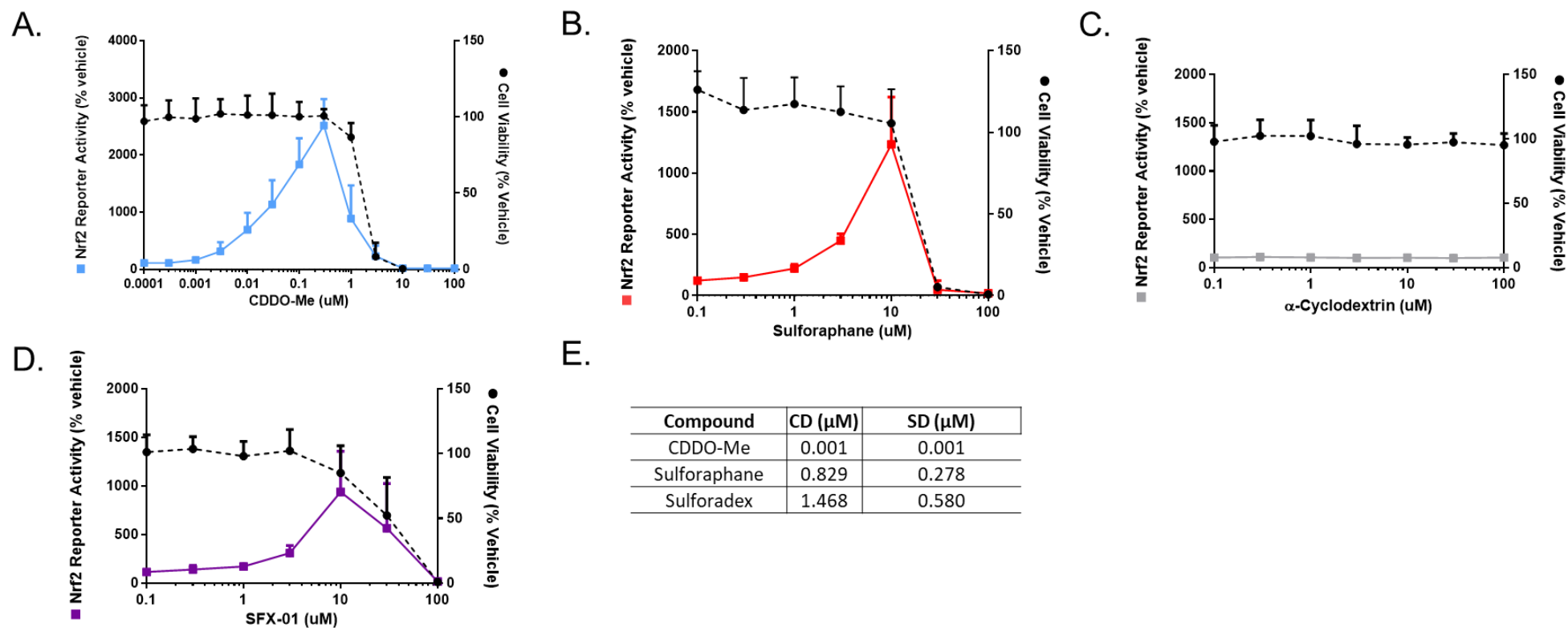


**Figure 5.1 Decreased luciferase NRF2-reporter activity following toxicity**

Potencies and toxicities of (A) CDDO-Me, (B) Sulforaphane, (C)  $\alpha$ -cyclodextrin and (D) Sulforadex<sup>®</sup> (SFX-01). H4IIE cells were exposed to the indicated concentrations of drug or vehicle control. Following 24 h exposure, luciferase-reporter activity (bold line) and ATP content (dotted line) were quantified (n=4). Mean and SD shown. CD values were calculated by non-linear regression (E).

To assess the relative potencies of the sulforaphane analogues compared to the parent compound, CD values were calculated from dose-response curves documenting activity of the H4Ile-8AREL reporter. Identification of analogues with similar potencies to sulforaphane may provide candidates for clinical application.

To calculate the CD values of the sulforaphane analogues, non-linear regression of the dose-response curve, excluding toxic concentrations associated with luminescence reduction was applied. Apart from five compounds (EVG07, EVG08, EVG11, EVG12 and EVG31), all analogues exerted a two-fold enhancement of luminescence in comparison with vehicle-treated controls (Fig A6). Seventeen compounds had CD values exceeding 20  $\mu$ M, ranging from between  $20.04 \pm 3.17$  to  $89.33 \pm 18.39$   $\mu$ M (Fig A7). Of these compounds, EVG15 had the lowest CD value (Fig A7 A), whereas EVG33 had the highest CD value (Fig A7 Q). Of the remaining compounds, CD values ranging from  $15.17 \pm 7.44$  to  $19.63 \pm 5.27$   $\mu$ M were observed from five analogues (Fig A8), whereas, fifteen of the compounds generated CD values below 15  $\mu$ M ranging from  $11.04 \pm 2.31$  to  $14.80 \pm 8.36$   $\mu$ M (Fig A9). EVG01 and EVG02, with CD values of  $1.453 \pm 0.24$  and  $5.493 \pm 2.28$   $\mu$ M respectively, exhibited potencies closest to the parent compound, sulforaphane (Fig A10).

Taken together, these findings demonstrate a broad range of potencies for the analogues of the SFX-01 development program. Additionally, all analogues are less potent than the parent compound and commercially-available sulforaphane.

### 5.3.2. Construction and validation of pGL4-5xARE reporter

To generate a bioluminescent reporter that could be transiently (and ultimately stably) transfected into human cells, wild-type (WT) and mutated (MUT) quintupled consensus ARE constructs (5xARE) were synthesised and sub-cloned into the luminescent pGL4.20 vector (Fig 5.2 A). The mutated ARE sequence was generated by replacing the nucleotide bases T with G and A with C, and vice-versa. A string of three cytosine nucleotides was used to separate each ARE repeat sequence, similar to the repeat regions within the eight-times repeated AREc32 reporter (Wang et al., 2006). Both WT and MUT constructs were successfully sequenced (Fig 5.2 B and C).

To validate successful generation of WT and MUT reporter constructs, luminescence was quantified in transiently transfected HepG2 cells exposed to 100 nM CDDO-Me for 24 h. This dose of CDDO-Me had previously been shown to induce the Nrf2-pathway in HepG2 cells (See Chapter 4). Following CDDO-Me exposure, HepG2 cells transfected with pGL4-5xARE WT produced significantly greater luminescence compared to those transfected with pGL4-5xARE MUT, when normalised to transfected cells treated with 0.5 % DMSO ( $P = 0.0018$ ) (Fig 5.3 A). Luminescence normalised to renilla luciferase signal in cells co-transfected with the pRL-SV40 construct, highlighted a similar increase in WT luminescence compared to controls (Fig 5.3 B). Therefore, this indicated that cell viability and transfection efficiency were not influencing the strength of luminescent responses.

To assess the reporter's sensitivity to other forms of NRF2 stimulation, the response of the 5xARE constructs to NRF2 overexpression, induced by doxycycline (DOX) exposure of HepG2 cells co-transfected with either WT or MUT reporter constructs and pSB-tet-NRF2 was also measured (Fig 5.4). Comparison against DMSO-treated controls, whereby NRF2 overexpression was not induced, demonstrated significantly greater luminescence from WT-transfected cells than in the MUT-transfected counterparts ( $P = 0.0052$ ).

As findings demonstrated that the pGL4-5xARE WT construct was more responsive to NRF2 induction by chemical and pharmacological stimuli than the mutant construct, I subsequently utilized this ARE reporter, in HepG2 cells, to characterise a subset of sulforaphane analogues with a range of potencies.

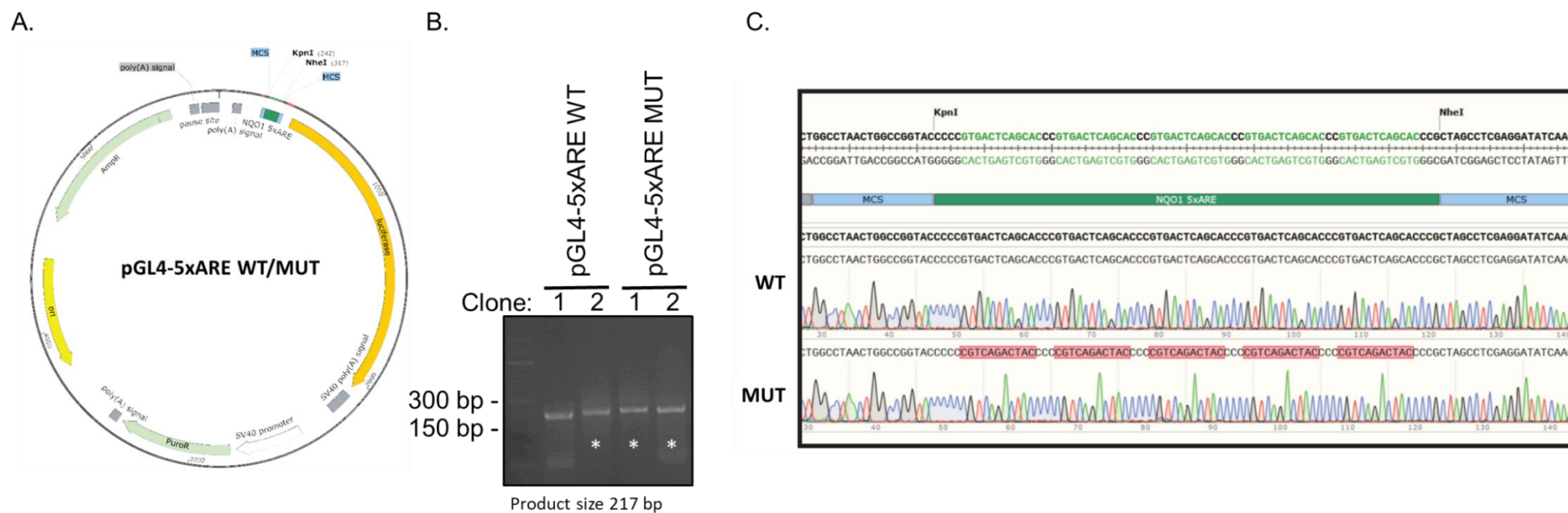


### Figure 5.2 5xARE reporter construction

The five times repeated ARE sequences (5xARE) of wild-type (WT) or mutated (MUT) human NQO1 were sub-cloned into the pGL4.20 vector (A). Miniprep DNA from bacterial colonies transformed with pGL4-5xARE WT or MUT constructs were screened (B) for successful insert ligation (\*) prior to sequencing. (C) Sanger sequencing confirmed insert integration (MUT ARE sequences highlighted red).



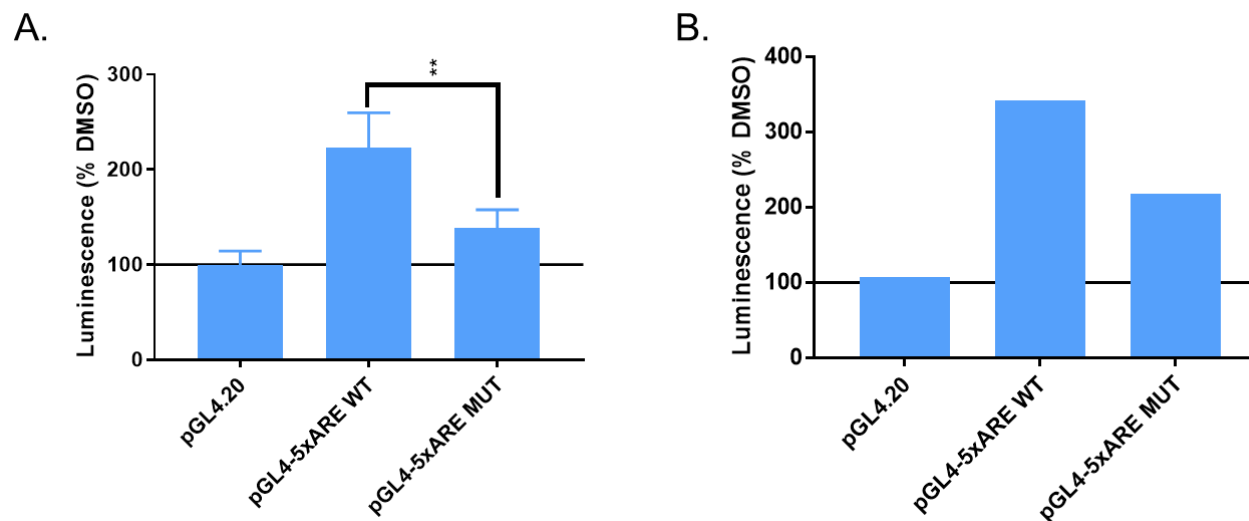


**Figure 5.3 Response of pGL4-5xARE reporter to CDDO-Me in HepG2 cells**

HepG2 cells transfected with wild-type (WT) or mutant (MUT) pGL4-reporter constructs exposed to either 100 nM CDDO-Me or 0.5 % DMSO and luminescence quantified after 24 h (A) (n=3). HepG2 cells co-transfected with pRL-SV40 and luminescence normalised to rLuc expression (B) (n=1). Significant difference in WT compared to MUT construct induction was calculated by Students T-test (\*\*  $p \leq 0.01$ ). Mean + SD shown. Solid line = baseline against which normalisation was performed.

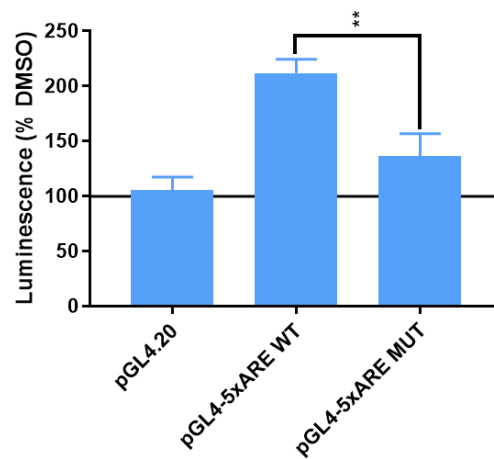


**Figure 5.4 Response of pGL4-5xARE reporter to NRF2 overexpression**

HepG2 cells co-transfected with pSB-tet-NRF2 and either wild-type (WT) or mutant (MUT) pGL4-reporter constructs. Cells were exposed to 6  $\mu\text{g/ml}$  Doxycycline or DMSO and luminescence quantified after 12 h ( $n=3$ ). Significant difference in WT compared to MUT construct induction was calculated by students t-test (\*\*  $p \leq 0.01$ ). Mean + SD shown. Solid line = baseline against which normalisation was performed.

### 5.3.3. pGL4-5xARE reporter activated by sulforaphane analogues in HepG2 cells

To investigate the human relevance of the ARE reporter screening approach, selected sulforaphane analogues from the SFX-01 development program were assessed for their potency to activate the pGL4-5xARE reporters and the pGL4-NQO1 WT plasmid (generated in chapter 4) in HepG2 cells. Cells transfected with the reporters were exposed to increasing concentrations of compounds shown previously to have high, medium or low CD values when evaluated in the H4Ile-8AREL cell line. These compounds were EVG33 (CD = 89.33  $\mu$ M) (Fig A7 Q), EVG40 (CD = 34.914  $\mu$ M) (Fig A7 N), and EVG01 (CD = 1.45  $\mu$ M) (Fig A10 A).

In cells transfected with pGL4-NQO1 WT, only EVG40 and EVG01 induced a two-fold greater luminescence than vehicle-treated controls (Fig 5.5 A), producing CD values of 2.009  $\mu$ M and 0.717  $\mu$ M respectively. In pGL4-5xARE-transfected cells, EVG40 and EVG01 had CD values of 8.035  $\mu$ M and 3.729  $\mu$ M respectively (Fig 5.5 B). These cells were also observed to display more variable luminescent responses than pGL4-NQO1 WT-transfected cells, based on the size of the standard deviation. Additionally, as mentioned, CD values of EV40 were vastly different between the two *NQO1*-based reporters (Fig 5.5 C).

In summary, here I observed a similar trend in the rank order of sulforaphane analogue potencies but absolute CD values varied greatly between cell lines and reporter constructs.

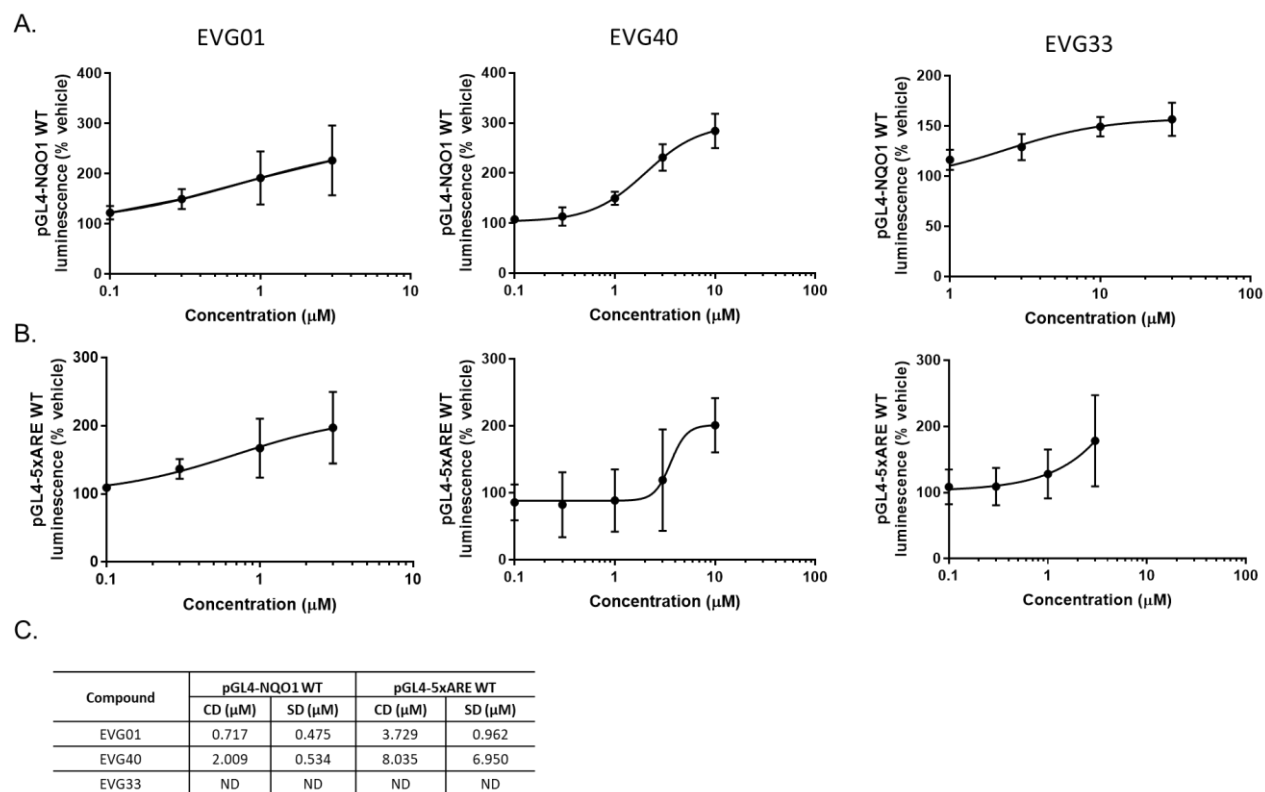


**Figure 5.5 Response of pGL4-NQO1 and 5xARE reporter constructs to sulforaphane analogues in HepG2 cells**

HepG2 cells, transfected with either pGL4-NQO1 WT (A) or pGL4-5xARE WT (B) and exposed to the parent compound EVG01 and analogues identified to induce the NRF2 pathway in the H4IIE cell line at high (EVG33), medium (EVG40) or low (EVG01) concentrations (n=3). After 24 h, luminescence was quantified. CD values (C) were calculated following non-linear regression analysis.

#### 5.4. Discussion

The data in this chapter summarises the characterisation of a range of sulforaphane analogues, generated as part of the SFX-01 development program. Here I show the application of the rat hepatoma cell line H4IIE-8AREL for the medium-throughput screening of these analogues, to assess the relative potencies needed to activate the NRF2 pathway. Following the construction of a similar luminescent reporter plasmid containing multiple consensus AREs (pGL4-5xARE WT), I hypothesised analogous luminescent responses would be induced in transiently transfected human hepatocarcinoma, HepG2 cells. The similar trend in rank order of analogue potencies towards activation of ARE-based reporters gives confidence in the ability of the 5xARE-reporter to predict the potencies of novel activators to induce the NRF2 pathway.

The potency of electrophilic, canonical NRF2 activators such as sulforaphane, are determined by their reactivity towards KEAP1 thiols including the highly reactive C151 but also cysteines within the KELCH domain (Hu et al., 2011). This is mediated by the highly reactive isothiocyanate group (-N=C=S). Previous assessment of sulforaphane analogue potencies have focused on the compounds ability to double NQO1 activity. Initially this was quantified using a colorimetric assay in which reduction of the dye 3-(4,5-dimethylthiazol-2-yl)-2,5-diphenyltetrazolium bromide (MTT) is proportional to enzyme activity (Prochaska and Santamaria, 1988). Utilizing this technique, Posner *et al.* assessed activity of linear sulforaphane analogues, replacing sulfoxide group (C-SO-C) with other polar groups, to induce Nqo1 in mouse Hepa1c1c7 cells (Posner et al., 1994). However, none were as potent as sulforaphane itself, indicating the importance of the sulfoxide group as well as the isothiocyanate group to activate NRF2. By replacing the isothiocyanate group with alternative sulfoxythiocarbamate groups, Ahn *et al.* produced analogues of sulforaphane capable of forming stable adducts with KEAP1 (Ahn et al., 2010). The length of the methylene bridge between the isothiocyanate and sulfoxide groups is also important as modification reduced potency (Zhang et al., 1992).

Although the focus of this chapter was not on deciphering detailed structure activity relationships of the analogues, it was apparent that most compounds with non-determined CD values contained a 'trioxaundecane' group. Additionally, many compounds containing the 'heptaotricosane-1-sulfinamide' group exhibited CD values greater than 25  $\mu$ M. The addition of extensive structures to the compound may cause steric hinderance, interfering with the interaction with its target site and reducing potency. None of the analogues

exhibited a modified isothiocyanate group. Modification of this region may yield analogues with greater potency towards the Nrf2 pathway.

Several ARE-based reporter assays have been established for the high-throughput screening of Nrf2 activating compounds. Previous work from our laboratory has demonstrated the application of the H4Ile-8AREL cell line for the assessment of therapeutic index of Nrf2 activating compounds such as CDDO-Me (Copple et al., 2014). In this chapter, induction of luminescence in HepG2 cells following exposure to EVG40, EVG33 or EVG01 resulted in a similar rank order of potencies towards activation of the pGL4-5xARE WT or pGL4-NQO1 WT reporter, established in chapter 4. This was comparable to the compounds' potency towards the 8AREL reporter in H4Ile cells, i.e. EVG01>EVG33>EVG40. This trend, observed in a limited number of compounds is encouraging. Previous assessment of NRF2 activators using the H4Ile cell line have shown strong correlation with potencies calculated by induction of Nqo1 in the murine Hepa1c1c7 cell line (Copple et al., 2014; Dinkova-Kostova et al., 2005). The contrast between absolute potencies observed in this chapter may be explained by the differences in cell line and reporter constructs.

While absolute CD values differed greatly between ARE-based reporters exposed to the same sulforaphane analogue, this is likely due to inherent differences in the assays. Inclusion of multiple repeated ARE sites have previously been shown to increase luciferase-based reporters sensitivity to pathway activation (Nguyen et al., 1994; Wang et al., 2006). Here, I observed lower CD values in cells transfected with pGL4-NQO1 WT rather than pGL4-5xARE WT. For example, EVG01 produced CD values of 0.717  $\mu$ M and 3.729  $\mu$ M respectively. Luminescence was more variable in the pGL4-5xARE transfected cells for all compounds measured when compared to the responses quantified in pGL4-NQO1 WT transfected cells. This may be due to the inclusion of the extended promoter region in the pGL4-NQO1 WT plasmid, providing opportunity for the recruitment of other cis-acting factors to aid transactivation compared to the limited five-times repeated consensus sequence incorporated within pGL4-5xARE.

One limitation of this dataset is the lack of transfection efficiency assessment. Although characterisation of the pGL4-5xARE reporter in response to CDDO-Me, showed no obvious detriment to cell viability or transfection efficiency (Fig 5.3 B). The application of *NQO1*-based reporters when basal expression of *NQO1* in HepG2 cell line is substantial (Gray et al., 2016), may also influence the lack of reporter induction in this cell line. Analysis of the induction of

pGL4-SRXN1 WT construct (previously characterised in Chapter 4) in HepG2 cells exposed to these compounds, would give credence to this theory. Comparison of the ability of selected sulforaphane analogues to activate the NQO1-based reporter in the recently established HUH7-1x-ARE-Luc cell line (Motahari et al., 2015), would also be of interest. Motahari *et al.* generated the pGL4.26-1x-ARE-Luc reporter consisting of a single copy of the 'extended' NQO1 ARE sequence (Motahari et al., 2015). HUH7 cells, stably transfected with this reporter, produced luminescence in response to both toxic (hydroquinone and p-benzoquinone) and therapeutic (Curcumin) activation of the NRF2 pathway.

A limitation of these ARE-based reporter assays is the inclusion of only one form of ARE sequence from a single NRF2-regulated gene. The data from previous chapters highlights the differential responses of the array of NRF2-regulated genes to different stimuli. Reporter constructs consisting of multiple ARE sequences could be advantageous, as reliance on expression of a single gene of interest may miss NRF2 pathway activation from exposure to certain compounds; ultimately generating false-negative results. To this effect, Rizzi *et al.* established a bicistronic reporter under the control of repeated ARE sequences from the promoter regions of *Hmox1*, *Nqo1*, *GstYa* and *Gsr* (Rizzi et al., 2017). These transgenic mice produced a bioluminescent response to ASN across tissues although interestingly, luminescence in muscle was not as high as the induction of endogenous *Hmox1* expression. It would be interesting to see the region of the multiple ARE reporter construct to which NRF2 binds as ARE sequence variation has been shown to influence binding affinity of NRF2-small MAF complexes (Kuosmanen et al., 2016).

Construction of an *Neh2*-Luc reporter facilitated the monitoring of Nrf2 stabilisation in response to drug exposure (Smirnova et al., 2011). The inclusion of the Nrf2 domain instead of an ARE-site from a downstream gene allows monitoring of direct Nrf2 activation but does not provide evidence that this accumulation leads to functional pathway induction. Inclusion of this site into a  $\beta$ -galactosidase (LacZ) reporter construct, generated a signal faster than ARE-based luciferase reporters within MEFs exposed to DEM and tBHQ (Hirotsu et al., 2011). However, inclusion of the *Neh2* region only, is not sensitive to NRF2 activators that do not target KEAP1 binding.

Within the extended ARE site included in the reporter assay developed by Hirotsu *et al.* is an AP-1 binding site (Hirotsu et al., 2011). Incorporation of multiple reporter assays would provide more evidence of off-target effects of compounds and the specificity of the drug to

activate the Nrf2 pathway. Off-target effects of sulforaphane include inhibition of histone deacetylase (Myzak et al., 2004), and reduced activation of NF- $\kappa$ B (Heiss et al., 2001). High-throughput toxicity screens are beginning to incorporate a range of reporters driven by 'hub' genes of major toxicity pathways to identify chemicals liable to toxicity (Herpers et al., 2016; Steinberg et al., 2017; Wink et al., 2017). Employment of a similar panel of redox sensitive transcription factors for screening Nrf2-activating compounds may aid the identification of off-target modification of cysteine residues by electrophilic compounds.

The utility of cell-based reporters for the screening of compound libraries is limited by the physiological relevance of current *in vitro* models. For instance, comparison of *in vivo* toxicity data from the ToxRefDB database with *in vitro* data from phase 1 of the ToxCast™ initiative, highlighted the inability of *in vitro* assays to mimic individual diversity, bioactivation of a compound and toxico-kinetics (Knudsen et al., 2011). Additionally, assessment of NRF2-pathway activation in a single cell line does not facilitate visualisation of the holistic pathway response. Extra-hepatic activation of the NRF2 pathway was not considered in these data. Luciferase reporter constructs have been utilised within 3D cultures to monitor cell viability in an environment more relevant to that seen *in vivo*. For instance, hepatocellular carcinoma HUH1 cells in 2D and 3D spheroids cultures expressing a  $\beta$ -catenin luciferase reporter produced differing responses when exposed to drugs known to inhibit wnt signalling (Takai et al., 2016). HCT116 cells stably transfected with a pTRAF-Nrf2 reporter were used to monitor transcription factor expression and localisation throughout spheroid formation (Kipp et al., 2017). The Nrf2-Luc mouse model described in chapter 2 offers insight into Nrf2 pathway activation across multiple tissues. Many compounds in the clinic pleiotropically activate NRF2, for instance the breast cancer drug, tamoxifen induces NQO1 (Krishnamurthy et al., 2012) and NSAIDs upregulate HMOX1 within the gastric mucosa (Aburaya et al., 2006). Assessment of off-target modifications of cysteine residues by electrophilic activators of NRF2 is essential to avoid adverse effects and ensure potency towards KEAP1 binding.

In conclusion, the H4Ile-8AREL luminescence-based reporter cell line can be applied on a medium throughput scale to screen compounds for their potency to activate the NRF2 pathway. Construction and characterisation of NQO1 ARE-based human reporter constructs, highlighted in this chapter, provide a model for assessment of NRF2 pathway activation within a human cell line. While absolute CD values differed between reporters exposed to the same compound, a similar trend in rank order of potencies across ARE-based reporters



in rat and human hepatocyte cell lines is encouraging. Development of sensitive assays for the *in vitro* assessment of Nrf2 activators are of increasing value as the number of therapeutic Nrf2-modulating compounds entering the clinic grows.

**Chapter 6**

**General discussion**

**Contents**

6.1.	<b>Introduction</b> .....	203
6.2.	<b>Key aims and major findings</b> .....	203
6.3.	<b>General discussion of findings</b> .....	204
6.3.1.	Expanding the tool box for monitoring NRF2 pathway activation .....	204
6.3.2.	Role of NRF2 in toxicity testing .....	205
6.3.3.	Future of NRF2-based therapeutics .....	207
6.4.	<b>Conclusions and future directions</b> .....	209

### 6.1. Introduction

The transcription factor NRF2 has been increasingly implicated in response to drug-induced toxicity. Electrophilic compounds have been found to directly modulate KEAP1 repression of the NRF2 pathway (Bryan et al., 2013). Activation of the NRF2 pathway to sub-toxic concentrations of compounds (Goldring et al., 2004), demonstrate the transcription factor's utility to provide sensitive insight into the mechanisms of a toxic chemical entity, making it an attractive pre-clinical marker of chemicals liable to cause toxicity. Additionally, a growing number of pathologies have been implicated with an underlying oxidative stress component. In response to this a range of NRF2-activating agents have begun clinical trials as antioxidant-based therapies (Fox et al., 2012; Gold et al., 2012; Liby and Sporn, 2012). Thorough characterisation of the NRF2-mediated oxidative stress response is therefore vital, not only to provide effective therapeutic strategies, but also to improve pre-clinical safety assessment of drugs liable to induce oxidative damage. This thesis aimed to assess novel methods of monitoring NRF2 pathway activation, to improve testing strategies to identify chemicals and drugs that are likely to provoke toxicity in humans and potent activators of the NRF2 pathway with therapeutic potential.

### 6.2. Key aims and major findings

The major aims of this thesis were:

1. To characterise the response of Nrf2-Luc mice to organ-specific toxicants APAP and cisplatin.
2. To assess Nrf2 pathway activity in whole blood as a means of monitoring Nrf2 pathway status *in vivo*.
3. To characterise putative novel Nrf2-regulated genes in human liver cells.
4. To develop and use novel Nrf2-responsive reporter platforms to evaluate the potencies of novel analogues of the Nrf2-activating compound, Sulforaphane.

The major findings of this thesis were:

1. Data from Nrf2-Luc mice studies show the sensitivity of the mouse model to organ-specific toxicity. The bioluminescent signal localizes to the site of toxicity and reflects the extent of damage.

2. Quantification of Nrf2-regulated mRNA in whole blood revealed their presence in circulation following DILI. Levels of these transcripts were muted following administration of NAC highlighting damaged hepatocytes as a potential source of the Nrf2-regulated mRNA.
3. Bioinformatic analysis of putative novel Nrf2-regulated genes corroborated microarray analysis of genes sensitive to Nrf2 modulation in PHH and identified potential ARE sequences responsible for regulation. However, mutational analysis indicated these sequences are not responsible for induction of *F2RL2*, *LOC344887* and *TRIM16L* on their own, i.e. without enhancer elements.
4. Data from promoter-reporter assays show that the sequence responsible for Nrf2-mediated activation of *SRXN1* consists of two consecutive ARE sites that are both essential for gene transcription.
5. Using well established and novel ARE-based luciferase reporters, I show similar rank order of potency of analogues of sulforaphane within the SFX-01 development program towards activation of NRF2 in rat and human hepatic cell lines.

### 6.3. General discussion of findings

#### 6.3.1. Expanding the tool box for monitoring NRF2 pathway activation

Novel methods for monitoring the activity of cytoprotective responses mediated by NRF2 is vital due to the lack of sensitive, non-invasive strategies currently used. The Nrf2-Luc mouse model offers, the ability to monitor whole-body activation of the NRF2 pathway non-invasively (Oikawa et al., 2012). The data presented in chapter 2 highlights the utility of the bioluminescent Nrf2-Luc mouse model to monitor activation of the pathway in response to organ-specific drug-induced toxicity. In response to hepatotoxic doses of APAP or nephrotoxic doses of Cisplatin, luminescence was measured non-invasively in organs undergoing damage. This bioluminescent signal correlated closely with traditional markers of toxicity and reflected pathological scoring of the affected tissues. Application of the Nrf2-Luc model in late stage pre-clinical toxicity testing on subgroup of compounds would facilitate the detection of chemicals liable to provoke chemical/oxidative stress *in vivo*. A key advantage of this model is the holistic visualization of NRF2 activation provides data on potential off-target effects, offering an overview of pathway modulation during late stage

preclinical assessment. Further development of immortalized cell lines from these mice, could also be utilized for HTP toxicity testing within specific tissues.

Additionally, methods for monitoring activation of the NRF2 pathway in peripheral, accessible tissues such as blood, may provide insight into pharmaceutical assessment. In chapter 3I aimed to assess the ability of the circulating NRF2-regulated transcriptome to reflect organ-specific toxicity. These data show a muted induction of NRF2-regulated transcripts in C57BL6 mice receiving the antidote for APAP-induced hepatotoxicity, NAC, compared to mice receiving APAP alone. This aligns with previous studies highlighting the correlation of many mRNA transcripts with the extent of APAP-induced liver damage in rodents (Umbright et al., 2010; K. Wang et al., 2013; Wetmore et al., 2010). Monitoring markers of the Nrf2-pathway in peripheral tissues that reflect organ-specific insult, may hold prognostic value in the clinic. While other biomarkers of DILI are elevated in the early stages of toxicity such as miR-122 (Starkey Lewis et al., 2011), Nrf2 activity may inform the cytoprotective capacity of the compromised organ, indicative of the extent of damage. Drug induced toxicity is a substantial burden to both the clinic and pharmaceutical industry. Implementation of peripheral tissue assessment during pre-clinical testing may aid the identification of drugs liable to toxicity and therefore enhance current assessment platforms.

### 6.3.2. Role of NRF2 in toxicity testing

Activation of the NRF2 pathway forms a common stage in many adverse outcome pathways. PHH are considered the gold standard for toxicity assessment, but little is known about the NRF2 pathway in these cells. In chapter 4I aimed to identify the ARE sites responsible for the activation of potentially novel Nrf2-regulated, implicated in PHH as being responsive to both *NRF2* and *KEAP1* knockdown. In comparison with other microarray datasets, it became apparent that *F2RL2*, *LOC344887* and *TRIM16L* were responsive to NRF2 modulation in additional cell lines and contained potentially active AREs close to their transcription start site. Unexpectedly, the data in this chapter suggests NRF2 does not directly regulate the above-mentioned genes via the ARE sites identified here. This may be due to lack of inclusion of vital enhancer sites. For instance, Johnson *et al.* identify the ARE site incorporated within our reporter assays as the site of Nrf2 binding to the *LOC344887* locus, via CHIP-seq (Johnson et al., 2016). However, an additional ARE sequence to which the authors show MAFG/K interacts, was not included in our reporter constructs. It is therefore likely that inclusion of

additional enhancer sites within the LOC344887 promoter region may be essential for Nrf2-dependent activation of the pseudogene. Assessment for other transcription factor binding sites may reveal indirect regulation of these genes by NRF2. A key finding from this chapter is the extended ARE sequence in the promoter of SRXN1 consists of two consecutive ARE sequences, identified by Soriano *et al.* and Singh *et al.* (Singh *et al.*, 2009; Soriano *et al.*, 2008). However, these data, for the first time, highlight the essential nature of both sequences for Nrf2-dependent activation.

Identification of the specific stimuli Nrf2 responds to and the downstream pathway activity in response to chemical/oxidative stressors will inform the utility of incorporating the pathway in risk assessment. For example, a distinct set of Nrf2-regulated genes were upregulated in response to carcinogens and DILI-related compounds with a propensity to induce hepatotoxicity (Souza *et al.*, 2017). Nrf2 has been shown to influence and be regulated by other stress response pathways (Rushworth *et al.*, 2012; Wakabayashi *et al.*, 2014), and therefore combining models from multiple stress-response pathways may be required to more completely predict risk of toxicity. Discussions from a recent workshop suggested a tiered approach to pathway-based toxicity risk assessment, moving away from animal-based toxic end-point analysis (Middleton *et al.*, 2017). Firstly, chemicals would be assessed for their ability to activate a broad range of stress response pathways in tissues liable to exposure such as the liver and kidneys. Following tiers would focus on impeded cell viability and function in relation to pharmacokinetic/pharmacodynamic data. Utilizing this approach, it would be interesting to see if chemicals liable to bioactivation are associated with perturbation of multiple stress response pathways or a specific subset.

Incorporation of Nrf2 pathway responses within predictive computational platforms to model the chemical and cellular events implicated in AOPs may aid risk assessment. Integration of data from *in vitro* ARE-based assays improved the sensitivity of predictive models of drug sensitivity assessment (Hirota *et al.*, 2018; Jaworska *et al.*, 2015). However, to minimize assumptions in computational models, generation of *in vitro* systems with greater physiological relevance is necessary. Acute exposure of single cell models cannot inform the effects of chronic exposure, especially as many cell lines exhibit impaired metabolic activity to primary cells (Hart *et al.*, 2010). Establishment of cell models, such as 3D HepG2 spheroid cultures that exhibited increased CYP450 metabolism compared to 2D cultures (Ramaiahgari *et al.*, 2014), that are amenable to HTP toxicity screening will better

inform modelling platforms. Further development of *in vitro* models combining multiple organs within a single bioreactor, such as the heart-lung-liver organ-on-a-chip model developed by Skardal et al. (Skardal et al., 2017) may provide insight into the influence of drug distribution on the likelihood of an organ-specific stress-response occurring *in vivo*. However, at present these assays cannot rival the context provided by *in vivo* models such as the Nrf2-Luc mouse.

A key factor that must be agreed is the level of NRF2 activation necessary to imply pre-emptive toxicity and not solely an adaptive response. Definition of these ‘tipping points’ corresponding to adverse or adaptive outcomes will inform risk assessment frameworks. For instance, activation of stress response pathways was dampened at toxic doses of the model oxidant, zinc, in bronchial epithelial cells, when compared to activation at recoverable exposures (Currier et al., 2016). Identification of the dose and time at which this threshold of activation is likely to be breached is challenging and will need further time-course analysis in physiologically relevant models to inform AOPs. To monitor pathways associated with overt toxicity instead of specific toxicological endpoints, these *in vitro* measurements must be related to *in vivo* exposure and responses of known chemicals liable to toxicity. Specifically, NRF2 activity in response to toxic moieties should be compared to the relative activity of the transcription factor induced by therapeutic drugs to gauge the likelihood of stress occurring in patients. Relating pathway activation in AOP models to actual levels of human exposure is also needed to increase the translational relevance of this framework. In patients, it is unlikely this threshold will be the same between individuals. Mutations within NRF2 and KEAP1 strongly influence pathway activity (Konstantinopoulos et al., 2011; Levings et al., 2017). Additional individual adaptive responses may be compromised due to co-pathologies, sub-clinical infections and polypharmacy.

### **6.3.3. Future of NRF2-based therapeutics**

Therapeutic activation of the NRF2 pathway has been shown to be beneficial in a variety of different disease pathologies. As more NRF2-activating compounds undergo clinical trials for the therapeutic pathway induction, it is vital to develop robust, translational ways to test their potency. The data presented in chapter 5, utilises the luminescent H4IIE-8AREL cell line to assess the potencies of sulforaphane analogues as part of the SFX-01 development program. A key finding of this chapter was the reduced potency towards NRF2 pathway



activation in all analogues, compared to the parent sulforaphane compound. In addition, following the development of luminescent reporter plasmids, a similar rank order of potencies of a small group of sulforaphane analogues to activate different ARE-based reporters in both H4Ile and HepG2 cells, was observed. Similar commercially available HepG2 cells expressing an ARE-Luc reporter (BPS bioscience San Diego, USA) have been used for the assessment of novel Nrf2 activating compounds, that correlated with endogenous Nrf2 pathway activation (Khoo et al., 2018). This cell line produced an EC<sub>50</sub> for sulforaphane at 1.16  $\mu$ M, similar to our findings, however, the exact ARE sequence in this reporter cell line is commercially protected.

Electrophilic compounds, such as CDDO-Me and sulforaphane, have the potential for off-target effects due to their pleiotropic modification of thiol groups. Considering this, a range of non-electrophilic activators of NRF2 are an exciting addition to therapeutic activators. This includes the development of peptides and small molecules that disrupt interactions between KEAP1-NRF2 via the ETGE sequence, KEAP1-CUL3 or homodimers of KEAP1 (Hancock et al., 2012; Jiang et al., 2014). These may be more specific than electrophilic NRF2-activators, however it is important to note KEAP1 interactions with other proteins such P62 through the STGE motif which shares significant homology to the ETGE sequence (Komatsu et al., 2010). Targeting of competitive binding partners for KEAP1 may reveal a potent class of NRF2-activating compounds. Alternatively, targeting other regulatory molecules that influence NRF2 such as those targeting the NEH6 phosphodegron (Rojo et al., 2012), or specific ubiquitin ligases (Lo et al., 2017, p. 23; T. Wu et al., 2014, p. 1) have been shown to activate the NRF2 pathway. Ultimately, further understanding of NRF2-pathway regulation and the location of specific deleterious ROS generation is vital for the development of effective, safe therapeutic activators of NRF2.

To this effect, robust screens for the development of novel NRF2 activators have been established. Many ARE-driven luciferase assays, in a variety of cell lines have been used to screen activators of the Nrf2 pathway, including astrocytes (Ajit et al., 2016), pulmonary cells (Thekkevedu et al., 2017), and hepatocytes (Copple et al., 2014). Conversely these reporters have also been used to screen for NRF2 inhibiting compounds (Choi et al., 2017). Methods to monitor Nrf2-pathway modulation in patients are limited to the analysis of peripheral tissues such as blood. Assessment of Nrf2-pathway activation in the DEFINE and CONFIRM clinical trials for the use of DMF to treat multiple sclerosis, was achieved by quantification of

*NQO1* and *HMOX1* mRNA in whole blood isolated from DMF-treated patients (Gopal et al., 2017). Significant induction of these genes was observed after 12 and 48 weeks respectively. The authors also assessed PBMCs cultured from healthy volunteers to ex vivo stimulation with DMF which also lead to up regulation of these Nrf2-regulated genes (Gopal et al., 2017). Reliable assays for the assessment of Nrf2-regulated proteins in circulation have yet to be established. Elevated Nrf2 pathway activity has also been observed in peripheral tissues of patients suffering from pathologies with an underlying oxidative stress component, including synovial fluid extracted from patients with rheumatoid or osteo-arthritis (*NRF2* mRNA correlated with preoperative reactive metabolite levels) (Kondo et al., 2017). The establishment of robust methods to monitor Nrf2 pathway modulation in accessible patient tissues will aid the pharmacodynamic assessment of Nrf2 activators and decipher the therapeutic role of NRF2 activation relative to other off target effects of a compound.

Additionally, the development of sensitive screening platforms will aid the generation of targeted antioxidant therapies. Oxidative eustress emphasises the beneficial effects of redox signalling that are not associated with oxidative damage (Sies, 2018). Targeted antioxidant therapies at specific intracellular locations of aberrant ROS generation are essential to avoid interference with reactive species necessary for stress-response hormesis. Additionally, the effects of sustained therapeutic NRF2 activation on the diverse role of the transcription factor to regulate processes such as protein turnover and glucose metabolism are yet to be assessed (Hirotsu et al., 2012). The risks and therapeutic effects of NRF2 pathway modulation in man are not fully understood. Further insight into chronic exposure of antioxidant therapies in disease models are needed and the emerging therapeutic strategies entering the clinic are well primed to provide answers.

#### **6.4. Conclusions and future directions**

The growing need to monitor NRF2 pathway activity in response to toxicological and therapeutic stimuli has prompted the generation of novel methods of assessing modulation of the transcription factor. This thesis has characterised both *in vivo* and *in vitro* novel methods of Nrf2 pathway assessment. The ability to monitor the status of the NRF2 pathway across the whole body, in the Nrf2-Luc mouse model, allows an overview of organs that might not have been assessed in the early stages of pre-clinical toxicity testing. Additionally, this study has assessed potential the Nrf2-dependent regulation of putative novel NRF2-

regulated genes. Understanding the regulation of the Nrf2 pathway fully will aid the development of novel NRF2 activating compounds but also improve toxicity assessment. Delineation of the specific expression profiles of NRF2-regulated genes following chemical insult may provide insight into the type of ROS being generated and its sub-cellular localisation. Identifying the point at which activation of the NRF2 pathway switches from providing an adaptive response to responding to adverse conditions will improve toxicity assessment by informing phenotypic outcomes. *In vitro* assays with increasing physiological relevance provide the context for NRF2 induction and resultant modulation of the pathway

Several further studies should be conducted to validate and build upon the findings of this thesis. In chapter 2, the Nrf2-Luc mouse model was assessed for its ability to respond to organ specific toxicity. Future studies utilising these mice should investigate the sensitivity of this model to respond to stress not associated with overt toxicity to identify major 'tipping points' within Nrf2 pathway activation. This would aid delineation of MIEs within AOPs. However, this would be dependent on the sensitivity of the transgene to subtle changes in Nrf2 activity. Additionally, application of Nrf2-Luc mice to assess a wider range of compounds liable to toxicity in various organs. This would aid the definition of the group of toxic moieties associated with Nrf2 activation during toxicity and will inform the integration of the model into preclinical screening of compounds.

In this thesis I describe the modulation of mRNA transcripts within murine whole blood in response to APAP-induced hepatotoxicity. Future work to establish the source of the Nrf2 regulated transcripts is vital to show whether these elevations reflect organ-specific injury. Our data highlights the muted induction of Nrf2-regulated transcripts in response to hepatotoxic intervention implicating damaged hepatocytes as a potential source. Assessment of hepatocyte secretions in culture media following APAP-induced toxicity may reveal the presence of vesicle/protein-bound Nrf2-regulated mRNA. The functionality of these Nrf2-regulated transcripts could be assessed by treatment of cells with Nrf2-regulated mRNA from exosomes/conditioned media to assess the ability of the transcripts to influence basal gene expression in recipient cells or provide protective effects against subsequent damage to recipient cells. One limitation of the data in this chapter is the lack of assessment in human whole blood. The human blood-based NRF2 pathway is modulated in response to type 2 diabetes (Siewert et al., 2013) and myeloproliferative neoplasms (Hasselbalch et al.,

2014). Measurement of Nrf2-regulated mRNA in blood samples from DILI patients may highlight the translational relevance of these findings.

This study has assessed ARE sites within the promoter-regions of potentially novel Nrf2-regulated genes for their ability to interact with NRF2. Further analysis of other ARE sites close-to or within the putative Nrf2-regulated genes transcription start site may identify the ARE sequence necessary for activation. Identification of these regions could be informed by ChIP-seq analysis of PHH to identify cell-specific NRF2 binding regions. Additionally, inclusion of enhancer sites within promoter-reporter constructs may facilitate NRF2 interactions. Identification of essential co-factors needed for gene activation could be assessed by stimulating Nrf2 activation in cells with specific MAFs knocked down. Aside from *F2RL2*, *LOC344887* and *TRIM16L* other genes from microarray analysis are worth investigating, such as Pannexin 2 (*PANX2*), EP300 interacting inhibitor of differentiation 3 (*EID3*) and Secreted phosphoprotein 1 (*SPP1*) as these genes were all modulated by stimuli in bioinformatic analysis.

Finally, the utility of ARE-based reporters for the screening of compounds has been demonstrated in this thesis. The generation of stably transfected human cell lines with lower basal Nrf2-pathway activity may facilitate a luciferase-based signal with greater range, that reflect endogenous Nrf2 pathway activation. Ultimately generation of reporter constructs such as those described by Rizzi *et al.* consisting of multiple ARE sequences, will facilitate a more sensitive, representative signal of pathway induction to various stimuli (Rizzi *et al.*, 2017).

## References

- Aatonen, M.T., Öhman, T., Nyman, T.A., Laitinen, S., Grönholm, M., Siljander, P.R.-M., 2014. Isolation and characterization of platelet-derived extracellular vesicles. *J. Extracell. Vesicles* 3. <https://doi.org/10.3402/jev.v3.24692>
- Abiko, Y., Miura, T., Phuc, B.H., Shinkai, Y., Kumagai, Y., 2011. Participation of Keap1 in the activation of Nrf2 by tert-butylbenzoquinone, an electrophilic metabolite of butylated hydroxyanisole. *Toxicol. Appl. Pharmacol.* 255, 32–39. <https://doi.org/10.1016/j.taap.2011.05.013>
- Aburaya, M., Tanaka, K.-I., Hoshino, T., Tsutsumi, S., Suzuki, K., Makise, M., Akagi, R., Mizushima, T., 2006. Haem oxygenase-1 protects gastric mucosal cells against non-steroidal anti-inflammatory drugs. *J. Biol. Chem.* 281, 33422–33432. <https://doi.org/10.1074/jbc.M602074200>
- A. Clulow, J., M. Storck, E., Lanyon-Hogg, T., A. Kalesh, K., H. Jones, L., W. Tate, E., 2017. Competition-based, quantitative chemical proteomics in breast cancer cells identifies new target profiles for sulforaphane. *Chem. Commun.* 53, 5182–5185. <https://doi.org/10.1039/C6CC08797C>
- Agyeman, A.S., Chaerkady, R., Shaw, P.G., Davidson, N.E., Visvanathan, K., Pandey, A., Kensler, T.W., 2012. Transcriptomic and proteomic profiling of KEAP1 disrupted and sulforaphane-treated human breast epithelial cells reveals common expression profiles. *Breast Cancer Res. Treat.* 132, 175–187. <https://doi.org/10.1007/s10549-011-1536-9>
- Ahn, Y.-H., Hwang, Y., Liu, H., Wang, X.J., Zhang, Y., Stephenson, K.K., Boronina, T.N., Cole, R.N., Dinkova-Kostova, A.T., Talalay, P., Cole, P.A., 2010. Electrophilic tuning of the chemoprotective natural product sulforaphane. *Proc. Natl. Acad. Sci.* 107, 9590–9595. <https://doi.org/10.1073/pnas.1004104107>
- Aitio, M.-L., 2006. N-acetylcysteine – passe-partout or much ado about nothing? *Br. J. Clin. Pharmacol.* 61, 5–15. <https://doi.org/10.1111/j.1365-2125.2005.02523.x>
- Ajit, D., Simonyi, A., Li, R., Chen, Z., Hannink, M., Fritsche, K.L., Mossine, V.V., Smith, R.E., Dobbs, T.K., Luo, R., Folk, W.R., Gu, Z., Lubahn, D.B., Weisman, G.A., Sun, G.Y., 2016. Phytochemicals and botanical extracts regulate NF- $\kappa$ B and Nrf2/ARE reporter activities in DI TNC1 astrocytes. *Neurochem. Int.* 97, 49–56. <https://doi.org/10.1016/j.neuint.2016.05.004>
- Akram, A., Han, B., Masoom, H., Peng, C., Lam, E., L. Litvack, M., Bai, X., Shan, Y., Hai, T., Batt, J., Slutsky, A.S., Zhang, H., Kuebler, W.M., Haitzma, J.J., Liu, M., dos Santos, C.C., 2010. Activating Transcription Factor 3 Confers Protection against Ventilator-induced Lung Injury. *Am. J. Respir. Crit. Care Med.* 182, 489–500. <https://doi.org/10.1164/rccm.200906-0925OC>
- Alam, J., Cook, J.L., 2007a. How Many Transcription Factors Does It Take to Turn On the Haem Oxygenase-1 Gene? *Am. J. Respir. Cell Mol. Biol.* 36, 166–174. <https://doi.org/10.1165/rcmb.2006-0340TR>
- Alam, J., Cook, J.L., 2007b. How Many Transcription Factors Does It Take to Turn On the Haem Oxygenase-1 Gene? *Am. J. Respir. Cell Mol. Biol.* 36, 166–174. <https://doi.org/10.1165/rcmb.2006-0340TR>
- Aleksunes, L.M., Goedken, M.J., Rockwell, C.E., Thomale, J., Manautou, J.E., Klaassen, C.D., 2010. Transcriptional regulation of renal cytoprotective genes by Nrf2 and its potential use as a therapeutic target to mitigate cisplatin-induced nephrotoxicity. *J. Pharmacol. Exp. Ther.* 335, 2–12. <https://doi.org/10.1124/jpet.110.170084>
- Anderton, B.H., Betts, J., Blackstock, W.P., Brion, J.P., Chapman, S., Connell, J., Dayanandan, R., Gallo, J.M., Gibb, G., Hanger, D.P., Hutton, M., Kardalidou, E., Leroy, K., Lovestone, S., Mack, T., Reynolds, C.H., Van Slegtenhorst, M., 2001. Sites of phosphorylation in tau and factors affecting their regulation. *Biochem. Soc. Symp.* 73–80.
- Ankley, G.T., Bennett, R.S., Erickson, R.J., Hoff, D.J., Hornung, M.W., Johnson, R.D., Mount, D.R., Nichols, J.W., Russom, C.L., Schmieder, P.K., Serrano, J.A., Tietge, J.E., Villeneuve, D.L., 2010. Adverse outcome pathways: A conceptual framework to support ecotoxicology research and risk assessment. *Environ. Toxicol. Chem.* 29, 730–741. <https://doi.org/10.1002/etc.34>
- Antoine, D.J., Dear, J.W., Lewis, P.S., Platt, V., Coyle, J., Masson, M., Thanacoody, R.H., Gray, A.J., Webb, D.J., Moggs, J.G., Bateman, D.N., Goldring, C.E., Park, B.K., 2013. Mechanistic biomarkers provide early and sensitive detection of acetaminophen-induced acute liver injury at first presentation to hospital. *Hepatol. Baltim. Md* 58, 777–787. <https://doi.org/10.1002/hep.26294>
- Antoine, D.J., Williams, D.P., Kipar, A., Jenkins, R.E., Regan, S.L., Sathish, J.G., Kitteringham, N.R., Park, B.K., 2009. High-mobility group box-1 protein and keratin-18, circulating serum proteins informative of acetaminophen-induced necrosis and apoptosis in vivo. *Toxicol. Sci. Off. J. Soc. Toxicol.* 112, 521–531. <https://doi.org/10.1093/toxsci/kfp235>
- Arinze, I.J., Kawai, Y., 2005. Transcriptional activation of the human Galphai2 gene promoter through nuclear factor-kappaB and antioxidant response elements. *J. Biol. Chem.* 280, 9786–9795. <https://doi.org/10.1074/jbc.M414006200>
- Arroyo, C.M., Kramer, J.H., Dickens, B.F., Weglicki, W.B., 1987. Identification of free radicals in myocardial ischemia/reperfusion by spin trapping with nitron DMPO. *FEBS Lett.* 221, 101–104. [https://doi.org/10.1016/0014-5793\(87\)80360-5](https://doi.org/10.1016/0014-5793(87)80360-5)
- Aschauer, L., Limonciel, A., Wilmes, A., Stanzel, S., Kopp-Schneider, A., Hewitt, P., Lukas, A., Leonard, M.O., Pfaller, W., Jennings, P., 2014. Application of RPTEC/TERT1 cells for investigation of repeat dose nephrotoxicity: A transcriptomic study. *Toxicol. In Vitro.* <https://doi.org/10.1016/j.tiv.2014.10.005>
- Ascherio, A., Weisskopf, M.G., O'reilly, E.J., Jacobs, E.J., McCullough, M.L., Calle, E.E., Cudkovicz, M., Thun, M.J., 2005. Vitamin E intake and risk of amyotrophic lateral sclerosis. *Ann. Neurol.* 57, 104–110. <https://doi.org/10.1002/ana.20316>
- Axworthy, D.B., Hoffmann, K.J., Streeter, A.J., Callemann, C.J., Pascoe, G.A., Baillie, T.A., 1988. Covalent binding of acetaminophen to mouse hemoglobin. Identification of major and minor adducts formed in vivo and implications for the nature of the arylating metabolites. *Chem. Biol. Interact.* 68, 99–116.
- Babior, B.M., Kipnes, R.S., Curnutte, J.T., 1973. Biological Defense Mechanisms. THE PRODUCTION BY LEUKOCYTES OF SUPEROXIDE, A POTENTIAL BACTERICIDAL AGENT. *J. Clin. Invest.* 52, 741–744.
- Bah, A., Chen, Z., Bush-Pelc, L.A., Mathews, F.S., Cera, E.D., 2007. Crystal structures of murine thrombin in complex with the extracellular fragments of murine protease-activated receptors PAR3 and PAR4. *Proc. Natl. Acad. Sci.* 104, 11603–11608. <https://doi.org/10.1073/pnas.0704409104>
- Banning, A., Deubel, S., Kluth, D., Zhou, Z., Brigelius-Flohé, R., 2005. The Gl-GPx gene is a target for Nrf2. *Mol. Cell. Biol.* 25, 4914–4923. <https://doi.org/10.1128/MCB.25.12.4914-4923.2005>
- Barajas, B., Che, N., Yin, F., Rowshanrad, A., Orozco, L.D., Gong, K.W., Wang, X., Castellani, L.W., Reue, K., Lusic, A.J., Araujo, J.A., 2011. NF-E2-related factor 2 promotes atherosclerosis by effects on plasma lipoproteins and cholesterol

- transport that overshadow antioxidant protection. *Arterioscler. Thromb. Vasc. Biol.* 31, 58–66. <https://doi.org/10.1161/ATVBAHA.110.210906>
- Belousov, V.V., Fradkov, A.F., Lukyanov, K.A., Staroverov, D.B., Shakhbazov, K.S., Tersikh, A.V., Lukyanov, S., 2006. Genetically encoded fluorescent indicator for intracellular hydrogen peroxide. *Nat. Methods* 3, 281–286. <https://doi.org/10.1038/nmeth866>
- Bilan, D.S., Pase, L., Joosen, L., Gorokhovatsky, A.Y., Ermakova, Y.G., Gadella, T.W.J., Grabher, C., Schultz, C., Lukyanov, S., Belousov, V.V., 2013. HyPer-3: a genetically encoded H<sub>2</sub>O<sub>2</sub> probe with improved performance for ratiometric and fluorescence lifetime imaging. *ACS Chem. Biol.* 8, 535–542. <https://doi.org/10.1021/cb300625g>
- Biteau, B., Labarre, J., Toledano, M.B., 2003. ATP-dependent reduction of cysteine–sulphinic acid by *S. cerevisiae* sulphiredoxin. *Nature* 425, 980–984. <https://doi.org/10.1038/nature02075>
- Bittner, G.C.V. de, Dubikovskaya, E.A., Bertozzi, C.R., Chang, C.J., 2010. In vivo imaging of hydrogen peroxide production in a murine tumor model with a chemoselective bioluminescent reporter. *Proc. Natl. Acad. Sci.* 107, 21316–21321. <https://doi.org/10.1073/pnas.1012864107>
- Bjelakovic, G., Nikolova, D., Gluud, L.L., Simonetti, R.G., Gluud, C., 2007. Mortality in randomized trials of antioxidant supplements for primary and secondary prevention: systematic review and meta-analysis. *JAMA* 297, 842–857. <https://doi.org/10.1001/jama.297.8.842>
- Black, C.N., Bot, M., Scheffer, P.G., Cuijpers, P., Penninx, B.W.J.H., 2015. Is depression associated with increased oxidative stress? A systematic review and meta-analysis. *Psychoneuroendocrinology*, This issue includes a Special Section on Biomarkers in the Military - New Findings from Prospective Studies 51, 164–175. <https://doi.org/10.1016/j.psyneuen.2014.09.025>
- Blanchard, N., Lankar, D., Faure, F., Regnault, A., Dumont, C., Raposo, G., Hivroz, C., 2002. TCR Activation of Human T Cells Induces the Production of Exosomes Bearing the TCR/CD3/ζ Complex. *J. Immunol.* 168, 3235–3241. <https://doi.org/10.4049/jimmunol.168.7.3235>
- Bloom, D.A., Jaiswal, A.K., 2003. Phosphorylation of Nrf2 at Ser40 by protein kinase C in response to antioxidants leads to the release of Nrf2 from IκB, but is not required for Nrf2 stabilization/accumulation in the nucleus and transcriptional activation of antioxidant response element-mediated NAD(P)H:quinone oxidoreductase-1 gene expression. *J. Biol. Chem.* 278, 44675–44682. <https://doi.org/10.1074/jbc.M307633200>
- Board, W.H.O.E., 1973. Handbook of resolutions and decisions of the World Health Assembly and the Executive Board. World Health Organization.
- Boom, R., Sol, C.J., Salimans, M.M., Jansen, C.L., Wertheim-van Dillen, P.M., van der Noordaa, J., 1990. Rapid and simple method for purification of nucleic acids. *J. Clin. Microbiol.* 28, 495–503.
- Boylston, J.A., Brenner, C., 2014. A knockdown with smoke model reveals FHIT as a repressor of Haem oxygenase 1. *Cell Cycle Georget. Tex* 13, 2913–2930. <https://doi.org/10.4161/15384101.2014.946858>
- Bradford, M.M., 1976. A rapid and sensitive method for the quantitation of microgram quantities of protein utilizing the principle of protein-dye binding. *Anal. Biochem.* 72, 248–254. [https://doi.org/10.1016/0003-2697\(76\)90527-3](https://doi.org/10.1016/0003-2697(76)90527-3)
- Brown, S.L., Sekhar, K.R., Rachakonda, G., Sasi, S., Freeman, M.L., 2008. Activating Transcription Factor 3 Is a Novel Repressor of the Nuclear Factor Erythroid-Derived 2-Related Factor 2 (Nrf2)-Regulated Stress Pathway. *Cancer Res.* 68, 364–368. <https://doi.org/10.1158/0008-5472.CAN-07-2170>
- Browne, S.E., Ferrante, R.J., Beal, M.F., 1999. Oxidative Stress in Huntington's Disease. *Brain Pathol.* 9, 147–163. <https://doi.org/10.1111/j.1750-3639.1999.tb00216.x>
- Bruce, C.R., Carey, A.L., Hawley, J.A., Febbraio, M.A., 2003. Intramuscular Heat Shock Protein 72 and Haem Oxygenase-1 mRNA Are Reduced in Patients With Type 2 Diabetes: Evidence That Insulin Resistance Is Associated With a Disturbed Antioxidant Defense Mechanism. *Diabetes* 52, 2338–2345. <https://doi.org/10.2337/diabetes.52.9.2338>
- Bryan, H.K., Olayanju, A., Goldring, C.E., Park, B.K., 2013. The Nrf2 cell defence pathway: Keap1-dependent and -independent mechanisms of regulation. *Biochem. Pharmacol.* 85, 705–717. <https://doi.org/10.1016/j.bcp.2012.11.016>
- Bulua, A.C., Simon, A., Maddipati, R., Pelletier, M., Park, H., Kim, K.-Y., Sack, M.N., Kastner, D.L., Siegel, R.M., 2011. Mitochondrial reactive oxygen species promote production of proinflammatory cytokines and are elevated in TNFR1-associated periodic syndrome (TRAPS). *J. Exp. Med.* 208, 519–533. <https://doi.org/10.1084/jem.20102049>
- Burkitt, M.J., Wardman, P., 2001. Cytochrome c Is a Potent Catalyst of Dichlorofluorescein Oxidation: Implications for the Role of Reactive Oxygen Species in Apoptosis. *Biochem. Biophys. Res. Commun.* 282, 329–333. <https://doi.org/10.1006/bbrc.2001.4578>
- Burnette, W.N., 1981. "Western Blotting": Electrophoretic transfer of proteins from sodium dodecyl sulfate-polyacrylamide gels to unmodified nitrocellulose and radiographic detection with antibody and radioiodinated protein A. *Anal. Biochem.* 112, 195–203. [https://doi.org/10.1016/0003-2697\(81\)90281-5](https://doi.org/10.1016/0003-2697(81)90281-5)
- Bushel, P.R., Heinloth, A.N., Li, J., Huang, L., Chou, J.W., Boorman, G.A., Malarkey, D.E., Houle, C.D., Ward, S.M., Wilson, R.E., Fannin, R.D., Russo, M.W., Watkins, P.B., Tennant, R.W., Paules, R.S., 2007. Blood gene expression signatures predict exposure levels. *Proc. Natl. Acad. Sci.* 104, 18211–18216. <https://doi.org/10.1073/pnas.0706987104>
- Butterfield, D.A., Drake, J., Pocernich, C., Castegna, A., 2001. Evidence of oxidative damage in Alzheimer's disease brain: central role for amyloid beta-peptide. *Trends Mol. Med.* 7, 548–554.
- Cahuana, G.M., Tejedro, J.R., Jiménez, J., Ramírez, R., Sobrino, F., Bedoya, F.J., 2004. Nitric oxide-induced carbonylation of Bcl-2, GAPDH and ANT precedes apoptotic events in insulin-secreting RINm5F cells. *Exp. Cell Res.* 293, 22–30.
- Cai, J., Wu, M., Nelson, K.C., Sternberg, P., Jones, D.P., 1999. Oxidant-induced apoptosis in cultured human retinal pigment epithelial cells. *Invest. Ophthalmol. Vis. Sci.* 40, 959–966.
- Chae, H.Z., Chung, S.J., Rhee, S.G., 1994. Thioredoxin-dependent peroxide reductase from yeast. *J. Biol. Chem.* 269, 27670–27678.
- Chan, K., Han, X.D., Kan, Y.W., 2001. An important function of Nrf2 in combating oxidative stress: detoxification of acetaminophen. *Proc. Natl. Acad. Sci. U. S. A.* 98, 4611–4616. <https://doi.org/10.1073/pnas.081082098>
- Chan, K., Lu, R., Chang, J.C., Kan, Y.W., 1996. NRF2, a member of the NFE2 family of transcription factors, is not essential for murine erythropoiesis, growth, and development. *Proc. Natl. Acad. Sci. U. S. A.* 93, 13943–13948.

- Chan, R.W.Y., Wong, J., Lai, P.B.S., Lo, Y.M.D., Chiu, R.W.K., 2013. The potential clinical utility of serial plasma albumin mRNA monitoring for the post-liver transplantation management. *Clin. Biochem.* 46, 1313–1319. <https://doi.org/10.1016/j.clinbiochem.2013.04.022>
- Chanas, S.A., Jiang, Q., McMahon, M., McWalter, G.K., McLellan, L.I., Elcombe, C.R., Henderson, C.J., Wolf, C.R., Moffat, G.J., Itoh, K., Yamamoto, M., Hayes, J.D., 2002. Loss of the Nrf2 transcription factor causes a marked reduction in constitutive and inducible expression of the glutathione S-transferase *Gsta1*, *Gsta2*, *Gstm1*, *Gstm2*, *Gstm3* and *Gstm4* genes in the livers of male and female mice. *Biochem. J.* 365, 405–416. <https://doi.org/10.1042/BJ20020320>
- Chen, P.-C., Vargas, M.R., Pani, A.K., Smeyne, R.J., Johnson, D.A., Kan, Y.W., Johnson, J.A., 2009. Nrf2-mediated neuroprotection in the MPTP mouse model of Parkinson's disease: Critical role for the astrocyte. *Proc. Natl. Acad. Sci. U. S. A.* 106, 2933–2938. <https://doi.org/10.1073/pnas.0813361106>
- Chen, X., Ba, Y., Ma, L., Cai, X., Yin, Y., Wang, K., Guo, J., Zhang, Y., Chen, J., Guo, X., Li, Q., Li, X., Wang, W., Zhang, Y., Wang, J., Jiang, X., Xiang, Y., Xu, C., Zheng, P., Zhang, J., Li, R., Zhang, H., Shang, X., Gong, T., Ning, G., Wang, J., Zen, K., Zhang, J., Zhang, C.-Y., 2008. Characterization of microRNAs in serum: a novel class of biomarkers for diagnosis of cancer and other diseases. *Cell Res.* 18, 997–1006. <https://doi.org/10.1038/cr.2008.282>
- Chen, X.-L., Zhang, Q., Zhao, R., Ding, X., Tummala, P.E., Medford, R.M., 2003. Rac1 and Superoxide Are Required for the Expression of Cell Adhesion Molecules Induced by Tumor Necrosis Factor- $\alpha$  in Endothelial Cells. *J. Pharmacol. Exp. Ther.* 305, 573–580. <https://doi.org/10.1124/jpet.102.047894>
- Cheung, S.T., Fan, S.T., Lee, Y.T., Chow, J.P., Ng, I.O., Fong, D.Y., Lo, C.M., 2008. Albumin mRNA in Plasma Predicts Post-Transplant Recurrence of Patients With Hepatocellular Carcinoma. *Transplantation* 85, 81. <https://doi.org/10.1097/01.tp.0000298003.88530.11>
- Chiarugi, P., Pani, G., Giannoni, E., Taddei, L., Colavitti, R., Raugei, G., Symons, M., Borrello, S., Galeotti, T., Ramponi, G., 2003. Reactive oxygen species as essential mediators of cell adhesion. *J. Cell Biol.* 161, 933–944. <https://doi.org/10.1083/jcb.200211118>
- Cho, H.-Y., Reddy, S.P.M., Yamamoto, M., Kleeberger, S.R., 2004. The transcription factor NRF2 protects against pulmonary fibrosis. *FASEB J. Off. Publ. Fed. Am. Soc. Exp. Biol.* 18, 1258–1260. <https://doi.org/10.1096/fj.03-1127fje>
- Cho, J.-M., Manandhar, S., Lee, H.-R., Park, H.-M., Kwak, M.-K., 2008. Role of the Nrf2-antioxidant system in cytotoxicity mediated by anticancer cisplatin: Implication to cancer cell resistance. *Cancer Lett.* 260, 96–108. <https://doi.org/10.1016/j.canlet.2007.10.022>
- Choi, E.-J., Jung, B.-J., Lee, S.-H., Yoo, H.-S., Shin, E.-A., Ko, H.-J., Chang, S., Kim, S.-Y., Jeon, S.-M., 2017. A clinical drug library screen identifies clobetasol propionate as an NRF2 inhibitor with potential therapeutic efficacy in KEAP1 mutant lung cancer. *Oncogene* 36, 5285–5295. <https://doi.org/10.1038/onc.2017.153>
- Chorley, B.N., Campbell, M.R., Wang, X., Karaca, M., Sambandan, D., Bangura, F., Xue, P., Pi, J., Kleeberger, S.R., Bell, D.A., 2012. Identification of novel NRF2-regulated genes by ChIP-Seq: influence on retinoid X receptor alpha. *Nucleic Acids Res.* 40, 7416–7429. <https://doi.org/10.1093/nar/gks409>
- Choucha Snouber, L., Bunescu, A., Naudot, M., Legallais, C., Brochet, C., Dumas, M.E., Elena-Herrmann, B., Leclerc, E., 2013. Metabolomics-on-a-chip of hepatotoxicity induced by anticancer drug flutamide and its active metabolite hydroxyflutamide using HepG2/C3a microfluidic biochips. *Toxicol. Sci. Off. J. Soc. Toxicol.* 132, 8–20. <https://doi.org/10.1093/toxsci/kfs230>
- Chowdhry, S., Zhang, Y., McMahon, M., Sutherland, C., Cuadrado, A., Hayes, J.D., 2013. Nrf2 is controlled by two distinct  $\beta$ -TrCP recognition motifs in its Neh6 domain, one of which can be modulated by GSK-3 activity. *Oncogene* 32, 3765–3781. <https://doi.org/10.1038/onc.2012.388>
- Chowdhury, I., Mo, Y., Gao, L., Kazi, A., Fisher, A.B., Feinstein, S.I., 2009. Oxidant stress stimulates expression of the human peroxiredoxin 6 gene by a transcriptional mechanism involving an antioxidant response element. *Free Radic. Biol. Med.* 46, 146–153. <https://doi.org/10.1016/j.freeradbiomed.2008.09.027>
- Cincin, Z.B., Unlu, M., Kiran, B., Bireller, E.S., Baran, Y., Cakmakoglu, B., 2014. Molecular Mechanisms of Quercitrin-induced Apoptosis in Non-small Cell Lung Cancer. *Arch. Med. Res.* 45, 445–454. <https://doi.org/10.1016/j.arcmed.2014.08.002>
- Cleasby, A., Yon, J., Day, P.J., Richardson, C., Tickle, I.J., Williams, P.A., Callahan, J.F., Carr, R., Concha, N., Kerns, J.K., Qi, H., Sweitzer, T., Ward, P., Davies, T.G., 2014. Structure of the BTB Domain of Keap1 and Its Interaction with the Triterpenoid Antagonist CDDO. *PLOS ONE* 9, e98896. <https://doi.org/10.1371/journal.pone.0098896>
- Converso, D.P., Taillé, C., Carreras, M.C., Jaitovich, A., Poderoso, J.J., Boczkowski, J., 2006. HO-1 is located in liver mitochondria and modulates mitochondrial haem content and metabolism. *FASEB J. Off. Publ. Fed. Am. Soc. Exp. Biol.* 20, 1236–1238. <https://doi.org/10.1096/fj.05-4204fje>
- Copple, I.M., Goldring, C.E., Jenkins, R.E., Chia, A.J.L., Randle, L.E., Hayes, J.D., Kitteringham, N.R., Park, B.K., 2008a. The hepatotoxic metabolite of acetaminophen directly activates the Keap1-Nrf2 cell defense system. *Hepatology* 48, 1292–1301. <https://doi.org/10.1002/hep.22472>
- Copple, I.M., Goldring, C.E., Kitteringham, N.R., Park, B.K., 2008b. The Nrf2–Keap1 defence pathway: Role in protection against drug-induced toxicity. *Toxicology, Includes Special Issue section on: New Technologies for Toxicology - Meeting Future Challenges in Drug Safety* 246, 24–33. <https://doi.org/10.1016/j.tox.2007.10.029>
- Copple, I.M., Lister, A., Obeng, A.D., Kitteringham, N.R., Jenkins, R.E., Layfield, R., Foster, B.J., Goldring, C.E., Park, B.K., 2010. Physical and functional interaction of sequestosome 1 with Keap1 regulates the Keap1-Nrf2 cell defense pathway. *J. Biol. Chem.* 285, 16782–16788. <https://doi.org/10.1074/jbc.M109.096545>
- Copple, I.M., Shelton, L.M., Walsh, J., Kratschmar, D.V., Lister, A., Odermatt, A., Goldring, C.E., Dinkova-Kostova, A.T., Honda, T., Park, B.K., 2014. Chemical tuning enhances both potency toward nrf2 and in vitro therapeutic index of triterpenoids. *Toxicol. Sci. Off. J. Soc. Toxicol.* 140, 462–469. <https://doi.org/10.1093/toxsci/kfu080>
- Correa, P., Fontham, E.T.H., Bravo, J.C., Bravo, L.E., Ruiz, B., Zarama, G., Realpe, J.L., Malcom, G.T., Li, D., Johnson, W.D., Mera, R., 2000. Chemoprevention of Gastric Dysplasia: Randomized Trial of Antioxidant Supplements and Anti-Helicobacter pylori Therapy. *J. Natl. Cancer Inst.* 92, 1881–1888. <https://doi.org/10.1093/jnci/92.23.1881>

- Costantini, D., Verhulst, S., 2009. Does high antioxidant capacity indicate low oxidative stress? *Funct. Ecol.* 23, 506–509. <https://doi.org/10.1111/j.1365-2435.2009.01546.x>
- Coughlin, S.R., 2000. Thrombin signalling and protease-activated receptors. *Nature* 407, 258–264. <https://doi.org/10.1038/35025229>
- Cullinan, S.B., Gordan, J.D., Jin, J., Harper, J.W., Diehl, J.A., 2004. The Keap1-BTB Protein Is an Adaptor That Bridges Nrf2 to a Cul3-Based E3 Ligase: Oxidative Stress Sensing by a Cul3-Keap1 Ligase. *Mol. Cell. Biol.* 24, 8477–8486. <https://doi.org/10.1128/MCB.24.19.8477-8486.2004>
- Currier, J.M., Cheng, W.-Y., Menendez, D., Conolly, R., Chorley, B.N., 2016. Developing a Gene Biomarker at the Tipping Point of Adaptive and Adverse Responses in Human Bronchial Epithelial Cells. *PLOS ONE* 11, e0155875. <https://doi.org/10.1371/journal.pone.0155875>
- Curtis, A., Calabro, K., Galarneau, J.-R., Bigio, I.J., Krucker, T., 2011. Temporal variations of skin pigmentation in C57BL/6 mice affect optical bioluminescence quantitation. *Mol. Imaging Biol. MIB Off. Publ. Acad. Mol. Imaging* 13, 1114–1123. <https://doi.org/10.1007/s11307-010-0440-8>
- Dahlin, D.C., Nelson, S.D., 1982. Synthesis, decomposition kinetics, and preliminary toxicological studies of pure N-acetyl-p-benzoquinone imine, a proposed toxic metabolite of acetaminophen. *J. Med. Chem.* 25, 885–886. <https://doi.org/10.1021/jm00350a001>
- Dai, G., He, L., Chou, N., Wan, Y.-J.Y., 2006. Acetaminophen Metabolism Does Not Contribute to Gender Difference in Its Hepatotoxicity in Mouse. *Toxicol. Sci.* 92, 33–41. <https://doi.org/10.1093/toxsci/kfj192>
- de Zeeuw, D., Akizawa, T., Audhya, P., Bakris, G.L., Chin, M., Christ-Schmidt, H., Goldsberry, A., Houser, M., Krauth, M., Lambers Heerspink, H.J., McMurray, J.J., Meyer, C.J., Parving, H.-H., Remuzzi, G., Toto, R.D., Vaziri, N.D., Wanner, C., Wittes, J., Wrolstad, D., Chertow, G.M., 2013. Bardoxolone Methyl in Type 2 Diabetes and Stage 4 Chronic Kidney Disease. *N. Engl. J. Med.* 369, 2492–2503. <https://doi.org/10.1056/NEJMoa1306033>
- DeNicola, G.M., Karreth, F.A., Humpston, T.J., Gopinathan, A., Wei, C., Frese, K., Mangal, D., Yu, K.H., Yeo, C.J., Calhoun, E.S., Scrimieri, F., Winter, J.M., Hruban, R.H., Iacobuzio-Donahue, C., Kern, S.E., Blair, I.A., Tuveson, D.A., 2011. Oncogene-induced Nrf2 transcription promotes ROS detoxification and tumorigenesis. *Nature* 475, 106–109. <https://doi.org/10.1038/nature10189>
- Dhakshinamoorthy, S., Jain, A.K., Bloom, D.A., Jaiswal, A.K., 2005. Bach1 competes with Nrf2 leading to negative regulation of the antioxidant response element (ARE)-mediated NAD(P)H:quinone oxidoreductase 1 gene expression and induction in response to antioxidants. *J. Biol. Chem.* 280, 16891–16900. <https://doi.org/10.1074/jbc.M500166200>
- Ding, V.W., Chen, R.-H., McCormick, F., 2000. Differential Regulation of Glycogen Synthase Kinase 3 $\beta$  by Insulin and Wnt Signaling. *J. Biol. Chem.* 275, 32475–32481. <https://doi.org/10.1074/jbc.M005342200>
- Dinkova-Kostova, A.T., Holtzclaw, W.D., Cole, R.N., Itoh, K., Wakabayashi, N., Katoh, Y., Yamamoto, M., Talalay, P., 2002. Direct evidence that sulfhydryl groups of Keap1 are the sensors regulating induction of phase 2 enzymes that protect against carcinogens and oxidants. *Proc. Natl. Acad. Sci. U. S. A.* 99, 11908–11913. <https://doi.org/10.1073/pnas.172398899>
- Dinkova-Kostova, A.T., Liby, K.T., Stephenson, K.K., Holtzclaw, W.D., Gao, X., Suh, N., Williams, C., Risingsong, R., Honda, T., Gribble, G.W., Sporn, M.B., Talalay, P., 2005. Extremely potent triterpenoid inducers of the phase 2 response: Correlations of protection against oxidant and inflammatory stress. *Proc. Natl. Acad. Sci. U. S. A.* 102, 4584–4589. <https://doi.org/10.1073/pnas.0500815102>
- Dreger, H., Westphal, K., Weller, A., Baumann, G., Stangl, V., Meiners, S., Stangl, K., 2009. Nrf2-dependent upregulation of antioxidant enzymes: a novel pathway for proteasome inhibitor-mediated cardioprotection. *Cardiovasc. Res.* 83, 354–361. <https://doi.org/10.1093/cvr/cvp107>
- Eakins, R., Walsh, J., Randle, L., Jenkins, R.E., Schuppe-Koistinen, I., Rowe, C., Lewis, P.S., Vasieva, O., Prats, N., Brilliant, N., Auli, M., Bayliss, M., Webb, S., Rees, J.A., Kitteringham, N.R., Goldring, C.E., Park, B.K., 2015. Adaptation to acetaminophen exposure elicits major changes in expression and distribution of the hepatic proteome. *Sci. Rep.* 5, 16423. <https://doi.org/10.1038/srep16423>
- Eastman, A., 1983. Characterization of the adducts produced in DNA by cis-diamminedichloroplatinum(II) and cis-dichloro(ethylenediamine)platinum(II). *Biochemistry (Mosc.)* 22, 3927–3933. <https://doi.org/10.1021/bi00285a031>
- Eisenstein, R.S., Garcia-Mayol, D., Pettingell, W., Munro, H.N., 1991. Regulation of ferritin and haem oxygenase synthesis in rat fibroblasts by different forms of iron. *Proc. Natl. Acad. Sci. U. S. A.* 88, 688–692.
- Eitas, T.K., Stepp, W., Sjeklocha, L., Long, C., Riley, C., Callahan, J., Sanchez, Y., Gough, P., Knowlin, L., van Duin, D., Ortiz-Pujols, S., Jones, S., Maile, R., Hong, Z., Berger, S., Cairns, B., 2017. Differential regulation of innate immune cytokine production through pharmacological activation of Nuclear Factor-Erythroid-2-Related Factor 2 (NRF2) in burn patient immune cells and monocytes. *PLoS ONE* 12. <https://doi.org/10.1371/journal.pone.0184164>
- Elaut, G., Hensens, T., Papeleu, P., Snykers, S., Vinken, M., Vanhaecke, T., Rogiers, V., 2006. Molecular mechanisms underlying the dedifferentiation process of isolated hepatocytes and their cultures. *Curr. Drug Metab.* 7, 629–660.
- Eldh, M., Ekström, K., Valadi, H., Sjöstrand, M., Olsson, B., Jernäs, M., Lötvall, J., 2010. Exosomes Communicate Protective Messages during Oxidative Stress; Possible Role of Exosomal Shuttle RNA. *PLOS ONE* 5, e15353. <https://doi.org/10.1371/journal.pone.0015353>
- El-Hefnawy, T., Raja, S., Kelly, L., Bigbee, W.L., Kirkwood, J.M., Luketich, J.D., Godfrey, T.E., 2004. Characterization of Amplifiable, Circulating RNA in Plasma and Its Potential as a Tool for Cancer Diagnostics. *Clin. Chem.* 50, 564–573. <https://doi.org/10.1373/clinchem.2003.028506>
- Emter, R., Ellis, G., Natsch, A., 2010. Performance of a novel keratinocyte-based reporter cell line to screen skin sensitizers in vitro. *Toxicol. Appl. Pharmacol.* 245, 281–290. <https://doi.org/10.1016/j.taap.2010.03.009>
- Emter, R., Natsch, A., 2015. Dual regulation of skin sensitizer-induced HMOX1 expression by Bach1 and Nrf2: Comparison to regulation of the AKR1C2-ARE element in the KeratinoSens cell line. *Toxicol. Appl. Pharmacol.* 288, 281–288. <https://doi.org/10.1016/j.taap.2015.07.027>



- Endo, H., Sugioka, Y., Nakagi, Y., Saijo, Y., Yoshida, T., 2008. A novel role of the NRF2 transcription factor in the regulation of arsenite-mediated keratin 16 gene expression in human keratinocytes. *Environ. Health Perspect.* 116, 873–879. <https://doi.org/10.1289/ehp.10696>
- Engelhart, M.J., Geerlings, M.I., Ruitenberg, A., van Swieten, J.C., Hofman, A., Witteman, J.C.M., Breteler, M.M.B., 2002. Dietary intake of antioxidants and risk of Alzheimer disease. *JAMA* 287, 3223–3229.
- Enomoto, A., Itoh, K., Nagayoshi, E., Haruta, J., Kimura, T., O'Connor, T., Harada, T., Yamamoto, M., 2001. High Sensitivity of Nrf2 Knockout Mice to Acetaminophen Hepatotoxicity Associated with Decreased Expression of ARE-Regulated Drug Metabolizing Enzymes and Antioxidant Genes. *Toxicol. Sci.* 59, 169–177. <https://doi.org/10.1093/toxsci/59.1.169>
- Erickson, A.M., Nevarea, Z., Gipp, J.J., Mulcahy, R.T., 2002. Identification of a variant antioxidant response element in the promoter of the human glutamate-cysteine ligase modifier subunit gene. Revision of the ARE consensus sequence. *J. Biol. Chem.* 277, 30730–30737. <https://doi.org/10.1074/jbc.M205225200>
- Fan, P.-C., Chen, C.-C., Chen, Y.-C., Chang, Y.-S., Chu, P.-H., 2016. MicroRNAs in acute kidney injury. *Hum. Genomics* 10. <https://doi.org/10.1186/s40246-016-0085-z>
- Fannin, R.D., Russo, M., O'Connell, T.M., Gerrish, K., Winnike, J.H., Macdonald, J., Newton, J., Malik, S., Sieber, S.O., Parker, J., Shah, R., Zhou, T., Watkins, P.B., Paules, R.S., 2010. Acetaminophen dosing of humans results in blood transcriptome and metabolome changes consistent with impaired oxidative phosphorylation. *Hepatology* 51, 227–236. <https://doi.org/10.1002/hep.23330>
- Fichtinger-Schepman, A.M.J., Van der Veer, J.L., Den Hartog, J.H.J., Lohman, P.H.M., Reedijk, J., 1985. Adducts of the antitumor drug cis-diamminedichloroplatinum(II) with DNA: formation, identification, and quantitation. *Biochemistry (Mosc.)* 24, 707–713. <https://doi.org/10.1021/bi00324a025>
- Finkel, T., 2011. Signal transduction by reactive oxygen species. *J. Cell Biol.* 194, 7–15. <https://doi.org/10.1083/jcb.201102095>
- Forootan, S.S., Mutter, F.E., Kipar, A., Iwawaki, T., Francis, B., Goldring, C.E., Park, B.K., Copple, I.M., 2017. Real-time in vivo imaging reveals localised Nrf2 stress responses associated with direct and metabolism-dependent drug toxicity. *Sci. Rep.* 7, 16084. <https://doi.org/10.1038/s41598-017-16491-2>
- Fox, R.J., Miller, D.H., Phillips, J.T., Hutchinson, M., Havrdova, E., Kita, M., Yang, M., Raghupathi, K., Novas, M., Sweetser, M.T., Vigiotta, V., Dawson, K.T., CONFIRM Study Investigators, 2012. Placebo-controlled phase 3 study of oral BG-12 or glatiramer in multiple sclerosis. *N. Engl. J. Med.* 367, 1087–1097. <https://doi.org/10.1056/NEJMoa1206328>
- Franco, R., Schoneveld, O., Georgakilas, A.G., Panayiotidis, M.I., 2008. Oxidative stress, DNA methylation and carcinogenesis. *Cancer Lett., Oxidative Stress and Carcinogenesis Special Issue* 266, 6–11. <https://doi.org/10.1016/j.canlet.2008.02.026>
- Fredriksson, L., Wink, S., Herpers, B., Benedetti, G., Hadi, M., de Bont, H., Groothuis, G., Luijten, M., Danen, E., de Graauw, M., Meerman, J., van de Water, B., 2014. Drug-induced endoplasmic reticulum and oxidative stress responses independently sensitize toward TNF $\alpha$ -mediated hepatotoxicity. *Toxicol. Sci. Off. J. Soc. Toxicol.* 140, 144–159. <https://doi.org/10.1093/toxsci/kfu072>
- Fried, M., Crothers, D.M., 1981. Equilibria and kinetics of lac repressor-operator interactions by polyacrylamide gel electrophoresis. *Nucleic Acids Res.* 9, 6505–6525.
- Fuse, Y., Nakajima, H., Nakajima-Takagi, Y., Nakajima, O., Kobayashi, M., 2015. Heme-mediated inhibition of Bach1 regulates the liver specificity and transience of the Nrf2-dependent induction of zebrafish heme oxygenase 1. *Genes Cells* 20, 590–600. <https://doi.org/10.1111/gtc.12249>
- Gacesa, R., Dunlap, W.C., Barlow, D.J., Laskowski, R.A., Long, P.F., 2016. Rising levels of atmospheric oxygen and evolution of Nrf2. *Sci. Rep.* 6, 27740. <https://doi.org/10.1038/srep27740>
- Gamboa, J.L., Billings, F.T., Bojanowski, M.T., Gilliam, L.A., Yu, C., Roshanravan, B., Roberts, L.J., Himmelfarb, J., Ikizler, T.A., Brown, N.J., 2016. Mitochondrial dysfunction and oxidative stress in patients with chronic kidney disease. *Physiol. Rep.* 4. <https://doi.org/10.14814/phy2.12780>
- Gao, A., Peng, Y., Deng, Y., Qing, H., 2013. Potential therapeutic applications of differentiated induced pluripotent stem cells (iPSCs) in the treatment of neurodegenerative diseases. *Neuroscience* 228, 47–59. <https://doi.org/10.1016/j.neuroscience.2012.09.076>
- Gao, B., Doan, A., Hybertson, B.M., 2014. The clinical potential of influencing Nrf2 signaling in degenerative and immunological disorders. *Clin. Pharmacol. Adv. Appl.* 6, 19–34. <https://doi.org/10.2147/CPAA.S35078>
- García, V., García, J.M., Peña, C., Silva, J., Domínguez, G., Lorenzo, Y., Díaz, R., Espinosa, P., de Sola, J.G., Cantos, B., Bonilla, F., 2008. Free circulating mRNA in plasma from breast cancer patients and clinical outcome. *Cancer Lett.* 263, 312–320. <https://doi.org/10.1016/j.canlet.2008.01.008>
- García-González, A., Gaxiola-Robles, R., Zenteno-Savín, T., 2015. Oxidative stress in patients with rheumatoid arthritis. *Rev. Investig. Clin. Organo Hosp. Enfermedades Nutr.* 67, 46–53.
- Garner, M.M., Revzin, A., 1981. A gel electrophoresis method for quantifying the binding of proteins to specific DNA regions: application to components of the Escherichia coli lactose operon regulatory system. *Nucleic Acids Res.* 9, 3047–3060.
- Giacco, F., Brownlee, M., 2010. Oxidative stress and diabetic complications. *Circ. Res.* 107, 1058–1070. <https://doi.org/10.1161/CIRCRESAHA.110.223545>
- Gold, R., Kappos, L., Arnold, D.L., Bar-Or, A., Giovannoni, G., Selmaj, K., Tornatore, C., Sweetser, M.T., Yang, M., Sheikh, S.I., Dawson, K.T., 2012. Placebo-Controlled Phase 3 Study of Oral BG-12 for Relapsing Multiple Sclerosis. *N. Engl. J. Med.* 367, 1098–1107. <https://doi.org/10.1056/NEJMoa1114287>
- Goldring, C.E.P., Kitteringham, N.R., Elsbey, R., Randle, L.E., Clement, Y.N., Williams, D.P., McMahon, M., Hayes, J.D., Itoh, K., Yamamoto, M., Park, B.K., 2004. Activation of hepatic Nrf2 in vivo by acetaminophen in CD-1 mice. *Hepatology* 39, 1267–1276. <https://doi.org/10.1002/hep.20183>
- Goldstein, L.D., Lee, J., Gnad, F., Klijn, C., Schaub, A., Reeder, J., Daemen, A., Bakalarski, C.E., Holcomb, T., Shames, D.S., Hartmaier, R.J., Chmielecki, J., Seshagiri, S., Gentleman, R., Stokoe, D., 2016. Recurrent Loss of NFE2L2 Exon 2 Is a Mechanism for Nrf2 Pathway Activation in Human Cancers. *Cell Rep.* 16, 2605–2617. <https://doi.org/10.1016/j.celrep.2016.08.010>

- Gómez-Lechón, M.J., Tolosa, L., Conde, I., Donato, M.T., 2014. Competency of different cell models to predict human hepatotoxic drugs. *Expert Opin. Drug Metab. Toxicol.* 10, 1553–1568. <https://doi.org/10.1517/17425255.2014.967680>
- Gonzales-Vitale, J.C., Hayes, D.M., Cvitkovic, E., Sternberg, S.S., 1977. The renal pathology in clinical trials of cis-platinum (II) diamminedichloride. *Cancer* 39, 1362–1371.
- Gopal, S., Mikulskis, A., Gold, R., Fox, R.J., Dawson, K.T., Amaravadi, L., 2017. Evidence of activation of the Nrf2 pathway in multiple sclerosis patients treated with delayed-release dimethyl fumarate in the Phase 3 DEFINE and CONFIRM studies. *Mult. Scler. J.* 23, 1875–1883. <https://doi.org/10.1177/1352458517690617>
- Gossen, M., Freundlieb, S., Bender, G., Müller, G., Hillen, W., Bujard, H., 1995. Transcriptional activation by tetracyclines in mammalian cells. *Science* 268, 1766–1769.
- Gray, J.P., Karandrea, S., Burgos, D.Z., Jaiswal, A.A., Heart, E.A., 2016. NAD(P)H-dependent Quinone Oxidoreductase 1 (NQO1) and Cytochrome P450 Oxidoreductase (CYP450OR) differentially regulate menadione-mediated alterations in redox status, survival and metabolism in pancreatic  $\beta$ -cells. *Toxicol. Lett.* 262, 1–11. <https://doi.org/10.1016/j.toxlet.2016.08.021>
- Greaney, A.J., Maier, N.K., Leppla, S.H., Moayeri, M., 2016. Sulforaphane inhibits multiple inflammasomes through an Nrf2-independent mechanism. *J. Leukoc. Biol.* 99, 189–199. <https://doi.org/10.1189/jlb.3A0415-155RR>
- Greenlee, H., Kwan, M.L., Kushi, L.H., Song, J., Castillo, A., Weltzien, E., Quesenberry, C.P., Caan, B.J., 2012. Antioxidant supplement use after breast cancer diagnosis and mortality in the Life After Cancer Epidemiology (LACE) cohort. *Cancer* 118, 2048–2058. <https://doi.org/10.1002/cncr.26526>
- Griendling, K.K., FitzGerald, G.A., 2003. Oxidative Stress and Cardiovascular Injury Part I: Basic Mechanisms and In Vivo Monitoring of ROS. *Circulation* 108, 1912–1916. <https://doi.org/10.1161/01.CIR.0000093660.86242.BB>
- Groen, J.N., Capraro, D., Morris, K.V., 2014. The emerging role of pseudogene expressed non-coding RNAs in cellular functions. *Int. J. Biochem. Cell Biol.* 54, 350–355. <https://doi.org/10.1016/j.biocel.2014.05.008>
- Hagemann, T.L., Gaeta, S.A., Smith, M.A., Johnson, D.A., Johnson, J.A., Messing, A., 2005. Gene expression analysis in mice with elevated glial fibrillary acidic protein and Rosenthal fibers reveals a stress response followed by glial activation and neuronal dysfunction. *Hum. Mol. Genet.* 14, 2443–2458. <https://doi.org/10.1093/hmg/ddi248>
- Haider, L., Fischer, M.T., Frischer, J.M., Bauer, J., Höftberger, R., Botond, G., Esterbauer, H., Binder, C.J., Witztum, J.L., Lassmann, H., 2011. Oxidative damage in multiple sclerosis lesions. *Brain* 134, 1914–1924. <https://doi.org/10.1093/brain/awr128>
- Hakim, T.S., Sugimori, K., Camporesi, E.M., Anderson, G., 1996. Half-life of nitric oxide in aqueous solutions with and without haemoglobin. *Physiol. Meas.* 17, 267–277.
- Halicka, H.D., Bedner, E., Darzynkiewicz, Z., 2000. Segregation of RNA and Separate Packaging of DNA and RNA in Apoptotic Bodies during Apoptosis. *Exp. Cell Res.* 260, 248–256. <https://doi.org/10.1006/excr.2000.5027>
- Halliwell, B., 2007. Oxidative stress and cancer: have we moved forward? *Biochem. J.* 401, 1–11. <https://doi.org/10.1042/BJ20061131>
- Halliwell, B., 2007. Biochemistry of oxidative stress. *Biochem. Soc. Trans.* 35, 1147–1150. <https://doi.org/10.1042/BST0351147>
- Hancock, R., Bertrand, H.C., Tsujita, T., Naz, S., El-Bakry, A., Laoruchupong, J., Hayes, J.D., Wells, G., 2012. Peptide inhibitors of the Keap1–Nrf2 protein–protein interaction. *Free Radic. Biol. Med.* 52, 444–451. <https://doi.org/10.1016/j.freeradbiomed.2011.10.486>
- Handa, O., Naito, Y., Yoshikawa, T., 2011. Redox biology and gastric carcinogenesis: the role of Helicobacter pylori. *Redox Rep. Commun. Free Radic. Res.* 16, 1–7. <https://doi.org/10.1179/174329211X12968219310756>
- Harman, D., 1956. Aging: A Theory Based on Free Radical and Radiation Chemistry. *J. Gerontol.* 11, 298–300. <https://doi.org/10.1093/geronj/11.3.298>
- Hart, S.N., Li, Y., Nakamoto, K., Subileau, E., Steen, D., Zhong, X., 2010. A Comparison of Whole Genome Gene Expression Profiles of HepaRG Cells and HepG2 Cells to Primary Human Hepatocytes and Human Liver Tissues. *Drug Metab. Dispos.* 38, 988–994. <https://doi.org/10.1124/dmd.109.031831>
- Hasselbalch, H.C., Thomassen, M., Riley, C.H., Kjær, L., Larsen, T.S., Jensen, M.K., Bjerrum, O.W., Kruse, T.A., Skov, V., 2014. Whole Blood Transcriptional Profiling Reveals Dereglulation of Oxidative and Antioxidative Defence Genes in Myelofibrosis and Related Neoplasms. Potential Implications of Downregulation of Nrf2 for Genomic Instability and Disease Progression. *PLOS ONE* 9, e112786. <https://doi.org/10.1371/journal.pone.0112786>
- Hatakeyama, S., 2011. TRIM proteins and cancer. *Nat. Rev. Cancer* 11, 792. <https://doi.org/10.1038/nrc3139>
- Hayakawa, M., Miyashita, H., Sakamoto, I., Kitagawa, M., Tanaka, H., Yasuda, H., Karin, M., Kikugawa, K., 2003. Evidence that reactive oxygen species do not mediate NF- $\kappa$ B activation. *EMBO J.* 22, 3356–3366. <https://doi.org/10.1093/emboj/cdg332>
- Hayes, J.D., Dinkova-Kostova, A.T., 2014. The Nrf2 regulatory network provides an interface between redox and intermediary metabolism. *Trends Biochem. Sci.* 39, 199–218. <https://doi.org/10.1016/j.tibs.2014.02.002>
- Heiss, E., Herhaus, C., Klimo, K., Bartsch, H., Gerhäuser, C., 2001. Nuclear factor kappa B is a molecular target for sulforaphane-mediated anti-inflammatory mechanisms. *J. Biol. Chem.* 276, 32008–32015. <https://doi.org/10.1074/jbc.M104794200>
- Held, K.D., Epp, E.R., Clark, E.P., Biaglow, J.E., 1988. Effect of Dimethyl Fumarate on the Radiation Sensitivity of Mammalian Cells in Vitro. *Radiat. Res.* 115, 495–502. <https://doi.org/10.2307/3577299>
- Hendriks, G., Atallah, M., Morolli, B., Calléja, F., Ras-Verloop, N., Huijskens, I., Raamsman, M., Water, B. van de, Vrieling, H., 2012. The ToxTracker Assay: Novel GFP Reporter Systems that Provide Mechanistic Insight into the Genotoxic Properties of Chemicals. *Toxicol. Sci.* 125, 285–298. <https://doi.org/10.1093/toxsci/kfr281>
- Herpers, B., Wink, S., Fredriksson, L., Di, Z., Hendriks, G., Vrieling, H., de Bont, H., van de Water, B., 2016. Activation of the Nrf2 response by intrinsic hepatotoxic drugs correlates with suppression of NF- $\kappa$ B activation and sensitizes toward TNF $\alpha$ -induced cytotoxicity. *Arch. Toxicol.* 90, 1163–1179. <https://doi.org/10.1007/s00204-015-1536-3>

- Hiemstra, S., Niemeijer, M., Koedoot, E., Wink, S., Klip, J.E., Vlasveld, M., de Zeeuw, E., van Os, B., White, A., Water, B. van de, 2017. Comprehensive Landscape of Nrf2 and p53 Pathway Activation Dynamics by Oxidative Stress and DNA Damage. *Chem. Res. Toxicol.* 30, 923–933. <https://doi.org/10.1021/acs.chemrestox.6b00322>
- Hinoi, E., Fujimori, S., Wang, L., Hojo, H., Uno, K., Yoneda, Y., 2006. Nrf2 Negatively Regulates Osteoblast Differentiation via Interfering with Runx2-dependent Transcriptional Activation. *J. Biol. Chem.* 281, 18015–18024. <https://doi.org/10.1074/jbc.M600603200>
- Hinson, J.A., Roberts, D.W., James, L.P., 2010. Mechanisms of Acetaminophen-Induced Liver Necrosis. *Handb. Exp. Pharmacol.* 369–405. [https://doi.org/10.1007/978-3-642-00663-0\\_12](https://doi.org/10.1007/978-3-642-00663-0_12)
- Hintze, K.J., Theil, E.C., 2005. DNA and mRNA elements with complementary responses to hemin, antioxidant inducers, and iron control ferritin-L expression. *Proc. Natl. Acad. Sci. U. S. A.* 102, 15048–15052. <https://doi.org/10.1073/pnas.0505148102>
- Hintze, K.J., Wald, K.A., Zeng, H., Jeffery, E.H., Finley, J.W., 2003. Thioredoxin Reductase in Human Hepatoma Cells Is Transcriptionally Regulated by Sulforaphane and Other Electrophiles via an Antioxidant Response Element-. *J. Nutr.* 133, 2721–2727.
- Hirota, M., Ashikaga, T., Kouzuki, H., 2018. Development of an artificial neural network model for risk assessment of skin sensitization using human cell line activation test, direct peptide reactivity assay, KeratinoSens™ and in silico structure alert parameter. *J. Appl. Toxicol.* 38, 514–526. <https://doi.org/10.1002/jat.3558>
- Hirotsu, Y., Katsuoka, F., Funayama, R., Nagashima, T., Nishida, Y., Nakayama, K., Douglas Engel, J., Yamamoto, M., 2012. Nrf2–MafG heterodimers contribute globally to antioxidant and metabolic networks. *Nucleic Acids Res.* 40, 10228–10239. <https://doi.org/10.1093/nar/gks827>
- Hirotsu, Y., Katsuoka, F., Itoh, K., Yamamoto, M., 2011. Nrf2 degron-fused reporter system: a new tool for specific evaluation of Nrf2 inducers. *Genes Cells Devoted Mol. Cell. Mech.* 16, 406–415. <https://doi.org/10.1111/j.1365-2443.2011.01496.x>
- Hirvonen, T., Pietinen, P., Virtanen, M., Ovaskainen, M.-L., Häkkinen, S., Albanes, D., Virtamo, J., 2001. Intake of Flavonols and Flavones and Risk of Coronary Heart Disease in Male Smokers. *Epidemiology* 12, 62–67.
- Hoeflich, K.P., Luo, J., Rubie, E.A., Tsao, M.S., Jin, O., Woodgett, J.R., 2000. Requirement for glycogen synthase kinase-3beta in cell survival and NF-kappaB activation. *Nature* 406, 86–90. <https://doi.org/10.1038/35017574>
- Höing, S., Rudhard, Y., Reinhardt, P., Glatza, M., Stehling, M., Wu, G., Peiker, C., Böcker, A., Parga, J.A., Bunk, E., Schwamborn, J.C., Slack, M., Sternecker, J., Schöler, H.R., 2012. Discovery of Inhibitors of Microglial Neurotoxicity Acting Through Multiple Mechanisms Using a Stem-Cell-Based Phenotypic Assay. *Cell Stem Cell* 11, 620–632. <https://doi.org/10.1016/j.stem.2012.07.005>
- Homma, S., Ishii, Y., Morishima, Y., Yamadori, T., Matsuno, Y., Haraguchi, N., Kikuchi, N., Satoh, H., Sakamoto, T., Hizawa, N., Itoh, K., Yamamoto, M., 2009. Nrf2 Enhances Cell Proliferation and Resistance to Anticancer Drugs in Human Lung Cancer. *Am. Assoc. Cancer Res.* 15, 3423–3432. <https://doi.org/10.1158/1078-0432.CCR-08-2822>
- Hong, D.S., Kurzrock, R., Supko, J.G., He, X., Naing, A., Wheler, J., Lawrence, D., Eder, J.P., Meyer, C.J., Ferguson, D.A., Mier, J., Konopleva, M., Konoplev, S., Andreeff, M., Kufe, D., Lazarus, H., Shapiro, G.I., Dezube, B.J., 2012. A phase I first-in-human trial of bardoxolone methyl in patients with advanced solid tumors and lymphomas. *Clin. Cancer Res. Off. J. Am. Assoc. Cancer Res.* 18, 3396–3406. <https://doi.org/10.1158/1078-0432.CCR-11-2703>
- Hsiao, Y.-W., Petersson, C., Svensson, M.A., Norinder, U., 2012. A Pragmatic Approach Using First-Principle Methods to Address Site of Metabolism with Implications for Reactive Metabolite Formation. *J. Chem. Inf. Model.* 52, 686–695. <https://doi.org/10.1021/ci200523f>
- Hu, C., Eggler, A.L., Mesecar, A.D., van Breemen, R.B., 2011. Modification of Keap1 Cysteine Residues by Sulforaphane. *Chem. Res. Toxicol.* 24, 515–521. <https://doi.org/10.1021/tx100389r>
- Hu, S., Leblanc, A., Gibson, A., Hong, K., Kim, J., Janke, L., Li, L., Vasilyeva, A., Finkelstein, D., Sprowl, J., Sweet, D., Schlatter, E., Ciarimboli, G., Schellens, J., Baker, S., Pabla, N., Sparreboom, A., 2017. Identification of OAT1/OAT3 as Contributors to Cisplatin Toxicity. *Clin. Transl. Sci.* n/a-n/a. <https://doi.org/10.1111/cts.12480>
- Huang, J., Shi, W., Zhang, J., Chou, J.W., Paules, R.S., Gerrish, K., Li, J., Luo, J., Wolfinger, R.D., Bao, W., Chu, T.-M., Nikolsky, Y., Nikolskaya, T., Dosymbekov, D., Tsyganova, M.O., Shi, L., Fan, X., Corton, J.C., Chen, M., Cheng, Y., Tong, W., Fang, H., Bushel, P.R., 2010. Genomic indicators in the blood predict drug-induced liver injury. *Pharmacogenomics J.* 10, 267–277. <https://doi.org/10.1038/tpj.2010.33>
- Huang, J., Tabbi-Anneni, I., Gunda, V., Wang, L., 2010. Transcription factor Nrf2 regulates SHP and lipogenic gene expression in hepatic lipid metabolism. *Am. J. Physiol. Gastrointest. Liver Physiol.* 299, G1211–1221. <https://doi.org/10.1152/ajpgi.00322.2010>
- Huang, R., Xia, M., Sakamuru, S., Zhao, J., Shahane, S.A., Attene-Ramos, M., Zhao, T., Austin, C.P., Simeonov, A., 2016. Modelling the Tox21 10 K chemical profiles for in vivo toxicity prediction and mechanism characterization. *Nat. Commun.* 7, 10425. <https://doi.org/10.1038/ncomms10425>
- Huh, S., Lee, J., Jung, E., Kim, S.-C., Kang, J.-I., Lee, J., Kim, Y.-W., Sung, Y.K., Kang, H.-K., Park, D., 2009. A cell-based system for screening hair growth-promoting agents. *Arch. Dermatol. Res.* 301, 381. <https://doi.org/10.1007/s00403-009-0931-0>
- Igarashi, Y., Nakatsu, N., Yamashita, T., Ono, A., Ohno, Y., Urushidani, T., Yamada, H., 2014. Open TG-GATEs: a large-scale toxicogenomics database. *Nucleic Acids Res.* gku955. <https://doi.org/10.1093/nar/gku955>
- Imai, T., Iwawaki, T., Akai, R., Suzue, K., Hirai, M., Taniguchi, T., Okada, H., Hisaeda, H., 2014. Evaluating experimental cerebral malaria using oxidative stress indicator OKD48 mice. *Int. J. Parasitol.* 44, 681–685. <https://doi.org/10.1016/j.ijpara.2014.06.002>
- Imran, M., Lim, I.K., 2013. Regulation of Btg2/TIS21/PC3 expression via reactive oxygen species–protein kinase C–NFkB pathway under stress conditions. *Cell. Signal.* 25, 2400–2412. <https://doi.org/10.1016/j.cellsig.2013.07.015>
- Ishihara, H., Connolly, A.J., Zeng, D., Kahn, M.L., Wu Zheng, Y., Timmons, C., Tram, T., Coughlin, S.R., 1997. Protease-activated receptor 3 is a second thrombin receptor in humans. *Nature* 386, 502–506. <https://doi.org/10.1038/386502a0>

- Ishikawa, K., Takenaga, K., Akimoto, M., Koshikawa, N., Yamaguchi, A., Imanishi, H., Nakada, K., Honma, Y., Hayashi, J.-I., 2008. ROS-Generating Mitochondrial DNA Mutations Can Regulate Tumor Cell Metastasis. *Science* 320, 661–664. <https://doi.org/10.1126/science.1156906>
- Itoh, K., Chiba, T., Takahashi, S., Ishii, T., Igarashi, K., Katoh, Y., Oyake, T., Hayashi, N., Satoh, K., Hatayama, I., Yamamoto, M., Nabeshima, Y., 1997. An Nrf2/small Maf heterodimer mediates the induction of phase II detoxifying enzyme genes through antioxidant response elements. *Biochem. Biophys. Res. Commun.* 236, 313–322.
- Itoh, K., Igarashi, K., Hayashi, N., Nishizawa, M., Yamamoto, M., 1995. Cloning and characterization of a novel erythroid cell-derived CNC family transcription factor heterodimerizing with the small Maf family proteins. *Mol. Cell. Biol.* 15, 4184–4193.
- Itoh, K., Wakabayashi, N., Katoh, Y., Ishii, T., Igarashi, K., Engel, J.D., Yamamoto, M., 1999. Keap1 represses nuclear activation of antioxidant responsive elements by Nrf2 through binding to the amino-terminal Neh2 domain. *Genes Dev.* 13, 76–86.
- Jacq, C., Miller, J.R., Brownlee, G.G., 1977. A pseudogene structure in 5S DNA of *Xenopus laevis*. *Cell* 12, 109–120.
- Jaeschke, H., Bajt, M.L., 2010. 9.21 - Mechanisms of Acetaminophen Hepatotoxicity, in: McQueen, C.A. (Ed.), *Comprehensive Toxicology* (Second Edition). Elsevier, Oxford, pp. 457–473. <https://doi.org/10.1016/B978-0-08-046884-6.01019-8>
- Janzen, E.G., Kotake, Y., Randall D., H., 1992. Stabilities of hydroxyl radical spin adducts of PBN-type spin traps. *Free Radic. Biol. Med.* 12, 169–173. [https://doi.org/10.1016/0891-5849\(92\)90011-5](https://doi.org/10.1016/0891-5849(92)90011-5)
- Jaworska, J.S., Natsch, A., Ryan, C., Strickland, J., Ashikaga, T., Miyazawa, M., 2015. Bayesian integrated testing strategy (ITS) for skin sensitization potency assessment: a decision support system for quantitative weight of evidence and adaptive testing strategy. *Arch. Toxicol.* 89, 2355–2383. <https://doi.org/10.1007/s00204-015-1634-2>
- Jennings, P., Limonciel, A., Felice, L., Leonard, M.O., 2013. An overview of transcriptional regulation in response to toxicological insult. *Arch. Toxicol.* 87, 49–72. <https://doi.org/10.1007/s00204-012-0919-y>
- Jia, X., McNeill, G., Avenell, A., 2008. Does taking vitamin, mineral and fatty acid supplements prevent cognitive decline? A systematic review of randomized controlled trials. *J. Hum. Nutr. Diet. Off. J. Br. Diet. Assoc.* 21, 317–336. <https://doi.org/10.1111/j.1365-277X.2008.00887.x>
- Jiang, Z.-Y., Lu, M.-C., Xu, L., Yang, T.-T., Xi, M.-Y., Xu, X.-L., Guo, X.-K., Zhang, X.-J., You, Q.-D., Sun, H.-P., 2014. Discovery of Potent Keap1–Nrf2 Protein–Protein Interaction Inhibitor Based on Molecular Binding Determinants Analysis. *J. Med. Chem.* 57, 2736–2745. <https://doi.org/10.1021/jm5000529>
- Johnson, D.A., Andrews, G.K., Xu, W., Johnson, J.A., 2002. Activation of the antioxidant response element in primary cortical neuronal cultures derived from transgenic reporter mice. *J. Neurochem.* 81, 1233–1241.
- Johnson, G., Beaver, L., Williams, D.E., Ho, E., Dashwood, R.H., 2015. Abstract B33: Regulation and function of Nrf2-associated long noncoding RNA. *Cancer Prev. Res. (Phila. Pa.)* 8, B33–B33. <https://doi.org/10.1158/1940-6215.PREV-14-B33>
- Johnson, G.S., Li, J., Beaver, L.M., Dashwood, W.M., Sun, D., Rajendran, P., Williams, D.E., Ho, E., Dashwood, R.H., 2016. A functional pseudogene, NMRAL2P, is regulated by Nrf2 and serves as a co-activator of NQO1 in sulforaphane-treated colon cancer cells. *Mol. Nutr. Food Res.* n/a-n/a. <https://doi.org/10.1002/mnfr.201600769>
- Jung, D., Biggs, H., Erikson, J., Ledyard, P.U., 1975. New Colorimetric Reaction for End-Point, Continuous-Flow, and Kinetic Measurement of Urea. *Clin. Chem.* 21, 1136–1140.
- Jung, K.-A., Choi, B., Nam, C.-W., Song, M., Kim, S.-T., Lee, J.Y., Kwak, M.-K., 2013. Identification of aldo-keto reductases as NRF2-target marker genes in human cells. *Toxicol. Lett.* 218, 39–49. <https://doi.org/10.1016/j.toxlet.2012.12.026>
- Kagan, V.E., Tyurin, V.A., Jiang, J., Tyurina, Y.Y., Ritov, V.B., Amoscato, A.A., Osipov, A.N., Belikova, N.A., Kapralov, A.A., Kini, V., Vlasova, I.I., Zhao, Q., Zou, M., Di, P., Svistunenko, D.A., Kurnikov, I.V., Borisenko, G.G., 2005. Cytochrome c acts as a cardiolipin oxygenase required for release of proapoptotic factors. *Nat. Chem. Biol.* 1, 223–232. <https://doi.org/10.1038/nchembio727>
- Kahn, M.L., Hammes, S.R., Botka, C., Coughlin, S.R., 1998. Gene and Locus Structure and Chromosomal Localization of the Protease-activated Receptor Gene Family. *J. Biol. Chem.* 273, 23290–23296. <https://doi.org/10.1074/jbc.273.36.23290>
- Kallifatidis, G., Rausch, V., Baumann, B., Apel, A., Beckermann, B.M., Groth, A., Mattern, J., Li, Z., Kolb, A., Moldenhauer, G., Altevogt, P., Wirth, T., Werner, J., Schemmer, P., Büchler, M.W., Salnikov, A.V., Herr, I., 2009. Sulforaphane targets pancreatic tumour-initiating cells by NF-kappaB-induced antiapoptotic signalling. *Gut* 58, 949–963. <https://doi.org/10.1136/gut.2008.149039>
- Kang, M.-I., Kobayashi, A., Wakabayashi, N., Kim, S.-G., Yamamoto, M., 2004. Scaffolding of Keap1 to the actin cytoskeleton controls the function of Nrf2 as key regulator of cytoprotective phase 2 genes. *Proc. Natl. Acad. Sci. U. S. A.* 101, 2046–2051. <https://doi.org/10.1073/pnas.0308347100>
- Kaspar, J.W., Jaiswal, A.K., 2010. An Autoregulatory Loop between Nrf2 and Cul3-Rbx1 Controls Their Cellular Abundance. *J. Biol. Chem.* 285, 21349–21358. <https://doi.org/10.1074/jbc.M110.121863>
- Kataoka, K., Ekuni, D., Tomofuji, T., Irie, K., Kunitomo, M., Uchida, Y., Fukuhara, D., Morita, M., 2016. Visualization of Oxidative Stress Induced by Experimental Periodontitis in Keap1-Dependent Oxidative Stress Detector-Luciferase Mice. *Int. J. Mol. Sci.* 17. <https://doi.org/10.3390/ijms17111907>
- Katoh, Y., Iida, K., Kang, M.-I., Kobayashi, A., Mizukami, M., Tong, K.I., McMahon, M., Hayes, J.D., Itoh, K., Yamamoto, M., 2005. Evolutionary conserved N-terminal domain of Nrf2 is essential for the Keap1-mediated degradation of the protein by proteasome. *Arch. Biochem. Biophys.* 433, 342–350. <https://doi.org/10.1016/j.abb.2004.10.012>
- Katoh, Y., Itoh, K., Yoshida, E., Miyagishi, M., Fukamizu, A., Yamamoto, M., 2001. Two domains of Nrf2 cooperatively bind CBP, a CREB binding protein, and synergistically activate transcription. *Genes Cells Devoted Mol. Cell. Mech.* 6, 857–868.
- Katsuoka, F., Motohashi, H., Engel, J.D., Yamamoto, M., 2005. Nrf2 Transcriptionally Activates the mafG Gene through an Antioxidant Response Element. *J. Biol. Chem.* 280, 4483–4490. <https://doi.org/10.1074/jbc.M411451200>
- Kaur, P., Kalia, S., Bansal, M.P., 2006. Effect of Diethyl Maleate Induced Oxidative Stress on Male Reproductive Activity in Mice: Redox Active Enzymes and Transcription Factors Expression. *Mol. Cell. Biochem.* 291, 55–61. <https://doi.org/10.1007/s11010-006-9195-6>

- Kelley, M.J., Glaser, E.M., Herndon, J.E., Becker, F., Bhagat, R., Zhang, Y.-J., Santella, R.M., Carmella, S.G., Hecht, S.S., Gallot, L., Schilder, L., Crowell, J.A., Perloff, M., Folz, R.J., Bergan, R.C., 2005. Safety and Efficacy of Weekly Oral Oltipraz in Chronic Smokers. *Cancer Epidemiol. Biomarkers Prev.* 14, 892–899. <https://doi.org/10.1158/1055-9965.EPI-04-0585>
- Keum, Y.-S., Yu, S., Chang, P.P.-J., Yuan, X., Kim, J.-H., Xu, C., Han, J., Agarwal, A., Kong, A.-N.T., 2006. Mechanism of action of sulforaphane: inhibition of p38 mitogen-activated protein kinase isoforms contributing to the induction of antioxidant response element-mediated haem oxygenase-1 in human hepatoma HepG2 cells. *Cancer Res.* 66, 8804–8813. <https://doi.org/10.1158/0008-5472.CAN-05-3513>
- Khoo, N.K.H., Li, L., Salvatore, S.R., Schopfer, F.J., Freeman, B.A., 2018. Electrophilic fatty acid nitroalkenes regulate Nrf2 and NF- $\kappa$ B signaling: A medicinal chemistry investigation of structure-function relationships. *Sci. Rep.* 8, 2295. <https://doi.org/10.1038/s41598-018-20460-8>
- Kim, J.Y., Kim, D.Y., Son, H., Kim, Y.J., Oh, S.H., 2014. Protease-activated receptor-2 activates NQO-1 via Nrf2 stabilization in keratinocytes. *J. Dermatol. Sci.* 74, 48–55. <https://doi.org/10.1016/j.jdermsci.2013.11.010>
- Kim, K.-H., Jeong, J.-Y., Surh, Y.-J., Kim, K.-W., 2010. Expression of stress-response ATF3 is mediated by Nrf2 in astrocytes. *Nucleic Acids Res.* 38, 48–59. <https://doi.org/10.1093/nar/gkp865>
- Kim, M.T., Huang, R., Sedykh, A., Wang, W., Xia, M., Zhu, H., 2016. Mechanism Profiling of Hepatotoxicity Caused by Oxidative Stress Using Antioxidant Response Element Reporter Gene Assay Models and Big Data. *Environ. Health Perspect.* 124, 634–641. <https://doi.org/10.1289/ehp.1509763>
- Kim, T.H., Eom, J.S., Lee, C.G., Yang, Y.M., Lee, Y.S., Kim, S.G., 2013. An active metabolite of oltipraz (M2) increases mitochondrial fuel oxidation and inhibits lipogenesis in the liver by dually activating AMPK. *Br. J. Pharmacol.* 168, 1647–1661. <https://doi.org/10.1111/bph.12057>
- Kim, Y.-C., Yamaguchi, Y., Kondo, N., Masutani, H., Yodoi, J., 2003. Thioredoxin-dependent redox regulation of the antioxidant responsive element (ARE) in electrophile response. *Oncogene* 22, 1860–1865. <https://doi.org/10.1038/sj.onc.1206369>
- Kim, Y.-J., Ahn, J.-Y., Liang, P., Ip, C., Zhang, Y., Park, Y.-M., 2007. Human prx1 gene is a target of Nrf2 and is up-regulated by hypoxia/reoxygenation: implication to tumor biology. *Cancer Res.* 67, 546–554. <https://doi.org/10.1158/0008-5472.CAN-06-2401>
- Kipp, A.P., Deubel, S., Arnér, E.S.J., Johansson, K., 2017. Time- and cell-resolved dynamics of redox-sensitive Nrf2, HIF and NF- $\kappa$ B activities in 3D spheroids enriched for cancer stem cells. *Redox Biol.* 12, 403–409. <https://doi.org/10.1016/j.redox.2017.03.013>
- Knudsen, T.B., Houck, K.A., Sipes, N.S., Singh, A.V., Judson, R.S., Martin, M.T., Weissman, A., Kleinstreuer, N.C., Mortensen, H.M., Reif, D.M., Rabinowitz, J.R., Setzer, R.W., Richard, A.M., Dix, D.J., Kavlock, R.J., 2011. Activity profiles of 309 ToxCast™ chemicals evaluated across 292 biochemical targets. *Toxicology* 282, 1–15. <https://doi.org/10.1016/j.tox.2010.12.010>
- Kobayashi, M., Li, L., Iwamoto, N., Nakajima-Takagi, Y., Kaneko, H., Nakayama, Y., Eguchi, M., Wada, Y., Kumagai, Y., Yamamoto, M., 2009. The Antioxidant Defense System Keap1-Nrf2 Comprises a Multiple Sensing Mechanism for Responding to a Wide Range of Chemical Compounds. *Mol. Cell. Biol.* 29, 493–502. <https://doi.org/10.1128/MCB.01080-08>
- Kola, I., Landis, J., 2004. Can the pharmaceutical industry reduce attrition rates? *Nat. Rev. Drug Discov.* 3, 711–716. <https://doi.org/10.1038/nrd1470>
- Komatsu, M., Kurokawa, H., Waguri, S., Taguchi, K., Kobayashi, A., Ichimura, Y., Sou, Y.-S., Ueno, I., Sakamoto, A., Tong, K.I., Kim, M., Nishito, Y., Iemura, S., Natsume, T., Ueno, T., Kominami, E., Motohashi, H., Tanaka, K., Yamamoto, M., 2010. The selective autophagy substrate p62 activates the stress responsive transcription factor Nrf2 through inactivation of Keap1. *Nat. Cell Biol.* 12, 213–223. <https://doi.org/10.1038/ncb2021>
- Kon, K., Kim, J.-S., Jaeschke, H., Lemasters, J.J., 2004. Mitochondrial permeability transition in acetaminophen-induced necrosis and apoptosis of cultured mouse hepatocytes. *Hepatology* 40, 1170–1179. <https://doi.org/10.1002/hep.20437>
- Kondo, N., Netsu, T., Arai, K., Kanai, T., Sano, H., Kijima, Y., Okumura, G., Fujisawa, J., Endo, N., 2017. Nuclear factor-erythroid 2-related 2 mRNA and protein are highly expressed in the synovium of patients with rheumatoid arthritis. *Internat J. Rheumatol. Clin. Immunol.* 5. <https://doi.org/10.15305/ijrci/v5i1/231>
- Konstantinopoulos, P.A., Spentzos, D., Fountzilas, E., Francoeur, N., Sanisetty, S., Grammatikos, A.P., Hecht, J.L., Cannistra, S.A., 2011. Keap1 Mutations and Nrf2 Pathway Activation in Epithelial Ovarian Cancer. *Cancer Res.* 71, 5081–5089. <https://doi.org/10.1158/0008-5472.CAN-10-4668>
- Kraft, A.D., Lee, J.-M., Johnson, D.A., Kan, Y.W., Johnson, J.A., 2006. Neuronal sensitivity to kainic acid is dependent on the Nrf2-mediated actions of the antioxidant response element. *J. Neurochem.* 98, 1852–1865. <https://doi.org/10.1111/j.1471-4159.2006.04019.x>
- Kratschmar, D.V., Calabrese, D., Walsh, J., Lister, A., Birk, J., Appenzeller-Herzog, C., Moulin, P., Goldring, C.E., Odermatt, A., 2012. Suppression of the Nrf2-Dependent Antioxidant Response by Glucocorticoids and 11 $\beta$ -HSD1-Mediated Glucocorticoid Activation in Hepatic Cells. *PLoS ONE* 7, e36774. <https://doi.org/10.1371/journal.pone.0036774>
- Krauskopf, J., Caiment, F., Claessen, S.M., Johnson, K.J., Warner, R.L., Schomaker, S.J., Burt, D.A., Aubrecht, J., Kleinjans, J.C., 2015. Application of High-Throughput Sequencing to Circulating microRNAs Reveals Novel Biomarkers for Drug-Induced Liver Injury. *Toxicol. Sci.* 143, 268–276. <https://doi.org/10.1093/toxsci/kfu232>
- Krishnamurthy, N., Hu, Y., Siedlak, S., Doughman, Y.Q., Watanabe, M., Montano, M.M., 2012. Induction of quinone reductase by tamoxifen or DPN protects against mammary tumorigenesis. *FASEB J. Off. Publ. Fed. Am. Soc. Exp. Biol.* 26, 3993–4002. <https://doi.org/10.1096/fj.12-208330>
- Kumar, B., Koul, S., Khandrika, L., Meacham, R.B., Koul, H.K., 2008. Oxidative Stress Is Inherent in Prostate Cancer Cells and Is Required for Aggressive Phenotype. *Cancer Res.* 68, 1777–1785. <https://doi.org/10.1158/0008-5472.CAN-07-5259>
- Kunsch, C., Medford, R.M., 1999. Oxidative stress as a regulator of gene expression in the vasculature. *Circ. Res.* 85, 753–766.
- Kuosmanen, S.M., Viitala, S., Laitinen, T., Peräkylä, M., Pölönen, P., Kansanen, E., Leinonen, H., Raju, S., Wienecke-Baldacchino, A., Närvänen, A., Poso, A., Heinänen, M., Heikkinen, S., Levonen, A.-L., 2016. The Effects of Sequence Variation on

- Genome-wide NRF2 Binding-New Target Genes and Regulatory SNPs. *Nucleic Acids Res.* 44, 1760–1775. <https://doi.org/10.1093/nar/gkw052>
- Kurian, G.A., Rajagopal, R., Vedantham, S., Rajesh, M., 2016. The Role of Oxidative Stress in Myocardial Ischemia and Reperfusion Injury and Remodeling: Revisited [WWW Document]. *Oxid. Med. Cell. Longev.* <https://doi.org/10.1155/2016/1656450>
- Kurz, E.U., Cole, S.P., Deeley, R.G., 2001. Identification of DNA-protein interactions in the 5' flanking and 5' untranslated regions of the human multidrug resistance protein (MRP1) gene: evaluation of a putative antioxidant response element/AP-1 binding site. *Biochem. Biophys. Res. Commun.* 285, 981–990. <https://doi.org/10.1006/bbrc.2001.5262>
- Kwak, M.-K., Itoh, K., Yamamoto, M., Kensler, T.W., 2002. Enhanced Expression of the Transcription Factor Nrf2 by Cancer Chemopreventive Agents: Role of Antioxidant Response Element-Like Sequences in the nrf2 Promoter. *Mol. Cell. Biol.* 22, 2883–2892. <https://doi.org/10.1128/MCB.22.9.2883-2892.2002>
- Lars Ernster, F.N., 1958. Soluble Diaphorase in Animal Tissues. *Acta Chem. Scand.* - ACTA CHEM SCAND 12, 595–595. <https://doi.org/10.3891/acta.chem.scand.12-0595>
- Lau, A., Tian, W., Whitman, S.A., Zhang, D.D., 2013. The Predicted Molecular Weight of Nrf2: It Is What It Is Not. *Antioxid. Redox Signal.* 18, 91–93. <https://doi.org/10.1089/ars.2012.4754>
- Lau, A., Wang, X.-J., Zhao, F., Villeneuve, N.F., Wu, T., Jiang, T., Sun, Z., White, E., Zhang, D.D., 2010. A noncanonical mechanism of Nrf2 activation by autophagy deficiency: direct interaction between Keap1 and p62. *Mol. Cell. Biol.* 30, 3275–3285. <https://doi.org/10.1128/MCB.00248-10>
- Lauderback, C.M., Hackett, J.M., Huang, F.F., Keller, J.N., Szveda, L.I., Markesbery, W.R., Butterfield, D.A., 2001. The glial glutamate transporter, GLT-1, is oxidatively modified by 4-hydroxy-2-nonenal in the Alzheimer's disease brain: the role of Abeta1-42. *J. Neurochem.* 78, 413–416.
- Lazarou, J., Pomeranz, B.H., Corey, P.N., 1998. Incidence of Adverse Drug Reactions in Hospitalized Patients: A Meta-analysis of Prospective Studies. *JAMA J. Am. Med. Assoc.* 279, 1200. <https://doi.org/10.1001/jama.279.15.1200>
- LeCluyse, E.L., Alexandre, E., Hamilton, G.A., Viollon-Abadie, C., Coon, D.J., Jolley, S., Richert, L., 2005. Isolation and culture of primary human hepatocytes. *Methods Mol. Biol. Clifton NJ* 290, 207–229.
- Lee, A.C., Murray, M., 2010. Up-regulation of human CYP2J2 in HepG2 cells by butylated hydroxyanisole is mediated by c-Jun and Nrf2. *Mol. Pharmacol.* 77, 987–994. <https://doi.org/10.1124/mol.109.062729>
- Lee, W., 2012. Acute Liver Failure. *Semin. Respir. Crit. Care Med.* 33, 36–45. <https://doi.org/10.1055/s-0032-1301733>
- Lehane, A.M., McDevitt, C.A., Kirk, K., Fidock, D.A., 2012. Degrees of chloroquine resistance in Plasmodium – Is the redox system involved? *Int. J. Parasitol. Drugs Drug Resist., Including Articles from Keystone Symposium on "Drug Discovery for Protozoan Parasites"*; pp. 230–270 2, 47–57. <https://doi.org/10.1016/j.ijpddr.2011.11.001>
- Leśniak, W., Szczepańska, A., Kuźnicki, J., 2005. Calcyclin (S100A6) expression is stimulated by agents evoking oxidative stress via the antioxidant response element. *Biochim. Biophys. Acta BBA - Mol. Cell Res.* 1744, 29–37. <https://doi.org/10.1016/j.bbamcr.2004.11.003>
- Levings, D., Wang, X., Kohlhase, D., Bell, D., Slattery, M., 2017. 139 - A Distinct Class of Antioxidant Response Elements is Consistently Activated in Tumors with Oncogenic NRF2 Mutations. *Free Radic. Biol. Med., SFRBM 2017 SFRBM's 24th Annual Meeting Program and Abstracts November 29 - December 2, 2017 Hilton Baltimore Baltimore, MD USA* 112, 101–102. <https://doi.org/10.1016/j.freeradbiomed.2017.10.152>
- Levonen, A.-L., Landar, A., Ramachandran, A., Ceaser, E.K., Dickinson, D.A., Zaroni, G., Morrow, J.D., Darley-Usmar, V.M., 2004. Cellular mechanisms of redox cell signalling: role of cysteine modification in controlling antioxidant defences in response to electrophilic lipid oxidation products. *Biochem. J.* 378, 373–382. <https://doi.org/10.1042/BJ20031049>
- Lewis, A., Park, C.S., Shen, Y., Lee, N.K., Lacorazza, H.D., 2017. Chemical Inhibition of the Macrophage Inhibitor Factor (MIF) Induces Cell Cycle Arrest and Apoptosis in Lymphoid and Myeloid Leukemia. *Blood* 130, 1329–1329.
- Li, W., Thakor, N., Xu, E.Y., Huang, Y., Chen, C., Yu, R., Holcik, M., Kong, A.-N., 2010. An internal ribosomal entry site mediates redox-sensitive translation of Nrf2. *Nucleic Acids Res.* 38, 778–788. <https://doi.org/10.1093/nar/gkp1048>
- Li, Y., Elashoff, D., Oh, M., Sinha, U., St John, M.A.R., Zhou, X., Abemayor, E., Wong, D.T., 2006. Serum Circulating Human mRNA Profiling and Its Utility for Oral Cancer Detection. *J. Clin. Oncol.* 24, 1754–1760. <https://doi.org/10.1200/JCO.2005.03.7598>
- Li, Y., Jaiswal, A.K., 1992. Regulation of human NAD(P)H:quinone oxidoreductase gene. Role of AP1 binding site contained within human antioxidant response element. *J. Biol. Chem.* 267, 15097–15104.
- Liby, K.T., Sporn, M.B., 2012. Synthetic oleanane triterpenoids: multifunctional drugs with a broad range of applications for prevention and treatment of chronic disease. *Pharmacol. Rev.* 64, 972–1003. <https://doi.org/10.1124/pr.111.004846>
- Liew, C.Y., Pan, C., Tan, A., Ang, K.X.M., Yap, C.W., 2012. QSAR classification of metabolic activation of chemicals into covalently reactive species. *Mol. Divers.* 16, 389–400. <https://doi.org/10.1007/s11030-012-9364-3>
- Limonciel, A., Mönks, K., Stanzel, S., Truisi, G.L., Parmentier, C., Aschauer, L., Wilmes, A., Richert, L., Hewitt, P., Mueller, S.O., Lukas, A., Kopp-Schneider, A., Leonard, M.O., Jennings, P., 2015. Transcriptomics hit the target: Monitoring of ligand-activated and stress response pathways for chemical testing. *Toxicol. Vitro Int. J. Publ. Assoc. BIBRA.* <https://doi.org/10.1016/j.tiv.2014.12.011>
- Lin, Q., Weis, S., Yang, G., Weng, Y.-H., Helston, R., Rish, K., Smith, A., Bordner, J., Polte, T., Gaunitz, F., Dennerly, P.A., 2007. Haem oxygenase-1 protein localizes to the nucleus and activates transcription factors important in oxidative stress. *J. Biol. Chem.* 282, 20621–20633. <https://doi.org/10.1074/jbc.M607954200>
- Linker, R.A., Lee, D.-H., Ryan, S., Dam, A.M. van, Conrad, R., Bista, P., Zeng, W., Hronowsky, X., Buko, A., Chollate, S., Ellrichmann, G., Brück, W., Dawson, K., Goelz, S., Wiese, S., Scannevin, R.H., Lukashev, M., Gold, R., 2011. Fumaric acid esters exert neuroprotective effects in neuroinflammation via activation of the Nrf2 antioxidant pathway. *Brain* 134, 678–692. <https://doi.org/10.1093/brain/awq386>
- Liu, J.-F., Hou, S.-M., Tsai, C.-H., Huang, C.-Y., Yang, W.-H., Tang, C.-H., 2012. Thrombin induces haem oxygenase-1 expression in human synovial fibroblasts through protease-activated receptor signaling pathways. *Arthritis Res. Ther.* 14, R91. <https://doi.org/10.1186/ar3815>

- Lo, J.Y., Spatola, B.N., Curran, S.P., 2017. WDR23 regulates NRF2 independently of KEAP1. *PLoS Genet.* 13, e1006762. <https://doi.org/10.1371/journal.pgen.1006762>
- Lobenhofer, E.K., Auman, J.T., Blackshear, P.E., Boorman, G.A., Bushel, P.R., Cunningham, M.L., Fostel, J.M., Gerrish, K., Heinloth, A.N., Irwin, R.D., Malarkey, D.E., Merrick, B.A., Sieber, S.O., Tucker, C.J., Ward, S.M., Wilson, R.E., Hurban, P., Tennant, R.W., Paules, R.S., 2008. Gene expression response in target organ and whole blood varies as a function of target organ injury phenotype. *Genome Biol.* 9, R100. <https://doi.org/10.1186/gb-2008-9-6-r100>
- Longbrake, E.E., Ramsbottom, M.J., Cantoni, C., Ghezzi, L., Cross, A.H., Piccio, L., 2016. Dimethyl fumarate selectively reduces memory T cells in multiple sclerosis patients. *Mult. Scler. J.* 22, 1061–1070. <https://doi.org/10.1177/1352458515608961>
- Lou, H., Du, S., Ji, Q., Stolz, A., 2006. Induction of AKR1C2 by Phase II Inducers: Identification of a Distal Consensus Antioxidant Response Element Regulated by NRF2. *Mol. Pharmacol.* 69, 1662–1672. <https://doi.org/10.1124/mol.105.019794>
- Lundbäck, P., Lea, J.D., Sowinska, A., Ottosson, L., Fürst, C.M., Steen, J., Aulin, C., Clarke, J.I., Kipar, A., Klevenvall, L., Yang, H., Palmblad, K., Park, B.K., Tracey, K.J., Blom, A.M., Andersson, U., Antoine, D.J., Erlandsson Harris, H., 2016. A novel high mobility group box 1 neutralizing chimeric antibody attenuates drug-induced liver injury and postinjury inflammation in mice. *Hepatology*. Md 64, 1699–1710. <https://doi.org/10.1002/hep.28736>
- Luo, M., Zhang, J., He, H., Su, D., Chen, Q., Gross, M.L., Kelley, M.R., Georgiadis, M.M., 2012. Characterization of the redox activity and disulfide bond formation in apurinic/aprimidinic endonuclease. *Biochemistry (Mosc.)* 51, 695–705. <https://doi.org/10.1021/bi201034z>
- MacLeod, A.K., McMahon, M., Plummer, S.M., Higgins, L.G., Penning, T.M., Igarashi, K., Hayes, J.D., 2009. Characterization of the cancer chemopreventive NRF2-dependent gene battery in human keratinocytes: demonstration that the KEAP1-NRF2 pathway, and not the BACH1-NRF2 pathway, controls cytoprotection against electrophiles as well as redox-cycling compounds. *Carcinogenesis* 30, 1571–1580. <https://doi.org/10.1093/carcin/bgp176>
- Malstrom, S.E., Jekic-McMullen, D., Sambucetti, L., Ang, A., Reeves, R., Purchio, A.F., Contag, P.R., West, D.B., 2004a. In vivo bioluminescent monitoring of chemical toxicity using haem oxygenase-luciferase transgenic mice. *Toxicol. Appl. Pharmacol.* 200, 219–228. <https://doi.org/10.1016/j.taap.2004.04.021>
- Malstrom, S.E., Jekic-McMullen, D., Sambucetti, L., Ang, A., Reeves, R., Purchio, A.F., Contag, P.R., West, D.B., 2004b. In vivo bioluminescent monitoring of chemical toxicity using haem oxygenase-luciferase transgenic mice. *Toxicol. Appl. Pharmacol.* 200, 219–228. <https://doi.org/10.1016/j.taap.2004.04.021>
- Markvicheva, K.N., Bilan, D.S., Mishina, N.M., Gorokhovatsky, A.Y., Vinokurov, L.M., Lukyanov, S., Belousov, V.V., 2011. A genetically encoded sensor for H<sub>2</sub>O<sub>2</sub> with expanded dynamic range. *Bioorg. Med. Chem.* 19, 1079–1084. <https://doi.org/10.1016/j.bmc.2010.07.014>
- Maruichi, T., Fukami, T., Nakajima, M., Yokoi, T., 2010. Transcriptional regulation of human carboxylesterase 1A1 by nuclear factor-erythroid 2 related factor 2 (Nrf2). *Biochem. Pharmacol.* 79, 288–295. <https://doi.org/10.1016/j.bcp.2009.08.019>
- Marzec, J.M., Christie, J.D., Reddy, S.P., Jedlicka, A.E., Vuong, H., Lanken, P.N., Aplenc, R., Yamamoto, T., Yamamoto, M., Cho, H.-Y., Kleeberger, S.R., 2007. Functional polymorphisms in the transcription factor NRF2 in humans increase the risk of acute lung injury. *FASEB J.* 21, 2237–2246. <https://doi.org/10.1096/fj.06-7759com>
- Matoba, T., Shimokawa, H., Nakashima, M., Hirakawa, Y., Mukai, Y., Hirano, K., Kanaide, H., Takeshita, A., 2000. Hydrogen peroxide is an endothelium-derived hyperpolarizing factor in mice. *J. Clin. Invest.* 106, 1521–1530. <https://doi.org/10.1172/JCI10506>
- Maurer, U., Preiss, F., Brauns-Schubert, P., Schlicher, L., Charvet, C., 2014. GSK-3 - at the crossroads of cell death and survival. *J. Cell Sci.* 127, 1369–1378. <https://doi.org/10.1242/jcs.138057>
- McCONKEY, S.E., Grant, D.M., Cribb, A.E., 2009. The role of para-aminophenol in acetaminophen-induced methemoglobinemia in dogs and cats. *J. Vet. Pharmacol. Ther.* 32, 585–595. <https://doi.org/10.1111/j.1365-2885.2009.01080.x>
- McConnachie, L.A., Mohar, I., Hudson, F.N., Ware, C.B., Ladiges, W.C., Fernandez, C., Chatterton-Kirchmeier, S., White, C.C., Pierce, R.H., Kavanagh, T.J., 2007. Glutamate Cysteine Ligase Modifier Subunit Deficiency and Gender as Determinants of Acetaminophen-Induced Hepatotoxicity in Mice. *Toxicol. Sci.* 99, 628–636. <https://doi.org/10.1093/toxsci/kfm165>
- McCord, J.M., Fridovich, I., 1969. Superoxide dismutase. An enzymic function for erythrocyte (hemocuprein). *J. Biol. Chem.* 244, 6049–6055.
- McGill, M.R., Lebofsky, M., Norris, H.-R.K., Slawson, M.H., Bajt, M.L., Xie, Y., Williams, C.D., Wilkins, D.G., Rollins, D.E., Jaeschke, H., 2013. Plasma and liver acetaminophen-protein adduct levels in mice after acetaminophen treatment: dose-response, mechanisms, and clinical implications. *Toxicol. Appl. Pharmacol.* 269, 240–249. <https://doi.org/10.1016/j.taap.2013.03.026>
- McLaughlin, J.N., Patterson, M.M., Malik, A.B., 2007. Protease-activated receptor-3 (PAR3) regulates PAR1 signaling by receptor dimerization. *Proc. Natl. Acad. Sci.* 104, 5662–5667. <https://doi.org/10.1073/pnas.0700763104>
- McMahon, M., Ding, S., Acosta-Jimenez, L.P., Frangova, T.G., Henderson, C.J., Wolf, C.R., 2018. Measuring in vivo responses to endogenous and exogenous oxidative stress using a novel haem oxygenase 1 reporter mouse. *J. Physiol.* 596, 105–127. <https://doi.org/10.1113/JP274915>
- McMahon, M., Itoh, K., Yamamoto, M., Chanas, S.A., Henderson, C.J., McLellan, L.I., Wolf, C.R., Cavin, C., Hayes, J.D., 2001. The Cap 'n' Collar Basic Leucine Zipper Transcription Factor Nrf2 (NF-E2 p45-related Factor 2) Controls Both Constitutive and Inducible Expression of Intestinal Detoxification and Glutathione Biosynthetic Enzymes. *Cancer Res.* 61, 3299–3307.
- McMahon, M., Lamont, D.J., Beattie, K.A., Hayes, J.D., 2010. Keap1 perceives stress via three sensors for the endogenous signaling molecules nitric oxide, zinc, and alkenals. *Proc. Natl. Acad. Sci. U. S. A.* 107, 18838–18843. <https://doi.org/10.1073/pnas.1007387107>
- McMahon, M., Thomas, N., Itoh, K., Yamamoto, M., Hayes, J.D., 2004. Redox-regulated Turnover of Nrf2 Is Determined by at Least Two Separate Protein Domains, the Redox-sensitive Neh2 Degron and the Redox-insensitive Neh6 Degron. *J. Biol. Chem.* 279, 31556–31567. <https://doi.org/10.1074/jbc.M403061200>

- Miao, W., Hu, L., Scrivens, P.J., Batist, G., 2005. Transcriptional regulation of NF-E2 p45-related factor (NRF2) expression by the aryl hydrocarbon receptor-xenobiotic response element signaling pathway: direct cross-talk between phase I and II drug-metabolizing enzymes. *J. Biol. Chem.* 280, 20340–20348. <https://doi.org/10.1074/jbc.M412081200>
- Middleton, A., Cooper, S., Cull, T., Stark, R., Adeleye, Y., Boekelheide, K., Clewell, R., Jennings, P., Guo, J., Liu, C., McMullen, P., Peng, S., Shah, I., Spencer, P., Subramanian, K., Thomas, R.S., van de Water, B., Westmoreland, C., White, A., Zhang, Q., Carmichael, P.L., 2017. Case Studies in Cellular Stress: Defining Adversity/Adaptation Tipping Points. *Appl. Vitro Toxicol.* 3, 199–210. <https://doi.org/10.1089/aivt.2017.0003>
- Miseta, A., Csutora, P., 2000. Relationship between the occurrence of cysteine in proteins and the complexity of organisms. *Mol. Biol. Evol.* 17, 1232–1239.
- Mitchell, P.S., Parkin, R.K., Kroh, E.M., Fritz, B.R., Wyman, S.K., Pogosova-Agadjanyan, E.L., Peterson, A., Noteboom, J., O'Briant, K.C., Allen, A., Lin, D.W., Urban, N., Drescher, C.W., Knudsen, B.S., Stirewalt, D.L., Gentleman, R., Vessella, R.L., Nelson, P.S., Martin, D.B., Tewari, M., 2008. Circulating microRNAs as stable blood-based markers for cancer detection. *Proc. Natl. Acad. Sci.* 105, 10513–10518. <https://doi.org/10.1073/pnas.0804549105>
- Mittal, C.K., Murad, F., 1977. Activation of guanylate cyclase by superoxide dismutase and hydroxyl radical: a physiological regulator of guanosine 3',5'-monophosphate formation. *Proc. Natl. Acad. Sci.* 74, 4360–4364.
- Mittal, M., Siddiqui, M.R., Tran, K., Reddy, S.P., Malik, A.B., 2014. Reactive Oxygen Species in Inflammation and Tissue Injury. *Antioxid. Redox Signal.* 20, 1126–1167. <https://doi.org/10.1089/ars.2012.5149>
- Miyagi, M.Y.S., Seelaender, M., Castoldi, A., de Almeida, D.C., Bacurau, A.V.N., Andrade-Oliveira, V., Enju, L.M., Pisciotano, M., Hayashida, C.Y., Hiyane, M.I., Brum, P.C., Camara, N.O.S., Amano, M.T., 2014. Long-Term Aerobic Exercise Protects against Cisplatin-Induced Nephrotoxicity by Modulating the Expression of IL-6 and HO-1. *PLoS ONE* 9. <https://doi.org/10.1371/journal.pone.0108543>
- Miyahara, E., Nishikawa, T., Takeuchi, T., Yasuda, K., Okamoto, Y., Kawano, Y., Horiuchi, M., 2014. Effect of myeloperoxidase inhibition on gene expression profiles in HL-60 cells exposed to 1, 2, 4,-benzenetriol. *Toxicology* 317, 50–57. <https://doi.org/10.1016/j.tox.2014.01.007>
- Miyamoto, M., Yanai, M., Ookubo, S., Awasaki, N., Takami, K., Imai, R., 2008. Detection of cell-free, liver-specific mRNAs in peripheral blood from rats with hepatotoxicity: a potential toxicological biomarker for safety evaluation. *Toxicol. Sci. Off. J. Soc. Toxicol.* 106, 538–545. <https://doi.org/10.1093/toxsci/kfn188>
- Mohar, I., Stamper, B.D., Rademacher, P.M., White, C.C., Nelson, S.D., Kavanagh, T.J., 2014. Acetaminophen-induced liver damage in mice is associated with gender-specific adduction of peroxiredoxin-6. *Redox Biol.* 2, 377–387. <https://doi.org/10.1016/j.redox.2014.01.008>
- Moi, P., Chan, K., Asunis, I., Cao, A., Kan, Y.W., 1994. Isolation of NF-E2-related factor 2 (Nrf2), a NF-E2-like basic leucine zipper transcriptional activator that binds to the tandem NF-E2/AP1 repeat of the beta-globin locus control region. *Proc. Natl. Acad. Sci. U. S. A.* 91, 9926–9930.
- Montano, M.M., Deng, H., Liu, M., Sun, X., Singal, R., 2004. Transcriptional regulation by the estrogen receptor of antioxidative stress enzymes and its functional implications. *Oncogene* 23, 2442–2453. <https://doi.org/10.1038/sj.onc.1207358>
- Mooradian, A.D., Haas, M.J., Wong, N.C.W., 2004. Transcriptional Control of Apolipoprotein A-I Gene Expression in Diabetes. *Diabetes* 53, 513–520. <https://doi.org/10.2337/diabetes.53.3.513>
- Morgan, M.J., Liu, Z., 2011. Crosstalk of reactive oxygen species and NF- $\kappa$ B signaling. *Cell Res.* 21, 103–115. <https://doi.org/10.1038/cr.2010.178>
- Motahari, P., Sadeghizadeh, M., Behmanesh, M., Sabri, S., Zolghadr, F., 2015. Generation of stable ARE- driven reporter system for monitoring oxidative stress. *DARU J. Pharm. Sci.* 23. <https://doi.org/10.1186/s40199-015-0122-9>
- Mrowietz, U., Altmeyer, P., Bieber, T., Röcken, M., Schopf, R.E., Sterry, W., 2007. Treatment of psoriasis with fumaric acid esters (Fumaderm®). *JDDG J. Dtsch. Dermatol. Ges.* 5, 716–717. <https://doi.org/10.1111/j.1610-0387.2007.06346.x>
- Mulcahy, R.T., Wartman, M.A., Bailey, H.H., Gipp, J.J., 1997. Constitutive and  $\beta$ -Naphthoflavone-induced Expression of the Human  $\gamma$ -Glutamylcysteine Synthetase Heavy Subunit Gene Is Regulated by a Distal Antioxidant Response Element/TRE Sequence. *J. Biol. Chem.* 272, 7445–7454. <https://doi.org/10.1074/jbc.272.11.7445>
- Muldrew, K.L., James, L.P., Coop, L., McCullough, S.S., Hendrickson, H.P., Hinson, J.A., Mayeux, P.R., 2002. Determination of Acetaminophen-Protein Adducts in Mouse Liver and Serum and Human Serum after Hepatotoxic Doses of Acetaminophen Using High-Performance Liquid Chromatography with Electrochemical Detection. *Drug Metab. Dispos.* 30, 446–451. <https://doi.org/10.1124/dmd.30.4.446>
- Münzel, P.A., Schmohl, S., Buckler, F., Jaehrling, J., Raschko, F.T., Köhle, C., Bock, K.W., 2003. Contribution of the Ah receptor to the phenolic antioxidant-mediated expression of human and rat UDP-glucuronosyltransferase UGT1A6 in Caco-2 and rat hepatoma 5L cells. *Biochem. Pharmacol.* 66, 841–847.
- Mutter, F.E., Park, B.K., Copple, I.M., 2015. Value of monitoring Nrf2 activity for the detection of chemical and oxidative stress. *Biochem. Soc. Trans.* 43, 657–662. <https://doi.org/10.1042/BST20150044>
- Myzak, M.C., Karplus, P.A., Chung, F.-L., Dashwood, R.H., 2004. A novel mechanism of chemoprotection by sulforaphane: inhibition of histone deacetylase. *Cancer Res.* 64, 5767–5774. <https://doi.org/10.1158/0008-5472.CAN-04-1326>
- Nakabeppu, Y., Tsuchimoto, D., Yamaguchi, H., Sakumi, K., 2007. Oxidative damage in nucleic acids and Parkinson's disease. *J. Neurosci. Res.* 85, 919–934. <https://doi.org/10.1002/jnr.21191>
- Nakamura, A., Nakajima, M., Higashi, E., Yamanaka, H., Yokoi, T., 2008. Genetic polymorphisms in the 5'-flanking region of human UDP-glucuronosyltransferase 2B7 affect the Nrf2-dependent transcriptional regulation. *Pharmacogenet. Genomics* 18, 709–720. <https://doi.org/10.1097/FPC.0b013e32830500c9>
- Nguyen, T., Rushmore, T.H., Pickett, C.B., 1994. Transcriptional regulation of a rat liver glutathione S-transferase Ya subunit gene. Analysis of the antioxidant response element and its activation by the phorbol ester 12-O-tetradecanoylphorbol-13-acetate. *J. Biol. Chem.* 269, 13656–13662.
- Nguyen, T., Sherratt, P.J., Huang, H.-C., Yang, C.S., Pickett, C.B., 2003. Increased Protein Stability as a Mechanism That Enhances Nrf2-mediated Transcriptional Activation of the Antioxidant Response Element DEGRADATION OF Nrf2 BY THE 26 S PROTEASOME. *J. Biol. Chem.* 278, 4536–4541. <https://doi.org/10.1074/jbc.M207293200>



- Nguyen, T., Sherratt, P.J., Nioi, P., Yang, C.S., Pickett, C.B., 2005. Nrf2 Controls Constitutive and Inducible Expression of ARE-driven Genes through a Dynamic Pathway Involving Nucleocytoplasmic Shuttling by Keap1. *J. Biol. Chem.* 280, 32485–32492. <https://doi.org/10.1074/jbc.M503074200>
- Nielsen, L.B., Wang, C., Sørensen, K., Bang-Berthelsen, C.H., Hansen, L., Andersen, M.-L.M., Hougaard, P., Juul, A., Zhang, C.-Y., Pociot, F., Mortensen, H.B., 2012. Circulating Levels of MicroRNA from Children with Newly Diagnosed Type 1 Diabetes and Healthy Controls: Evidence That miR-25 Associates to Residual Beta-Cell Function and Glycaemic Control during Disease Progression [WWW Document]. *J. Diabetes Res.* <https://doi.org/10.1155/2012/896362>
- Nioi, P., McMahon, M., Itoh, K., Yamamoto, M., Hayes, J.D., 2003. Identification of a novel Nrf2-regulated antioxidant response element (ARE) in the mouse NAD(P)H:quinone oxidoreductase 1 gene: reassessment of the ARE consensus sequence. *Biochem. J.* 374, 337–348. <https://doi.org/10.1042/BJ20030754>
- Nioi, P., Nguyen, T., Sherratt, P.J., Pickett, C.B., 2005. The Carboxy-Terminal Neh3 Domain of Nrf2 Is Required for Transcriptional Activation. *Mol. Cell. Biol.* 25, 10895–10906. <https://doi.org/10.1128/MCB.25.24.10895-10906.2005>
- Nishikawa, T., Edelstein, D., Du, X.L., Yamagishi, S., Matsumura, T., Kaneda, Y., Yorek, M.A., Beebe, D., Oates, P.J., Hammes, H.-P., Giardino, I., Brownlee, M., 2000. Normalizing mitochondrial superoxide production blocks three pathways of hyperglycaemic damage. *Nature* 404, 787. <https://doi.org/10.1038/35008121>
- Niture, S.K., Jain, A.K., Jaiswal, A.K., 2009. Antioxidant-induced modification of INrf2 cysteine 151 and PKC- $\delta$ -mediated phosphorylation of Nrf2 serine 40 are both required for stabilization and nuclear translocation of Nrf2 and increased drug resistance. *J. Cell Sci.* 122, 4452–4464. <https://doi.org/10.1242/jcs.058537>
- Niture, S.K., Jaiswal, A.K., 2012. Nrf2 Protein Up-regulates Antiapoptotic Protein Bcl-2 and Prevents Cellular Apoptosis. *J. Biol. Chem.* 287, 9873–9886. <https://doi.org/10.1074/jbc.M111.312694>
- Noel, S., Zheng, L., Navas-Acien, A., Fuchs, R.J., 2014. THE EFFECT OF EX VIVO CDDO-ME ACTIVATION ON NUCLEAR FACTOR ERYTHROID 2-RELATED FACTOR 2 PATHWAY IN WHITE BLOOD CELLS FROM PATIENTS WITH SEPTIC SHOCK. *Shock Augusta Ga* 42, 392–399. <https://doi.org/10.1097/SHK.0000000000000236>
- Nunomura, A., Perry, G., Aliev, G., Hirai, K., Takeda, A., Balraj, E.K., Jones, P.K., Ghanbari, H., Wataya, T., Shimohama, S., Chiba, S., Atwood, C.S., Petersen, R.B., Smith, M.A., 2001. Oxidative damage is the earliest event in Alzheimer disease. *J. Neuropathol. Exp. Neurol.* 60, 759–767.
- Nyström-Persson, J., Igarashi, Y., Ito, M., Morita, M., Nakatsu, N., Yamada, H., Mizuguchi, K., 2013. Toxygates: interactive toxicity analysis on a hybrid microarray and linked data platform. *Bioinformatics* 29, 3080–3086. <https://doi.org/10.1093/bioinformatics/btt531>
- Oikawa, D., Akai, R., Tokuda, M., Iwawaki, T., 2012. A transgenic mouse model for monitoring oxidative stress. *Sci. Rep.* 2. <https://doi.org/10.1038/srep00229>
- Okawa, H., Motohashi, H., Kobayashi, A., Aburatani, H., Kensler, T.W., Yamamoto, M., 2006. Hepatocyte-specific deletion of the keap1 gene activates Nrf2 and confers potent resistance against acute drug toxicity. *Biochem. Biophys. Res. Commun.* 339, 79–88. <https://doi.org/10.1016/j.bbrc.2005.10.185>
- Okubo, S., Miyamoto, M., Takami, K., Kanki, M., Ono, A., Nakatsu, N., Yamada, H., Ohno, Y., Urushidani, T., 2013. Identification of Novel Liver-Specific mRNAs in Plasma for Biomarkers of Drug-Induced Liver Injury and Quantitative Evaluation in Rats Treated With Various Hepatotoxic Compounds. *Toxicol. Sci.* 132, 21–31. <https://doi.org/10.1093/toxsci/kfs340>
- Olson, H., Betton, G., Robinson, D., Thomas, K., Monro, A., Kolaja, G., Lilly, P., Sanders, J., Sipes, G., Bracken, W., Dorato, M., Van Deun, K., Smith, P., Berger, B., Heller, A., 2000. Concordance of the toxicity of pharmaceuticals in humans and in animals. *Regul. Toxicol. Pharmacol.* RTP 32, 56–67. <https://doi.org/10.1006/rtp.2000.1399>
- Onakpoya, I.J., Heneghan, C.J., Aronson, J.K., 2016. Post-marketing withdrawal of 462 medicinal products because of adverse drug reactions: a systematic review of the world literature. *BMC Med.* 14. <https://doi.org/10.1186/s12916-016-0553-2>
- Paek, J., Lo, J.Y., Narasimhan, S.D., Nguyen, T.N., Glover-Cutter, K., Robida-Stubbs, S., Suzuki, T., Yamamoto, M., Blackwell, T.K., Curran, S.P., 2012. Mitochondrial SKN-1/Nrf Mediates a Conserved Starvation Response. *Cell Metab.* 16, 526–537. <https://doi.org/10.1016/j.cmet.2012.09.007>
- Pan, J.-A., Sun, Y., Jiang, Y.-P., Bott, A.J., Jaber, N., Dou, Z., Yang, B., Chen, J.-S., Catanzaro, J.M., Du, C., Ding, W.-X., Diaz-Meco, M.T., Moscat, J., Ozato, K., Lin, R.Z., Zong, W.-X., 2016. TRIM21 Ubiquitylates SQSTM1/p62 and Suppresses Protein Sequestration to Regulate Redox Homeostasis. *Mol. Cell* 61, 720–733. <https://doi.org/10.1016/j.molcel.2016.02.007>
- Papp, D., Lenti, K., Módos, D., Fazekas, D., Dúl, Z., Túrei, D., Földvári-Nagy, L., Nussinov, R., Csermely, P., Korcsmáros, T., 2012. The NRF2-related interactome and regulome contain multifunctional proteins and fine-tuned autoregulatory loops. *FEBS Lett.* 586, 1795–1802. <https://doi.org/10.1016/j.febslet.2012.05.016>
- Pareek, T.K., Belkadi, A., Kesavapany, S., Zaremba, A., Loh, S.L., Bai, L., Cohen, M.L., Meyer, C., Liby, K.T., Miller, R.H., Sporn, M.B., Letterio, J.J., 2011. Triterpenoid modulation of IL-17 and Nrf-2 expression ameliorates neuroinflammation and promotes remyelination in autoimmune encephalomyelitis. *Sci. Rep.* 1, srep00201. <https://doi.org/10.1038/srep00201>
- Park, E.Y., Rho, H.M., 2002. The transcriptional activation of the human copper/zinc superoxide dismutase gene by 2,3,7,8-tetrachlorodibenzo-p-dioxin through two different regulator sites, the antioxidant responsive element and xenobiotic responsive element. *Mol. Cell. Biochem.* 240, 47–55. <https://doi.org/10.1023/A:1020600509965>
- Parrish, A.R., Chen, G., Burghardt, R.C., Watanabe, T., Morisseau, C., Hammock, B.D., 2009. Attenuation of cisplatin nephrotoxicity by inhibition of soluble epoxide hydrolase. *Cell Biol. Toxicol.* 25, 217–225. <https://doi.org/10.1007/s10565-008-9071-0>
- Pei, B., Sisu, C., Frankish, A., Howald, C., Habegger, L., Mu, X.J., Harte, R., Balasubramanian, S., Tanzer, A., Diekhans, M., Reymond, A., Hubbard, T.J., Harrow, J., Gerstein, M.B., 2012. The GENCODE pseudogene resource. *Genome Biol.* 13, R51. <https://doi.org/10.1186/gb-2012-13-9-r51>
- Pellegrini, K.L., Han, T., Bijol, V., Saikumar, J., Craciun, F.L., Chen, W.W., Fuscoe, J.C., Vaidya, V.S., 2014. MicroRNA-155 Deficient Mice Experience Heightened Kidney Toxicity When Dosed with Cisplatin. *Toxicol. Sci.* 141, 484–492. <https://doi.org/10.1093/toxsci/kfu143>

- Peters, T.R., Tosk, J.M., Goulbourne, E.A., 1990. Lucigenin chemiluminescence as a probe for measuring reactive oxygen species production in *Escherichia coli*. *Anal. Biochem.* 186, 316–319. [https://doi.org/10.1016/0003-2697\(90\)90087-P](https://doi.org/10.1016/0003-2697(90)90087-P)
- Pirmohamed, M., James, S., Meakin, S., Green, C., Scott, A.K., Walley, T.J., Farrar, K., Park, B.K., Breckenridge, A.M., 2004. Adverse drug reactions as cause of admission to hospital: prospective analysis of 18 820 patients. *BMJ* 329, 15–19. <https://doi.org/10.1136/bmj.329.7456.15>
- Pompella, A., Sies, H., Wacker, R., Brouns, F., Grune, T., Biesalski, H.K., Frank, J., 2014. The use of total antioxidant capacity as surrogate marker for food quality and its effect on health is to be discouraged. *Nutrition* 30, 791–793. <https://doi.org/10.1016/j.nut.2013.12.002>
- Ponchel, F., Toomes, C., Bransfield, K., Leong, F.T., Douglas, S.H., Field, S.L., Bell, S.M., Combaret, V., Puisieux, A., Mighell, A.J., Robinson, P.A., Inglehearn, C.F., Isaacs, J.D., Markham, A.F., 2003. Real-time PCR based on SYBR-Green I fluorescence: An alternative to the TaqMan assay for a relative quantification of gene rearrangements, gene amplifications and micro gene deletions. *BMC Biotechnol.* 3, 18. <https://doi.org/10.1186/1472-6750-3-18>
- Posner, G.H., Cho, C.G., Green, J.V., Zhang, Y., Talalay, P., 1994. Design and synthesis of bifunctional isothiocyanate analogs of sulforaphane: correlation between structure and potency as inducers of anticarcinogenic detoxication enzymes. *J. Med. Chem.* 37, 170–176.
- Poss, K.D., Tonegawa, S., 1997. Haem oxygenase 1 is required for mammalian iron reutilization. *Proc. Natl. Acad. Sci.* 94, 10919–10924. <https://doi.org/10.1073/pnas.94.20.10919>
- Prochaska, H.J., Santamaria, A.B., 1988. Direct measurement of NAD(P)H:quinone reductase from cells cultured in microtiter wells: A screening assay for anticarcinogenic enzyme inducers. *Anal. Biochem.* 169, 328–336. [https://doi.org/10.1016/0003-2697\(88\)90292-8](https://doi.org/10.1016/0003-2697(88)90292-8)
- Qiu, L.-Q., Abey, S., Harris, S., Shah, R., Gerrish, K.E., Blackshear, P.J., 2015. Global Analysis of Posttranscriptional Gene Expression in Response to Sodium Arsenite. *Environ. Health Perspect.* 123, 324–330. <https://doi.org/10.1289/ehp.1408626>
- Rachakonda, G., Xiong, Y., Sekhar, K.R., Stamer, S.L., Liebler, D.C., Freeman, M.L., 2008. Covalent Modification at Cys151 Dissociates the Electrophile Sensor Keap1 from the Ubiquitin Ligase CUL3. *Chem. Res. Toxicol.* 21, 705–710. <https://doi.org/10.1021/tx700302s>
- Rada, P., Rojo, A.I., Chowdhry, S., McMahon, M., Hayes, J.D., Cuadrado, A., 2011. SCF/β-TrCP Promotes Glycogen Synthase Kinase 3-Dependent Degradation of the Nrf2 Transcription Factor in a Keap1-Independent Manner. *Mol. Cell. Biol.* 31, 1121–1133. <https://doi.org/10.1128/MCB.01204-10>
- Rada, P., Rojo, A.I., Evrard-Todeschi, N., Innamorato, N.G., Cotte, A., Jaworski, T., Tobón-Velasco, J.C., Devijver, H., García-Mayoral, M.F., Leuven, F.V., Hayes, J.D., Bertho, G., Cuadrado, A., 2012. Structural and Functional Characterization of Nrf2 Degradation by the Glycogen Synthase Kinase 3/β-TrCP Axis. *Mol. Cell. Biol.* 32, 3486–3499. <https://doi.org/10.1128/MCB.00180-12>
- Radjendirane, V., Joseph, P., Lee, Y.-H., Kimura, S., Klein-Szanto, A.J.P., Gonzalez, F.J., Jaiswal, A.K., 1998. Disruption of the DT Diaphorase (NQO1) Gene in Mice Leads to Increased Menadione Toxicity. *J. Biol. Chem.* 273, 7382–7389. <https://doi.org/10.1074/jbc.273.13.7382>
- Radom-Aizik, S., Zaldivar, F., Leu, S.-Y., Galassetti, P., Cooper, D.M., 2008. Effects of 30 min of aerobic exercise on gene expression in human neutrophils. *J. Appl. Physiol. Bethesda Md* 1985 104, 236–243. <https://doi.org/10.1152/jappphysiol.00872.2007>
- Rahman, I., Kode, A., Biswas, S.K., 2007. Assay for quantitative determination of glutathione and glutathione disulfide levels using enzymatic recycling method. *Nat. Protoc.* 1, 3159–3165. <https://doi.org/10.1038/nprot.2006.378>
- Ramaiahgari, S.C., den Braver, M.W., Herpers, B., Terpstra, V., Commandeur, J.N.M., van de Water, B., Price, L.S., 2014. A 3D in vitro model of differentiated HepG2 cell spheroids with improved liver-like properties for repeated dose high-throughput toxicity studies. *Arch. Toxicol.* 88, 1083–1095. <https://doi.org/10.1007/s00204-014-1215-9>
- Ramkumar, K.M., Sekar, T.V., Foygel, K., Elango, B., Paulmurugan, R., 2013. Reporter Protein Complementation Imaging Assay to Screen and Study Nrf2 Activators in Cells and Living Animals. *Anal. Chem.* 85, 7542–7549. <https://doi.org/10.1021/ac401569j>
- Ramos-Gomez, M., Dolan, P.M., Itoh, K., Yamamoto, M., Kensler, T.W., 2003. Interactive effects of nrf2 genotype and oltipraz on benzo[a]pyrene–DNA adducts and tumor yield in mice. *Carcinogenesis* 24, 461–467. <https://doi.org/10.1093/carcin/24.3.461>
- Randle, L.E., Goldring, C.E.P., Benson, C.A., Metcalfe, P.N., Kitteringham, N.R., Park, B.K., Williams, D.P., 2008. Investigation of the effect of a panel of model hepatotoxins on the Nrf2-Keap1 defence response pathway in CD-1 mice. *Toxicology* 243, 249–260. <https://doi.org/10.1016/j.tox.2007.10.011>
- Reichard, J.F., Motz, G.T., Puga, A., 2007. Haem oxygenase-1 induction by NRF2 requires inactivation of the transcriptional repressor BACH1. *Nucleic Acids Res.* 35, 7074–7086. <https://doi.org/10.1093/nar/gkm638>
- Reisman, S.A., Lee, C.-Y.I., Meyer, C.J., Proksch, J.W., Sonis, S.T., Ward, K.W., 2014. Topical Application of the Synthetic Triterpenoid RTA 408 Protects Mice from Radiation-Induced Dermatitis. *Radiat. Res.* 181, 512–520. <https://doi.org/10.1667/RR13578.1>
- Richard, A.M., Judson, R.S., Houck, K.A., Grulke, C.M., Volarath, P., Thillainadarajah, I., Yang, C., Rathman, J., Martin, M.T., Wambaugh, J.F., Knudsen, T.B., Kancharla, J., Mansouri, K., Patlewicz, G., Williams, A.J., Little, S.B., Crofton, K.M., Thomas, R.S., 2016. ToxCast Chemical Landscape: Paving the Road to 21st Century Toxicology. *Chem. Res. Toxicol.* 29, 1225–1251. <https://doi.org/10.1021/acs.chemrestox.6b00135>
- Rizzi, N., Rebecchi, M., Levandis, G., Ciana, P., Maggi, A., 2017. Identification of novel loci for the generation of reporter mice. *Nucleic Acids Res.* 45, e37. <https://doi.org/10.1093/nar/gkw1142>
- Rohrer, P.R., Rudraiah, S., Goedken, M.J., Manautou, J.E., 2014. Is Nuclear Factor Erythroid 2–Related Factor 2 Responsible for Sex Differences in Susceptibility to Acetaminophen-Induced Hepatotoxicity in Mice? *Drug Metab. Dispos.* 42, 1663–1674. <https://doi.org/10.1124/dmd.114.059006>
- Rojo, A.I., Medina-Campos, O.N., Rada, P., Zúñiga-Toalá, A., López-Gazcón, A., Espada, S., Pedraza-Chaverri, J., Cuadrado, A., 2012. Signaling pathways activated by the phytochemical nordihydroguaiaretic acid contribute to a Keap1-

- independent regulation of Nrf2 stability: Role of glycogen synthase kinase-3. *Free Radic. Biol. Med.* 52, 473–487. <https://doi.org/10.1016/j.freeradbiomed.2011.11.003>
- Rushmore, T.H., Morton, M.R., Pickett, C.B., 1991. The antioxidant responsive element. Activation by oxidative stress and identification of the DNA consensus sequence required for functional activity. *J. Biol. Chem.* 266, 11632–11639.
- Rushworth, S.A., Zaitseva, L., Murray, M.Y., Shah, N.M., Bowles, K.M., MacEwan, D.J., 2012. The high Nrf2 expression in human acute myeloid leukemia is driven by NF- $\kappa$ B and underlies its chemo-resistance. *Blood* 120, 5188–5198. <https://doi.org/10.1182/blood-2012-04-422121>
- Russell, W.M.S., Burch, R.L., 1959. The principles of humane experimental technique. Wheathampstead (UK): Universities Federation for Animal Welfare. Universities Federation for Animal Welfare., Wheathampstead (UK).
- Russmann, S., Kullak-Ublick, G.A., Grattagliano, I., 2009. Current concepts of mechanisms in drug-induced hepatotoxicity. *Curr. Med. Chem.* 16, 3041–3053.
- Salazar, M., Rojo, A.I., Velasco, D., Sagarra, R.M. de, Cuadrado, A., 2006. Glycogen Synthase Kinase-3 $\beta$  Inhibits the Xenobiotic and Antioxidant Cell Response by Direct Phosphorylation and Nuclear Exclusion of the Transcription Factor Nrf2. *J. Biol. Chem.* 281, 14841–14851. <https://doi.org/10.1074/jbc.M513737200>
- Schneider, C.A., Rasband, W.S., Eliceiri, K.W., 2012. NIH Image to ImageJ: 25 years of image analysis. *Nat Meth* 9, 671–675. <https://doi.org/10.1038/nmeth.2089>
- Schoonbroodt, S., Ferreira, V., Best-Belpomme, M., Boelaert, J.R., Legrand-Poels, S., Korner, M., Piette, J., 2000. Crucial role of the amino-terminal tyrosine residue 42 and the carboxyl-terminal PEST domain of I kappa B alpha in NF-kappa B activation by an oxidative stress. *J. Immunol. Baltim. Md 1950* 164, 4292–4300.
- Schwarzländer, M., Wagner, S., Ermakova, Y.G., Belousov, V.V., Radi, R., Beckman, J.S., Buettner, G.R., Demaux, N., Duchon, M.R., Forman, H.J., Fricker, M.D., Gems, D., Halestrap, A.P., Halliwell, B., Jakob, U., Johnston, I.G., Jones, N.S., Logan, D.C., Morgan, B., Müller, F.L., Nicholls, D.G., Remington, S.J., Schumacker, P.T., Winterbourn, C.C., Sweetlove, L.J., Meyer, A.J., Dick, T.P., Murphy, M.P., 2014. The 'mitoflash' probe cpYFP does not respond to superoxide. *Nature* 514, E12–E14. <https://doi.org/10.1038/nature13858>
- Segal, L., Katz, L.S., Shapira, H., Sandbank, J., Geras-Raaka, E., Gershengorn, M.C., Oron, Y., 2014. PAR-3 Knockdown Enhances Adhesion Rate of PANC-1 Cells via Increased Expression of Integrin $\alpha$ v and E-Cadherin. *PLoS ONE* 9, e93879. <https://doi.org/10.1371/journal.pone.0093879>
- Sekhar, K.R., Soltaninassab, S.R., Borrelli, M.J., Xu, Z.Q., Meredith, M.J., Domann, F.E., Freeman, M.L., 2000. Inhibition of the 26S proteasome induces expression of GLCLC, the catalytic subunit for gamma-glutamylcysteine synthetase. *Biochem. Biophys. Res. Commun.* 270, 311–317. <https://doi.org/10.1006/bbrc.2000.2419>
- Sharkey, J., 2013. Molecular Biomarkers and Regulators of Susceptibility to Drug-Induced Kidney Injury (PhD thesis). University of Liverpool.
- Sharma, S., Gao, P., Steele, V.E., 2006. The chemopreventive efficacy of inhaled oltipraz particulates in the B[a]P-induced A/J mouse lung adenoma model. *Carcinogenesis* 27, 1721–1727. <https://doi.org/10.1093/carcin/bg1052>
- Shelton, L.M., Lister, A., Walsh, J., Jenkins, R.E., Wong, M.H.L., Rowe, C., Ricci, E., Ressel, L., Fang, Y., Demougin, P., Vukojevic, V., O'Neill, P.M., Goldring, C.E., Kitteringham, N.R., Park, B.K., Odermatt, A., Copple, I.M., 2015. Integrated transcriptomic and proteomic analyses uncover regulatory roles of Nrf2 in the kidney. *Kidney Int.* 88, 1261–1273. <https://doi.org/10.1038/ki.2015.286>
- Sherratt, P.J., McLellan, L.I., Hayes, J.D., 2003. Positive and negative regulation of prostaglandin E2 biosynthesis in human colorectal carcinoma cells by cancer chemopreventive agents. *Biochem. Pharmacol.* 66, 51–61.
- Shimomura, O., 1985. Bioluminescence in the sea: photoprotein systems. *Symp. Soc. Exp. Biol.* 39, 351–372.
- Shin, S., Wakabayashi, N., Misra, V., Biswal, S., Lee, G.H., Agoston, E.S., Yamamoto, M., Kensler, T.W., 2007. NRF2 Modulates Aryl Hydrocarbon Receptor Signaling: Influence on Adipogenesis. *Mol. Cell. Biol.* 27, 7188–7197. <https://doi.org/10.1128/MCB.00915-07>
- Shord, S.S., Thompson, D.M., Krempel, G.A., Hanigan, M.H., 2006. Effect of concurrent medications on cisplatin-induced nephrotoxicity in patients with head and neck cancer. *Anticancer. Drugs* 17, 207–215.
- Shuhendler, A.J., Pu, K., Cui, L., Uetrecht, J.P., Rao, J., 2014. Real-time imaging of oxidative and nitrosative stress in the liver of live animals for drug-toxicity testing. *Nat. Biotechnol.* 32, 373–380. <https://doi.org/10.1038/nbt.2838>
- Shukla, S.J., Huang, R., Simmons, S.O., Tice, R.R., Witt, K.L., VanLeer, D., Ramabhadran, R., Austin, C.P., Xia, M., 2012. Profiling Environmental Chemicals for Activity in the Antioxidant Response Element Signaling Pathway Using a High Throughput Screening Approach. *Environ. Health Perspect.* 120, 1150–1156. <https://doi.org/10.1289/ehp.1104709>
- Sies, H., 2018. On the history of oxidative stress: Concept and some aspects of current development. *Curr. Opin. Toxicol.* 7, 122–126. <https://doi.org/10.1016/j.cotox.2018.01.002>
- Sies, H., 2015. Oxidative stress: a concept in redox biology and medicine. *Redox Biol.* 4, 180–183. <https://doi.org/10.1016/j.redox.2015.01.002>
- Siewert, S., González, I., Santillán, L., Lucero, R., Ojeda, M.S., Gimenez, M.S., 2013. Downregulation of Nrf2 and HO-1 expression contributes to oxidative stress in type 2 diabetes mellitus: A study in Juana Koslay City, San Luis, Argentina. *J. Diabetes Mellit.* 03, 71. <https://doi.org/10.4236/jdm.2013.32011>
- Silva, J., García, V., García, J.M., Peña, C., Domínguez, G., Díaz, R., Lorenzo, Y., Hurtado, A., Sánchez, A., Bonilla, F., 2007. Circulating Bmi-1 mRNA as a possible prognostic factor for advanced breast cancer patients. *Breast Cancer Res. BCR* 9, R55. <https://doi.org/10.1186/bcr1760>
- Simmons, S.O., Fan, C.-Y., Yeoman, K., Wakefield, J., Ramabhadran, R., 2011. NRF2 Oxidative Stress Induced by Heavy Metals is Cell Type Dependent. *Curr. Chem. Genomics* 5, 1–12. <https://doi.org/10.2174/1875397301105010001>
- Simões, B.M., Alférez, D., Eyre, R., Spence, K., Santiago-Gomez, A., Tanaka, I., Kohler, B., Howat, D., Howell, S.J., Clarke, R.B., 2015. Abstract 2319: Sulforadex targets breast cancer stem-like cells in patient-derived cells and xenograft tumors. *Cancer Res.* 75, 2319–2319. <https://doi.org/10.1158/1538-7445.AM2015-2319>
- Singh, A., Happel, C., Manna, S.K., Acquaah-Mensah, G., Carrerero, J., Kumar, S., Nasipuri, P., Krausz, K.W., Wakabayashi, N., Dewi, R., Boros, L.G., Gonzalez, F.J., Gabrielson, E., Wong, K.K., Girnun, G., Biswal, S., 2013. Transcription factor NRF2

- regulates miR-1 and miR-206 to drive tumorigenesis. *J. Clin. Invest.* 123, 2921–2934. <https://doi.org/10.1172/JCI66353>
- Singh, A., Ling, G., Suhasini, A.N., Zhang, P., Yamamoto, M., Navas-Acien, A., Cosgrove, G., Tuder, R.M., Thomas, W.K., Watson, W.H., Biswal, S., 2009. Nrf2 Dependent Sulfiredoxin-1 Expression Protects Against Cigarette Smoke-induced Oxidative Stress in Lungs. *Free Radic. Biol. Med.* 46, 376–386. <https://doi.org/10.1016/j.freeradbiomed.2008.10.026>
- Singh, K., Connors, S.L., Macklin, E.A., Smith, K.D., Fahey, J.W., Talalay, P., Zimmerman, A.W., 2014. Sulforaphane treatment of autism spectrum disorder (ASD). *Proc. Natl. Acad. Sci.* 111, 15550–15555. <https://doi.org/10.1073/pnas.1416940111>
- Skardal, A., Murphy, S.V., Devarasetty, M., Mead, I., Kang, H.-W., Seol, Y.-J., Zhang, Y.S., Shin, S.-R., Zhao, L., Aleman, J., Hall, A.R., Shupe, T.D., Kleensang, A., Dokmeci, M.R., Lee, S.J., Jackson, J.D., Yoo, J.J., Hartung, T., Khademhosseini, A., Soker, S., Bishop, C.E., Atala, A., 2017. Multi-tissue interactions in an integrated three-tissue organ-on-a-chip platform. *Sci. Rep.* 7, 8837. <https://doi.org/10.1038/s41598-017-08879-x>
- Skog, J., Wurdinger, T., van Rijn, S., Meijer, D., Gainche, L., Sena-Estevés, M., Curry, W.T., Carter, R.S., Krichevsky, A.M., Breakefield, X.O., 2008. Glioblastoma microvesicles transport RNA and protein that promote tumor growth and provide diagnostic biomarkers. *Nat. Cell Biol.* 10, 1470–1476. <https://doi.org/10.1038/ncb1800>
- Skokos, D., Panse, S.L., Villa, I., Rousselle, J.-C., Peronet, R., David, B., Namane, A., Mécheri, S., 2001. Mast Cell-Dependent B and T Lymphocyte Activation Is Mediated by the Secretion of Immunologically Active Exosomes. *J. Immunol.* 166, 868–876. <https://doi.org/10.4049/jimmunol.166.2.868>
- Smirnova, N.A., Haskew-Layton, R.E., Basso, M., Hushpulia, D.M., Payappilly, J.B., Speer, R.E., Ahn, Y.-H., Rakhman, I., Cole, P.A., Pinto, J.T., Ratan, R.R., Gazaryan, I.G., 2011. Development of Neh2-Luciferase Reporter and Its Application for High Throughput Screening and Real-Time Monitoring of Nrf2 Activators. *Chem. Biol.* 18, 752–765. <https://doi.org/10.1016/j.chembiol.2011.03.013>
- Soriano, F.X., Léveillé, F., Papadia, S., Higgins, L.G., Varley, J., Baxter, P., Hayes, J.D., Hardingham, G.E., 2008. Induction of sulfiredoxin expression and reduction of peroxiredoxin hyperoxidation by the neuroprotective Nrf2 activator 3H-1,2-dithiole-3-thione. *J. Neurochem.* 107, 533–543. <https://doi.org/10.1111/j.1471-4159.2008.05648.x>
- Souza, T.M., Kleinjans, J.C.S., Jennen, D.G.J., 2017. Dose and Time Dependencies in Stress Pathway Responses during Chemical Exposure: Novel Insights from Gene Regulatory Networks. *Front. Genet.* 8. <https://doi.org/10.3389/fgene.2017.00142>
- Srivastava, A., Ramachandran, S., Hameed, S.P., Ahuja, V., Hosagrahara, V.P., 2014. Identification and Mitigation of a Reactive Metabolite Liability Associated with Aminoimidazoles. *Chem. Res. Toxicol.* 27, 1586–1597. <https://doi.org/10.1021/tx500212c>
- Starkey Lewis, P.J., Dear, J., Platt, V., Simpson, K.J., Craig, D.G.N., Antoine, D.J., French, N.S., Dhaun, N., Webb, D.J., Costello, E.M., Neoptolemos, J.P., Moggs, J., Goldring, C.E., Park, B.K., 2011. Circulating microRNAs as potential markers of human drug-induced liver injury. *Hepatology* 54, 1767–1776. <https://doi.org/10.1002/hep.24538>
- Steghens, J.-P., Min, K.-L., Bernengo, J.-C., 1998. Firefly luciferase has two nucleotide binding sites: effect of nucleoside monophosphate and CoA on the light-emission spectra. *Biochem. J.* 336, 109–113. <https://doi.org/10.1042/bj3360109>
- Steinberg, P., Behnisch, P.A., Besselink, H., Brouwer, A.A., 2017. Screening of molecular cell targets for carcinogenic heterocyclic aromatic amines by using CALUX® reporter gene assays. *Cell Biol. Toxicol.* 33, 283–293. <https://doi.org/10.1007/s10565-016-9373-6>
- Stewart, D., Killeen, E., Naquin, R., Alam, S., Alam, J., 2003. Degradation of Transcription Factor Nrf2 via the Ubiquitin-Proteasome Pathway and Stabilization by Cadmium. *J. Biol. Chem.* 278, 2396–2402. <https://doi.org/10.1074/jbc.M209195200>
- Stirban, A., 2008. Drugs for the treatment of diabetes complications. Zycose: a new player in the field? *Drugs Today Barc. Spain* 1998 44, 783–796. <https://doi.org/10.1358/dot.2008.44.10.1183086>
- Sun, H., Shamy, M., Kluz, T., Muñoz, A.B., Zhong, M., Lailicht, F., Alghamdi, M.A., Khoder, M.I., Chen, L.-C., Costa, M., 2012. Gene expression profiling and pathway analysis of human bronchial epithelial cells exposed to airborne particulate matter collected from Saudi Arabia. *Toxicol. Appl. Pharmacol.* 265. <https://doi.org/10.1016/j.taap.2012.10.008>
- Sun, L., Zhao, Y., Gu, S., Mao, Y., Ji, C., Xin, X., 2014. Regulation of the HMOX1 gene by the transcription factor AP-2δ with unique DNA binding site. *Mol. Med. Rep.* 10, 423–428. <https://doi.org/10.3892/mmr.2014.2196>
- Suttner, D.M., Sridhar, K., Lee, C.S., Tomura, T., Hansen, T.N., Dennery, P.A., 1999. Protective effects of transient HO-1 overexpression on susceptibility to oxygen toxicity in lung cells. *Am. J. Physiol.* 276, L443–451.
- Switzar, L., Kwast, L.M., Lingeman, H., Giera, M., Pieters, R.H.H., Niessen, W.M.A., 2013. Identification and quantification of drug-albumin adducts in serum samples from a drug exposure study in mice. *J. Chromatogr. B Analyt. Technol. Biomed. Life. Sci.* 917–918, 53–61. <https://doi.org/10.1016/j.jchromb.2012.12.033>
- Szent-Gyorgyi, C., Ballou, B.T., Dagnal, E., Bryan, B., 1999. Cloning and characterization of new bioluminescent proteins. Presented at the Biomedical Imaging: Reporters, Dyes, and Instrumentation, pp. 4–11. <https://doi.org/10.1117/12.351015>
- Takabe, W., Matsukawa, N., Kodama, T., Tanaka, K., Noguchi, N., 2006. Chemical structure-dependent gene expression of proteasome subunits via regulation of the antioxidant response element. *Free Radic. Res.* 40, 21–30. <https://doi.org/10.1080/10715760500354430>
- Takai, A., Fako, V., Dang, H., Forgues, M., Yu, Z., Budhu, A., Wang, X.W., 2016. Three-dimensional Organotypic Culture Models of Human Hepatocellular Carcinoma. *Sci. Rep.* 6, 21174. <https://doi.org/10.1038/srep21174>
- Takayama, K., Morisaki, Y., Kuno, S., Nagamoto, Y., Harada, K., Furukawa, N., Ohtaka, M., Nishimura, K., Imagawa, K., Sakurai, F., Tachibana, M., Sumazaki, R., Noguchi, E., Nakanishi, M., Hirata, K., Kawabata, K., Mizuguchi, H., 2014. Prediction of interindividual differences in hepatic functions and drug sensitivity by using human iPSC-derived hepatocytes. *Proc. Natl. Acad. Sci. U. S. A.* 111, 16772–16777. <https://doi.org/10.1073/pnas.1413481111>
- Tannenbaum, J., Bennett, B.T., 2015. Russell and Burch's 3Rs Then and Now: The Need for Clarity in Definition and Purpose. *J. Am. Assoc. Lab. Anim. Sci. JAALAS* 54, 120–132.

- Tenhunen, R., Marver, H.S., Schmid, R., 1968. The enzymatic conversion of haem to bilirubin by microsomal haem oxygenase. *Proc. Natl. Acad. Sci. U. S. A.* 61, 748–755.
- Thakur, S., Sarkar, B., Cholia, R.P., Gautam, N., Dhiman, M., Mantha, A.K., 2014. APE1/Ref-1 as an emerging therapeutic target for various human diseases: phytochemical modulation of its functions. *Exp. Mol. Med.* 46, e106. <https://doi.org/10.1038/emm.2014.42>
- Thekkeveedu, R.K., Chu, C., Basu, S.K., Moorthy, B., 2017. Role of NF-E2 Related Factor (Nrf2) in Hyperoxic Lung Injury: Implications for Bronchopulmonary Dysplasia and Acute Respiratory Distress Syndrome. *Pediatrics* 140, 53–53. [https://doi.org/10.1542/peds.140.1\\_MeetingAbstract.53](https://doi.org/10.1542/peds.140.1_MeetingAbstract.53)
- Théry, C., Boussac, M., Véron, P., Ricciardi-Castagnoli, P., Raposo, G., Garin, J., Amigorena, S., 2001. Proteomic Analysis of Dendritic Cell-Derived Exosomes: A Secreted Subcellular Compartment Distinct from Apoptotic Vesicles. *J. Immunol.* 166, 7309–7318. <https://doi.org/10.4049/jimmunol.166.12.7309>
- Thierry-Mieg, D., Thierry-Mieg, J., 2006. AceView: a comprehensive cDNA-supported gene and transcripts annotation. *Genome Biol.* 7, S12. <https://doi.org/10.1186/gb-2006-7-s1-s12>
- THIMMULAPPA, R.K., FUCHS, R.J., MALHOTRA, D., SCOLLICK, C., TRAORE, K., BREM, J.H., TRUSH, M.A., LIBY, K.T., SPORN, M.B., KENSLE, T.W., BISWAL, S., 2007. Preclinical Evaluation of Targeting the Nrf2 Pathway by Triterpenoids (CDDO-Im and CDDO-Me) for Protection from LPS-Induced Inflammatory Response and Reactive Oxygen Species in Human Peripheral Blood Mononuclear Cells and Neutrophils. *Antioxid. Redox Signal.* 9, 1963–1970. <https://doi.org/10.1089/ars.2007.1745>
- Thompson, R.A., Isin, E.M., Ogese, M.O., Mettetal, J.T., Williams, D.P., 2016. Reactive Metabolites: Current and Emerging Risk and Hazard Assessments. *Chem. Res. Toxicol.* 29, 505–533. <https://doi.org/10.1021/acs.chemrestox.5b00410>
- Tian, C., Gao, L., Zucker, I.H., 2017. Myocardial infarction-induced miRNA-enriched exosomes contribute to Nrf2 dysregulation in chronic heart failure. *FASEB J.* 31, 721.5–721.5.
- Tobón-Velasco, J.C., Limón-Pacheco, J.H., Orozco-Ibarra, M., Macías-Silva, M., Vázquez-Victorio, G., Cuevas, E., Ali, S.F., Cuadrado, A., Pedraza-Chaverri, J., Santamaría, A., 2013. 6-OHDA-induced apoptosis and mitochondrial dysfunction are mediated by early modulation of intracellular signals and interaction of Nrf2 and NF-κB factors. *Toxicology* 304, 109–119. <https://doi.org/10.1016/j.tox.2012.12.011>
- Tong, K.I., Kobayashi, A., Katsuoka, F., Yamamoto, M., 2006. Two-site substrate recognition model for the Keap1-Nrf2 system: a hinge and latch mechanism. *Biol. Chem.* 387, 1311–1320. <https://doi.org/10.1515/BC.2006.164>
- Tsamandouras, N., Chen, W.L.K., Edington, C.D., Stokes, C.L., Griffith, L.G., Cirit, M., 2017. Integrated Gut and Liver Microphysiological Systems for Quantitative <Emphasis Type="Italic">In Vitro</Emphasis> Pharmacokinetic Studies. *AAPS J.* 19, 1499–1512. <https://doi.org/10.1208/s12248-017-0122-4>
- Tsuji, Y., 2005. JunD activates transcription of the human ferritin H gene through an antioxidant response element during oxidative stress. *Oncogene* 24, 7567–7578. <https://doi.org/10.1038/sj.onc.1208901>
- Uetrecht, J., Naisbitt, D.J., 2013. Idiosyncratic Adverse Drug Reactions: Current Concepts. *Pharmacol. Rev.* 65, 779–808. <https://doi.org/10.1124/pr.113.007450>
- Umbricht, C., Sellamuthu, R., Li, S., Kashon, M., Luster, M., Joseph, P., 2010. Blood gene expression markers to detect and distinguish target organ toxicity. *Mol. Cell. Biochem.* 335, 223–234. <https://doi.org/10.1007/s11010-009-0272-5>
- Valadi, H., Ekström, K., Bossios, A., Sjöstrand, M., Lee, J.J., Lötvall, J.O., 2007. Exosome-mediated transfer of mRNAs and microRNAs is a novel mechanism of genetic exchange between cells. *Nat. Cell Biol.* 9, 654–659. <https://doi.org/10.1038/ncb1596>
- van der Linden, S.C., von Bergh, A.R.M., van Vught-Lussenburg, B.M.A., Jonker, L.R.A., Teunis, M., Krul, C.A.M., van der Burg, B., 2014. Development of a panel of high-throughput reporter-gene assays to detect genotoxicity and oxidative stress. *Mutat. Res. Toxicol. Environ. Mutagen.* 760, 23–32. <https://doi.org/10.1016/j.mrgentox.2013.09.009>
- van Erk, M.J., Blom, W.A.M., van Ommen, B., Hendriks, H.F.J., 2006. High-protein and high-carbohydrate breakfasts differentially change the transcriptome of human blood cells. *Am. J. Clin. Nutr.* 84, 1233–1241.
- Vandeputte, C., Guizon, I., Genestie-Denis, I., Vannier, B., Lorenzon, G., 1994. A microtiter plate assay for total glutathione and glutathione disulfide contents in cultured/isolated cells: performance study of a new miniaturized protocol. *Cell Biol. Toxicol.* 10, 415–421.
- Vasquez, K.O., Peterson, J.D., 2017. Early Detection of Acute Drug-Induced Liver Injury in Mice by Noninvasive Near-Infrared Fluorescence Imaging. *J. Pharmacol. Exp. Ther.* 361, 87–98. <https://doi.org/10.1124/jpet.116.238378>
- Velayutham, M., Villamena, F.A., Fishbein, J.C., Zweier, J.L., 2005. Cancer chemopreventive oltipraz generates superoxide anion radical. *Arch. Biochem. Biophys.* 435, 83–88. <https://doi.org/10.1016/j.abb.2004.11.028>
- Venugopal, R., Jaiswal, A.K., 1996. Nrf1 and Nrf2 positively and c-Fos and Fra1 negatively regulate the human antioxidant response element-mediated expression of NAD(P)H:quinone oxidoreductase1 gene. *Proc. Natl. Acad. Sci. U. S. A.* 93, 14960–14965.
- Vinken, M., 2013. The adverse outcome pathway concept: A pragmatic tool in toxicology. *Toxicology* 312, 158–165. <https://doi.org/10.1016/j.tox.2013.08.011>
- Vinken, M., Landesmann, B., Goumenou, M., Vinken, S., Shah, I., Jaeschke, H., Willett, C., Whelan, M., Rogiers, V., 2013. Development of an adverse outcome pathway from drug-mediated bile salt export pump inhibition to cholestatic liver injury. *Toxicol. Sci. Off. J. Soc. Toxicol.* 136, 97–106. <https://doi.org/10.1093/toxsci/kft177>
- Vivekananthan, D.P., Penn, M.S., Sapp, S.K., Hsu, A., Topol, E.J., 2003. Use of antioxidant vitamins for the prevention of cardiovascular disease: meta-analysis of randomised trials. *Lancet Lond. Engl.* 361, 2017–2023. [https://doi.org/10.1016/S0140-6736\(03\)13637-9](https://doi.org/10.1016/S0140-6736(03)13637-9)
- Wakabayashi, N., Itoh, K., Wakabayashi, J., Motohashi, H., Noda, S., Takahashi, S., Imakado, S., Kotsuji, T., Otsuka, F., Roop, D.R., Harada, T., Engel, J.D., Yamamoto, M., 2003. Keap1-null mutation leads to postnatal lethality due to constitutive Nrf2 activation. *Nat. Genet.* 35, 238–245. <https://doi.org/10.1038/ng1248>
- Wakabayashi, N., Skoko, J.J., Chartoumpekis, D.V., Kimura, S., Slocum, S.L., Noda, K., Palliyaguru, D.L., Fujimuro, M., Boley, P.A., Tanaka, Y., Shigemura, N., Biswal, S., Yamamoto, M., Kensler, T.W., 2014. Notch-Nrf2 axis: regulation of Nrf2 gene

- expression and cytoprotection by notch signaling. *Mol. Cell. Biol.* 34, 653–663. <https://doi.org/10.1128/MCB.01408-13>
- Walsh, J., Jenkins, R.E., Wong, M., Olayanju, A., Powell, H., Copple, I., O'Neill, P.M., Goldring, C.E.P., Kitteringham, N.R., Park, B.K., 2014. Identification and quantification of the basal and inducible Nrf2-dependent proteomes in mouse liver: Biochemical, pharmacological and toxicological implications. *J. Proteomics* 108, 171–187. <https://doi.org/10.1016/j.jprot.2014.05.007>
- Wang, G.-K., Zhu, J.-Q., Zhang, J.-T., Li, Q., Li, Y., He, J., Qin, Y.-W., Jing, Q., 2010. Circulating microRNA: a novel potential biomarker for early diagnosis of acute myocardial infarction in humans. *Eur. Heart J.* 31, 659–666. <https://doi.org/10.1093/eurheartj/ehq013>
- Wang, K., Yuan, Y., Li, H., Cho, J.-H., Huang, D., Gray, L., Qin, S., Galas, D.J., 2013. The Spectrum of Circulating RNA: A Window into Systems Toxicology. *Toxicol. Sci.* 132, 478–492. <https://doi.org/10.1093/toxsci/kft014>
- Wang, W., Jaiswal, A.K., 2006. Nuclear factor Nrf2 and antioxidant response element regulate NRH:quinone oxidoreductase 2 (NQO2) gene expression and antioxidant induction. *Free Radic. Biol. Med.* 40, 1119–1130. <https://doi.org/10.1016/j.freeradbiomed.2005.10.063>
- Wang, X., Fang, H., Huang, Z., Shang, W., Hou, T., Cheng, A., Cheng, H., 2013. Imaging ROS signaling in cells and animals. *J. Mol. Med. Berl. Ger.* 91, 917–927. <https://doi.org/10.1007/s00109-013-1067-4>
- Wang, X., Tomso, D.J., Chorley, B.N., Cho, H.-Y., Cheung, V.G., Kleeberger, S.R., Bell, D.A., 2007. Identification of polymorphic antioxidant response elements (AREs) in the human genome. *Hum. Mol. Genet.* 16, 1188–1200. <https://doi.org/10.1093/hmg/ddm066>
- Wang, X.J., Hayes, J.D., Wolf, C.R., 2006. Generation of a stable antioxidant response element-driven reporter gene cell line and its use to show redox-dependent activation of nrf2 by cancer chemotherapeutic agents. *Cancer Res.* 66, 10983–10994. <https://doi.org/10.1158/0008-5472.CAN-06-2298>
- Wang, Y., Xiao, L., Thiagalingam, A., Nelkin, B.D., Casero, R.A., 1998. The identification of a cis-element and a trans-acting factor involved in the response to polyamines and polyamine analogues in the regulation of the human spermidine/spermine N1-acetyltransferase gene transcription. *J. Biol. Chem.* 273, 34623–34630.
- Warabi, E., Wada, Y., Kajiwara, H., Kobayashi, M., Koshihara, N., Hisada, T., Shibata, M., Ando, J., Tsuchiya, M., Kodama, T., Noguchi, N., 2004. Effect on endothelial cell gene expression of shear stress, oxygen concentration, and low-density lipoprotein as studied by a novel flow cell culture system. *Free Radic. Biol. Med.* 37, 682–694. <https://doi.org/10.1016/j.freeradbiomed.2004.05.020>
- Ward, J., Kanchagar, C., Veksler-Lublinsky, I., Lee, R.C., McGill, M.R., Jaeschke, H., Curry, S.C., Ambros, V.R., 2014. Circulating microRNA profiles in human patients with acetaminophen hepatotoxicity or ischemic hepatitis. *Proc. Natl. Acad. Sci.* 111, 12169–12174. <https://doi.org/10.1073/pnas.1412608111>
- Wasserman, W.W., Fahl, W.E., 1997. Functional antioxidant responsive elements. *Proc. Natl. Acad. Sci. U. S. A.* 94, 5361–5366.
- Wasserman, W.W., Fahl, W.E., 1997. Functional antioxidant responsive elements. *Proc. Natl. Acad. Sci. U. S. A.* 94, 5361–5366.
- Watai, Y., Kobayashi, A., Nagase, H., Mizukami, M., McEvoy, J., Singer, J.D., Itoh, K., Yamamoto, M., 2007. Subcellular localization and cytoplasmic complex status of endogenous Keap1. *Genes Cells Devoted Mol. Cell. Mech.* 12, 1163–1178. <https://doi.org/10.1111/j.1365-2443.2007.01118.x>
- Watanabe, T., Tahara, M., Todo, S., 2008. The novel antioxidant edaravone: from bench to bedside. *Cardiovasc. Ther.* 26, 101–114. <https://doi.org/10.1111/j.1527-3466.2008.00041.x>
- Wayner, D. d. m., Burton, G. w., Ingold, K. u., Locke, S., 1985. Quantitative measurement of the total, peroxy radical-trapping antioxidant capability of human blood plasma by controlled peroxidation. *FEBS Lett.* 187, 33–37. [https://doi.org/10.1016/0014-5793\(85\)81208-4](https://doi.org/10.1016/0014-5793(85)81208-4)
- Weerachayaphorn, J., Cai, S.-Y., Soroka, C.J., Boyer, J.L., 2009. NF-E2-related factor 2 (Nrf2) is a positive regulator of human bile salt export pump (BSEP) expression. *Hepatology* 50, 1588–1596. <https://doi.org/10.1002/hep.23151>
- Wester, K., Jönsson, A.K., Spigset, O., Druid, H., Hägg, S., 2008. Incidence of fatal adverse drug reactions: a population based study. *Br. J. Clin. Pharmacol.* 65, 573–579. <https://doi.org/10.1111/j.1365-2125.2007.03064.x>
- Wetmore, B.A., Brees, D.J., Singh, R., Watkins, P.B., Andersen, M.E., Loy, J., Thomas, R.S., 2010. Quantitative analyses and transcriptomic profiling of circulating messenger RNAs as biomarkers of rat liver injury. *Hepatology* 51, 2127–2139. <https://doi.org/10.1002/hep.23574>
- Williamson, T.P., Amirahmadi, S., Joshi, G., Kaludov, N.K., Martinov, M.N., Johnson, D.A., Johnson, J.A., 2012. Discovery of potent, novel Nrf2 inducers via quantum modeling, virtual screening and in vitro experimental validation. *Chem. Biol. Drug Des.* 80, 810–820. <https://doi.org/10.1111/cbdd.12040>
- Wilmes, A., Crean, D., Aydin, S., Pfaller, W., Jennings, P., Leonard, M.O., 2011. Identification and dissection of the Nrf2 mediated oxidative stress pathway in human renal proximal tubule toxicity. *Toxicol. Vitro Int. J. Publ. Assoc. BIBRA* 25, 613–622. <https://doi.org/10.1016/j.tiv.2010.12.009>
- Wilmes, A., Limonciel, A., Aschauer, L., Moenks, K., Bielow, C., Leonard, M.O., Hamon, J., Carpi, D., Ruzek, S., Handler, A., Schmal, O., Herrgen, K., Bellwon, P., Burek, C., Trusi, G.L., Hewitt, P., Di Consiglio, E., Testai, E., Blaauboer, B.J., Guillou, C., Huber, C.G., Lukas, A., Pfaller, W., Mueller, S.O., Bois, F.Y., Dekant, W., Jennings, P., 2013. Application of integrated transcriptomic, proteomic and metabolomic profiling for the delineation of mechanisms of drug induced cell stress. *J. Proteomics* 79, 180–194. <https://doi.org/10.1016/j.jprot.2012.11.022>
- Wilson, L.A., Gemin, A., Espiritu, R., Singh, G., 2005. ets-1 is transcriptionally up-regulated by H<sub>2</sub>O<sub>2</sub> via an antioxidant response element. *FASEB J.* 19, 2085–2087. <https://doi.org/10.1096/fj.05-4401fje>
- Wink, S., Hiemstra, S., Herpers, B., van de Water, B., 2017. High-content imaging-based BAC-GFP toxicity pathway reporters to assess chemical adversity liabilities. *Arch. Toxicol.* 91, 1367–1383. <https://doi.org/10.1007/s00204-016-1781-0>
- Wink, S., Hiemstra, S., Huppelschoten, S., Danen, E., Niemeijer, M., Hendriks, G., Vrieling, H., Herpers, B., van de Water, B., 2014. Quantitative high content imaging of cellular adaptive stress response pathways in toxicity for chemical safety assessment. *Chem. Res. Toxicol.* 27, 338–355. <https://doi.org/10.1021/tx4004038>
- Wong, M.H.L., Bryan, H.K., Copple, I.M., Jenkins, R.E., Chiu, P.H., Bibby, J., Berry, N.G., Kitteringham, N.R., Goldring, C.E., O'Neill, P.M., Park, B.K., 2016. Design and Synthesis of Irreversible Analogues of Bardoxolone Methyl for the Identification

- of Pharmacologically Relevant Targets and Interaction Sites. *J. Med. Chem.* 59, 2396–2409. <https://doi.org/10.1021/acs.jmedchem.5b01292>
- Woo, H.A., Jeong, W., Chang, T.-S., Park, K.J., Park, S.J., Yang, J.S., Rhee, S.G., 2005. Reduction of cysteine sulfinic acid by sulfiredoxin is specific to 2-cys peroxiredoxins. *J. Biol. Chem.* 280, 3125–3128. <https://doi.org/10.1074/jbc.C400496200>
- Woo, H.A., Yim, S.H., Shin, D.H., Kang, D., Yu, D.-Y., Rhee, S.G., 2010. Inactivation of peroxiredoxin I by phosphorylation allows localized H<sub>2</sub>O<sub>2</sub> accumulation for cell signaling. *Cell* 140, 517–528. <https://doi.org/10.1016/j.cell.2010.01.009>
- WRÓBLEWSKI, F., JERVIS, G., LADUE, J.S., 1956. THE DIAGNOSTIC, PROGNOSTIC AND EPIDEMIOLOGIC SIGNIFICANCE OF SERUM GLUTAMIC OXALOACETIC TRANSAMINASE (SGO-T) ALTERATIONS IN ACUTE HEPATITIS\*. *Ann. Intern. Med.* 45, 782–800. <https://doi.org/10.7326/0003-4819-45-5-782>
- Wrona, M., Patel, K., Wardman, P., 2005. Reactivity of 2',7'-dichlorodihydrofluorescein and dihydrorhodamine 123 and their oxidized forms toward carbonate, nitrogen dioxide, and hydroxyl radicals. *Free Radic. Biol. Med.* 38, 262–270. <https://doi.org/10.1016/j.freeradbiomed.2004.10.022>
- Wu, K.C., McDonald, P.R., Liu, J., Klaassen, C.D., 2014. Screening of Natural Compounds as Activators of the Keap1-Nrf2 Pathway. *Planta Med.* 80, 97–104. <https://doi.org/10.1055/s-0033-1351097>
- Wu, K.C., McDonald, P.R., Liu, J.J., Chaguturu, R., Klaassen, C.D., 2012. Implementation of a High-Throughput Screen for Identifying Small Molecules to Activate the Keap1-Nrf2-ARE Pathway. *PLOS ONE* 7, e44686. <https://doi.org/10.1371/journal.pone.0044686>
- Wu, T., Zhao, F., Gao, B., Tan, C., Yagishita, N., Nakajima, T., Wong, P.K., Chapman, E., Fang, D., Zhang, D.D., 2014. Hrd1 suppresses Nrf2-mediated cellular protection during liver cirrhosis. *Genes Dev.* 28, 708–722. <https://doi.org/10.1101/gad.238246.114>
- Xanthoudakis, S., Miao, G., Wang, F., Pan, Y.C., Curran, T., 1992. Redox activation of Fos-Jun DNA binding activity is mediated by a DNA repair enzyme. *EMBO J.* 11, 3323–3335.
- Xu, J.J., Diaz, D., O'Brien, P.J., 2004. Applications of cytotoxicity assays and pre-lethal mechanistic assays for assessment of human hepatotoxicity potential. *Chem. Biol. Interact.* 150, 115–128. <https://doi.org/10.1016/j.cbi.2004.09.011>
- Yaekashiwa, M., Wang, L.-H., 2003. Nrf2 regulates thromboxane synthase gene expression in human lung cells. *DNA Cell Biol.* 22, 479–487. <https://doi.org/10.1089/10445490360708883>
- Yamamoto, T., Kyo, M., Kamiya, T., Tanaka, T., Engel, J.D., Motohashi, H., Yamamoto, M., 2006. Predictive base substitution rules that determine the binding and transcriptional specificity of Maf recognition elements. *Genes Cells Devoted Mol. Cell. Mech.* 11, 575–591. <https://doi.org/10.1111/j.1365-2443.2006.00965.x>
- Yamashita, S., Masuda, D., Ohama, T., Arai, H., Bujo, H., Kagimura, T., Kita, T., Matsuzaki, M., Saito, Y., Fukushima, M., Matsuzawa, Y., PROSPECTIVE Study Group, 2016. Rationale and Design of the PROSPECTIVE Trial: Probuocol Trial for Secondary Prevention of Atherosclerotic Events in Patients with Prior Coronary Heart Disease. *J. Atheroscler. Thromb.* 23, 746–756. <https://doi.org/10.5551/jat.32813>
- Yang, H., Magilnick, N., Lee, C., Kalmaz, D., Ou, X., Chan, J.Y., Lu, S.C., 2005. Nrf1 and Nrf2 Regulate Rat Glutamate-Cysteine Ligase Catalytic Subunit Transcription Indirectly via NF-κB and AP-1. *Mol. Cell. Biol.* 25, 5933–5946. <https://doi.org/10.1128/MCB.25.14.5933-5946.2005>
- Yazdani, M., 2015. Concerns in the application of fluorescent probes DCDHF-DA, DHR 123 and DHE to measure reactive oxygen species in vitro. *Toxicol. Vitro Int. J. Publ. Assoc. BIBRA* 30, 578–582. <https://doi.org/10.1016/j.tiv.2015.08.010>
- Yeager, R.L., Reisman, S.A., Aleksunes, L.M., Klaassen, C.D., 2009. Introducing the “TCDD-Inducible AhR-Nrf2 Gene Battery.” *Toxicol. Sci.* 111, 238–246. <https://doi.org/10.1093/toxsci/kfp115>
- Yoshino, Y., Ishioka, C., 2015. Inhibition of glycogen synthase kinase-3 beta induces apoptosis and mitotic catastrophe by disrupting centrosome regulation in cancer cells. *Sci. Rep.* 5, 13249. <https://doi.org/10.1038/srep13249>
- Yu, Y., Huang, X., Zhang, J., Liu, J., Hu, Y., Yang, Y., Cai, J., Huang, Y., Qin, Q., 2016. Fish TRIM16L exerts negative regulation on antiviral immune response against grouper iridoviruses. *Fish Shellfish Immunol.* 59, 256–267. <https://doi.org/10.1016/j.fsi.2016.10.044>
- Yuan, X., Xu, C., Pan, Z., Keum, Y.-S., Kim, J.-H., Shen, G., Yu, S., Oo, K.T., Ma, J., Kong, A.-N.T., 2006. Butylated hydroxyanisole regulates ARE-mediated gene expression via Nrf2 coupled with ERK and JNK signaling pathway in HepG2 cells. *Mol. Carcinog.* 45, 841–850. <https://doi.org/10.1002/mc.20234>
- Yueh, M.-F., Tukey, R.H., 2007. Nrf2-Keap1 signaling pathway regulates human UGT1A1 expression in vitro and in transgenic UGT1 mice. *J. Biol. Chem.* 282, 8749–8758. <https://doi.org/10.1074/jbc.M610790200>
- Zhang, D.D., Hannink, M., 2003. Distinct Cysteine Residues in Keap1 Are Required for Keap1-Dependent Ubiquitination of Nrf2 and for Stabilization of Nrf2 by Chemopreventive Agents and Oxidative Stress. *Mol. Cell. Biol.* 23, 8137–8151. <https://doi.org/10.1128/MCB.23.22.8137-8151.2003>
- Zhang, D.D., Lo, S.-C., Cross, J.V., Templeton, D.J., Hannink, M., 2004. Keap1 Is a Redox-Regulated Substrate Adaptor Protein for a Cul3-Dependent Ubiquitin Ligase Complex. *Mol. Cell. Biol.* 24, 10941–10953. <https://doi.org/10.1128/MCB.24.24.10941-10953.2004>
- Zhang, D.D., Lo, S.-C., Sun, Z., Habib, G.M., Lieberman, M.W., Hannink, M., 2005. Ubiquitination of Keap1, a BTB-Kelch Substrate Adaptor Protein for Cul3, Targets Keap1 for Degradation by a Proteasome-independent Pathway. *J. Biol. Chem.* 280, 30091–30099. <https://doi.org/10.1074/jbc.M501279200>
- Zhang, J., Goering, P.L., Espandiari, P., Shaw, M., Bonventre, J.V., Vaidya, V.S., Brown, R.P., Keenan, J., Kilty, C.G., Sadrieh, N., Hanig, J.P., 2009. Differences in Immunolocalization of Kim-1, RPA-1, and RPA-2 in Kidneys of Gentamicin-, Cisplatin-, and Valproic Acid-Treated Rats: Potential Role of iNOS and Nitrotyrosine. *Toxicol. Pathol.* 37, 629–643. <https://doi.org/10.1177/0192623309339605>
- Zhang, L., Bushel, P.R., Chou, J., Zhou, T., Watkins, P.B., 2012. Identification of Identical Transcript Changes in Liver and Whole Blood during Acetaminophen Toxicity. *Front. Genet.* 3. <https://doi.org/10.3389/fgene.2012.00162>
- Zhang, W., Feng, J.Q., Harris, S.E., Contag, P.R., Stevenson, D.K., Contag, C.H., 2001a. Rapid in vivo functional analysis of transgenes in mice using whole body imaging of luciferase expression. *Transgenic Res.* 10, 423–434.

- Zhang, W., Feng, J.Q., Harris, S.E., Contag, P.R., Stevenson, D.K., Contag, C.H., 2001b. Rapid in vivo functional analysis of transgenes in mice using whole body imaging of luciferase expression. *Transgenic Res.* 10, 423–434.
- Zhang, Y., Talalay, P., Cho, C.G., Posner, G.H., 1992. A major inducer of anticarcinogenic protective enzymes from broccoli: isolation and elucidation of structure. *Proc. Natl. Acad. Sci.* 89, 2399–2403.
- Zhao, F., Wu, T., Lau, A., Jiang, T., Huang, Z., Wang, X.-J., Chen, W., Wong, P.K., Zhang, D.D., 2009. Nrf2 promotes neuronal cell differentiation. *Free Radic. Biol. Med.* 47, 867–879. <https://doi.org/10.1016/j.freeradbiomed.2009.06.029>
- Zhong, X.Y., Holzgreve, W., Huang, D.J., 2008. Isolation of Cell-Free RNA from Maternal Plasma, in: *Prenatal Diagnosis, Methods in Molecular Biology™*. Humana Press, pp. 269–273. [https://doi.org/10.1007/978-1-59745-066-9\\_21](https://doi.org/10.1007/978-1-59745-066-9_21)
- Ziegler, D., Nowak, H., Kempler, P., Vargha, P., Low, P.A., 2004. Treatment of symptomatic diabetic polyneuropathy with the antioxidant alpha-lipoic acid: a meta-analysis. *Diabet. Med. J. Br. Diabet. Assoc.* 21, 114–121.
- Zou, W., Liu, X., Yue, P., Zhou, Z., Sporn, M.B., Lotan, R., Khuri, F.R., Sun, S.-Y., 2004. c-Jun NH2-terminal kinase-mediated up-regulation of death receptor 5 contributes to induction of apoptosis by the novel synthetic triterpenoid methyl-2-cyano-3,12-dioxooleana-1,9-dien-28-oate in human lung cancer cells. *Cancer Res.* 64, 7570–7578. <https://doi.org/10.1158/0008-5472.CAN-04-1238>
- Zweier, J.L., Kuppusamy, P., Lutty, G.A., 1988. Measurement of endothelial cell free radical generation: evidence for a central mechanism of free radical injury in postischemic tissues. *Proc. Natl. Acad. Sci.* 85, 4046–4050.



## Appendix

**Table A1 Putative NRF2-regulated gene bioinformatic analysis**

Green = Genes identified for further analysis (- = not measured in dataset, \* = not present in top 1000 genes upregulated by drug).

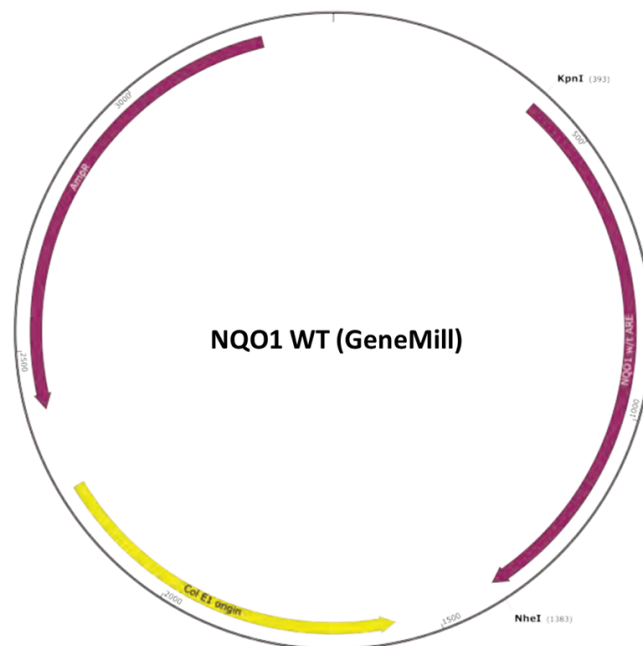
Gene symbol	Gene description	Average mRNA level						
		+ siNRF2 in PHH (% siCON)	+ siKEAP1 in PHH (% siCON)	+ siNRF2 (% Non-targeting siRNA) (Singh et al., 2013)	+ siKEAP1 (% Non-targeting siRNA) (Agyeman et al., 2012)	+ sulforaphane (% vehicle) (Agyeman et al., 2012)	+ 200 µM BHA dose (% vehicle) (Igarashi et al., 2014)	+ 1500 µM DEM dose (% vehicle) (Igarashi et al., 2014)
<i>F2RL2</i>	Coagulation factor II (thrombin) receptor-like 2 (F2RL2), transcript variant 1, mRNA [NM_004101]	6%	1828%	15%	603%	4858%	175%	1532%
<i>LOC344887</i>	NmrA-like family domain containing 1 pseudogene (LOC344887), non-coding RNA [NR_033752]	13%	1714%	15%	11815%	7225%	256%	271%
<i>AKR1B15</i>	Aldo-keto reductase family 1, member B15 (AKR1B15), mRNA [NM_001080538]	20%	1215%	-	-	-	*	*
<i>NQO1</i>	NAD(P)H dehydrogenase, quinone 1 (NQO1), transcript variant 1, mRNA [NM_000903]	26%	550%	38%	699%	517%	200%	154%
<i>ALDH3A1</i>	Aldehyde dehydrogenase 3 family, member A1 (ALDH3A1), transcript variant 2, mRNA [NM_000691]	27%	431%	16%	2761%	482%	*	*
<i>AKR1CL1</i>	Aldo-keto reductase family 1, member C-like 1 (AKR1CL1), non-coding RNA [NR_027916]	33%	199%	-	-	-	*	*
<i>TRIM16L</i>	Tripartite motif containing 16-like (TRIM16L), mRNA [NM_001037330]	40%	372%	91%	327%	556%	123%	*
<i>PANX2</i>	Pannexin 2 (PANX2), transcript variant 1, mRNA [NM_052839]	41%	241%	86%	180%	962%	189%	133%
<i>THC2521366</i>	Unknown	41%	214%	-	-	-	142%	*
<i>LUCAT1</i>	Lung cancer associated transcript 1 (non-protein coding) [Source:HGNC Symbol;Acc:48498] [ENST00000513626]	45%	700%	-	-	-	*	*
<i>EID3</i>	EP300 interacting inhibitor of differentiation 3 (EID3), mRNA [NM_001008394]	46%	263%	63%	528%	802%	237%	407%
<i>LOC101927592</i>	Uncharacterized LOC101927592 (LOC101927592), long non-coding RNA [NR_104646]	46%	404%	94%	109%	135%	*	*
<i>UGDH</i>	UDP-glucose 6-dehydrogenase (UGDH), transcript variant 1, mRNA [NM_003359]	49%	185%	75%	196%	324%	*	*
<i>MAP2</i>	Microtubule-associated protein 2 (MAP2), transcript variant 1, mRNA [NM_002374]	49%	286%	14%	614%	6073%	*	*
<i>GSTA7P</i>	Glutathione S-transferase alpha 7, pseudogene (GSTA7P), non-coding RNA [NR_033760]	49%	260%	-	-	-	*	*
<i>AKR1C4</i>	Aldo-keto reductase family 1, member C4 (AKR1C4), mRNA [NM_001818]	50%	172%	67%	80%	86%	*	*
<i>AFP</i>	Alpha-fetoprotein (AFP), mRNA [NM_001134]	50%	176%	70%	144%	105%	*	191%
<i>XLOC_014512</i>	linc BROAD Institute lincRNA (XLOC_014512), lincRNA [TCONS_ID_00013854]	50%	169%	-	-	-	247%	*
<i>FAM223A</i>	Family with sequence similarity 223, member A (non-protein coding) (FAM223A), long non-coding RNA [NR_027401]	50%	184%	95%	-	-	163%	*
<i>A_33_P3328284</i>	Unknown	51%	181%	-	-	-	*	*
<i>BTBD11</i>	Family with sequence similarity 162, member A (FAM162A), mRNA [NM_014367]	54%	255%	65%	92%	118%	276%	*
<i>ALDH1A1</i>	Aldehyde dehydrogenase 1 family, member A1 (ALDH1A1), mRNA [NM_000689]	54%	196%	101%	49%	63%	*	*
<i>LOC101927136</i>	Uncharacterized LOC101927136 (LOC101927136), long non-coding RNA [NR_110840]	54%	204%	-	-	-	*	*
<i>SLCO1B1</i>	Solute carrier organic anion transporter family, member 1B1 (SLCO1B1), mRNA [NM_006446]	56%	162%	100%	98%	98%	*	*
<i>IKBKG</i>	Inhibitor of kappa light polypeptide gene enhancer in B-cells, kinase gamma (IKBKG), transcript variant 3, mRNA [NM_003639]	57%	145%	93%	312%	428%	298%	141%
<i>ENST00000449602</i>	Q8HCZ3_PT1PL (Q8HCZ3) Nicotinamide dehydrogenase subunit 2	59%	179%	-	-	-	*	*

	(Fragment), partial (5%) [THC2646287]							
<b>SRXN1</b>	<b>Sulfiredoxin 1 (SRXN1), mRNA [NM_080725]</b>	<b>59%</b>	<b>264%</b>	<b>26%</b>	<b>425%</b>	<b>706%</b>	<b>360%</b>	<b>343%</b>
<i>LOC101927258</i>	Uncharacterized LOC101927258 (LOC101927258), transcript variant X2, ncRNA [XR_426391]	59%	163%	-	-	-	*	*
<i>SPP1</i>	Secreted phosphoprotein 1 (SPP1), transcript variant 1, mRNA [NM_001040058]	59%	172%	34%	556%	1576%	320%	237%
<i>SFN</i>	Stratifin (SFN), mRNA [NM_006142]	60%	323%	31%	181%	312%	129%	167%
<i>LOC101927171</i>	Uncharacterized LOC101927171 (RP11-345L23.1), ncRNA [XR_242040]	62%	137%	-	-	-	*	*
<i>SULT1A2</i>	Sulfotransferase family, cytosolic, 1A, phenol-preferring, member 2 (SULT1A2), transcript variant 2, mRNA [NM_177528]	62%	168%	97%	238%	528%	*	*
<i>MROH2A</i>	Maestro heat-like repeat family member 2A (MROH2A), mRNA [NM_001287395]	65%	194%	88%	106%	101%	*	*
<i>ALDH1L1</i>	Aldehyde dehydrogenase 1 family, member L1 (ALDH1L1), transcript variant 2, mRNA [NM_012190]	65%	187%	93%	125%	90%	168%	*
<i>DKK3</i>	Dickkopf WNT signaling pathway inhibitor 3 (DKK3), transcript variant 1, mRNA [NM_015881]	65%	142%	93%	111%	575%	*	*
<i>MLLT11</i>	Myeloid/lymphoid or mixed-lineage leukemia (trithorax homolog, Drosophila); translocated to, 11 (MLLT11), mRNA [NM_006818]	65%	182%	53%	238%	213%	209%	180%
<i>BHMT2</i>	Betaine--homocysteine S-methyltransferase 2 (BHMT2), transcript variant 1, mRNA [NM_017614]	66%	134%	94%	97%	95%	147%	*
<i>ZDHHC18</i>	Zinc finger, DHHC-type containing 18 (ZDHHC18), mRNA [NM_032283]	66%	178%	79%	202%	176%	*	287%
<i>CCND1</i>	Cyclin D1 (CCND1), mRNA [NM_053056]	67%	146%	60%	96%	253%	*	*
<i>ENST00000479830</i>	Uncharacterized LOC101928885 (RP11-141O11.2), transcript variant X1, ncRNA [XR_241811]	67%	194%	-	-	-	*	*
<i>ENST00000430247</i>	Uncharacterized LOC102724420 (LOC102724420), ncRNA [XR_425263]	67%	150%	-	-	-	*	*
<i>L3HYPDH</i>	L-3-hydroxyproline dehydratase (trans-) (L3HYPDH), mRNA [NM_144581]	67%	151%	66%	179%	263%	*	*
<i>ADHFE1</i>	Alcohol dehydrogenase, iron containing, 1 (ADHFE1), mRNA [NM_144650]	69%	171%	99%	274%	934%	256%	*
<i>MYEOV</i>	Myeloma overexpressed (MYEOV), transcript variant 2, mRNA [NM_138768]	69%	156%	47%	104%	103%	*	*
<i>ABHD4</i>	Abhydrolase domain containing 4 (ABHD4), mRNA [NM_022060]	69%	173%	65%	263%	565%	234%	182%
<i>CES5A</i>	Carboxylesterase 5A (CES5A), transcript variant 2, mRNA [NM_145024]	70%	180%	103%	92%	122%	*	*
<i>ITGA7</i>	Integrin, alpha 7 (ITGA7), transcript variant 2, mRNA [NM_002206]	70%	230%	86%	126%	217%	148%	*
<i>LOC100505985</i>	Uncharacterized LOC100505985 (LOC100505985), ncRNA [XR_108661]	71%	196%	-	-	-	*	226%
<i>CNTNAP3B</i>	Contactin associated protein-like 3B (CNTNAP3B), mRNA [NM_001201380]	72%	136%	-	-	-	182%	*
<i>KYNU</i>	Kynureninase (KYNU), transcript variant 2, mRNA [NM_001032998]	72%	163%	40%	368%	493%	402%	191%
<i>LOC102723323</i>	Uncharacterized LOC102723323 (LOC102723323), ncRNA [XR_424702]	72%	152%	-	-	-	*	*
<i>SLC48A1</i>	Solute carrier family 48 (haem transporter), member 1 (SLC48A1), mRNA [NM_017842]	74%	148%	76%	141%	324%	*	*
<i>ENST00000479351</i>	Contactin associated protein-like 3B (CNTNAP3) [Source:HGNC Symbol;Acc:32035] [ENST00000479351]	74%	144%	-	-	-	*	*
<i>GBE1</i>	Glucan (1,4-alpha-), branching enzyme 1 (GBE1), mRNA [NM_000158]	76%	154%	94%	105%	354%	164%	*
<i>CCAT1</i>	Colon cancer associated transcript 1 (non-protein coding) (CCAT1), long non-coding RNA [NR_108049]	76%	158%	-	127%	115%	*	*
<i>SULT1A4</i>	Sulfotransferase family, cytosolic, 1A, phenol-preferring, member 4 (SULT1A4), mRNA [NM_001017390]	76%	162%	100%	-	-	*	*
<i>ENST00000521815</i>	Cancer susceptibility candidate 19 (non-protein coding) [Source:HGNC Symbol;Acc:49476] [ENST00000521815]	77%	148%	-	-	-	*	*
<i>MPP3</i>	Membrane protein, palmitoylated 3 (MAGUK p55 subfamily member 3) (MPP3), transcript variant 1, mRNA [NM_001932]	77%	145%	82%	149%	317%	118%	*
<i>CDC14B</i>	Cell division cycle 14B (CDC14B), transcript variant 2, mRNA [NM_033331]	78%	138%	85%	106%	177%	175%	265%
<i>GSTA5</i>	Glutathione S-transferase alpha 5 (GSTA5), mRNA [NM_153699]	78%	180%	-	173%	297%	*	*
<i>AOC3</i>	Amine oxidase, copper containing 3 (AOC3), transcript variant 1, mRNA [NM_003734]	78%	123%	101%	89%	450%	*	198%
<i>OTOS</i>	Otopiralin (OTOS), mRNA [NM_148961]	78%	130%	99%	88%	132%	*	*
<i>CES1P2</i>	Carboxylesterase 1 pseudogene 2 (CES1P2), non-coding RNA [NR_033740]	79%	156%	-	-	-	187%	137%

<i>ALDH3A2</i>	Aldehyde dehydrogenase 3 family, member A2 (ALDH3A2), transcript variant 1, mRNA [NM_001031806]	79%	147%	48%	196%	144%	*	*
<i>TDRD6</i>	Tudor domain containing 6 (TDRD6), transcript variant 1, mRNA [NM_001010870]	81%	125%	92%	130%	130%	*	*
<i>NLN</i>	Neurolysin (metallopeptidase M3 family) (NLN), mRNA [NM_020726]	81%	134%	51%	160%	148%	116%	*
<i>NRG1</i>	Neuregulin 1 (NRG1), transcript variant HRG-gamma, mRNA [NM_004495]	81%	129%	46%	133%	791%	393%	150%
<i>AADAC</i>	Arylacetamide deacetylase (AADAC), mRNA [NM_001086]	82%	117%	100%	85%	96%	162%	*
<i>SFXN5</i>	Sideroflexin 5 (SFXN5), mRNA [NM_144579]	82%	119%	88%	175%	120%	*	*
<i>SCCPDH</i>	Saccharopine dehydrogenase (putative) (SCCPDH), mRNA [NM_016002]	82%	135%	100%	121%	124%	156%	*
<i>FAM162A</i>	Family with sequence similarity 162, member A (FAM162A), mRNA [NM_014367]	83%	116%	98%	123%	57%	117%	*
<i>CUTC</i>	CutC copper transporter (CUTC), mRNA [NM_015960]	83%	129%	57%	134%	116%	194%	*
<i>TCEB3</i>	Transcription elongation factor B (SIII), polypeptide 3 (110kDa, elongin A) (TCEB3), mRNA [NM_003198]	84%	126%	73%	107%	126%	124%	271%
<i>SLC22A3</i>	Solute carrier family 22 (organic cation transporter), member 3 [Source:HGNC Symbol;Acc:10967] [ENST00000392145]	84%	120%	99%	96%	64%	*	*
<i>ENST00000594829</i>	Uncharacterized protein [ENST00000594829]	85%	117%	-	-	-	*	*
<i>LOC100506922</i>	Basic proline-rich protein-like (LOC100506922), mRNA [XM_005263848]	86%	120%	41%	-	-	*	*
<i>ICK</i>	Intestinal cell (MAK-like) kinase (ICK), transcript variant 2, mRNA [NM_016513]	86%	114%	104%	204%	97%	*	*
<i>PPARA</i>	Peroxisome proliferator-activated receptor alpha (PPARA), transcript variant 5, mRNA [NM_005036]	88%	119%	93%	218%	392%	203%	182%
<i>OR5T3</i>	Olfactory receptor family 5 subfamily T member 3 (OR5T3), mRNA [NM_001004747.1]	104%	102%	-	-	-	*	*

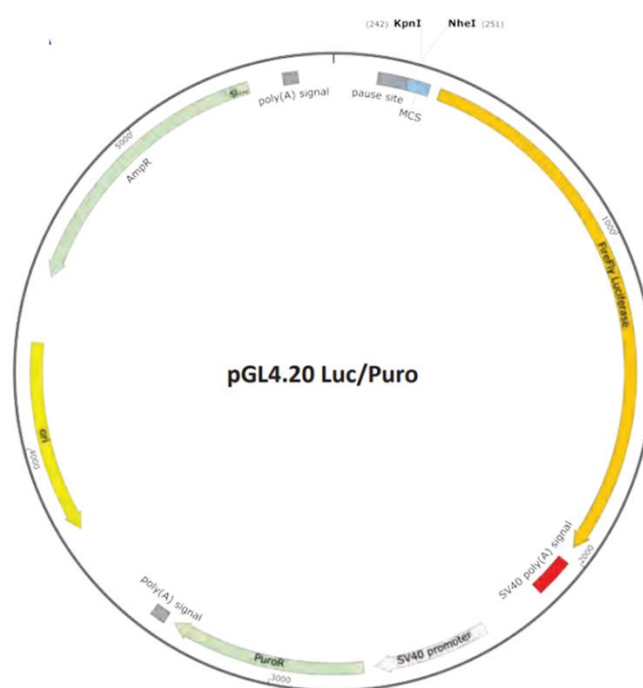
**Figure A1 NQO1 WT GeneMill plasmid map**

Plasmid map of NQO1 WT, a representative construct from GeneMill.



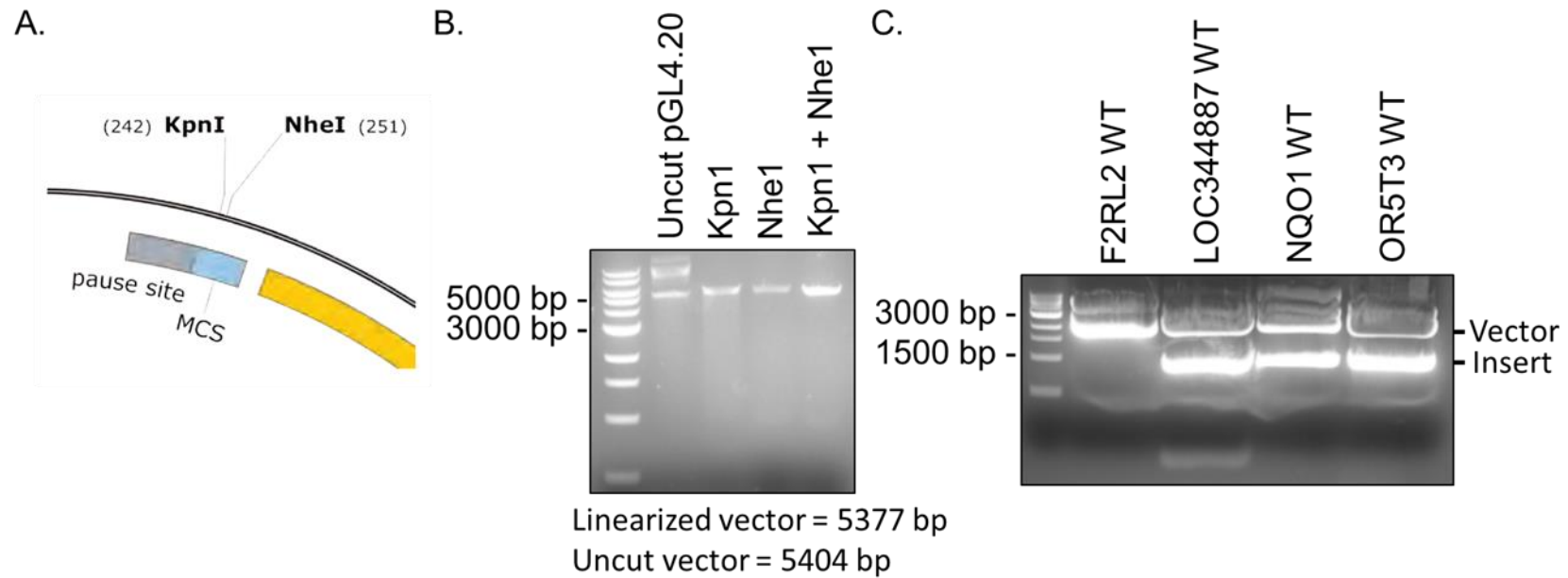
**Figure A2 pGL4.20 plasmid map**

Plasmid map of pGL4.20 Luc/Puro vector.



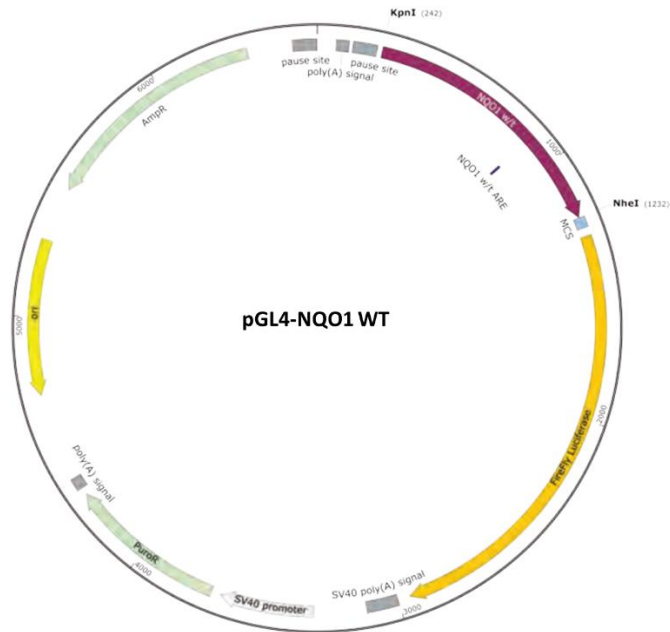
**Figure A3 Sub-cloning promoter regions into the pGL4.20 vector**

(A) Multiple cloning site (MCS) of pGL4.20 and (B) a gel to show digestion of the vector with Kpn1 and Nhe1. (C) Removal of promoter inserts from GeneMill constructs following restriction digest with the enzymes Kpn1 and Nhe1



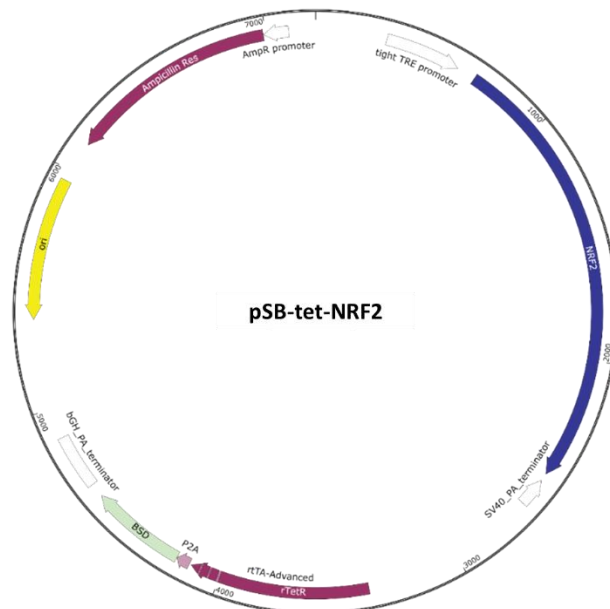
**Figure A4 NQO1 WT GeneMill plasmid map**

Final promoter-reporter plasmid following insertion into pGL4.20. Location of the ARE highlighted blue.



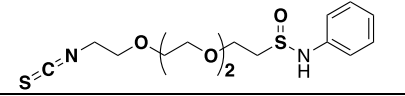
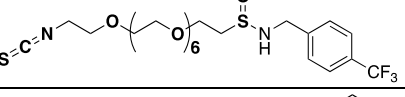
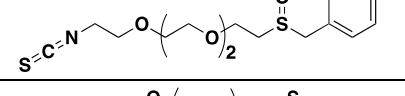
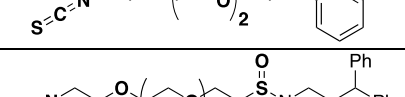
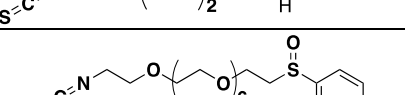
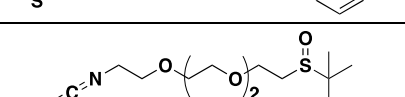
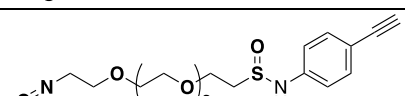
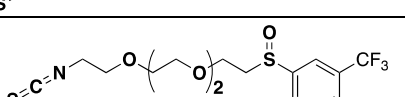
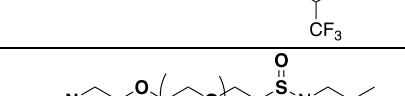
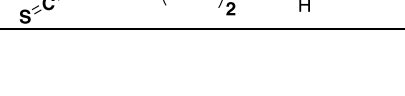
**Figure A5 pSB-tet-Nrf2 plasmid map**

Map of the inducible Nrf2 over-expression plasmid pSB-tet-Nrf2.

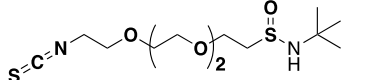
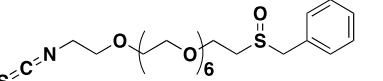
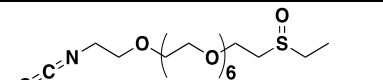
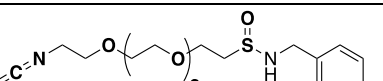
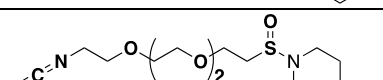
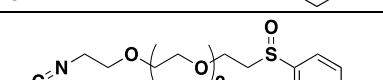
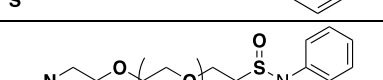
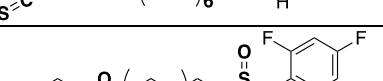
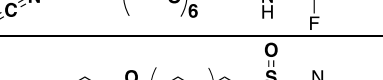


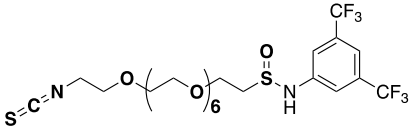
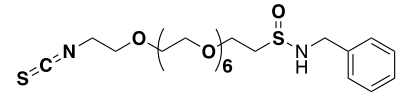
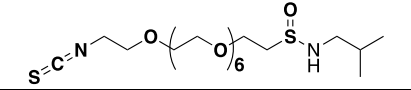
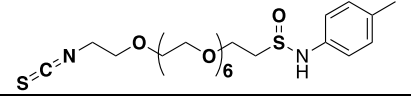
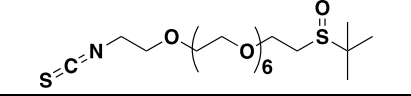
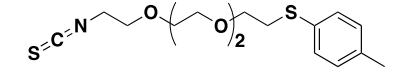
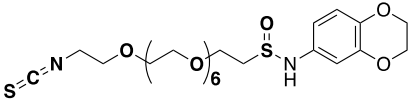
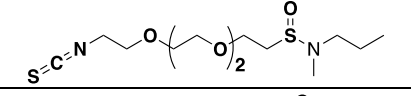
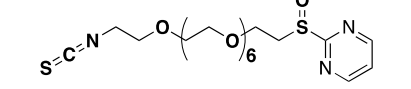
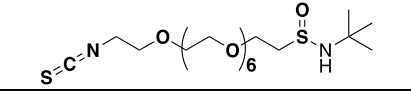
**Table A2 Summary of EVGEN analogue potencies**

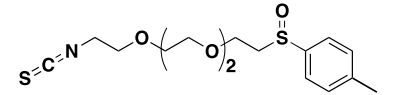
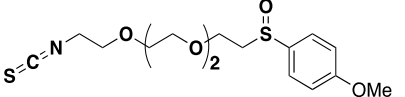
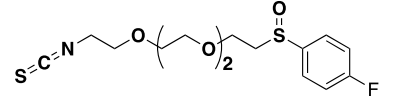
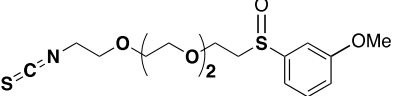
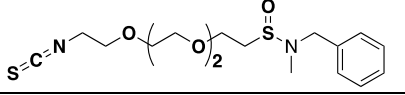
Evgen ID	Compound Structure	Compound Name	CD ( $\mu\text{M}$ )	SD ( $\mu\text{M}$ )
EVG01 (sulforaphane)		1-isothiocyanato-4-(methylsulfinyl)butane	1.45	0.24
EVG02		1-isothiocyanato-2-(2-(2-(methylsulfinyl)ethoxy)ethoxy)ethane	5.49	2.28
EVG14		1-isothiocyanato-23-(methylsulfinyl)-3,6,9,12,15,18,21-heptaoxatricosane	11.04	2.31
EVG22		1-isothiocyanato-23-(o-trifluoromethyl-phenylsulfinyl)-3,6,9,12,15,18,21-heptaoxatricosane	11.14	0.48
EVG09		1-isothiocyanato-11-(pyridine-2-sulfinyl)-3,6,9-trioxaundecane	11.27	0.45
EVG25		N-(isopentyl)-N-(methyl)-11-isothiocyanato-3,6,9-trioxaundecane-1-sulfinamide	11.78	6.24
EVG03		1-isothiocyanato-11-(butylsulfinyl)-3,6,9-trioxaundecane	11.94	3.46
EVG18		1-isothiocyanato-23-(p-tolylsulfinyl)-3,6,9,12,15,18,21-heptaoxatricosane	12.33	1.42
EVG13		1-isothiocyanato-11-(1,1,1-trifluoromethyl-ethanesulfinyl)-3,6,9-trioxaundecane	12.47	1.00
EVG23		1-isothiocyanato-23-(3,5-bis-trifluoromethyl-phenylsulfinyl)-3,6,9,12,15,18,21-heptaoxatricosane	12.88	1.96

EVG32		11-isothiocyanato-N-(phenyl)-3,6,9-trioxaundecane-1-sulfinamide	13.27	3.63
EVG42		23-isothiocyanato-N-(4-trifluoromethylbenzyl)-3,6,9,12,15,18,21-heptaotricosane-1-sulfinamide	13.46	1.77
EVG05		1-isothiocyanato-11-(benzylsulfinyl)-3,6,9-trioxaundecane	13.90	5.57
EVG06a		1-isothiocyanato-11-(thiophenyl)-3,6,9-trioxaundecane	14.13	4.67
EVG24		<i>N</i> -(isopentyl)-11-isothiocyanato-3,6,9-trioxaundecane-1-sulfinamide	14.29	2.81
EVG17		1-isothiocyanato-23-(phenylsulfinyl)-3,6,9,12,15,18,21-heptaotricosane	14.32	4.05
EVG04		1-isothiocyanato-11-(tert-butylsulfinyl)-3,6,9-trioxaundecane	14.80	8.36
EVG37		<i>N</i> -(4-ethynylphenyl)-23-isothiocyanato-3,6,9,12,15,18,21-heptaotricosane-1-sulfinamide	15.17	7.44
EVG10		1-isothiocyanato-11-(3,5-bis-trifluoromethyl-phenylsulfinyl)-3,6,9-trioxaundecane	15.56	2.36
EVG27		11-isothiocyanato-N-(propyl)-3,6,9-trioxaundecane-1-sulfinamide	18.54	5.97



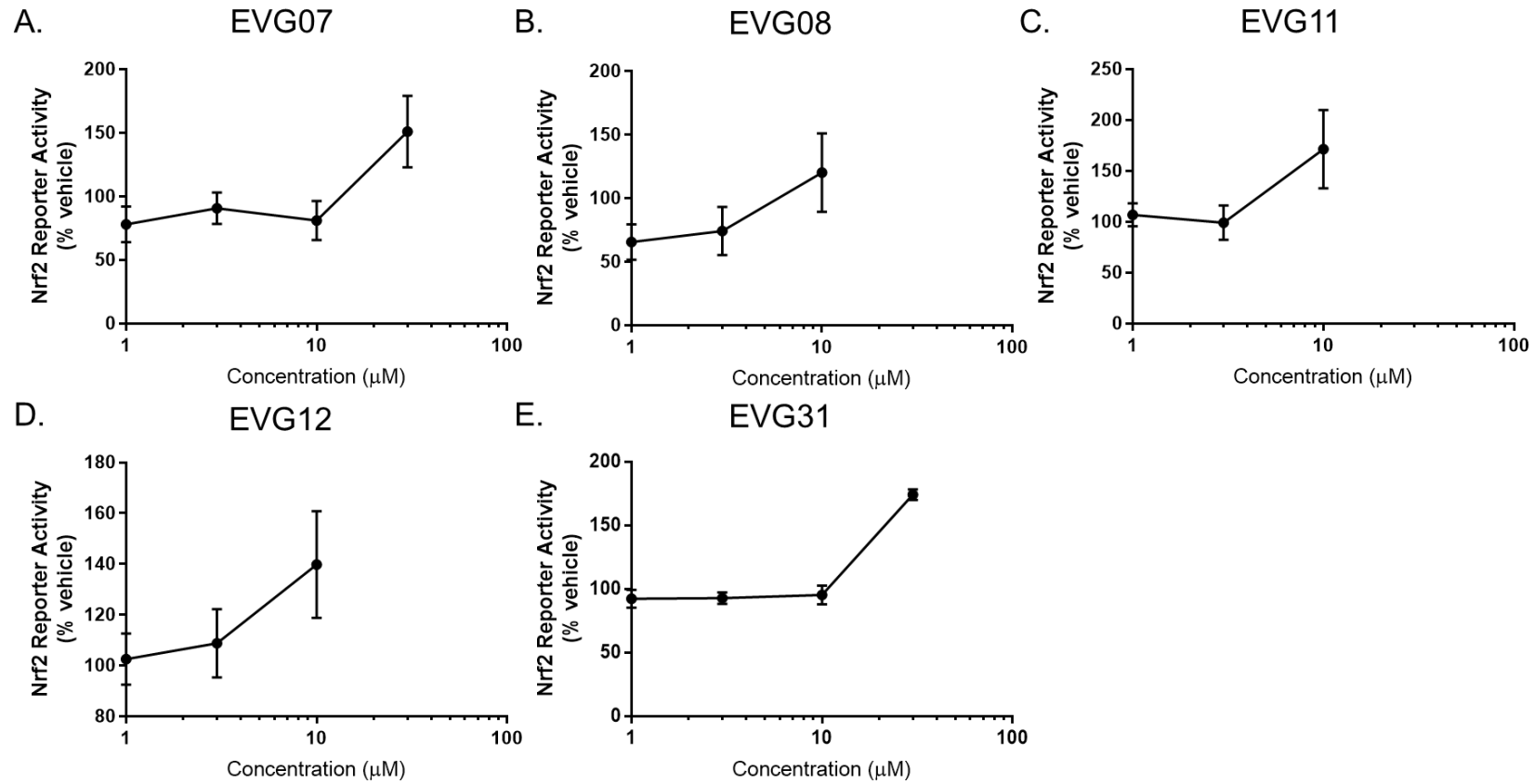
EVG26		<i>N-(tert-butyl)-11-isothiocyanato-3,6,9-trioxaundecane-1-sulfinamide</i>	19.54	5.79
EVG19		1-isothiocyanato-23-(benzylsulfinyl)-3,6,9,12,15,18,21-heptaotricosane	19.63	5.27
EVG15		1-isothiocyanato-23-(ethylsulfinyl)-3,6,9,12,15,18,21-heptaotricosane	20.04	3.17
EVG30		<i>N-(benzyl)-11-isothiocyanato-3,6,9-trioxaundecane-1-sulfinamide</i>	20.09	2.40
EVG29		1-((2-(2-(2-(2-isothiocyanatoethoxy)ethoxy)ethoxy)ethyl)sulfinyl)piperidine	20.94	2.39
EVG06		1-isothiocyanato-11-(phenylsulfinyl)-3,6,9-trioxaundecane	21.18	6.60
EVG35		23-isothiocyanato-N-phenyl-3,6,9,12,15,18,21-heptaotricosane-1-sulfinamide	25.00	5.71
EVG38		23-isothiocyanato-N-(2,4,6-trifluorophenyl)-3,6,9,12,15,18,21-heptaotricosane-1-sulfinamide	25.37	7.99
EVG20		1-isothiocyanato-23-(pyridine-2-sulfinyl)-3,6,9,12,15,18,21-heptaotricosane	25.53	2.06

EVG39		<i>N</i> -(3,5-bis(trifluoromethyl)phenyl)-23-isothiocyanato-3,6,9,12,15,18,21-heptaoxatricosane-1-sulfinamide	25.63	3.25
EVG41		<i>N</i> -benzyl-23-isothiocyanato-3,6,9,12,15,18,21-heptaoxatricosane-1-sulfinamide	27.04	4.83
EVG34		<i>N</i> -isobutyl-23-isothiocyanato-3,6,9,12,15,18,21-heptaoxatricosane-1-sulfinamide	27.80	1.17
EVG36		23-isothiocyanato-N-(p-tolyl)-3,6,9,12,15,18,21-heptaoxatricosane-1-sulfinamide	29.72	4.72
EVG16		1-isothiocyanato-23-(tert-butylsulfinyl)-3,6,9,12,15,18,21-heptaoxatricosane	32.50	9.71
EVG07a		1-isothiocyanato-11-(4-methyl-thiophenyl)-3,6,9-trioxaundecane	33.34	13.94
EVG40		<i>N</i> -(2,3-dihydrobenzo[b][1,4]dioxin-6-yl)-23-isothiocyanato-3,6,9,12,15,18,21-heptaoxatricosane-1-sulfinamide	34.91	1.95
EVG28		11-isothiocyanato- N-(propyl)-N-(methyl)-3,6,9-trioxaundecane-1-sulfinamide	48.08	19.07
EVG21		1-isothiocyanato-23-(pyrimidine-2-sulfinyl)-3,6,9,12,15,18,21-heptaoxatricosane	71.12	15.61
EVG33		<i>N</i> -(tert-butyl)-23-isothiocyanato-3,6,9,12,15,18,21-heptaoxatricosane-1-sulfinamide	89.33	18.39

EVG07		1-isothiocyanato-11-(p-tolylsulfinyl)-3,6,9-trioxaundecane	ND	
EVG08		1-isothiocyanato-11-(p-methoxy-phenylsulfinyl)-3,6,9-trioxaundecane	ND	
EVG11		1-isothiocyanato-11-(p-fluoro-phenylsulfinyl)-3,6,9-trioxaundecane	ND	
EVG12		1-isothiocyanato-11-(m-methoxy-phenylsulfinyl)-3,6,9-trioxaundecane	ND	
EVG31		<i>N-(benzyl)-N-(methyl)-11-isothiocyanato-3,6,9-trioxaundecane-1-sulfinamide</i>	ND	

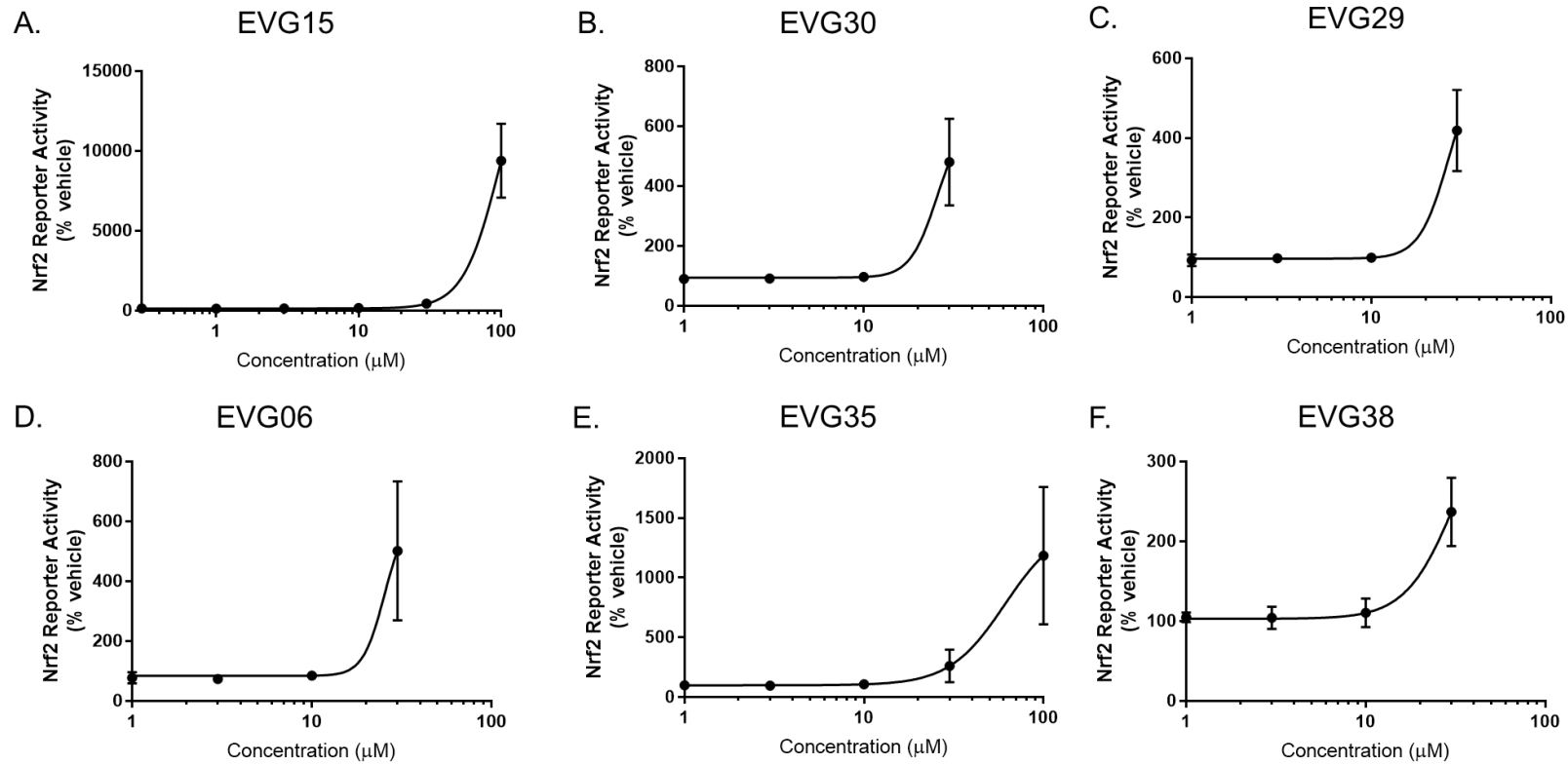
**Figure A6 Sulforaphane analogues with non-defined CD values**

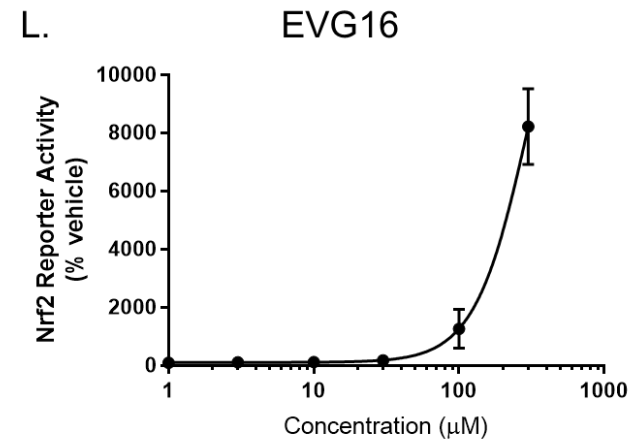
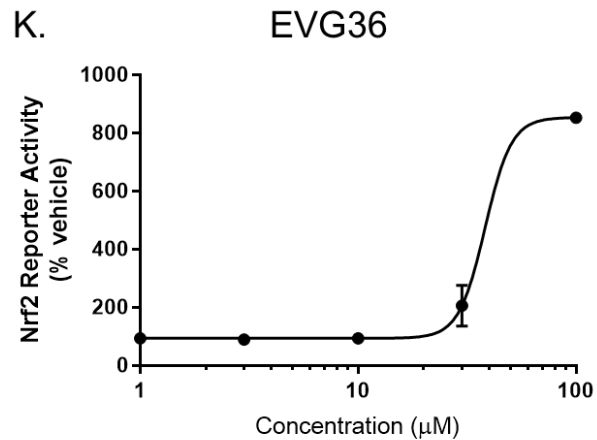
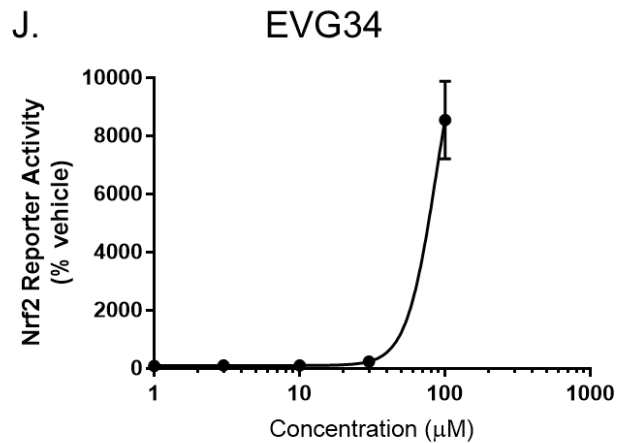
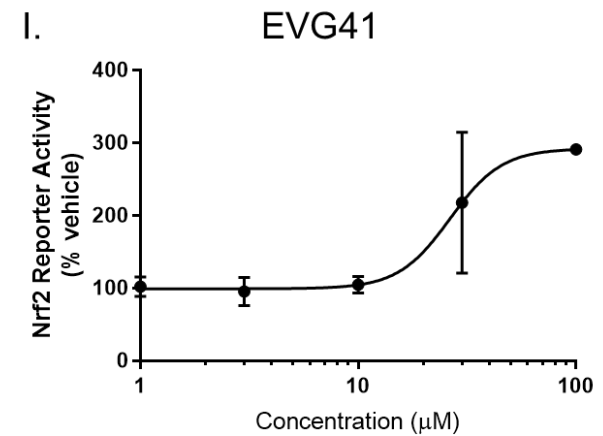
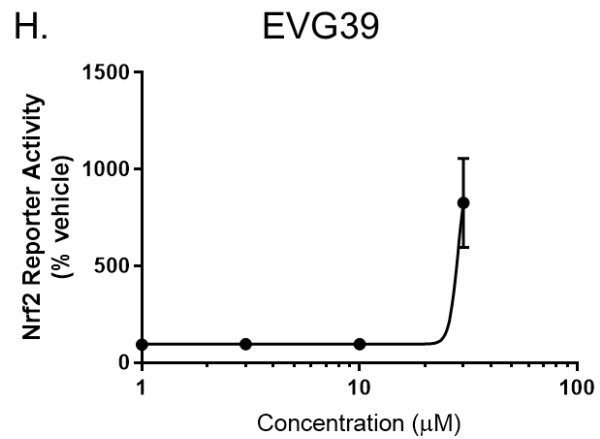
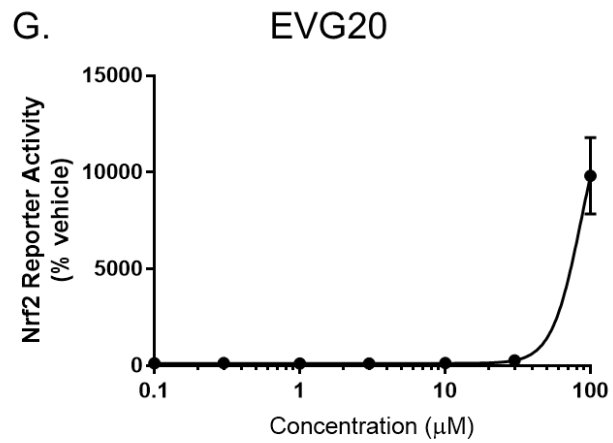
Concentration-response curves of 8AREL reporter luminescence in the H4IIE cells, after 24 h exposure to sulforaphane analogues (n=3): EVG07 (A), EVG08 (B), EVG11 (C), EVG12 (D) and EVG31 (E). CD values undetermined. Mean and SD shown.

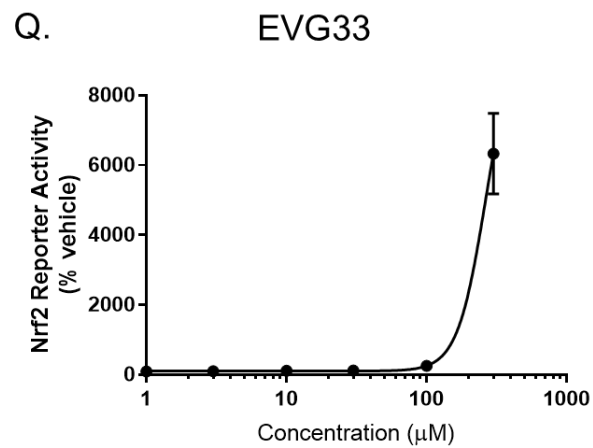
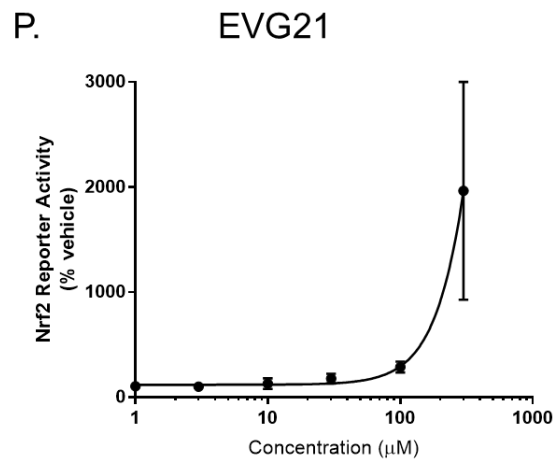
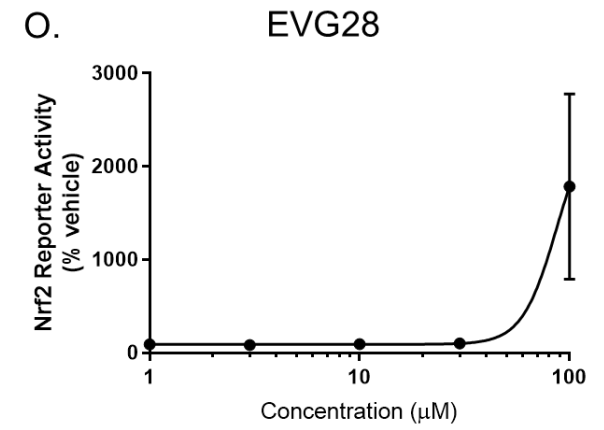
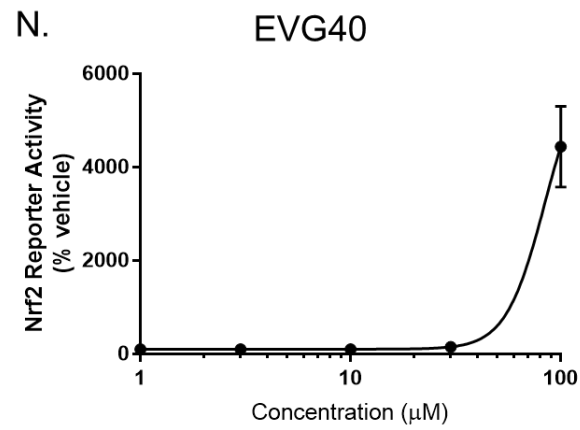
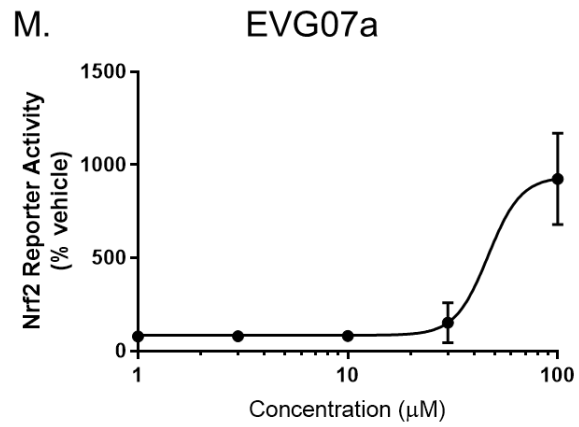


**Figure A7 Sulforaphane analogues with CD values greater than 20  $\mu\text{M}$**

Concentration-response curves of 8AREL reporter luminescence in the H4IIE cells, after 24 h exposure to sulforaphane analogues (n=3) (A-Q). Curve fit calculated via non-linear regression. Mean and SD shown.

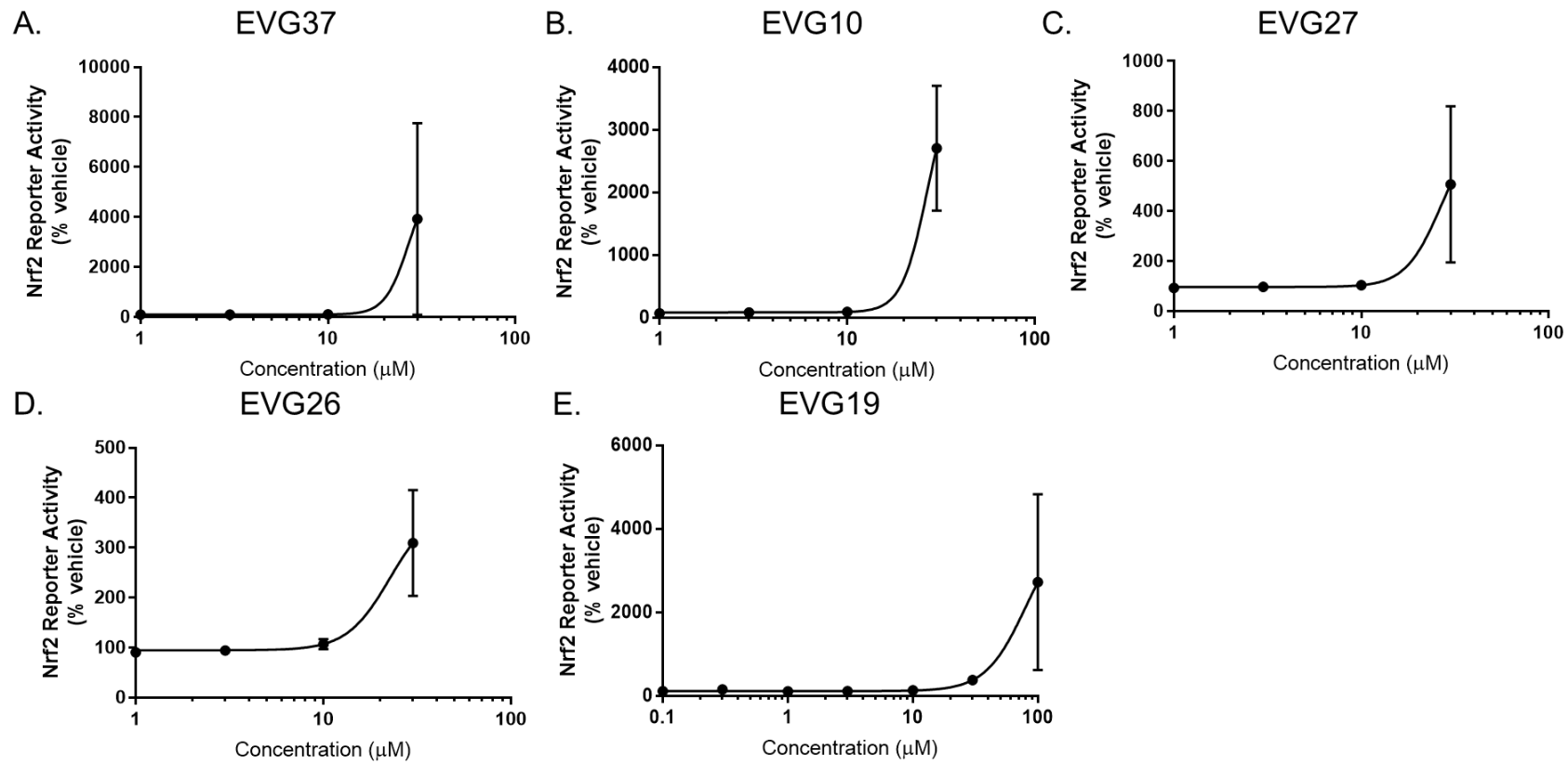






**Figure A8 Sulforaphane analogues with CD values between 15 and 20  $\mu\text{M}$**

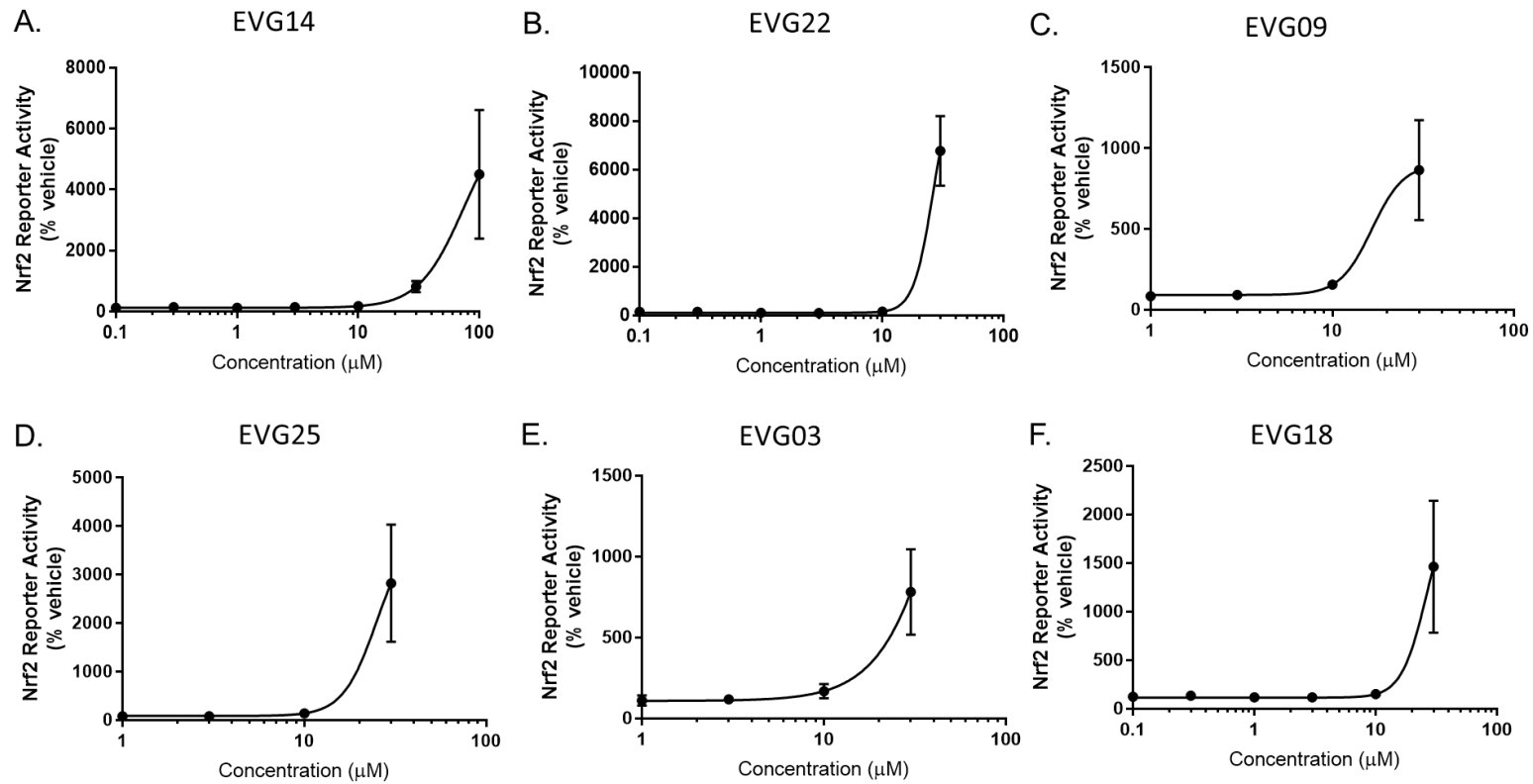
Concentration-response curves of 8AREL reporter luminescence in the H4IIE cells, after 24 h exposure to sulforaphane analogues (n=3) (A-E). Curve fit calculated via non-linear regression. Mean and SD shown.

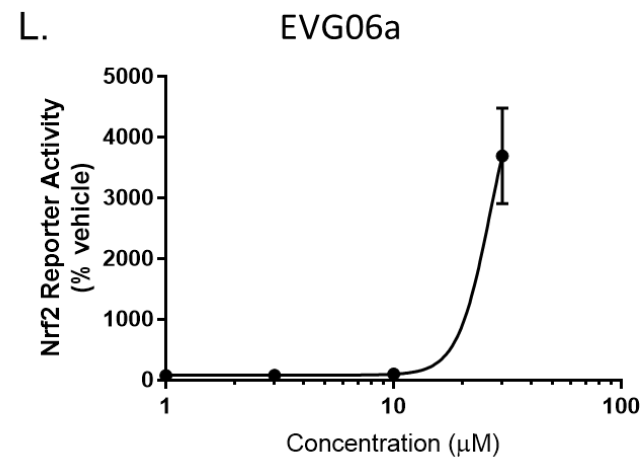
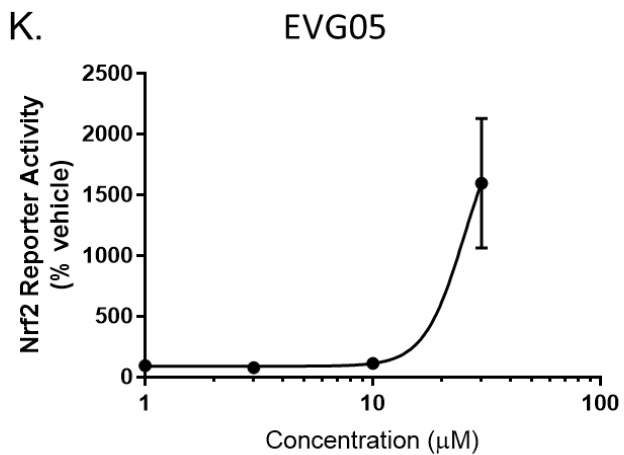
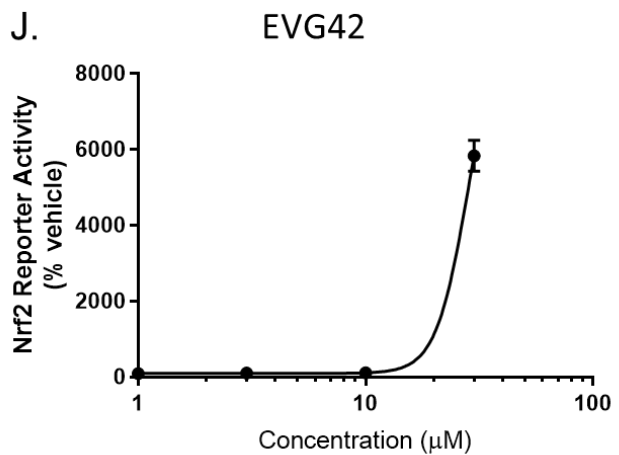
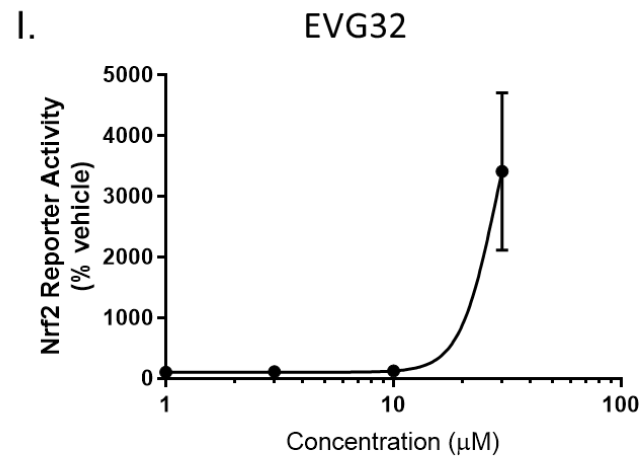
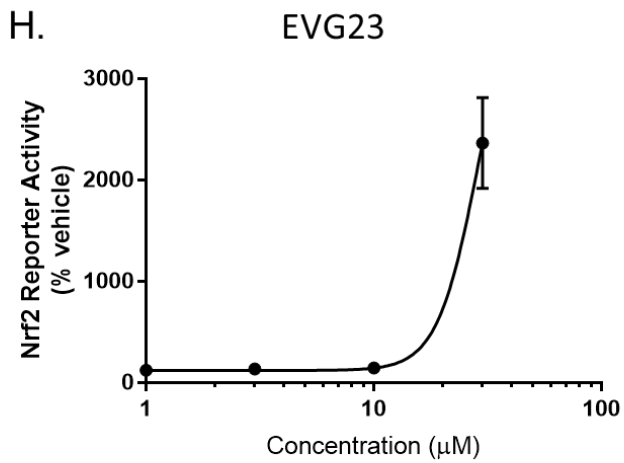
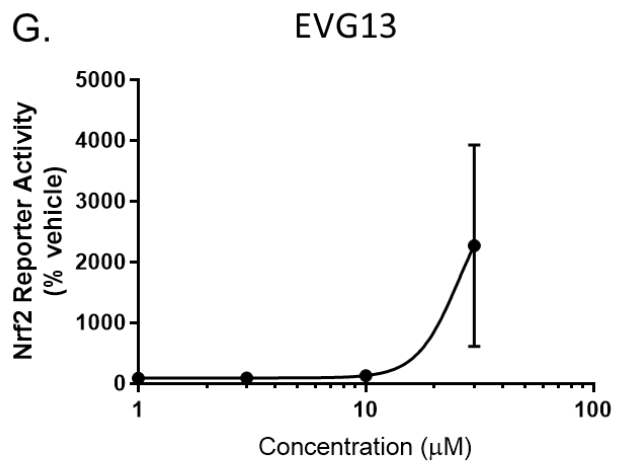




**Figure A9 Sulforaphane analogues with CD values between 10 and 15  $\mu\text{M}$**

Concentration-response curves of 8AREL reporter luminescence in the H4IIE cells, after 24 h exposure to sulforaphane analogues (n=3) (A-O): EVG14(A), EVG22 (B), EVG09 (C), EVG25 (D), EVG03 (E), EVG18 (F), EVG13 (G), EVG23 (H), EVG32 (I), EVG42 (J), EVG05 (K), EVG06a (L), EVG24 (M), EVG17 (N) and EVG04 (O). Curve fit calculated via non-linear regression. Mean and SD shown.





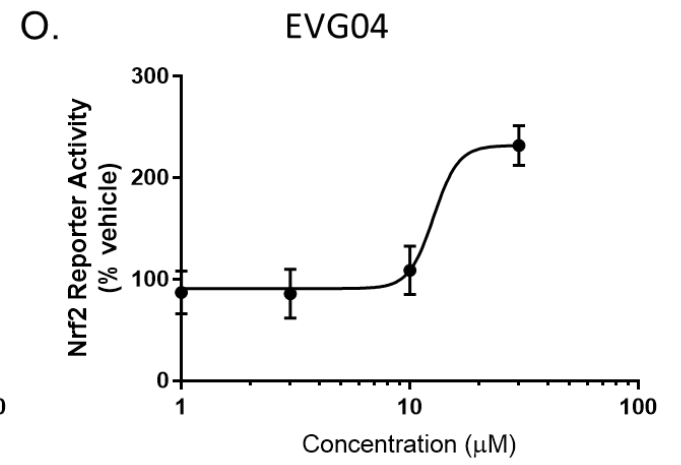
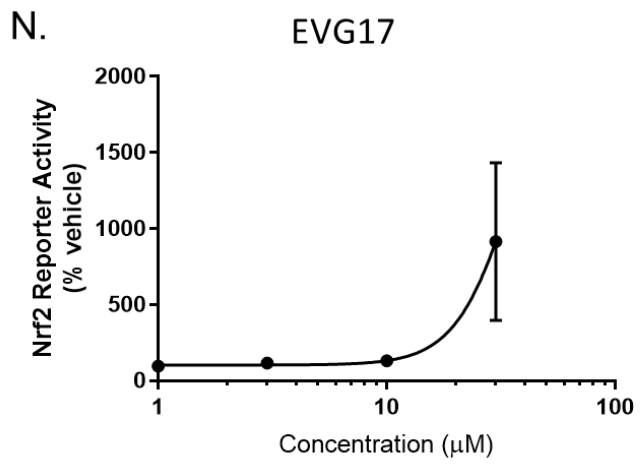
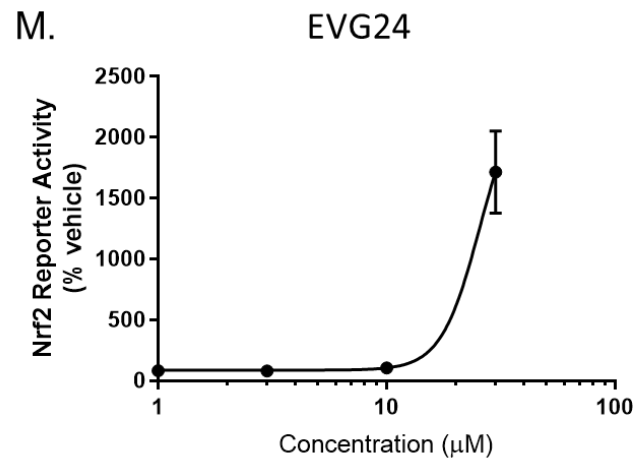


**Figure A10 Compounds in the SFX-01 program with CD values less than 10  $\mu\text{M}$**

Concentration-response curves of 8AREL reporter luminescence in the H4IIE cells, after 24 h exposure to sulforaphane analogues (n=3): EVG01 (A) and EVG02 (B). Curve fit calculated via non-linear regression. Mean and SD shown.

